The recent history of the Antarctic Ice Sheet: constraints from sea-level change.

Daniel Peter Zwartz
September 1995

A thesis submitted for the degree of Doctor of Philosophy of The Australian National University.

The work described in this thesis was carried out while I was a full-time student at the Research School of Earth Sciences, at The Australian National University, between June 1991 and September 1995. Except where mentioned in the text, the research described here is my own. No part of this thesis has been submitted to any other university or similar institution.

Dan Zwartz
September 1995

Acknowledgments

Now that I am finally near the end of this thesis, I feel deeply grateful to everyone who has helped me along the way, both at work and at play. I was lucky to have an excellent supervisory panel. Kurt Lambeck's supervision contained suitable proportions of encouragement and persuasion, and his perseverence in constructively reviewing my final drafts under difficult conditions is greatly appreciated. John Stone and Herb McQueen always provided good advice and their assistance is gratefully acknowledged. Many people assisted me in my data collection, and without them the work would not have been possible. John Stone and Michael Bird let me join their Vestfold Hills expedition, and were excellent companions. They also generously let me use the results of analyses they conducted on the Antarctic samples. David Hopley was always helpful and his expertise was much appreciated during field work on the Great Barrier Reef. Claudine Stirling, Jeremy Taylor, and Mark and Geoff on the R.V. Kirby were also invaluable at this time. Permission for field work in Queensland was granted by the Great Barrier Reef Marine Park Authority, and the National Tidal Facility at Flinders University and the Queensland Ministry of Transport provided tidal data. Unpublished reef core data from the Great Barrier Reef were generously provided by David Hopley and John Marshall. Dick Jenssen kindly provided me with ice and bedrock maps of Antarctica in digital form, thus saving me a great deal of work. My colleagues in Geodynamics have helped make my time here enjoyable, and I would particularly like to thank Jean Braun, Paul Johnston, Tony Purcell, Vivien Gleeson and Janine Dolton for their assistance in various fields whenever it was needed. Sharing an office with Deb Scott was a stimulating experience which I enjoyed immensely, and learned a great deal from. It has taken two people to replace her, but Tony Purcell and Geoff Batt have done a good job of filling the gap. I have enjoyed the company of my fellow students at RSES, particularly Adam Kent, Melita Keywood, Dave John Brown, Steve Pell, Alfredo Camacho, Sue Keay, Claudine Stirling and Geoff Fraser, among others. Finally, for their comments on drafts of this thesis, I would like to thank John Stone, Michael Bird, Paul Johnston and Herb McQueen.

My time in Canberra will be memorable for the range of diversions which kept me away from work, and the people who accompanied me. Dylan Harrison and Alusha Mamchak were wonderful housemates, and tolerated the "last stages" of my thesis for a long time. A significant fraction of my spare time was spent getting tired and dirty on bicycles, and I always enjoyed the company I had doing this: thanks to the main protagonists: Dylan, Pete, Gill, Adam, and Melita. For films, frisbee, coffee, climbs, squash, jokes, beer and more bike rides I thank Amanda, Angus, Greg, Kym, Penny, Rosie, Steve, and many others. Thanks also to Ulli, who was a constant source of motivation, humour, affection and liquorice. Finally, I would like to thank my parents, who have given support and encouragement throughout my education. I owe the enjoyment of my four years in Canberra to their efforts over a much longer period of time.

Abstract

The rheology of the earth and the history of ice sheets, which have a major contributing role in climate change, are both subjects of considerable interest in earth sciences, and the study of sea-level change provides insight into both. Sea-level change since the last glacial maximum (LGM), about 18,000 years ago, can be explained as the sum of three contributions: the sea-level rise due to melting of the Pleistocene ice sheets; the isostatic and gravitational response to the melting of these ice sheets; and the isostatic and gravitational response to the water added to the oceans. Thus, sea-level change varies with location, and is dependent on the volume and distribution of the ice removed, the shape of the oceans, and the rheological structure of the earth. Using sea-level records from appropriate locations, and numerical models of the response of the earth to surface loads, constraints can be placed on some of these parameters. In this thesis, I use new sea-level observations from Antarctica and Queensland to estimate the former distribution of ice at several Antarctic sites, the total amount of extra ice which was stored in Antarctica at the LGM compared to the present, and the eustatic sea-level change which has occurred in the last 6,000 years.

I present a new high-resolution sea-level record from the Vestfold Hills, Antarctica, obtained by dating the lacustrine-marine and marine-lacustrine transitions in sediment cores from lakes which were formerly connected to the sea. A sea-level maximum ~9 m above present sea-level 6,000 years ago is documented. Sea-level observations from other Antarctic sites have been compiled and compared with predictions derived from simplified models of melting at the ice sheet margin. The results indicate that at the LGM the East Antarctic ice sheet margin was 25 - 100 km beyond its present position, resulting in ice thicknesses of 500 - 1000 m at sites now on the coast.

Eustatic sea-level change in the last 6,000 years can be estimated from the difference between sea-level predictions and observations at sites unaffected by details of the ice sheet reconstructions. Using new sea-level observations and a compilation of published data from north Queensland, a eustatic sea-level rise of 3 - 6 m in the last 6,000 years is inferred, with the rate of rise decreasing towards the present.

The reconstructions described here, if applied to the entire Antarctic Ice Sheet margin, would amount to 8.6 - 12.1 m equivalent sea-level. When combined with the ~90 m contribution from the better-constrained northern hemisphere ice sheets, this is insufficient to make up the observed ~120 m of postglacial eustatic sea-level rise. The additional water may have been stored (i) in the Antarctic Ice Sheet at locations far from the sites studied here, such as the West Antarctic Ice Sheet, or (ii) in another reservoir elsewhere on the planet. When corrections are made for all other known contributions, the observed sea-levels in eastern Australia show a gradient in latitude consistent with the removal of a large volume of ice from Antarctica, supporting the former scenario.

Contents

1 Introduction: Sea-level change, ice sheets and climate....1
1.1 What can sea-level tell us about climate and climate history? 1
1.1.1 What forces climatic cyclicity?....2
1.1.2 How much ice was on Antarctica at the LGM?....3
1.1.3 How was it distributed?....3
1.1.4 When did it melt?....4
1.2 Modelling sea-level change....5
1.2.1 Glacio-hydro-isostasy....5
1.2.2 Previous results from glacio-hydro-isostasy....5
1.3 Content of this thesis....7
1.3.1 Some definitions....8

Part I : Sea-level and ice sheet observations....9

2 Sea-level Observations from Far North Queensland....11
2.1 Introduction....11
2.2 Methods....13
2.2.1 Microatolls....13
2.2.2 Reef core data....16
2.2.3 Beachrock....17
2.2.4 Chenier plains....17
2.2.5 Oyster shells....18
2.2.6 Other methods....19
2.3 Previous work....20
2.3.1 LGM sea-level....20
2.3.2 The postglacial transgression....21
2.3.1 Sea-level change since ~6 ka....27
Microatolls....28
Oyster shell deposits....31
Drill core data....33
Beach ridges....33
2.4 Sea-level change at Orpheus Island....35
2.4.1 Introduction....35
2.4.2 Study sites....35
Pioneer Bay....35
Pioneer Bay South....35
Little Pioneer Bay....36
Iris Point....36
Hazard Bay....37
2.4.3 Sampling procedure....37
Microatolls....37
Clam shells....37
Levelling....37

Reduction of levelling data 37
2.4.4 Radiocarbon dates 38
Preparation of samples 38
Results 38
2.4.5 Interpretation 40
Pioneer Bay South 40
Discussion 42
2.5 Northern GBR microatolls 44
2.5.1 Introduction 44
2.5.2 Sample collection 46
2.5.3 Results 46
Microatolls 46
Oysters 49
2.5.4 Discussion 50
2.6 Drillcore data 52
2.6.1 Introduction 52
2.6.2 Data sources 52
2.6.3 Sites studied 53
2.6.4 Results 54

3 Sea-level Observations from Antarctica 57
3.1 Introduction 57
3.2 Methods 59
3.2.1 Raised Beaches 59
3.2.2 Isolated Lakes 59
3.2.3 Marine Limit 62
3.2.4 Limiting Observations 62
3.2.5 Radiocarbon dating 62
3.3 Vestfold Hills 65
3.3.1 Previous work 65
3.3.2 New observations 70
Collection of cores 70
Core stratigraphy and sediment characteristics 71
Interpretation 76
Dating the marine-lacustrine transitions 77
Sea-level history of the Vestfold Hills 80
3.4 Victoria Land 83
3.4.1 McMurdo Sound region 84
3.4.2 Terra Nova Bay 87
3.4.3 Marine limits 89
3.4.4 Miscellaneous sea-level observations 91
3.5 Windmill Islands 92
3.5.1 Marine limits 93
3.5.2 Lake sediment cores 94
3.6 Bunger Hills 96
3.7 Larsemann Hills 99
3.8 Sôya Coast 100
3.9 Antarctic Peninsula 103
3.10 Summary 105

4 The Antarctic Ice Sheet **107**
4.1 Introduction 107
4.2 Glacial Geology 109
4.2.1 Vestfold Hills 109
Lake sediment ages 109
Carbon analyses 111
Cosmogenic isotope measurements 114
Discussion 116
4.2.2 Other coastal oases 117
Larsemann Hills 117
Bunger Hills 117
Windmill Islands 118
Sôya Coast 118
4.2.3 Ross Sea Region 120
4.2.4 Lambert Glacier 121
4.2.5 Sør Rondane Mountains 124
4.2.6 Antarctic Peninsula 124
4.3 Marine Geology 125
4.3.1 Weddell Sea 125
4.3.2 Prydz Bay 125
4.3.3 Ross Sea 125
4.3.4 Wilkes Coast 126
4.3.5 Antarctic Peninsula 126
4.4 Ice Cores 127
4.4.1 Total gas content 127
4.4.2 Isotopic records 129
4.4.3 Cores from coastal regions 131
4.4.4 Ice temperature profile 131
4.4.5 Discussion 131
4.5 Theoretical Models 133
4.6 Estimates of Modern Mass Balance 135
4.7 Summary 136

Part II : Modelling sea-level change **137**

5 Basics of glacio-hydro-isostasy **139**
5.1 Introduction 139
5.2 The sea-level equation 142
5.3 Axisymmetric models 143
5.3.1 Axisymmetric ice sheet models 143
5.3.2 Ocean models 144
5.3.3 Earth rheological model 145
5.4 Sea-level predictions for axisymmetric models 147
5.4.1 Near field sea-level change 147
Ice-load component 147
Water-load component 149
Total sea-level change 151
5.4.2 Far field sea-level change 152
Ice-load component 153
Water-load component 154

5.4.3 Moving coastlines in the far field 155
5.5 Realistic models 158

6 Modelling sea-level change in North Queensland 159
6.1 Introduction 159
6.2 Sea-level at the Last Glacial Maximuum (LGM) 161
6.3 The post-glacial transgression 165
6.3.1 Introduction 165
6.3.2 Time at which present sea-level first attained 165
Model predictions 165
Comparison with observations 171
6.3.3 Sea-level stillstands and regressions 176
6.4 Mid-late Holocene sea-level 178
6.4.1 Introduction 178
6.4.2 Late Holocene eustatic sea-level change 179
Spatial variation 183

7 The Antarctic ice sheet and sea-level change 185
7.1 Objectives of this chapter 185
7.2 Previous work 186
7.2.1 The former Antarctic Ice Sheet 186
7.2.2 Rheological models of the Earth 189
7.3 Methods 191
7.3.1 Ice sheet configuration 191
7.3.2 Regional models 192
Ice sheet retreat 194
Distribution of ice removed 194
Timing of melting 195
7.3.3 Continental-scale models 197
Distribution of ice removed 197
Timing of melting 198
7.3.4 Ocean models 199
Static coastline models 199
Moving coastline models 201
Iterations of the sea-level equation 203
7.3.5 Earth model 203
7.3.6 Estimation of total relative sea-level change 203
7.4 Results - Regional models 204
7.4.1 Pattern of deformation 204
7.4.2 Shape of the RSL curve 204
7.4.3 ESL model 207
7.4.4 Ice load distribution 209
7.4.5 Ice volume 211
7.4.6 Lithospheric thickness 212
7.4.7 Upper mantle viscosity 214
7.4.8 Lower Mantle Viscosity 216
7.4.9 Time extent of models 217
7.4.10 Summary 217
7.5 Continental models 219

7.5.1 Elevation change inland 219
7.5.2 Distant effects 223
7.6 Regional models - Comparison with Antarctic observations 226
7.6.1 Calculation of variance 226
7.6.2 Optimum ice model 227
Ice thickness and retreat distance 227
Distribution of removed ice 231
Timing of melting 233
Late Holocene melting 234
7.6.3 Optimum Earth model 235
Lithospheric thickness 235
Upper mantle viscosity 235
Lower mantle viscosity 236
7.6.4 Local spatial gradients in sea-level change 236
7.6.5 Discussion 239
7.7 Continental-scale models - Comparison with observations 241
7.7.1 Elevation change inland 241
7.8 Comparison with Australian Holocene sea-levels 242
7.9 Realistic models 248
7.9.1 Estimating the total volume change of the Antarctic Ice Sheet 248
7.10 Summary 252

8 Conclusion 253
8.1 New Antarctic sea-level observations 253
8.2 Regional ice sheet reconstructions 254
8.3 Total Antarctic ice sheet volume change 255
8.4 Late Holocene melting 256

Appendix : Site Reports 259

Bibliography 269

List of Figures

2.1 A guide to tidal planes 13
2.2 Living and fossil microatolls at Iris Point, Orpheus Island 14
2.3 The response of microatolls to different patterns of sea-level change 15
2.4 Dated mangrove peat and shell material from sediment cores in Princess Charlotte Bay 24
2.5 Dated mangrove and shell material from cores on the northern Great Barrier Reef near Cooktown 24
2.6 Eustatic sea-level record for the last glacial cycle 27
2.7 Location map of the central to north Great Barrier Reef 30
2.8 Height-age relationship for dated microatolls from the central to north Great Barrier Reef 31
2.9 Relationship between microatolls and oyster shell beds at Magnetic Island. 32
2.10 Proposed 5000 yr sea-level isobase 34
2.11 Location map of Orpheus Island 36
2.12 All coral and clam shell dates from Orpheus Island 41
2.13 Dated coral and clam shell samples from Pioneer Bay South 41
2.14 Dated microatolls from Orpheus Island 42
2.15 Location map of the Lizard Island - Princess Charlotte Bay region, Great Barrier Reef 45
2.16 All dated microatolls from the Lizard Island - Princess Charlotte Bay region 48
2.17 Dated microatolls from the Lizard Island - Princess Charlotte Bay region, by location 49
2.18 Reef core location map 53
2.19 All dated coral samples from reef cores in the Great Barrier Reef 55
2.20 Possible sources of error when inferring sea-level from a dated core sample 56

3.1 Location map of Antarctica 58
3.2 Schematic representation of lake sedimentation in a changing sea-level environment 60
3.3 Reconstruction of sea-level history from lake sediment records 61
3.4 Published radiocarbon ages from the Vestfold Hills 66
3.5 Total emergence and inferred average emergence rate in the Vestfold Hills 67
3.6 Published constraints on the sea-level curve for the Vestfold Hills 67
3.7 Map of Watts/Nicholson/Anderson lake system 68
3.8 Aerial view of Anderson Lake, Watts Lake and Ellis Fjord 69
3.9 Locations of lakes cored in the Vestfold Hills 72
3.10 The relative sea-level history of the Vestfold Hills 82

3.11 Location map for Victoria Land 83
3.12 Sea-level curve for McMurdo Sound 86
3.13 Sea-level curve for Terra Nova Bay 89
3.14 Elevation of the marine limit in Victoria Land 90
3.15 Location map for Windmill Islands 92
3.16 Sea-level curve for Windmill Islands 95
3.17 Sea-level curve for the Bunger Hills 98
3.18 Location map for Lützow-Holm Bay 100
3.19 Sea-level curve for Skarvsnes, in Lützow-Holm Bay 101
3.20 Sea-level observations from King George Island 104
3.21 Summary of sea-level observations for Antarctic sites 105

4.1 Location map of Antarctica 108
4.2 TOC and $\delta^{13}C$ profiles from Scale Lake and Lake McCallum 113
4.3 Cosmogenic isotope exposure ages from the Vestfold Hills. 115
4.4 Location map for Lützow-Holm Bay 119
4.5 Profiles of drift sheets in the Transantarctic Mountains 122
4.6 Reconstructions of the Ross Ice Sheet 123
4.7 Total gas volume measurements in the Vostok ice core 129
4.8 Maximum reconstruction of the LGM Antarctic Ice Sheet 134

5.1 Schematic illustration of glacio-hydro-isostatic sea-level changes 140
5.2 Profiles of axisymmetric ice sheet models 144
5.3 The ice-load component in the near field 148
5.4 The water-load component in the near field 150
5.5 Components of predicted sea-level change for one and two iterations of the water load 151
5.6 The ice-load component in the far-field 153
5.7 The second iteration of the water load in the far field 154
5.8 Total predicted sea-level change at three far field sites 155
5.9 Bathymetric profiles of the far field coastline 157
5.10 The second iteration of the water-load component at the far field coastline 157

6.1 Predicted sea-level at the LGM, 18 000 years ago 162
6.2 Predicted sea-level at the LGM in the Australian region 164
6.3 Predicted sea-level curves at sites on a transect of the GBR. 166
6.4 Predicted sea-level histories on a transect of the north Queensland coast, ... 167
6.5 Predicted time at which sea-level first reached its present level in the Australian region. 168
6.6 Predicted first attainment time in the study area on the GBR 169
6.7 Same as Figure 6.6, but for models with a 50 km lithosphere. 170
6.8 Predicted and observed spatial gradients in the first attainment time 171
6.9 Same as Figure 6.8, for models with a 50 km lithosphere. 172
6.10 Same as Figure 6.8, but including 1.7 m of late Holocene melting 174

6.11 Same as Figure 6.9, but including 1.7 m of late Holocene melting....174
6.12 Same as Figure 6.8, but including 3 m of late Holocene melting....175
6.13 Same as Figure 6.9, but including 3 m of late Holocene melting....175
6.14 Predicted relative sea-level curves at Barbados and Halifax Bay....177
6.15 Predicted relative sea-level curves for inner and outer margins of continental shelves....178
6.16 Observed-predicted sea-level residuals for mid-late Holocene observations in north Queensland....180
6.17 Same as for Figure 6.16, but for an earth model with 100 km lithosphere and a uniform mantle viscosity of 10^{21} Pa.s....181
6.18 Comparison of sea-level residuals from north Queensland with the result of Lambeck (1993b)....182
6.19 Spatial variation in observed-predicted sea-level residuals....183

7.1 Published models for the Antarctic meltwater contribution....187
7.2 Example predicted and observed far-field sea-level curves....187
7.3 Distribution of ice load for axisymmetric models....192
7.4 Transects of the Antarctic Ice Sheet at study sites....193
7.5 Distribution of ice removed for constant-height and constant-b models....195
7.6 Three melting curves used for the regional-scale ice sheet models....196
7.7 Calculation of the load of ice grounded below sea-level....202
7.8 Sea-level change due to the regional model....205
7.9 Comparison of regional models with the actual Antarctic Ice Sheet....206
7.10 Predicted RSL history at a site on the present ice sheet margin....207
7.11 Effect of late Holocene melting on the RSL at a coastal site....208
7.12 Ice load component of sea-level change at a coastal site predicted by the three regional ice-melting curves....209
7.13 Predicted relative sea-level curves at a coastal site for constant-h and constant-b ice sheets and three melting histories....210
7.14 The effect on the predicted relative sea-level history at a coastal site of the volume of the regional ice sheet model....211
7.15 The effect of lithospheric thickness on RSL at a coastal site....212
7.16 The effect of upper mantle viscosity on RSL at a coastal site....214
7.17 The effect of lower mantle viscosity on RSL at a coastal site....216
7.18 Subdivision of an ice load into annular rings....220
7.19 The distribution of removed ice for several melting styles and two values of total ice volume....222
7.20 The effect of ice volume and distribution on predicted sea-level change in the region beyond the peripheral bulge....224
7.21 The effect of upper mantle viscosity on predicted sea-level change in the region beyond the peripheral bulge....225
7.22 The effect of lithospheric thickness on predicted sea-level change in the region beyond the peripheral bulge....225
7.23 Normalised variance between regional model predictions and sea-level observations....232

7.24 Comparison between observed and predicted sea-level in the Australasian region. 245
7.25 The ANT3 reconstruction of the LGM Antarctic Ice Sheet 248
7.26 The ICE-3G reconstruction of the LGM Antarctic Ice Sheet 249

List of Tables

2.1 Depths and ages of drowned shorelines in the central GBR 22
2.2 Radiocarbon ages of samples from sediment cores in Princess Charlotte Bay 23
2.3 Radiocarbon ages of mangrove muds from the transgressive unit, northern GBR 25
2.4 Proposed transgressive sea-level stillstands 25
2.5 Radiocarbon ages of raised *Porites* microatolls 29
2.6 Radiocarbon ages of coral samples from Orpheus Island 39
2.7 Radiocarbon ages of *Tridacna* clam shell samples 40
2.8 Study sites in the central and northern GBR 46
2.9 Radiocarbon dates from central and northern GBR 47
2.10 Comparison of elevations of modern and ancient oyster shell deposits 50
2.11 Locations of sites for which borehole data have been compiled 54

3.1 Locations of Antarctic sites discussed in this chapter 57
3.2 Estimates of the marine reservoir correction at some locations in East Antarctica 63
3.3 Radiocarbon assays from modern algae from the Vestfold Hills 64
3.4 Radiocarbon ages from marine organisms in emerged marine terraces in the Vestfold Hills 65
3.5 Published former sea-levels derived from isolation of lakes in the Vestfold Hills. 70
3.6 Lakes cored in the Vestfold Hills 73
3.7 Descriptions of cores taken from lakes in the Vestfold Hills 75
3.8 Conventional radiocarbon ages obtained from cores from lakes in the Vestfold Hills 78
3.9 Ages of marine-lacustrine transitions in lakes in the Vestfold Hills 80
3.10 Radiocarbon ages from emerged marine sediments in McMurdo Sound 85
3.11 Radiocarbon ages from Terra Nova Bay 88
3.12 Marine limit observations from the Windmill Islands 93
3.13 Radiocarbon ages from sediments in lakes in the Windmill Islands 94
3.14 Radiocarbon ages from the Bunger Hills 98

4.1 Age of lowest organic-rich lacustrine sediments in lakes of the Vestfold Hills. 110
4.2 Radiocarbon ages from till in cores from the Vestfold Hills 110

6.1 Rheological models used in this chapter 160
6.2 Observations and predictions of relative sea-level at the LGM at some far field sites. 163

6.3 Scatter of observed-predicted sea-level residuals 181

7.1 - Regional contributions to postglacial sea-level rise from the Antarctic Ice Sheet, ... 189
7.2 The three regional ice sheet ESL models 197
7.3 ESL models used in the continental-scale ice sheet models 198
7.4 Removed ice distribution models in the continental-scale ice sheet models. 198
7.5 Initial and final dimensions of the continental-scale ice sheet models 199
7.6 Rheological models in this chapter. 203
7.7 Effect on RSL curve of varying the model parameters 218
7.8 Surface elevation changes at the centre of the ice sheet 222
7.9 Estimated former ice thicknesses and margin retreat distances at sites in East Antarctica. 228
7.10 Estimated former ice thicknesses and margin retreat distances at sites in East Antarctica, using a standard earth model and only considering models which include significant late-Holocene melting 229
7.11 Predicted spatial gradient in the height of the 6 ka sea-level highstand. 238
7.12 Components of RSL at 6 ka at several East Australian sites 244
7.13 Estimated contribution to global sea-level change from regions of the Antarctic Ice Sheet since the LGM. 250

Chapter 1

Introduction: Sea-level change, ice sheets and climate

1.1 What can sea-level tell us about climate and climate history?

The history of Earth's climate in the Cenozoic is dominated by gradual cooling and associated accumulation of ice on land since the Oligocene. Although the primary control on the onset of glaciation is tectonic, namely the isolation of the Antarctic continent allowing the formation of the circum-polar current, ice sheets themselves play a critical role in the global climate system. For example, their high albedo influences the net solar radiation retained by the earth; the formation of sea ice at their margins controls the production of deep cold ocean currents, which are an important global heat reservoir; and they store significant amounts of water, controlling global sea-levels. Sea-level in turn influences the pattern of ocean currents, the distribution of land and water on the continental shelves, and hence the patterns of vegetation, wind and rainfall which constitute the earth's climate. A record of sea-level, then, when compared to other climatic records, provides us with an opportunity to establish some of the mechanisms operating between different aspects of the climatic system. Also, the former sea-level is a measure of the amount of ice on land, so the interrelationships between ice sheets, sea-level and climate can be investigated through sea-level studies.

Naturally, these interrelationships, and many others which comprise the climate system, are very complex and are the subject of a great deal of current research. General Circulation Models (GCMs) are used to study the physical and thermodynamic interaction of the atmosphere and oceans, and produce predictions for temperature, wind and precipitation patterns. These all depend primarily on short-term processes, and require that the climate-influencing features such as ice distribution and sea-level, which change on longer time scales, be given as part of the initial conditions. The predictions produced are then compared with climate records such as those derived from vegetation histories, deep sea sediments and ice cores. The degree of agreement between predictions and observations is used to assess the validity of the modelling and the significance of the processes which are modelled. Thus, if the climate system is to be properly understood using this method, a good record of sea-level change and ice distribution and an understanding of the relationship between them is essential.

The link between sea-level and global climate on shorter time scales is under close scrutiny, too, as it appears more and more certain that the earth is warming due to the enhanced Greenhouse Effect. Predictions of sea-level

change due to global warming involve estimating the effects of sea-level rise due to thermal expansion of the oceans and increased melting of ice, balanced against the possibility of sea-level fall due to increased snowfall onto existing ice sheets, in a warmer, more humid environment (eg Warrick and Oerlemans 1990).

Determining the relative importance of these effects involves comparing global temperature and sea-level records, which are generally only available with sufficient resolution for the past few decades. The sea-level history, as recorded by tide gauges, is noisy and the component due to global warming can only be determined if all other effects are accounted for. The continuing sea-level changes due to the deglaciation which was largely complete 6,000 years ago may still be significant in this regard.

Some of the major outstanding problems of Quaternary climate change which may be addressed by studies of ice sheets and sea-level change are discussed below.

1.1.1 What forces climatic cyclicity?

The most striking feature of the Quaternary climate record is its cyclicity: glacial and interglacial periods have alternated with a period of around 100,000 years for most of this time. Analysis of oxygen isotope records from deep sea cores shows that frequencies of around 23,000, 41,000 and 100,000 years are significant. These match well with the periodic variations in the earth's orbital parameters, which control the amount of the sun's radiation the planet receives and its distribution with latitude and throughout the year. This suggests a strong link between insolation and climate, but by no means an exclusive one. Other possible controls on periodic climate change include the irregular cyclicity inherent in complex systems with feedback mechanisms, and singular events such as volcanic eruptions, which may reduce the earth's insolation by injecting dust into the atmosphere, or induce warming by the addition of greenhouse gases.

The growth and decay of ice sheets in the northern hemisphere matches the insolation record calculated from the variation in orbital parameters, assuming that the combination of warm winters and cool summers results in the accumulation of snow which leads to the growth of ice sheets. When this seasonality occurs in the northern hemisphere, the opposite case (cold winters and hot summers) occurs in the southern hemisphere. Nevertheless, the conclusion that climate cycles are forced by northern hemisphere ice sheet growth and decay is not unreasonable, as that is where continents exist at latitudes where a small change in temperature can tip the balance between ice melt and ice accumulation. However, well-dated records from Huon Peninsula, Papua New Guinea (Stein and others 1993) and Devil's Hole, USA (Winograd and others 1992) suggest that the height of the last interglacial period may lead the insolation peak by several thousand years, suggesting that although the insolation cycle may modulate climate change, other factors may be important in initiating the growth and

decay of ice sheets. To resolve this problem, the various climate records must be well constrained in time, so that the leads and lags between the associated processes can be determined.

1.1.2 How much ice was on Antarctica at the LGM?

As mentioned above, the eustatic sea-level record is a direct measure of the amount of terrestrial ice, but only the total volume is indicated. For a record of the spatial distribution of ice, we need independent evidence from the continents where the ice was located. Most of this is the geomorphological signature of ice masses - moraines, striated pavements, roches moutonées, and other glacial and periglacial features. Along coastlines, the record of post-glacial rebound also describes the distribution of former ice sheets. Because of the usually destructive nature of glacial advances, and the fact that the earth's time constant for isostatic relaxation is around a few thousand years, the records from geomorphological and rebound data respectively are useful only for the last cycle of deglaciation. Luckily, this time period falls completely within the range of radiocarbon dating.

The existence and approximate size of former ice sheets in North America, Fennoscandia and Britain and their effects on sea-level had been established from geomorphological evidence long before the sea-level record was discovered. More recently, significant ice over the Barents Sea region has been established primarily using rebound data (Lambeck 1995), bringing the total northern hemisphere contribution to ~90 m (Nakada and Lambeck 1988, Tushingham and Peltier 1991). Observations of sea-level at the last glacial maximum range from -114 to -175 m (eg Veeh and Veevers 1970, Carter and Johnson 1986), so it is apparent that large bodies of ice must have existed elsewhere as well. Comparison of models and observations (Nakada and Lambeck 1988, Tushingham and Peltier 1991) indicates that around 25 - 35 m of equivalent sea-level was contributed from other sites. Antarctica is the most favoured candidate for this ice, but other sites such as eastern or western Siberia remain as unproven possibilities (Grosswald 1980). A better determination of the total volume of the Antarctic ice sheet at the last glacial maximum is therefore a useful addition to reconstructing global climate at that time.

1.1.3 How was it distributed?

The distribution of former Antarctic ice controls isostatic rebound and hence sea-level at coastal Antarctic locations, and even exerts an influence on sea-level as far away as Australia. This control implies that sea-level records from near Antarctica can be used to constrain the shape of the ice sheet at the last glacial maximum. This is useful information, as in combination with climatic reconstructions for the time it allows us to study how the ice sheet responds to changes in temperature and humidity - valuable knowledge in the light of possible changes in the near future. Previous work in reconstructing the Antarctic ice sheet has been based on geomorphological evidence such as moraines, striations and trimlines (eg

Denton and others 1991), as well as isotopic studies of ice cores (eg Lorius and others 1985) and some isostatic rebound observations (eg Colhoun and others 1992). These studies indicate that at the last glacial maximum, the Antarctic ice sheet was considerably wider than at present, extending to the edge of the continental shelf, but that the central height was about the same or perhaps even lower. More observations and detailed isostatic modelling will add to the understanding of ice sheet dynamics.

1.1.4 When did it melt?

The melting history of the Antarctic ice sheet is crucial information in the investigation of the processes which force climate change. In particular, was the deglaciation of Antarctica initiated in response to sea-level rise due to the melting of northern hemisphere ice; did they respond simultaneously to the same external force; or did the melting of Antarctic ice trigger the end of the glacial period globally? Unlike the northern hemisphere ice sheets, there is little datable material in Antarctic moraines to constrain the timing of the beginning of deglaciation. Thus, local rebound and global sea-level histories may be the best methods of resolving this problem. New methods of dating the retreat of ice in the absence of datable organic material, for example by the accumulation of cosmogenic isotopes, may also add to the story.

1.2 Modelling sea-level change

1.2.1 Glacio-hydro-isostasy

Reliable climate records are not sufficient to establish the processes which link the many observable aspects of climate, past and present: we need to describe the relationship between causes and effects quantitatively. As is the case in GCM studies, the problem is approached by using a model and a set of initial conditions to make a prediction, which is compared with observations. In this study, the system being modelled is the isostatic response of the whole earth to changing loads at the surface. Schematically, we may consider the system as a set of forces F producing a response R filtered according to an earth model E.

The forces, F, are the changing loads of ice and water on the earth's surface, as mass is moved from the oceans onto the high-latitude land masses during glacial periods, and then redistributed when the ice sheets melt.

The parameters of the model E are the rheological properties of the earth - density, elasticity, and viscosity, and their variation with depth. The radial variation in the elastic moduli has been estimated from seismological data, and one of the models thus obtained (PREM, Dziewonski and Anderson 1981) is used for this work. The earth's rheological properties are time-scale-dependant, and in studying climate-related processes, we are interested in timescales of 1,000 to 100,000 years, compared with seconds to hours in seismological studies. Similarly, the loads we are interested in are oceans and ice sheets (hundreds of metres to a few kilometres thick, and tens to thousands of km wide), and the responses are observable as vertical movements of up to hundreds of metres, compared with the small ground displacements recorded by seismometers. Similar studies have been made made on these long timescales by looking at changes in the earth's rotation rate, also due to changing ice loads, and other loading problems on the crust and upper mantle.

Because the processes which link different aspects of climate are complex, nonlinear systems, I won't try to solve them directly from the observations as an inverse problem. Instead, I will use the mathematical model to produce predictions from a range of plausible models and use sets of observations to identify the effects of the different variables and select the best-fitting solution.

1.2.2 Previous results from glacio-hydro-isostasy

Investigation of the earth's rheology from isostatic studies began with studies near the sites of the largest former loads - for example, the Laurentide ice sheet in North America (Walcott 1970), Lake Bonneville in Utah (Crittenden 1963, Lambeck and Nakiboglu 1981), and seamounts (Lambeck 1981). The realisation that these isostatic processes could cause measurable sea-level change worldwide, not just close to the load, led to the

formulation of theoretical techniques to calculate these effects (Farrell and Clarke 1976). Refinement of these techniques, discussed later, and the availability of sufficient computing power to use them efficiently brought these studies to the point where the mechanical properties of the crust and mantle could be estimated by comparison of calculated sea-level changes with those observed in the field (eg Chappell and others 1983, Nakada and Lambeck 1989, Tushingham and Peltier 1992). These developments represented a new source of data for evaluating the earth's rheological properties. The interpreted models are usually of a three-layered radially-symmetric earth, as the data available do not justify proposing more complex structures. Independent studies, using similar methods and observations, do not presently concur. For example, Nakada and Lambeck (1989) suggest an effective lithospheric thickness of around 60-100 km, and upper mantle viscosity (to 670 km depth) of 1-2 x 10^{20} Pa.s. and a lower mantle viscosity of about 10^{22} Pa.s. In contrast, Tushingham and Peltier (1992) suggest values of 120 km, 10^{21} Pa.s, and 2-4 x 10^{21} Pa.s. for the same parameters. The discrepancy between these results is largely due to the incomplete search of parameter space by Tushingham and Peltier (1992), though some may also be due to the locations of the sea-level observations used, since lithospheric thickness, for example, is known to vary laterally.

Although an estimate of the former ice distribution is required in order to generate sea-level predictions, the predictions can be compared with observations to iteratively improve the ice history model. For example, by removing the components of sea-level change due to distant ice sheets, the sea-level record near a former ice sheet can provide more accurate information about the local ice history. This is especially useful in locations where the presence or magnitude of a former ice sheet is difficult to estimate. The North Sea is an example of such a site, where modelling indicates that the British ice sheet did not join the Fennoscandian ice sheet at the last glacial maximum, as had previously been suggested (Lambeck 1993). Similarly, the existence and size of an ice sheet over the Barents Sea region during the last glaciation can be inferred (Lambeck 1995). These examples are from a region which is well covered by sea-level observations, in space and time. To perform a similar analysis on the Antarctic ice sheet would require more observational data than are presently available or easily collected, but some progress should be possible.

1.3 Content of this thesis

This thesis addresses some of the problems discussed above, using sea-level and ice sheet observations from Antarctica and Australia, and numerical models of sea-level change. The thesis is divided into two parts. Part I presents the observations, with little discussion of their wider implications. In Part II, glacio-hydro-isostatic models of sea-level change are presented, and the observations from Part I are used to constrain several aspects of the ice sheet/earth/sea-level system.

In Chapter 2, new sea-level observations from north Queensland are presented. These observations are all from the mid-late Holocene, when sea-level has been at roughly its present level. In particular, former sea-levels were recorded for several islands in the Lizard Island - Princess Charlotte Bay region, and a detailed record is obtained for Orpheus Island, in Halifax Bay near Townsville. In addition to the new data, published and unpublished sea-level observations are compiled and reviewed, including a large data set of dated coral from reef flat cores, which constrain sea-level during the period of rapid rise before 6000 years ago.

Records of Antarctic sea-level change are presented in Chapter 3. A new record from the Vestfold Hills, based on the isolation of lakes from the sea, defines sea-level for the last 6000 - 7000 years with much greater precision than can be obtained by dating raised beach features, which has been the main source of Antarctic sea-level observations. Published records from several sites distributed around East Antarctica are also compiled and reviewed.

The recent history of the Antarctic ice sheet is discussed in Chapter 4, particularly addressing the problem of how much additional ice was stored there during the last glaciation. First, the evidence from glacial geology in the coastal oases and the Transantarctic Mountains is discussed, including new observations from the Vestfold Hills. Results from marine geology, ice cores and theoretical models are also compiled.

Part II begins with a general presentation of the principles of glacio-hydro-isostasy in Chapter 5. Using the theory and numerical models of Johnston (1993), some implications for sea-level change of melting a circular ice sheet similar in size to the former Fennoscandian ice sheet are investigated. Particular attention is paid to coastal sites both close to the ice sheet and a long distance from it, as these are analogous to the Antarctic and Australian observation sites, respectively.

In Chapter 6, the predictions of geographically realistic glacio-hydro-isostatic models are compared with the sea-level observations from north Australia previously presented in Chapter 2. The predicted time at which present sea-level is first attained is investigated in detail, including the effects of location, earth rheology, and the amount of eustatic sea-level change which

has occurred in the late Holocene. The last of these components is also studied using the compiled sea-level observations from the last 6000 years.

The melting history of the Antarctic ice sheet is modelled in Chapter 7. Two types of model ice sheets are investigated, in order to investigate two aspects of the ice sheet history on which we have observational constraints. Both classes of models are circular, with parabolic cross-section, and do not realistically simulate the detailed geographical distribution of ice. First, regional models are constructed, which are intended to simulate the history of a part of the ice sheet margin on the scale of ~1000 km. These models are used to estimate the former ice thickness at those coastal sites from which sea-level records have been obtained (Chapter 3). The second type of model simulates the entire Antarctic ice sheet on the continental scale. These models are used to investigate the predicted elevation change in the centre of the ice sheet, and the isostatic effects of changes in the Antarctic ice sheet on sea-level change in eastern Australia. These sea-level changes are mainly dependant on the total ice volume change, and Australian sea-level observations are compared with the predictions in an attempt to better constrain this.

1.3.1 Some definitions

Sea-level can appear to vary as a result of many processes, such as eustasy (ie water volume changes), regional isostasy, tectonism and changing tidal range. As these processes are global, regional and local, the term "sea-level change" can cause some confusion. In this work, any change in the position of the sea surface relative to the land is referred to as relative sea-level change (RSL), which is the height of mean sea-level at that time above or below present mean sea-level. Thus, tectonic uplift of a site due to an earthquake causes an instantaneous fall in RSL, and an average uplift rate of 5 mm/yr implies that RSL 1000 years ago was +5 m (assuming that the sum of all other causes of sea-level change is zero).

Periods of time in which RSL is positive (ie sea-level was higher than present) are called highstands, and similarly times of negative RSL are called lowstands. If sea-level remains at one level for an extended period of time, this is termed a stillstand.

This thesis is concerned with the period of time since the last glacial maximum (LGM), around 18000 years ago. The term "postglacial" is used to refer to the entire period of time since the LGM. In some other works, particularly those dealing with the northern hemisphere, the term "late glacial" is used for the time until the ice sheets were completely melted, and "postglacial" is used from then until the present. Because this thesis deals mainly with the Antarctic ice sheet, which may have continued melting significantly throughout the Holocene and has not completely melted since the LGM, the term "postglacial" is used for the whole period.

Part I

Sea-level and ice sheet observations

Chapter 2 : Sea-level Observations from Far North Queensland 11

Chapter 3 : Sea-level Observations from Antarctica 57

Chapter 4 : The Antarctic Ice Sheet 107

Chapter 2

Sea-level Observations from Far North Queensland

2.1 Introduction

To constrain the parameters of a glacio-hydro-isostatic model, it is necessary to have a knowledge of sea-level change both close to and distant from the former ice sheets. Sea-level change in the formerly glaciated regions is dominated by the effects of glacio-isostatic rebound, and these observations are necessary to constrain the former distribution of ice and its melting history. The large amplitude of the rebound, however, makes the near field record insensitive to some aspects of the sea-level model, such as the amount of eustatic sea-level rise in the late Holocene. In contrast, sea-level change at distant coastlines is dominated by the eustatic sea-level rise and the hydro-isostatic response of the coastal region to this water-load. Sea-level change after 6 ka, when significant melting of the ice sheets ceased, is most sensitive to this response. Also, if the geometry of the former ice sheet is not well known, then a number of different ice/earth model combinations may adequately describe the observed sea-level change in the near field. Sea-level change in the far field, however, is insensitive to the geometry of the ice load, so better constraints on the mantle rheology may be obtained. These processes are discussed in detail in Chapter 5. North Queensland is a suitable far field region, because it is on the margin of a tectonically stable continent, and the natural environment of the Great Barrier Reef (GBR) is highly sensitive to sea-level change, and may preserve records of it.

The vast length and breadth of the GBR make it a suitable region in which to investigate the differences in the sea-level record along transects both perpendicular to the coastline and, with observations from the rest of eastern Australia and Tasmania, along a line roughly radial to the Antarctic ice sheet. Also, the proximity of the Gulf of Carpentaria, which was entirely above sea-level during the last glacial maximum and thus forms a large postglacial water load, makes North Queensland an ideal region to investigate the effects of large migrations of the coastline on sea-level change.

Since the GBR was first observed by explorers and naturalists in the eighteenth and nineteenth centuries, attempts have been made to understand its form and origin. As its vast extent makes it unique among the coral reefs of the world, the Royal Society has sponsored two major expeditions this century to the Reef, in 1928-29 and 1973, in order to expand our understanding of the processes which control its existence and

evolution. The emphasis of these studies was not specifically on sea-level change, although the three major problems under examination - morphology, structure and history of the reef (Stoddart, 1978) - are all related more or less directly to sea-level. In particular, the large-scale location, morphology and structure of reefs are related to the underlying Pleistocene geology on which they grew as sea-level rose after the last glacial maximum; and on a smaller scale, other geomorphological features are dependant on the smaller sea-level changes in the late Holocene. A good understanding of sea-level in the last 20,000 years is thus important in understanding the GBR, and similarly, geomorphological observations from this sea-level-sensitive environment can be used to infer the sea-level history.

2.2 Methods

This section summarises some of the principal methods used to reconstruct the sea-level history of north Queensland. Not all these methods have been used in this study, but all are found in the large body of literature on the subject. All methods relate a geomorphic feature to some part of the tidal range, and thus all are susceptible to error due to possible change in the tidal range. It is assumed throughout this work that the tidal range has remained constant through time, and this is a reasonable assumption for small reef islands in the last 6 ka, which are surrounded by ocean and have not grown sufficiently to impede tidal water flow. This may not be the case for mainland coastal sites, where sediment deposition may have changed water depth enough to alter tidal range. A guide to tidal planes referred to in this chapter is shown in Figure 2.1.

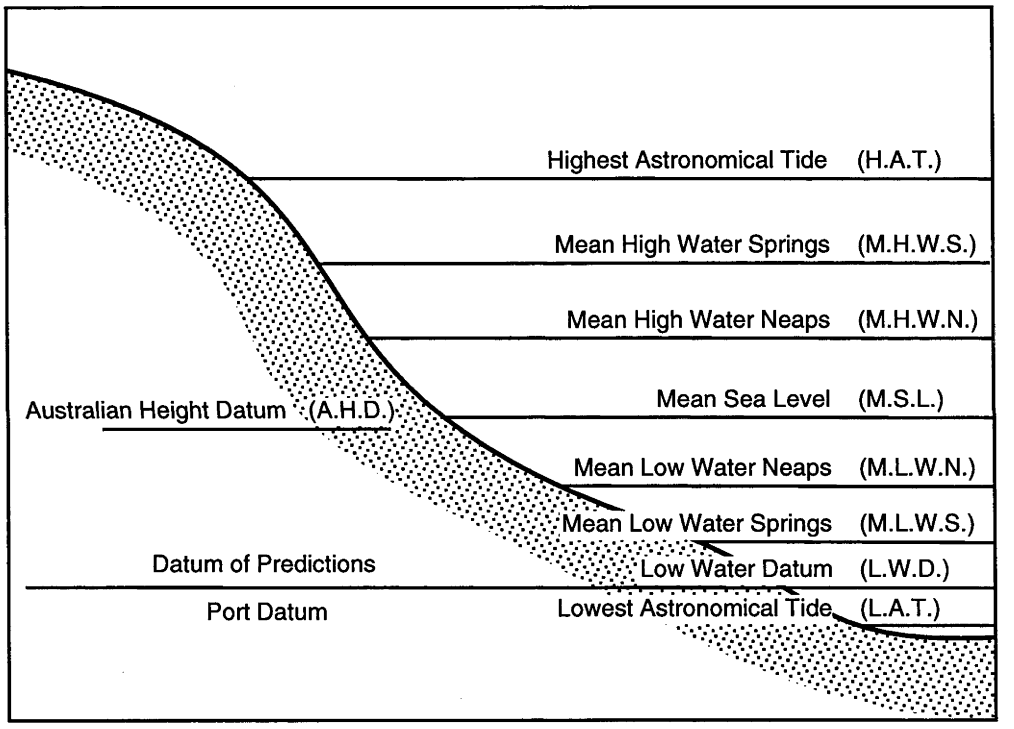

Figure 2.1 : A guide to tidal planes and their relationship to Australian Height Datum. (From 1992 Tidal Notes, Queensland Ministry of Transport).

2.2.1 Microatolls

Individual coral colonies with atoll-like form were described last century by Darwin and Dana, among others, but conflicting definitions were present until the Royal Society expedition to the GBR in 1973. Scoffin and Stoddart (1978) defined microatolls as those coral colonies with dead, flat tops and living perimeters which result from the restriction of upward growth by the air/water interface (Figure 2.2). They noted that in open water, the level of the upper surface of a microatoll corresponds to the level of mean low-water spring tides.

a)

b)

Figure 2.2 : a) Living, and b) fossil microatolls at Iris Point, Orpheus Island, on the Great Barrier Reef. Hammer is 32 cm long.

In addition, they described the various forms which can result from the complex histories possible during the lifetime of a coral colony. It must be remembered that the changes in "relative sea-level" that a coral experiences on a reef flat are not necessarily those experienced by the region as a whole. For instance, the formation of rubble ramparts can cause water to be moated on the reef flat at low tide, allowing microatolls to grow with an artificially high surface. Moat-forming ramparts may be created and destroyed during the lifetime of a single coral, producing complex forms on its surface (Scoffin and Stoddart, 1978). Some of these forms are illustrated in Figure 2.3. Since we are fairly sure that relative sea-level does not change this rapidly on a regional scale in tectonically stable areas, complex microatoll forms may be an indication of former moating, and these colonies should be used carefully to infer former sea-levels. In other circumstances, moats may last long enough to form microatolls which are indistinguishable from open-water examples, and these would provide incorrect estimates of sea-level change.

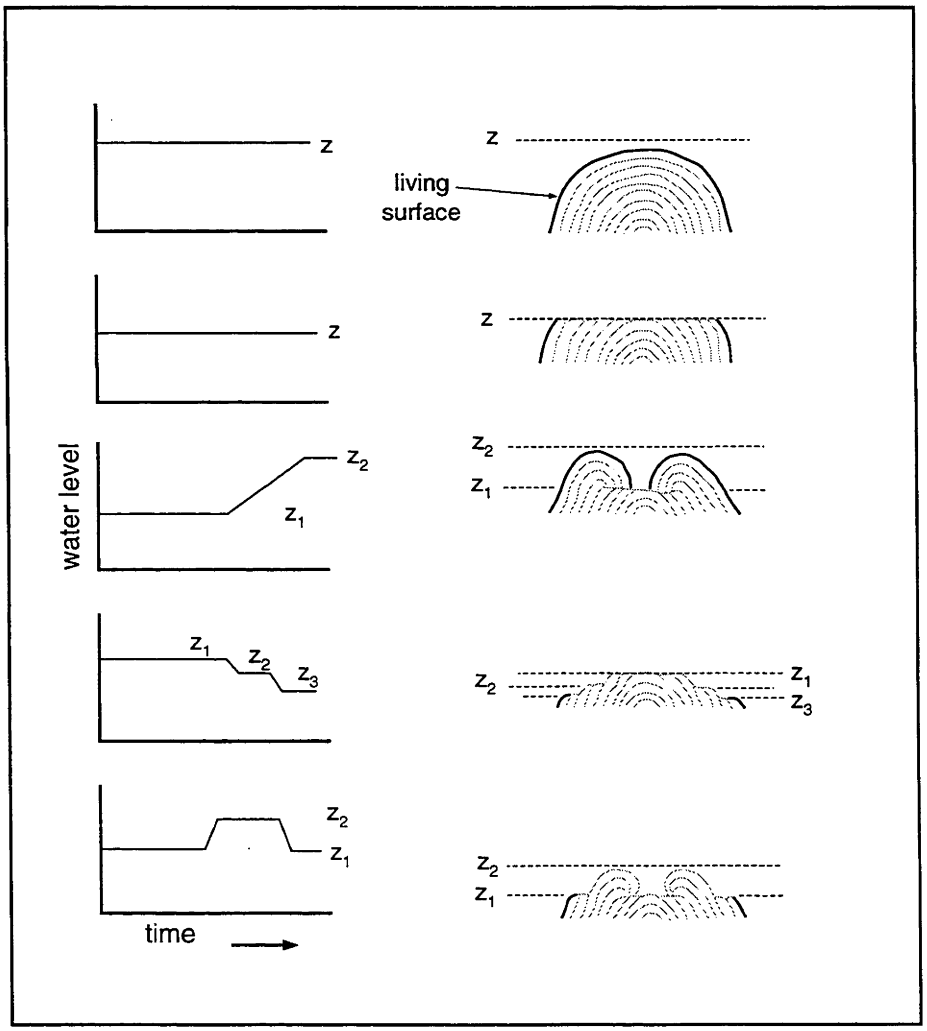

Figure 2.3 : The response of microatolls to different patterns of sea-level change. From Woodroffe and McLean (1990).

Moats may form on the reef flat when coral rubble accumulates there, thrown up from the front of the reef during storms. For this to occur, the reef flat must be relatively wide, and there must be a significant amount of coral growth nearby as source material for the rubble. These conditions were unlikely to be fulfilled when sea-level first reached its present level, as the reefs were mainly growing upwards, to keep up with the rapid sea-level rise. Microatolls of this age are therefore likely to be reliable sea-level indicators. After a few thousand years, however, the reef flat becomes sufficiently mature to accumulate rubble, as shown by the ages obtained from cemented rubble terraces on reef islands. Sea-level reached its present level around 6 ka, yet the terrace material dated by McLean and others (1978) formed predominantly between 4 ka and 2 ka. Microatolls of this age and younger are therefore more likely to have been moated when they occur on broad reef flats.

Because they form at sea-level, the sea-level record from fossil microatolls exposed on reef flats only covers the time since the mid Holocene, when sea-level has been relatively stable. Microatolls would be difficult to identify in drill core, and it would be impossible to determine whether moating had occurred on the reef flat when they formed, so the record is unlikely to extend further back than it does at present. In any case, the period of rapid sea-level rise may have prevented the formation of reef flats on which microatolls could have formed. The last time sea-level was stable was at the last glacial maximum, 18-20 ka, and preserved *in-situ* microatolls of this age would provide a precise estimate of sea-level at that time. Such samples are probably at depths of 120-130 m, and would almost certainly have to be collected using a submersible vehicle.

2.2.2 Reef core data

Bore holes drilled through reef flats can provide information about the nature of reef growth at that point. Unfortunately, the rate of upward reef growth is almost always lower than the rate of sea-level rise through most of the postglacial transgression, so the reef growth curve is not necessarily a sea-level curve (Hopley 1986b). No species on the GBR can be used as a "zone coral" such as *Acropora palmata* in the Caribbean, which now grows within a precise depth range on the reef crest (Lighty and others 1982). Nevertheless, knowing that coral growth is restricted to less than ~30 m water depth, with enough borehole data it is possible to construct an envelope of sea-level change (eg Grindrod and Rhodes, 1984). Problems associated with this type of record include uncertainty that any coral sample from a core is in growth position, and the difficulty of extracting a stratigraphically correct core when the reef flat is composed of large amounts of coral rubble.

If a core penetrates the entire Holocene reef, then the age of the basal *in situ* coral may indicate the time sea-level reached that elevation. Some delay may have occurred between inundation of the Pleistocene surface and colonisation by corals, due to water turbidity, but this delay is thought to be

small (Hopley 1986b). The advantage of this type of record, compared to the use of microatolls, is that it can be extended much further back in time. The depth to the Pleistocene surface ranges from sea-level in Torres Strait to in excess of 30 m in the central GBR (Hopley 1986b), so it is theoretically possible to obtain a sea-level record over this depth range.

2.2.3 Beachrock

The term "beachrock" has been used to describe a wide range of lithified materials in the littoral zone, but have been more rigidly defined as "beach sediments found within the intertidal zone, and cemented by calcium carbonate" (Hopley 1986a). If beachrock is to be used as a paleo-sea-level indicator, then we must know the elevation range in which it presently forms. A conservative estimate of sea-level change would then be the difference in elevation between the beachrock and the maximum elevation at which it presently forms. Hopley (1986a) supports the argument for the formation of aragonite cement by inorganic precipitation from sea-water, which suggests that the uppermost level of cementation would lie between mean high water spring tides and the highest astronomical tide. However, cementation above this level is also possible if the water table is temporarily raised by storm conditions, for example. Cementation can occur over periods of time ranging from months to decades (Hopley 1986a), so the range of possible formation elevations is large. McLean and others (1978) examined beachrock deposits throughout the northern GBR, and concluded that there was no positive evidence of sea-level change.

In addition to the uncertainty regarding the elevation at which it formed, the precise dating of beachrock is a difficult problem. If unrecrystallised fragments of the clast material can be obtained, then a maximum age for the deposit can be ascertained, although the time between growth of the clast and its incorporation into the beachrock may range from years to thousands of years (Hopley 1986a). If it can be isolated, the radiocarbon age of the cement may provide the age of cementation, although recrystallisation is possible and undetectable. Hopley (1971) reports that at Herald Island, near Townsville, a clast consisting of a shell of *Trochus* sp. gave an age of 4280±100 BP, while a whole-rock sample of fine-grained beachrock, containing up to 50% cement, was dated at only 3540±90 BP.

Despite the relatively large uncertainties in determining the age of a sample and its relationship to sea-level at that time, beachrock may prove to be a useful indicator of sea-level at the Last Glacial Maximum (LGM). Few samples from this time have been collected, and the uncertainty in LGM sea-level is greater than the uncertainty in the formation range of beachrock.

2.2.4 Chenier plains

The term "chenier" has been used to describe a wide variety of beach ridges on prograding coastlines. A precise definition is "a beach ridge, resting on silty or clayey deposits, which becomes isolated from the shore by a band of

tidal mudflats" (Otvos and Price 1979). This implies formation in an environment where mudflat progradation is interrupted by chenier formation. Cheniers are distinct from "true" beach ridges in that they are shallow-rooted and rest on mudflat deposits, while the latter are based on shoreface deposits and represent the top of a laterally extensive beach deposit. This difference makes cheniers much more useful for interpreting paleo-sea-levels, because the base of a chenier forms in the intertidal zone, while other beach ridge deposits may have no clearly defined base. The elevation of the crest of a chenier or beach ridge is less appropriate as an indicator of sea-level change, because it is initially controlled by the wave energy at the time of formation, which is unrelated to sea-level, and may be altered later by erosion.

Cheniers may form by a variety of processes, which involve interruption of the progradation of the mudflat (Augustinus 1989). The coarse sediment may develop by wave-winnowing and subsequent concentration in an offshore bar, or arrive by longshore transport of a shallow-based spit. Combinations of both usually occur (Augustinus 1989). After formation, the ridge may migrate landwards due to continuing or episodic reworking, until it is beyond the range of storm waves and spring tides. Continuing progradation of the mudflat seaward of the ridge may also halt its landward migration.

Chenier plains preserve a less reliable record of sea-level change than microatolls do, as they are formed within a wider sea-level range, and are affected by slow sediment compaction. Smart (1976) noted that some chenier ridges appear to have most of their volume above sea-level, while others have a considerable volume below it. This could be caused by variable compaction of the underlying sediment. Nevertheless, they are useful because they occur on the continental coast where the mid-Holocene highstand was the greatest, and where corals cannot grow because of the abundance of terrigenous sediment. Example of such sites are Karumba, in the southeast Gulf of Carpentaria (Rhodes 1980), and Princess Charlotte Bay, described by Chappell and Grindrod (1984).

2.2.5 Oyster shells

On rocky coasts in northern Queensland, oysters form distinctive cemented shell beds in the intertidal zone between mean sea-level (MSL) and mean high-water neaps (MHWN) (Endean and others 1956). In the conditions of falling sea-level that have occurred in the last few thousand years, oysters have been stranded above their growth range, and fossil shell beds may be found on rocks on sheltered parts of the coast. The actual growth range of modern oysters probably varies between areas experiencing different wave energies, but where both fossil and modern shells occur an estimate of former sea-level can be made by measuring the height difference between the fossil shells and the highest modern shells. Because the shells grow densely on top of each other, such deposits preserve well, and contain sufficient material for radiocarbon dating.

Estimating the former sea-level represented by an oyster shell deposit is subject to several errors. The nominal growth range of the oyster *Saccostrea* cited above represents a vertical range of 0.2 - 0.3 m above MSL in the GBR region (Queensland Ministry of Transport 1992). However, Beaman and others (1994) reported the upper limit of the modern oyster bed on Magnetic Island, near Townsville, to be 0.4 m above AHD (Australian Height Datum, which in the Townsville area is equivalent to MSL). Other measurements, presented later in this chapter, show the limit to be up to +0.8 m MSL on exposed rocks at West Cliff Island, which places it between the levels of MHWS and MHWN, although this measurement depends on the validity of correlating the tidal range from Flinders Island. Furthermore, on Lizard Island the upper limit of modern oyster growth was seen to range from +0.46 m MSL on exposed rocks to +0.53 m MSL at a sheltered site in the same bay. This suggests that fossil oyster beds, which are usually found in protected cracks and caves, grew above the range of contemporary oysters in exposed sites and would thus indicate a larger sea-level change than had in fact occurred. The uncertainty in estimated sea-level change using fossil oyster beds is thus around ±0.35 m, neglecting any uncertainty in surveying the level of the sample. This is considerably larger than the 0.14 m implied by Beaman and others (1994).

Problems may also be encountered in dating, as the finely-foliated nature of the shells means that clean surfaces rapidly absorb CO_2 containing modern carbon from the atmosphere during sample processing. This can be avoided either by preparing samples under a nitrogen atmosphere, or removing surface material with acid immediately before dating.

2.2.6 Other methods

Sea-floor sediment cores may provide useful evidence of sea-level during the period of postglacial sea-level rise. If the core penetrates paleosols which formed during the LGM, then the age of the overlying marine sediments provides the time of marine transgression (eg Smart 1977, in the Gulf of Carpentaria). On the GBR, it is more usual to penetrate an intertidal mangrove deposit associated with the transgression, which provides similar information. These have been widely used to infer sea-level change (eg Carter and others 1993, Larcombe and others 1995), and represent levels within a few metres of mean sea-level, although the possibility that they were reworked and deposited in deeper water must always be considered.

Shallow marine seismic surveys have also been used to infer the rate of sea-level change from the geometry of Holocene sediment packages on the continental shelf (eg Carter and others 1993). Constraints derived in this way may be ambiguous, since sediment deposition is influenced by several factors, of which sea-level is one. The distribution of submerged erosional shorelines and reef features, imaged using sidescan sonar, has also been used (Carter and Johnson 1986)

2.3 Previous work

This section reviews previous work on late Pleistocene and Holocene sea-level change in north Queensland. It is presented in three sections, each of which have a different significance for glacio-hydro-isostatic modelling. First, I review observations of sea-level at the last glacial maximum (LGM). The minimum sea-level at this time constrains the total volume of ice that must have existed on land. Second, the period of rapid sea-level rise until ~6 ka. Evidence of either steady or episodic sea-level rise during this period has direct implications for the nature of the disintegration of the large ice sheets, which is not well understood. Third, sea-level change in the mid-late Holocene. Precise sea-level observations are most abundant in this period, and the spatial and temporal variation supplies information on the rheology of the earth and recent eustatic sea-level change.

2.3.1 LGM sea-level

Glacio-hydro-isostatic modelling of sea-level change is hampered by the fact that the total amount of water taken from the oceans to form the ice sheets of the LGM is only approximately known. At present, different workers use values which are consistent with their own ice sheet reconstructions and sea-level observations, but too few observations are available from LGM times to constrain the total ice volume tightly. The model of Nakada and Lambeck (1988) contains a total ice volume of 129.3 m equivalent sea-level, while that of Peltier (1994) uses 105.2 m. It is important to establish the actual value, because the figure is not only used in global isostatic calculations, but also in comparisons of sea-level and isotope records (Chappell and Shackleton 1986, Shackleton 1987) on which many paleo-climate studies are based.

Sea-level at the LGM varies spatially, because of the effects of isostasy as well as local tectonism. This variation will be examined in Chapter 6. Here, we will review published observations of LGM sea-level from Queensland and northern Australia.

Veeh and Veevers (1970) dated a sample of beach rock from -150 m and a shallow water coral, *Galaxea clavus*, from a terrace at -175 m off One Tree Island in the Capricorn Group. Radiocarbon dates of 13 860 ± 220 and 13 600 ± 220 were obtained for the samples. A U-Th age of 17 000 ± 1000 was also obtained for the coral. As the coral can grow to at least 25 m depth and occasionally as deep as 75 m (Veeh and Veevers 1970), these samples could represent a lowstand of 150 m, with the coral growing 25 m below sea-level. Veeh and Veevers, however, consider it more likely that the coral grew in shallow water, and that sea-level stood near -175 m sometime between 13 600 and 17 000 years ago.

In the Timor Sea, van Andel and Veevers (1967) reported a change from lagoonal to marine sedimentation in a sediment core at 132 m water depth at the edge of the continental shelf, between 18 900 ± 1500 and 17 400 ± 1000

BP. Jongsma (1970) reported beachrock observed from a submarine in the Arafura Sea, and a sample dredged from about the same depth gave an age of 18 700 ± 350 BP.

Carter and Johnson (1986) used PDR (precision depth recorder) profiles to identify several bathymetric steps on the continental slope in the central GBR. A prominent terrace at -133 m has a sediment cover up to 10 m thick, which wedges out at a slightly eroded edge around -114 m. No dates are available for the sediment, and the LGM shoreline could be either the -114 m notch or the -133 m terrace. Carter and Johnson also consider the possibility that a higher terrace, at -103 m, could mark the LGM sea-level minimum.

2.3.2 The postglacial transgression

On a general scale, the rate at which the LGM ice sheets melted is known from oxygen isotope records and far field sea-level observations. The most rapid period of sea-level rise was between 14 ka and 8 ka, with an average rate of about 15 mm/yr. However, the question of whether sea-level rise was continuous or episodic remains.

Recent evidence from Greenland ice cores (Alley and others 1993, Dansgaard and others 1993, Taylor and others 1993) and North Atlantic sediment cores (Bond and others 1992, Lehman and Keigwin 1992) suggest that the last deglaciation involved sudden reorganisation of the global climate system. Collapse events in the Laurentide and Antarctic ice sheets are among the processes which are inferred to have occurred (Blanchon and Shaw 1995). These would cause episodic eustatic sea-level rise, the effects of which would vary spatially, due to isostatic effects. In the sea-level record from Barbados, Blanchon and Shaw (1995) propose three periods of "catastrophic sea-level rise" which they associate with ice sheet collapse events: two in the Laurentide and one in the Antarctic. In this section, I review the sea-level record for the same period of time in North Queensland. Comparison between the predicted and observed effects of episodic sea-level rise will be made in Chapter 6.

Maxwell (1968, p61) interpreted widespread bathymetric features of constant depth as former strandlines, and suggested a sequence of sea-level transgressions and stillstands which could have formed them. He proposed stillstands in the postglacial sea-level rise at 102 m, 88 m, 66 m and 29 m, followed by a fall to 59 m (depths rounded to the nearest metre). Further rise was punctuated by stillstands at 37 m and 18 m.

Carter and Johnson (1986) identified ten shorelines between 18 ka and the present from PDR profiles of the continental shelf in the central GBR, which are summarised in Table 2.1. An error of ±2 m was assigned to the depths of these shorelines, due to unknown tidal variations. Only the shorelines shallower than 25 m could be dated from radiocarbon ages of organic

material in the associated sediment bodies, and the remainder were assigned ages by comparison with the sea-level curve from New Zealand of Gibb (1985). Since sea-level varies spatially, the New Zealand record cannot be considered to be a eustatic curve, and dates obtained in this way are dubious unless corrected for glacio-hydro-isostatic effects. Where terrace-covering sediments can be dated, they provide a lower limit for sea-level at that time. Carter and Johnson (1986) interpreted the sequence as the result of a history of alternating stillstands and rapid sea-level rise. In a more localised study of Cleveland Bay, offshore from Townsville, Carter and others (1993) found evidence "consistent with pauses or slowdowns in the post-glacial sea-level rise" corresponding with shorelines S2 and S3, although the feature corresponding with S2 was found at -10 m.

Table 2.1: Depths and ages of drowned shorelines in the central GBR. From Carter and Johnson (1986).

shoreline	age (ka)	depth (m)
S8	18	114
S7	17	88
S6	15	75
S5	12	56
S4	11	45
S4a	10	39
S3	9.5	28
S3a	9	23
S2	7.5	9
S1	6.5	0

Of these shorelines, S7 and S3 correlate with Maxwell's observations, and S4a is within 2 m of another, which is the stated error for Carter and Johnson's depths. Also, the 103 m shoreline mentioned by Carter and Johnson (1986), but not included in their list of transgressive shorelines, matches closely with the 102 level of Maxwell (1968). Apart from these, the terrace levels do not correspond.

While these shorelines may have been formed during the post-glacial sea-level transgression, the conclusion that they represent stillstands is not necessarily warranted, because processes other than sea-level influence the distribution of coastal sediment. Lateral migration of sediment distribution channels, for example leaves a sediment record at any given point which could be interpreted as indicative of episodic sedimentation. One of the most powerful arguments in favour of stillstands is that the shorelines apparently persist laterally at roughly constant depth over wide areas, although this is not always the case and could also be explained by climate changes which affect the supply of sediment throughout the region.

Another form of evidence of sea-level change during the post-glacial transgression is the existence of submerged mangrove deposits, inferred to have formed in the intertidal zone, by analogy with modern mangrove

swamp environments. Salama (1990) recovered mangrove "peats" and unspecified shells from several sediment cores taken in Princess Charlotte Bay. Radiocarbon ages of these samples are summarised in Table 2.2 and Figure 2.4. Apart from two mangrove samples, the data form a reasonable trend for sea-level rise between -40 and -10 m. There is not sufficient sample resolution to determine whether the rise was continuous or episodic, but it is worth noting that the five peat samples between 23.3 m and 24.5 m form a plateau, in agreement with the 23 m shoreline (S3a) of Carter and Johnson (1986).

Table 2.2: Radiocarbon ages of samples from sediment cores in Princess Charlotte Bay, from Salama (1990). The marine reservoir correction applied to the dates from shells is -450±35 yr (Gillespie and Polach, 1979). The two samples older than 20 000 years are considered to be reworked, and are not included in Figure 2.4.

field code	S lat.	E long.	lab. number	depth below MSL (m)	conventional age (yr BP)	corrected age (yr BP)	sample
8/1/220	14.10	144.34	SAU 2373	33.9	31100 ± 800	30650 ± 800	shells
15/1/125	14.20	144.30	SAU 2374	22.7	29900 ± 600	29450 ± 601	shells
18/2/240	14.12	144.08	SAU 2375	31.6	9190 ± 140	8740 ± 144	shells
28/3/287	14.11	144.13	BETA 5814	36.8	8810 ± 100	8810 ± 100	peat
29/2/180	14.18	144.15	BETA 9283	23.9	8570 ± 140	8570 ± 140	peat
29/2/205	14.18	144.15	BETA 9284	24.2	8980 ± 200	8980 ± 200	peat
29/2/240	14.18	144.15	SAU 2375	24.5	8640 ± 120	8640 ± 120	peat
36/3/224	14.21	144.02	BETA 5814	16.7	8280 ± 70	8280 ± 70	peat
41/2/170	14.42	144.06	BETA 5816	10.1	7220 ± 120	7220 ± 120	peat
49/1/355	14.42	143.98	SAU 2377	9.0	6730 ± 180	6280 ± 183	crab
55/2/75	14.16	144.06	BETA 9285	24.1	8570 ± 140	8570 ± 140	peat
57/1/320	13.91	143.80	BETA 21804	23.3	8800 ± 90	8800 ± 90	peat
125/1/60	14.14	143.90	SAU 2378	18.4	8100 ± 140	8100 ± 140	peat
134/1/113	14.29	143.89	BETA 22248	12.8	8760 ± 140	8760 ± 140	peat
220/3/325	14.09	144.09	BETA 6648	27.8	9020 ± 90	9020 ± 90	peat
224/1/110A	14.07	144.18	SAU 2379	33.2	8920 ± 70	8470 ± 78	shells
224/1/110B	14.07	144.18	SAU 2380	33.2	9320 ± 120	9320 ± 120	peat
228/1/97	14.04	144.18	SAU 2381	42.0	9510 ± 120	9060 ± 125	shells
241/1/140	13.99	144.98	SAU 2382	31.0	9360 ± 150	8910 ± 154	shells

Similar submerged mangrove sediments from the GBR near Cooktown dated by Marshall (1995) (Table 2.3 and Figure 2.5) do not form a coherent indicator of sea-level change. In general, samples appear younger than the expected age for the depth in which they were collected, compared to the predicted relative sea-level curve of Nakada and Lambeck (1988), suggesting that sample contamination may have occurred.

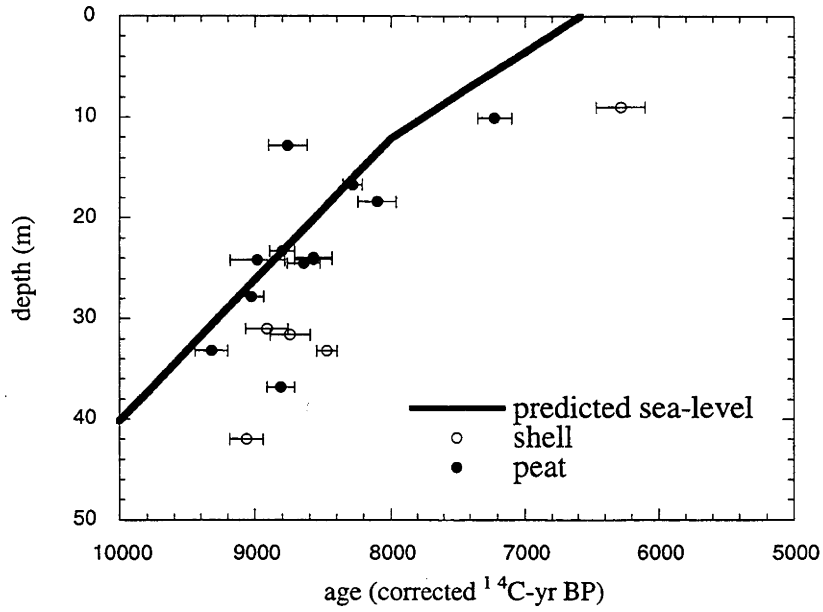

Figure 2.4 : Dated mangrove peat and shell material from sediment cores in Princess Charlotte Bay, from Salama (1990). The solid line is a sea-level prediction for a site in Princess Charlotte Bay using the ice models ARC3+ANT3 and a standard earth rheology. A marine reservoir correction of -450±35 yr has been applied to shell samples (Gillespie and Polach 1979).

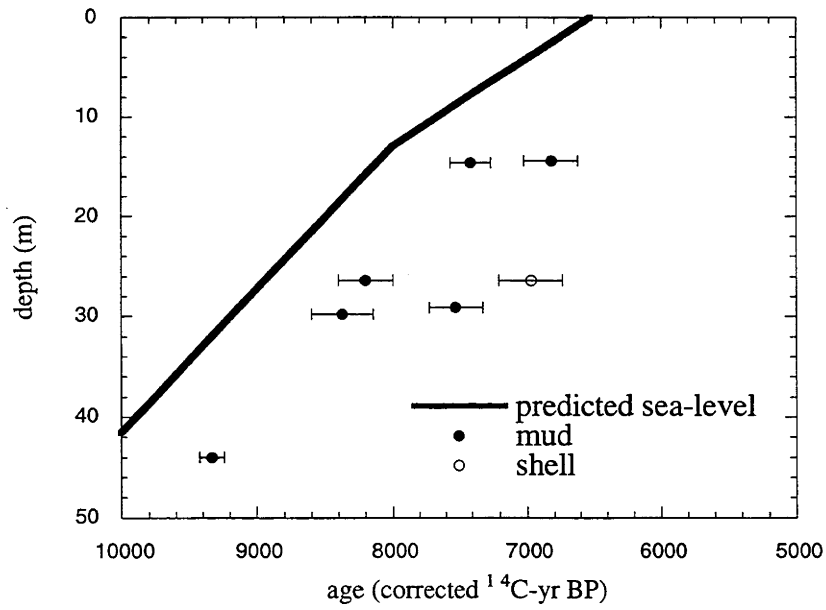

Figure 2.5: Dated mangrove and shell material from cores on the northern Great Barrier Reef near Cooktown, from Marshall (in prep). The solid line is a sea-level prediction for Boulder Reef using the ice models ARC3+ANT3 and a standard earth rheology. A marine reservoir correction of -450±35 yr has been applied to shell samples (Gillespie and Polach 1979).

Table 2.3: Radiocarbon ages of the organic fraction of mangrove muds from the transgressive unit, northern GBR, from Marshall (1995). The marine reservoir correction applied to the shell sample is -450±35 yr (Gillespie and Polach, 1979).

core	S lat.	E long.	lab. number	depth below MSL (m)	conventional age (yr BP)	corrected age (yr BP)	material
16	15.48	145.55	ANU-4586	36.9	6500 ± 450	6500 ± 450	mud
16	15.48	145.55	ANU-4587	43.1	7070 ± 320	7070 ± 320	mud
17	15.45	145.48	ANU-4588	37.0	5630 ± 300	5630 ± 300	mud
20	15.43	145.40	ANU-4589	26.4	8200 ± 200	8200 ± 200	mud
20	15.43	145.40	ANU-4590	26.4	7420 ± 230	6970 ± 232	shell
21	15.43	145.38	ANU-4591	29.1	7520 ± 200	7520 ± 200	mud
22	15.37	145.43	ANU-4593	29.8	8370 ± 230	8370 ± 230	mud
27	15.29	145.34	ANU-4594	14.4	6820 ± 200	6820 ± 200	mud
27	15.29	145.34	ANU-4595	14.6	7410 ± 150	7410 ± 150	mud
59	15.44	145.70	ANU-4596	44.0	9330 ± 90	9330 ± 90	mud

Larcombe and others (1995) compiled a large set of dates from mangrove sediments in cores from throughout the central GBR, and proposed the existence of five sea-level stillstands above -45 m, including the mid-Holocene maximum (Table 2.4). The three lowest stillstands are supported mainly by clusters of radiocarbon dates obtained from individual regions, which suggests that they may reflect local sedimentation patterns rather than regional sea-level. Core coverage is not uniform, however, and collection of further data may resolve this issue.

Table 2.4: Transgressive sea-level stillstands proposed by Larcombe and others (1995).

Depth (m)	Suggested ^{14}C age (kyr BP)
+1.7 ± 0.15	5.5 - 3.7
5 ± 2	7.8 - 6.8
17 ± 3	8.2
11 ± 2	8.5
45 ± ?	10.5

The most notable feature of this sea-level curve is the proposed 6 m regression between 8.5 and 8.2 ka, based on a simple interpretation of clusters of radiocarbon dates at these times. This proposed regression occurs in too short a time to be resolvable on other sea-level records, including the high-resolution record from Barbados (Fairbanks 1989, Blanchon and Shaw 1995). The regression of 6 m in 300 years requires an average sea-level fall of 20 mm/yr, while the fastest rate in the last glacial cycle is thought to be 15 mm/yr (Chappell 1994) and 5 mm/yr is more usual. If the regression was due to an increase in the volume of ice sheets on land, then the required accumulation in 300 years is approximately half the size of the Fennoscandian ice sheet at the LGM, yet no indication of an ice advance is seen in the moraine records of Europe or North America at this time.

Another stillstand in the post-glacial sea-level rise was suggested by Gagan and others (1994), on the basis of sediment distribution in two coastal embayments near Cairns in the central GBR. In that study, both a high-energy and a low-energy environment show interrupted sedimentation around 6.8 ka, when sea-level was 5 m lower than present.

An alternative to the hypothesis of episodic postglacial sea-level rise is that the observed terrace and shoreline features are developed on pre-existing surfaces which formed before the LGM. This is the opinion of Walbran (1994), who investigated the evolution of John Brewer Reef, in the central GBR near Townsville. On a set of seismic profiles crossing the reef, he identified a steep-sided platform forming a base for the Holocene reef. This platform is characterised by three terrace surfaces, at -20 m, -32 m and -40 m with respect to low water datum. This datum is about 1.7 m below mean sea-level at Townsville (Queensland Ministry of Transport 1992), so these depths correspond to about -22 m, -34 m and -42 m (rounded to the nearest metre) with respect to the same datum as was used by Carter and Johnson (1986).

Walbran (1994) considers the -22 m terrace to be either a reef flat which grew in the 50 ka interstadial period (Figure 2.6), or the erosional surface from that period of an earlier reef flat at a similar level. If the former explanation is correct, we would expect this surface to be higher than erosional shorelines of the same age, since the reef flat is approximately at the level of low tide, while erosional platforms form at the base of wave activity. This may in fact be the case, since the S3a shoreline of Carter and Johnson (1986) observed nearby at Townsville lies at -23 m, or lower if the thickness of Holocene sediment is taken into account (Carter and Johnson (1986) take the levels of their shorelines from the top of the Holocene sediment package). The -34 m terrace is smaller, and is thought to be a fringing reef which grew in a late-Pleistocene sea-level stillstand (Walbran 1994). It appears to have no analogue in the shoreline sequence of Carter and Johnson (1986). The -42 m surface appears to be erosional in origin (Walbran 1994). This level falls between shorelines S4 (-45 m) and S4a (-39 m) of Carter and Johnson (1986), but could correlate with either, depending on the thickness of Holocene sediment which overlies the erosional platform.

While these platforms on the antecedant surface to John Brewer Reef have been major sites of coral growth, they are not represented by terraces in the present reef morphology, which is consistent with continuous post-glacial sea-level rise (Walbran 1994).

A detailed survey of submerged reefs and terraces from throughout the central GBR (Harris and Davies 1989) revealed several depth ranges at which these features occur with greater frequency, and identified several components of a drowned barrier reef complex thought to have formed during the Pleistocene (Symonds and others 1983). Although there was some clustering, drowned features were found in almost every 2 m depth interval between 40 m and 170 m water depth, and many terrace features

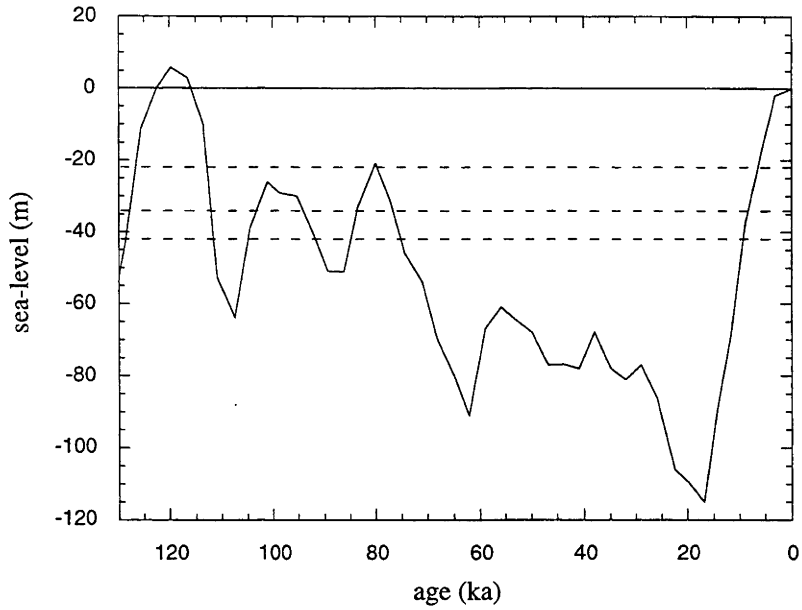

Figure 2.6 : Eustatic sea-level record for the last glacial cycle (Chappell 1994), indicating the depths of the terraces on the antecedant surface at John Brewer Reef.

could not be traced between adjacent transects, which were sometimes only 2 km apart (Harris and Davies 1989). Many submerged features thus appear to be of only local significance, and caution should be used when interpreting them in terms of sea-level change. Harris and Davies (1989) conclude that the observed features represent numerous Pleistocene sea-level oscillations, rather than a single episodic Holocene transgression.

In summary, a large number of submerged "terrace" or "shoreline" features have been identified on the GBR, but in no case has it been shown that these features represent pauses in the postglacial sea-level rise. The difficulty in correlating such features between sites where they are observed means that it is difficult to identify individual features which may show spatial variation in depth due to isostatic effects. In future, comparison of sea-level predictions with accurately located terrace observations may indicate whether they are postglacial features, or older.

2.3.1 Sea-level change since ~6 ka

Prior to the 1973 Royal Society expedition, evidence of former high sea-levels on the GBR had been noted, but almost no age control was available. Agassiz (1898) recorded a "coarse beach rock" elevated 2.4 m above high water on Three Isles, and the two distinct cemented platforms in the Turtle

and Howick Groups at around 1.5 m and 4.0 m had been noted by Steers (1929, 1937, 1938) and Spender (1930).

One of the aims of the 1973 Royal Society expedition was to determine which geomorphic features were useful for inferring former sea-levels. Many geomorphic features were investigated and dated, including cemented coral rubble terraces, beach rock (carbonate-cemented beach sand and shells), mangrove deposits, and microatolls (McLean and others 1978). Microatolls (described in section 2.3) proved to be the least ambiguous sea-level indicator, and these indicated that sea-level reached its present level around 6 ka, and was higher than present shortly afterwards. Because of the wide range of investigations, insufficient fossil microatolls were dated to obtain a coherent sea-level curve. The elevations of other geomorphic features of reef islands were found to be more dependant on the degree of reef flat development than on sea-level. While reef development and sea-level change are intimately linked, the relationship varies from reef to reef, so reef development is not an accurate indicator of sea-level change.

Hopley (1978) presented a compilation of radiometrically dated coastal features from eastern Queensland, which show apparently higher mid-Holocene sea-levels in the central GBR offshore from Townsville and Bowen than to the north and south. In this region, mid-Holocene sea-levels of up to 5 m above present had been interpreted, while 1 m is a more common value throughout the GBR, and no highstand was observed in the far north (Raine Island) or south (Coolum). Hopley (1978) noted a correlation between the maximum Holocene sea-level and the basement geological structure, but rejected the suggestion that broad tectonic warping might account for the spatial variation in sea-level change, as the rates of movement required seemed excessive for tectonism in a mid-plate setting. He suggested that hydro-isostasy was the major influence, and noted several trends which supported this, but could not confirm this as adequate modelling of glacio-hydro-isostatic processes was not available at the time. Examination of the data on which the observation of differential uplift were based, however, reveal that almost all the high elevation samples are of beach rock, which has since been discarded as an accurate sea-level indicator. Dated coral samples in the same data set show no trend of higher sea-levels in the central GBR region.

Microatolls

Chappell and others (1983) collected a reliable set of dated and levelled microatolls from sites throughout the GBR , shown in Table 2.5 and Figure 2.7. Although glacio-hydro-isostatic models available at that time (Chappell and others 1982) predicted sea-level variation between sites near the coast and sites further offshore, this data set did not have sufficient resolution to test this, and this work concluded a highstand of one metre, 6000 years ago, with sea-level falling uniformly to the present throughout the region (Figure 2.8).

Table 2.5: Radiocarbon ages of raised *Porites* microatolls from several locations in the central and northern GBR, from Chappell and others (1983). The reservoir-corrected age is obtained by subtracting 450 ± 35 yr from the conventional age (Gillespie and Polach, 1979).
† ANU numbers were not published for some samples.

field code	ANU number†	corrected age (BP)	height above MLWS (m)
KING ISLAND, 14° 06' S 144° 20' E			
KI/8	2324	5050 ± 135	0.75 ± 0.25
KI/7	2323	5110 ± 105	0.75 ± 0.25
KI/6	2322	3950 ± 100	0.55 ± 0.25
KI/5	2321	3960 ± 100	0.45 ± 0.25
FLINDERS ISLAND, 14° 10' S 144° 15' E			
FI/1	2319	5660 ± 205	0.95 ± 0.25
FI/2	2320	5600 ± 105	0.65 ± 0.25
YULE POINT, 16° 35' S 145° 30' E			
EWY-1		4420 ± 105	1.20 ± 0.20
EWY-2		3605 ± 100	1.05 ± 0.20
EWY-3		4475 ± 125	0.70 ± 0.20
EWY-6		1305 ± 70	0.55 ± 0.20
EWY-4		1150 ± 65	0.35 ± 0.20
DUNK ISLAND, 17° 58' S 146° 10' E			
EWD-1		5725 ± 105	0.85 ± 0.25
EWD-3		5295 ± 100	0.70 ± 0.25
EWD-5		5355 ± 80	0.35 ± 0.25
EWD-4		4645 ± 105	0.45 ± 0.25
GOOLD ISLAND, 18° 11' S 146° 10' E			
EWG-1		5855 ± 145	1.25 ± 0.25
EWG-2		5215 ± 115	0.95 ± 0.25
EWG-3		3050 ± 80	0.55 ± 0.25
ORPHEUS ISLAND, 18° 36' S 146° 30' E			
EWO/4	2471	4860 ± 90	0.95 ± 0.20
EWO/3	2476	4300 ± 80	0.65 ± 0.20
EWO/2	2473	3020 ± 80	0.40 ± 0.20
EWO/1	2470	2460 ± 80	0.20 ± 0.15
FANTOME ISLAND, 18° 40' S 146° 31' E			
FA/5	2477	5340 ± 80	1.00 ± 0.20
FA/4	2464	5520 ± 100	0.90 ± 0.20
FA/3	2478	4320 ± 90	0.65 ± 0.20
FA/1	2463	2550 ± 90	0.45 ± 0.20
FA/2	2469	2540 ± 90	0.35 ± 0.20
GREAT PALM ISLAND, 18° 42' S 146° 36' E			
GP/5	2466	4990 ± 115	0.85 ± 0.20
GP/4	2474	4390 ± 90	0.85 ± 0.20
GP/3	2465	5490 ± 100	0.80 ± 0.20
MAGNETIC ISLAND, 19° 09' S 146° 52' E			
EWM/4		5325 ± 80	1.20 ± 0.20
EWM/5		4770 ± 80	1.00 ± 0.20
EWM/6		4530 ± 105	0.50 ± 0.20
EWM/7		4765 ± 115	0.70 ± 0.20
EWM/8		360 ± 70	0.15 ± 0.05

Table 2.5 (continued)

field code	ANU number†	corrected age (BP)	height above MLWS (m)
CAMP ISLAND, 19° 52' S 147° 53' E			
EWC/1		5820 ± 115	0.90 ± 0.20
EWC/2		5020 ± 105	0.70 ± 0.20
EWC/3		1280 ± 105	0.50 ± 0.20
STONE ISLAND, 20° 02' S 148° 16' E			
EWS/1		5925 ± 115	1.08 ± 0.18
EWS/2		5285 ± 135	1.08 ± 0.18
EWS/3		5755 ± 105	0.98 ± 0.17
EWS/4		5250 ± 100	0.62 ± 0.18

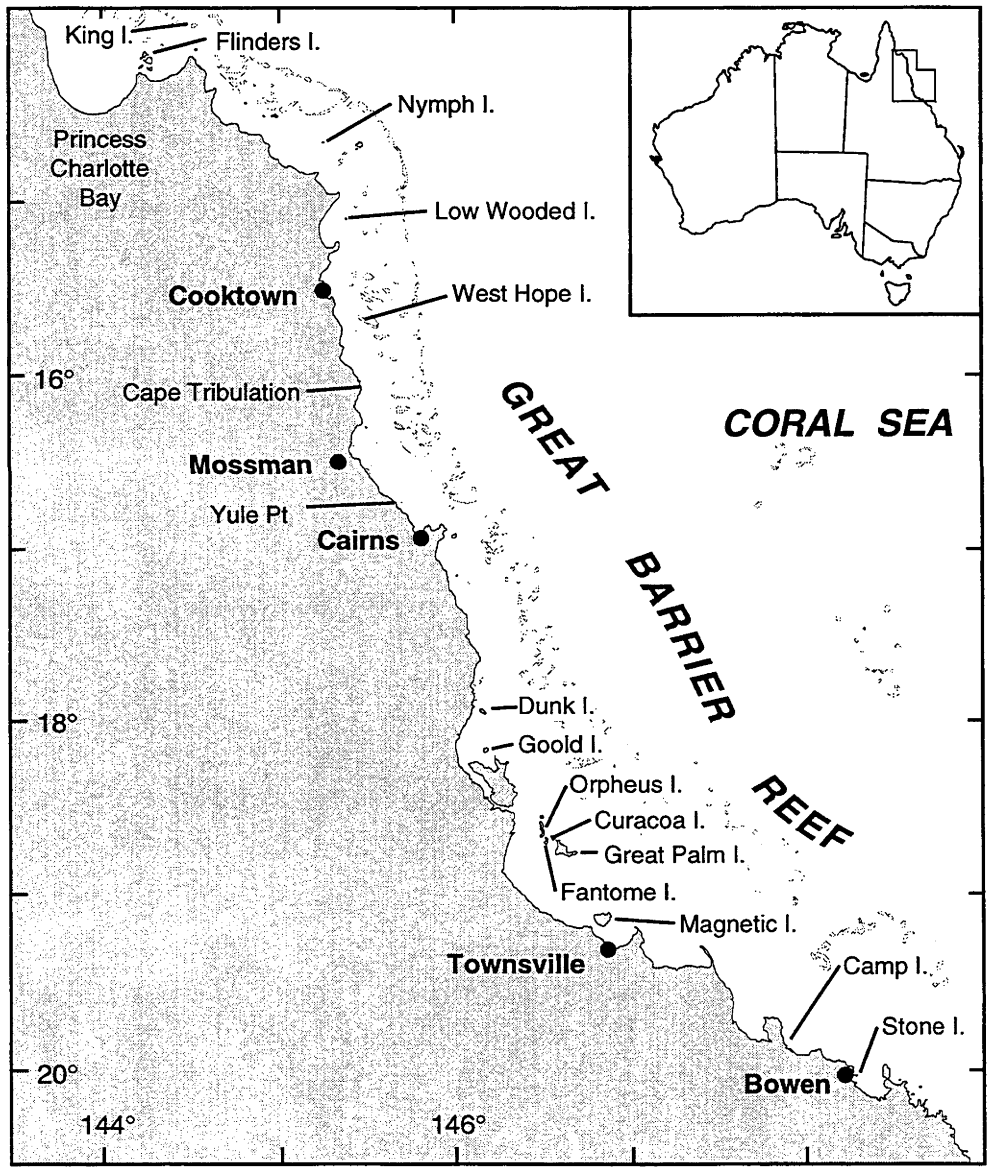

Figure 2.7 : Location map of the central to north Great Barrier Reef, showing the sites at which microatolls were studied by Chappell and others (1983).

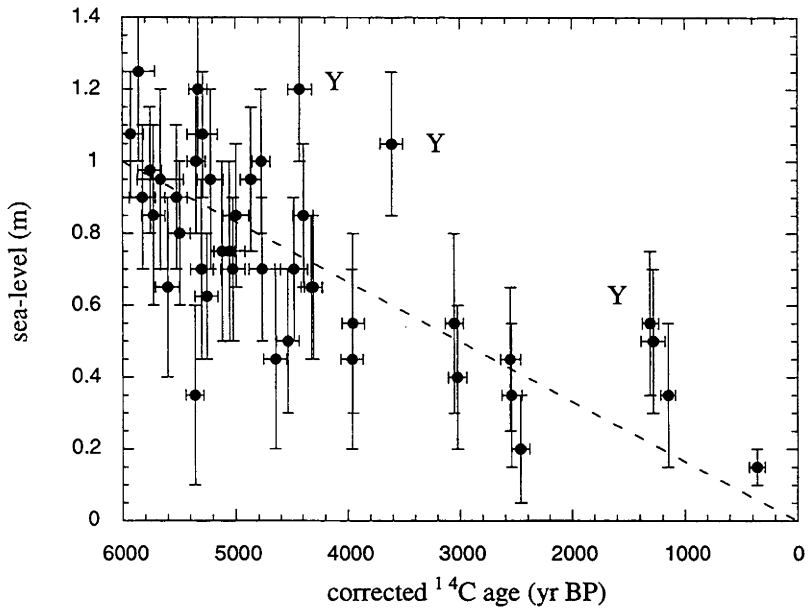

Figure 2.8 : Height-age relationship for dated microatolls from the central to north Great Barrier Reef, from Chappell and others (1983). A linear sea-level fall from 1.0 m 6000 years ago is indicated. Points marked 'Y' are from Yule Point, and consistently lie above the rest of the data.

Oyster shell deposits

On Magnetic Island, offshore from Townsville in the central GBR, Beaman and others (1994) dated fossil oyster beds of intertidal origin, which indicated that the Holocene sea-level highstand was attained there before 5660 ± 50 yr BP (conventional uncorrected radiocarbon age), and remained at 1.6-1.7 m above the present level until 4040 ± 50 yr BP. This estimate of sea-level change is well constrained by comparison with modern oyster beds in the same location. However, as discussed in Section 2.2 above, the sea-level change proposed may be too large, due to an unrealistic estimate of the growth range of oysters. This possibility is supported by the observation that the oyster deposits indicate a sea-level maximum which is 0.6 - 0.7 m higher than that indicated by microatolls (Chappell and others 1983). Beaman and others (1994) contend that the oysters indicate the correct value, but while it is possible for the oysters to indicate a sea-level change which is too large, as discussed in Section 2.2, it is impossible for microatolls to produce an underestimate, since they cannot form below the level of MLWS.

The only explanation which can accommodate both data sets is that tidal range has decreased by 0.6 - 0.7 m since the sea-level highstand (Figure 2.9). Whether this has occurred or not is unknown, although a paleo-tidal reconstruction of Cook and Mayo (1977) in Broad Sound (Southern GBR) suggests that tidal range may have increased by 1 m in the last 6 ka as the

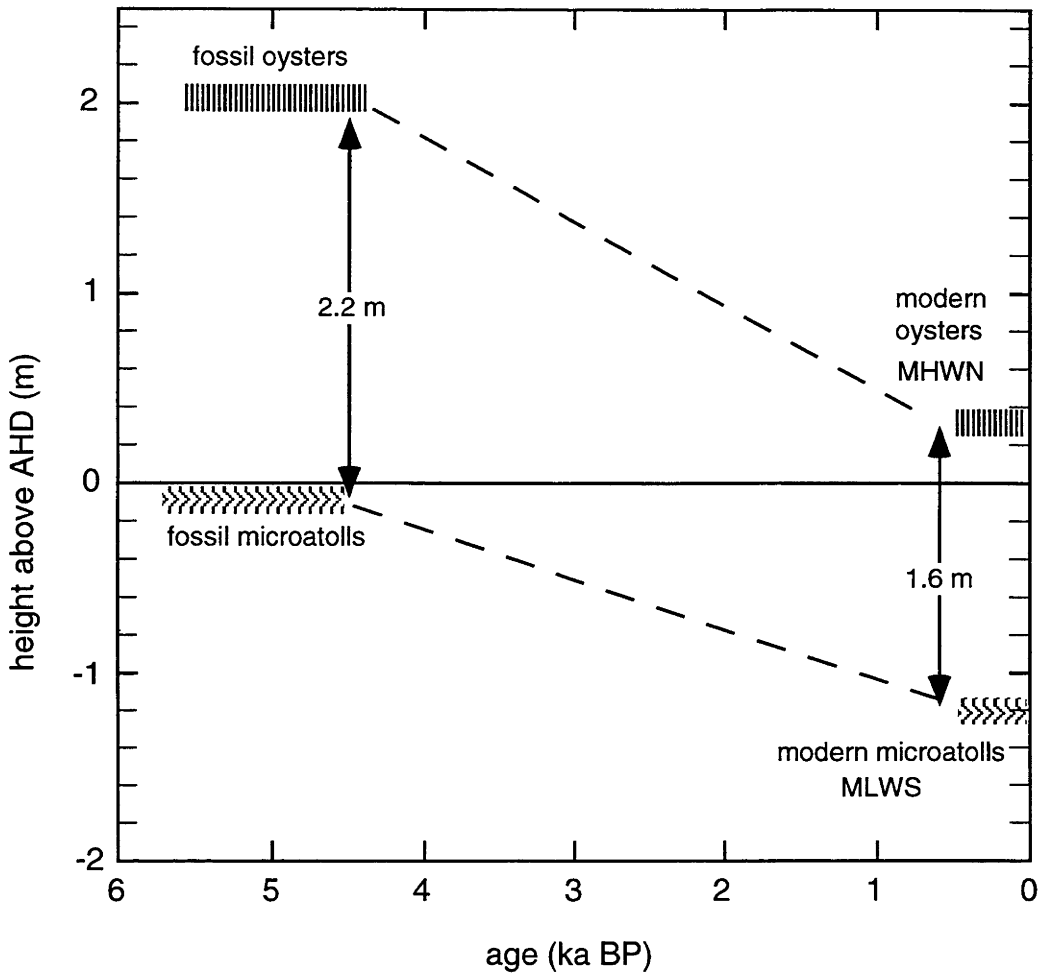

Figure 2.9 : Relationship between microatolls and oyster shell beds at Magnetic Island. If the environmental conditions which control the growth elevations of these features have not changed then a decrease in tidal range of ~0.6 m is indicated since mid-Holocene time.

coastline became more funnel-shaped. No mechanism for a decrease in tidal range has been proposed, and it is not considered likely.

Beaman and others (1994) obtained four radiocarbon ages from oyster shells at the same elevation ranging from 5660 ± 50 yr BP (WK-2919, conventional uncorrected radiocarbon age) to 4040 ± 50 yr BP (WK-2917). They interpret this as evidence of a sea-level stillstand which again is at odds with the microatoll data from the same region (Chappell and others 1983, and this work, Section 2.4), which indicate falling sea-level over this time. Using the same arguments as above, it is seen that it is possible to reconcile these data is either by an increase in the tidal range over this period or by noting that the oysters could have grown progressively closer to the top of their range. An increase in the tidal range over the period 5.5 - 4 ka, followed by a larger decrease until the present is an implausible scenario, and it is far more likely that the oyster-derived data are in error, or should at least be assigned much larger uncertainties.

Drill core data

Hopley (1983) presented a contour map of the 5000 yr BP sea-level surface for the central GBR (Figure 2.10). This map was based on a large number of corals dated from drill cores and the surface of reef flats, assuming that the corals grew close to MLWS. Seaward tilting of the continental shelf is apparent, with sea-level fall since 5000 yr BP only in a narrow band close to the coast. Elsewhere, sea-level has risen, with the amount of rise increasing offshore to a maximum of about 6 m at the shelf edge.

Beach ridges

In the eastern Gulf of Carpentaria, chenier plains have been studied at three locations as an indicator of former sea-levels. At Cape Keerweer, Smart (1976, 1977) concluded that the sea reached its present level 6500 - 7000 yr BP and has remained within 1 m of its present level since then. At Edward River, sea-level 5500 yr BP was 0.2 - 1.4 m above present, and further to the south at Karumba, sea-level at the same time was 1.7 - 3.1 m above present (Rhodes 1980, Chappell and others 1982).

Gagan and others (1994) found tentative support for a mid-Holocene highstand of ~1 m at Wyvuri Embayment, near Cairns. Here, the elevation of the base of the highest Holocene beach barrier is about 0.9 m above its modern equivalent.

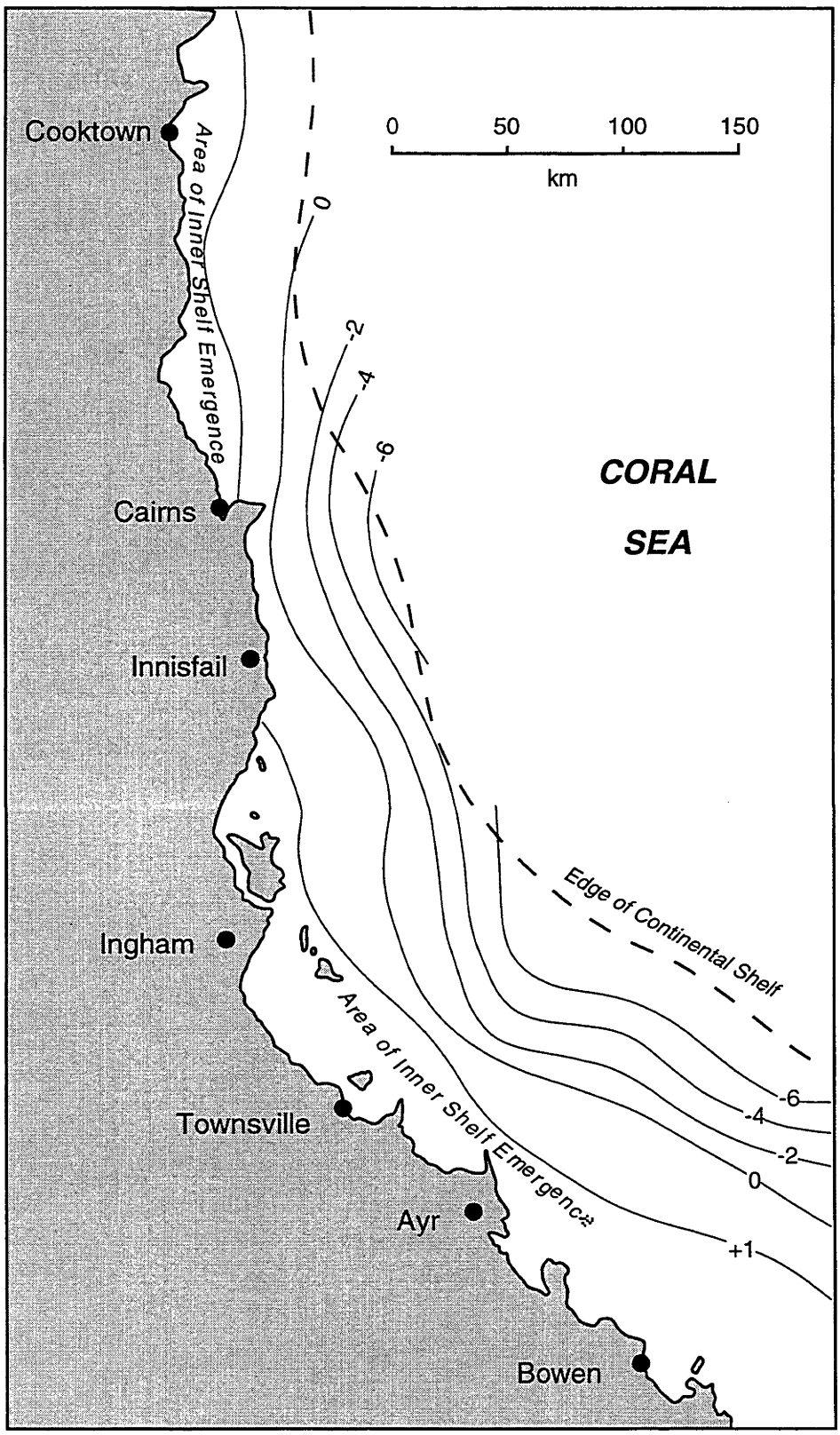

Figure 2.10 : The 5000 yr sea-level isobase proposed by Hopley (1982) on the basis of dated reef flat corals.

2.4 Sea-level change at Orpheus Island

2.4.1 Introduction

Orpheus Island (18.36 S, 146.30 E) is located in the Palm Group, on the North end of Halifax Bay near Townsville, Queensland (Figures 2.7 and 2.11). The island is about 10 km long and 1-2 km wide, and lies about 20 km offshore from Ingham, where the edge of the GBR (and most of the reefs) is about 100 km offshore. This location, about 80 km inland of the shoreline during the last glacial maximum, would be expected to show a mid-Holocene sea-level highstand, due to the isostatic response to sea-level rise when the late-Pleistocene ice sheets melted (see Chapter 6). Although Orpheus Island lies within the GBR, it is not a reef island, but consists of an igneous basement surrounded by fringing reefs. These fringing reefs provide an excellent opportunity to find the Holocene sea-level highstand preserved - unlike reef islands, which must build their own substrate to near sea-level before microatolls may form, the bedrock island always provides a substrate for microatolls to grow on, regardless of how fast sea-level may be rising.

The sea-level record on Orpheus Island has already been studied by Chappell and others (1983) as part of an extensive study of microatolls in the central GBR. This work, including sites on Curacoa, Fantome and Great Palm Islands, in the Palm Group, concluded that sea-level reached a highstand of 1 metre above the present level 6,000 years ago, and has fallen linearly since then. The growth and development of the fringing reefs has also been studied (Barnes 1984, Slocombe 1981).

2.4.2 Study sites

Five sites on Orpheus Island were studied (Figure 2.11): two in Pioneer Bay, on the west side of the island, where James Cook University has a Research Station; one in Little Pioneer Bay, to the north; in Hazard Bay, to the south; and at Iris Point, on the northern end of the island.

Pioneer Bay

The first Pioneer Bay site is on the reef flat directly in front of the research station, close to the transect studied by Chappell and others (1983). The landward side of the reef flat here ends at a beach, at the level of high tide. The inter-tidal region consists of dead coral colonies, surrounded and covered by mud and sand. Small *Tridacna* clams live on this part of the reef flat. At the seaward end, there are live corals and microatolls at the edge of the fringing reef. Thirteen microatoll samples have been dated from this site.

Pioneer Bay South

At the southern end of Pioneer Bay, the upper part of the reef flat is covered by boulders. At the site studied the boulders have been moved aside to form

a boat ramp for the research station. The corals beneath the boulders form a seaward-sloping surface, unlike the microatolls at other sites, which have level upper surfaces. The sloping coral surface has *Tridacna* clam shells embedded in it. Seven coral and four clam samples have been dated from here.

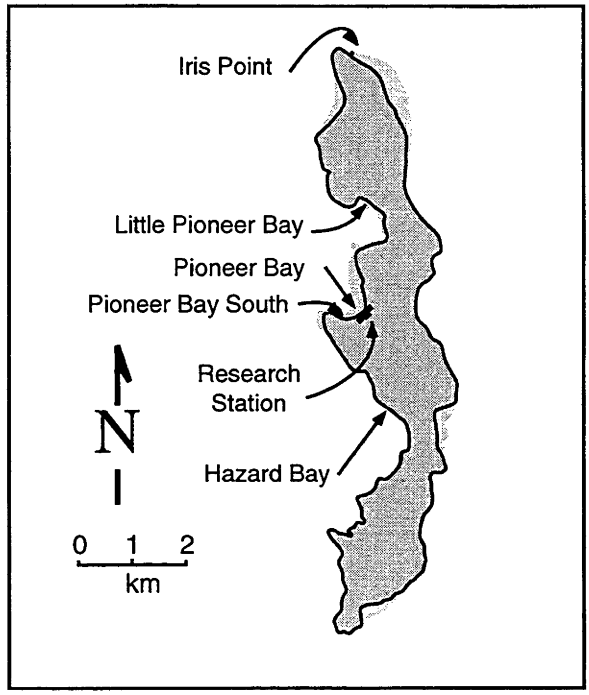

Figure 2.11 : Location map of Orpheus Island, showing sample sites.

Little Pioneer Bay

Little Pioneer Bay has a wide fringing reef similar to that in Pioneer Bay. Four microatoll samples collected by K. and A. Lambeck and one clam shell from here have been dated.

Iris Point

The fringing reef at Iris Point has a boulder beach on the landward side, a wide area of reef flat which is moated at low tide by a series of low algal and coral rubble terraces. Live coral colonies are present at the edge of the reef and microatolls are forming in the moated pools. Two samples were collected here by K. Lambeck and D. Hopley from between the boulders of the boulder beach, well above the limit of present moating, and also two from large (>2 m diameter) dead microatolls at the west end of the fringing reef, which earlier studies (Barnes, 1984) indicate is the youngest part of the reef, so is unlikely to have been moated, as moating requires the existence of a reef flat and enough coral rubble to form ramparts.

Hazard Bay

Three coral samples were collected from the reef flat at Hazard Bay by K. Lambeck.

2.4.3 Sampling procedure

Microatolls

The ideal sample for measuring sea-level change at these sites is a coral microatoll of the genus *Porites*. These have a level surface which may be levelled easily, and which is known to correspond to the level of Mean Low Water Springs when they were alive (provided they were not moated), and have a dense coral structure, more resistant to erosion, burrowing and contamination than other types of coral.

When ideal samples are not available, other types of coral can be used, especially Faviids, which are fairly common and also form microatoll structures.

Clam shells

Where clam shells are found embedded in the surface of a coral colony, in growth position, they must obviously be younger than the coral itself. Thus they provide a possible test of the origin of the surface: if the shells and coral have very similar ages, then the surface must be uneroded, and could relate to sea-level change; if the clams are much younger than the coral, it is possible that the surface at this site was formed after the death of the corals, by wave erosion, or movement of the boulders in a boulder beach. The only thing that this test can potentially provide conclusive evidence of is that the surface is original - a young clam shell in the surface of an old coral proves nothing about the age of the surface.

Levelling

Heights of samples were levelled using a staff and a 'dumpy' level mounted on a tripod. On microatolls, the level was taken from the highest part of the level upper surface, to minimise the effect of erosion. Samples were levelled to a local datum, usually the height of the dumpy level itself, or to a relocatable benchmark, if the tripod had to be moved. To convert the local datum at each site to tidal datum, the tide level was also recorded several times at each site. Whenever possible, these measurements were taken around the turn of the tide, to allow the easiest correlation with the tide tables.

Reduction of levelling data

To correlate the tide measurements made at each site with local tidal datum, tide records were obtained from the National Tidal Facility at Flinders

University in South Australia. For the sites on Orpheus Island, the tide record used was from Lucinda Jetty, about 20 km away, on the mainland. The observations were used, rather than the predictions (which are more widely available) to remove possible error due to regional air pressure and wind forcing on the day of observation. Normal weather patterns involve atmospheric pressure fluctuations of around 10 hPa, which causes a sea-level change of 10 cm. The lowest pressures which occur in this region are associated with tropical cyclones, which may cause a sea-level rise of over 1 m at their centre. The difference between the tidal predictions and observations over the period of this study was up to 10 cm, and removing it significantly reduced the scatter of the data. The resulting precision of the measurements is estimated to be about 10 cm.

The elevations of the samples are expressed relative to the height of mean low water spring tide (MLWS), which is the elevation at which modern microatolls grow (Scoffin and Stoddart 1978). The elevation of a fossil microatoll with respect to this level thus represents the sea-level change since that coral was alive.

2.4.4 Radiocarbon dates

Preparation of samples

Coral and clam shell samples were prepared for radiocarbon dating by cutting into chips, and removing all obvious recrystallised parts, burrows, and badly stained material. The remaining material was then rinsed in demineralised water and washed in an ultrasonic bath to flush out any carbonate sand. The samples were then dried, and the cleanest 50 - 60 grams submitted for dating. A small sample of each coral was also powdered for X-ray diffraction analysis. This would reveal if recrystallisation had taken place, as coral polyps precipitate their skeleton as aragonite, which is metastable at standard temperature and pressure. Recrystallisation of the coral under these conditions would convert the aragonite to calcite. XRD showed that the amount of calcite in the samples submitted for dating was undetectable or negligible (less than 1%).

Results

The conventional radiocarbon ages and levels of samples from Orpheus Island are summarised in Tables 2.6 and 2.7, separated according to sample type:

Table 2.6 : Radiocarbon ages of coral samples from Orpheus Island. All dates were determined by the Quaternary Dating Research Centre, ANU. Samples with the field code EWO are from Chappell and others (1983). The reservoir-corrected age is obtained by subtracting 450 ± 35 yr from the conventional age (Gillespie and Polach 1979).

field code	ANU number	conventional age (BP)	corrected age (BP)	height above MLWS (m)
PIONEER BAY				
PB 1	7903	210 ± 70	-240 ± 78	0.09 ± 0.1
PB 2	7994	2980 ± 70	2530 ± 78	0.26 ± 0.1
PB 3	7902	3480 ± 70	3030 ± 78	0.34 ± 0.1
PB 4	7995	5190 ± 70	4740 ± 78	0.54 ± 0.1
PB 5	7901	6280 ± 80	5830 ± 87	0.59 ± 0.1
PB 6	7996	5870 ± 70	5420 ± 78	0.67 ± 0.1
PB 7	7900	5930 ± 80	5480 ± 87	0.80 ± 0.1
PB 7a	7997	7040 ± 190	6590 ± 193	0.86 ± 0.1
PB 7b	8048	6130 ± 60	5680 ± 69	0.86 ± 0.1
PB 8	8049	6080 ± 60	5630 ± 69	0.86 ± 0.1
PBB 1	8810	6170 ± 70	5720 ± 78	0.80 ± 0.1
PBB 3	8811	6140 ± 70	5690 ± 78	0.77 ± 0.1
PBB 4	8812	6230 ± 70	5780 ± 78	0.77 ± 0.1
EWO/4	2471	5310 ± 90	4860 ± 96	0.95 ± 0.1
EWO/3	2476	4750 ± 80	4300 ± 87	0.60 ± 0.1
EWO/2	2473	3470 ± 80	3020 ± 87	0.40 ± 0.1
EWO/1	2470	2910 ± 80	2460 ± 87	0.20 ± 0.1
LITTLE PIONEER BAY				
LPB 1	8002	5780 ± 70	5330 ± 78	1.03 ± 0.1
LPB 2	8003	5790 ± 70	5340 ± 78	0.89 ± 0.1
LPB 3	8004	5710 ± 70	5260 ± 78	1.09 ± 0.1
LPB 4	8005	3980 ± 70	3530 ± 78	0.49 ± 0.1
IRIS POINT				
IP 1	6953	5840 ± 70	5390 ± 78	0.96 ± 0.1
IP 2	6952	5740 ± 70	5290 ± 78	1.01 ± 0.1
IPB 1	8467	5580 ± 80	5130 ± 87	0.55 ± 0.1
IPB 2	8468	5790 ± 80	5340 ± 87	0.58 ± 0.1
PIONEER BAY SOUTH				
PBS 1	8041	5910 ± 60	5460 ± 69	1.31 ± 0.1
PBS 2	8042	5850 ± 60	5400 ± 69	1.05 ± 0.1
PBS 3	8043	6040 ± 60	5590 ± 69	0.74 ± 0.1
PBS 4	8044	5890 ± 60	5440 ± 69	0.65 ± 0.1
PBS 5	8045	5870 ± 60	5420 ± 69	0.57 ± 0.1
PBS 6	8046	5800 ± 60	5350 ± 69	0.43 ± 0.1
PBS 7	8047	5970 ± 60	5520 ± 69	0.16 ± 0.1
HAZARD BAY				
HB 1	8298	5620 ± 60	5170 ± 69	0.73 ± 0.1
HB 2	8299	5600 ± 70	5150 ± 78	0.76 ± 0.1
HB 4	8300	4070 ± 60	3620 ± 69	0.46 ± 0.1

Table 2.7 : Radiocarbon ages of *Tridacna* clam shell samples from Orpheus Island.

field code	ANU number	conventional age (BP)	corrected age (BP)	height above MLWS (m)
LITTLE PIONEER BAY				
LPBB 1	9219	5760 ± 90	5310 ± 96	1.00 ± 0.2
PIONEER BAY SOUTH				
PBSB 1	9216	5820 ± 90	5370 ± 96	0.74 ± 0.2
PBSB 2	9215	5850 ± 80	5400 ± 87	0.70 ± 0.2
PBSB 3	9218	5940 ± 90	5490 ± 96	0.90 ± 0.2
PBSB 4	9217	5560 ± 80	5110 ± 87	1.18 ± 0.2

2.4.5 Interpretation

The plot of all age/height data from Orpheus Island (Figure 2.12) shows sea-level falling from a highstand of about 1 metre 6,000 years ago. This observation is in agreement with that of Chappell and others (1983) who used microatoll heights and ages from throughout the central GBR to conclude that the sea-level change could be described by a linear fall from 1 metre 6,000 years ago (Figure 2.6). The new data show less scatter than that of Chappell and others, which may be attributable to regional variation in the relative sea-level history, since the latter data were obtained from several sites. However, there is a lack of data after 3 ka, and a large scatter in the data points around 6 ka. This is discussed below.

Pioneer Bay South

The corals sampled from Pioneer Bay South (Figure 2.13) fall within a narrow age range, but have a large range of heights. Thus, these corals are not interpreted as microatolls, but as large coral heads eroded to form a flat sloping surface by the action of the boulder beach which over-ran them. Since the corals must have grown sub-tidally, they thus indicate that sea-level was at or above 1.3 m at 5500 BP.

The clam shells from this surface show radiocarbon ages very similar to the corals in which they are embedded. This implies that the erosion of the corals and the subsequent growth of the clams took place shortly after the growth of the corals themselves. The corals show no sign of having grown within the boulder beach, unlike corals at Iris Point which have grown around boulders. Thus, the boulder beach at Pioneer Bay South seems to have formed rapidly, eroded the corals, and then stabilised sufficiently to allow the clams to grow. Alternatively, the boulder beach may not be the cause of erosion, but formed later, over the pre-existing eroded surface colonised by clams.

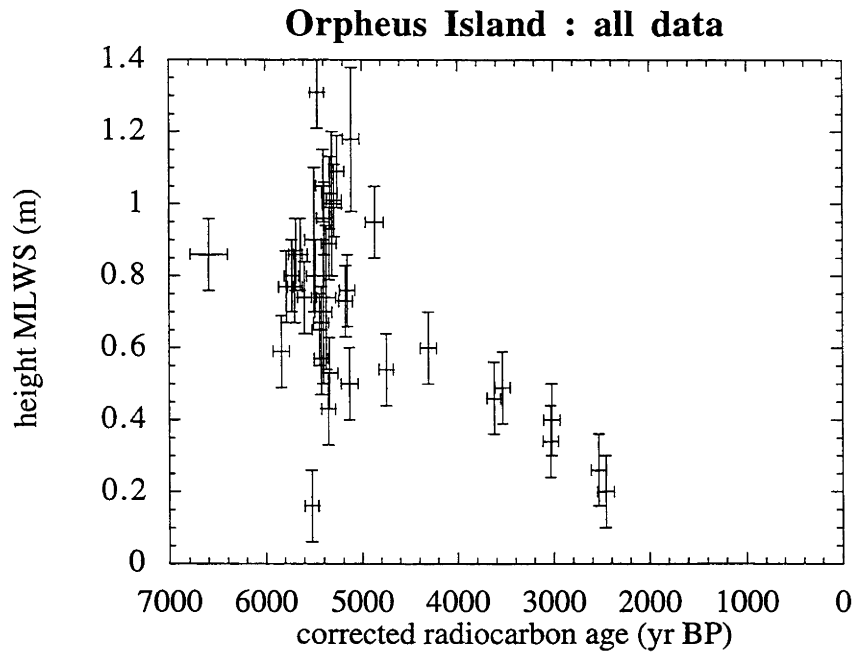

Figure 2.12 : All coral and clam shell data from Orpheus Island. A marine reservoir correction of -450±35 yr has been applied (Gillespie and Polach 1979).

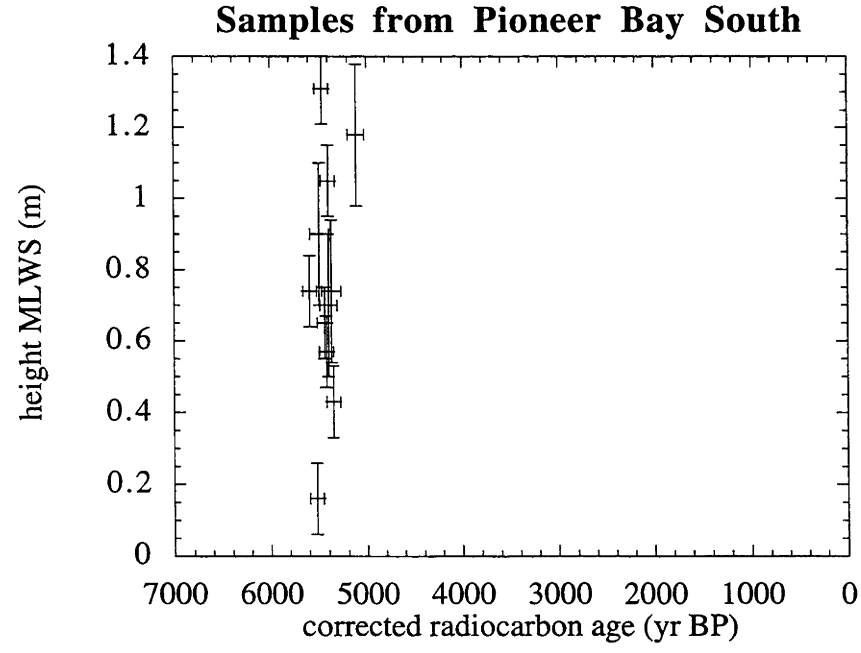

Figure 2.13 : Dated coral and clam shell samples from the Pioneer Bay South site (PBS). The large vertical range in a short time interval indicates that the coral surfaces were eroded into a sloping surface and are not microatolls.

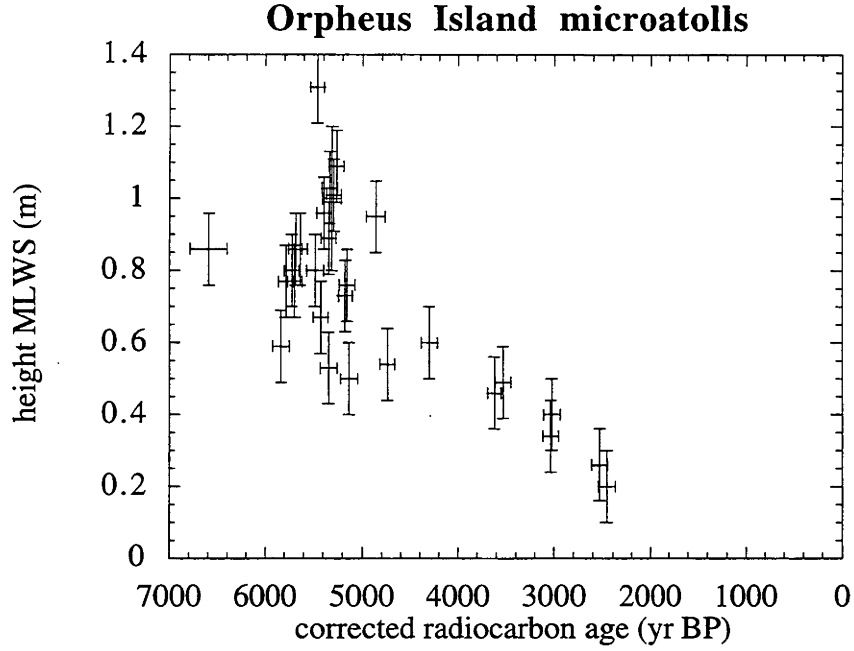

Figure 2.14 : Dated microatolls from Orpheus Island, without most samples from Pioneer Bay South. The data suggest a sea-level highstand of ~1 m at 5500 yr BP.

Discussion

Including only the limiting data point from Pioneer Bay South (Figure 2.14), the data set shows a good linear trend between 5 ka and 3 ka, and a cluster of points between 6 ka and 5 ka at 0.6 to 1.1 m above present. Since the maximum height of the highstand is an important constraint on eustatic sea-level curve and the rheological parameters of the earth, it is vital to determine this correctly from the observed data. If all the samples were perfectly-preserved microatolls, then we would have to assume that MLWS at any time was at or below the level of the lowest microatoll of that age, since microatolls can form above MLWS, in moated pools, but not below. This would imply a maximum highstand of 0.6 m, and moating of at least 0.7 m at that time (sample PBS1). However, the original upper surface of the microatolls sampled was usually not present, as this part of the coral is most exposed to physical erosion on the reef flat, and to bio-erosion from organisms living on the dead coral, and often within the small pools which form on top of many microatolls. The true level of MLWS probably lies within the range of heights around 6 ka, and extrapolation of the trend from 5 to 3 ka by a linear or an exponential curve indicates a highstand of 0.9 to 1.0 m.

Chappell and others (1983) concluded a linear fall of sea-level because their data had too much scatter to justify a more complex estimate. With this data set from a single location, the sea-level curve can be described in more

detail. It is immediately obvious from Figure 2.14 that the majority of points fall below the linear sea-level curve drawn from the highstand to the origin. An exponential fall from a highstand of around 1 m describes the data well. This agrees in form, if not in magnitude, with the predictions of a hydro-isostatic model of sea-level change. There is no indication of fluctuations in sea-level in the last 6 ka.

2.5 Northern GBR microatolls

2.5.1 Introduction

The spatial variation in sea-level change in the GBR predicted by glacio-hydro-isostatic models (eg Thom and Chappell 1978, Nakada and Lambeck 1989) is mostly due to the effect of the increased water load in the ocean due to postglacial sea-level rise. In coastal regions, the effect of this load is a seaward tilting of the continental margin, so that a site on the coast experiences uplift, or relative sea-level fall. This uplift begins as soon as the water load begins to increase (ie at the start of deglaciation) and continues after the melting has ceased until isostatic equilibrium is reached. Because uplift is continuous, the older the record the more uplift we expect to observe, and hence the greatest spatial variation in the sea-level record. The greatest predicted variation occurs for relative sea-level at the onset of melting, ie the LGM sea-level lowstand. Unfortunately, older sea-level records are more scarce and generally have much larger associated error, to the extent that we do not know LGM sea-levels in most places. If we are to observe spatial variation, we must use records whose error is small compared to the magnitude of the expected variation.

The best chance of meeting these conditions is in the mid-late Holocene. Sea-level indicators from this period are above or close to present sea-level, so that they are easier to locate than pre-Holocene indicators, and the factors which affect the accuracy of each observations, such as reef flat morphology, are relatively easy to identify and assess. The existence of the sea-level maximum at many sites during this time also makes records of past sea-level easier to find, since the sea-level stillstand allows the formation of more prominent indicators.

The region of the northern GBR between Lizard Island in the south and Princess Charlotte Bay in the north (Figure 2.15) was chosen for this study for several reasons. First, the observations of Chappell and others (1983) provide a good base on which to build new work. Secondly, the deep embayment of Princess Charlotte Bay provides sites which are effectively further inland, as far as hydro-isostatic processes are concerned, because the lithosphere tends to filter the effects of short-wavelength loads and produce deformation which appears to be in response to an "average" coastline. As well as the inshore sites in Princess Charlotte Bay, reef islands are present in this region which allow examination of onshore-offshore transects which should exhibit variation in sea-level change. Thirdly, the region was investigated during the 1973 Royal Society Expedition, so maps of the reef islands were available as well as some indication of where the best sea-level records might be found. In addition to this region in the northern GBR, three fringing reefs at Cape Tribulation were investigated.

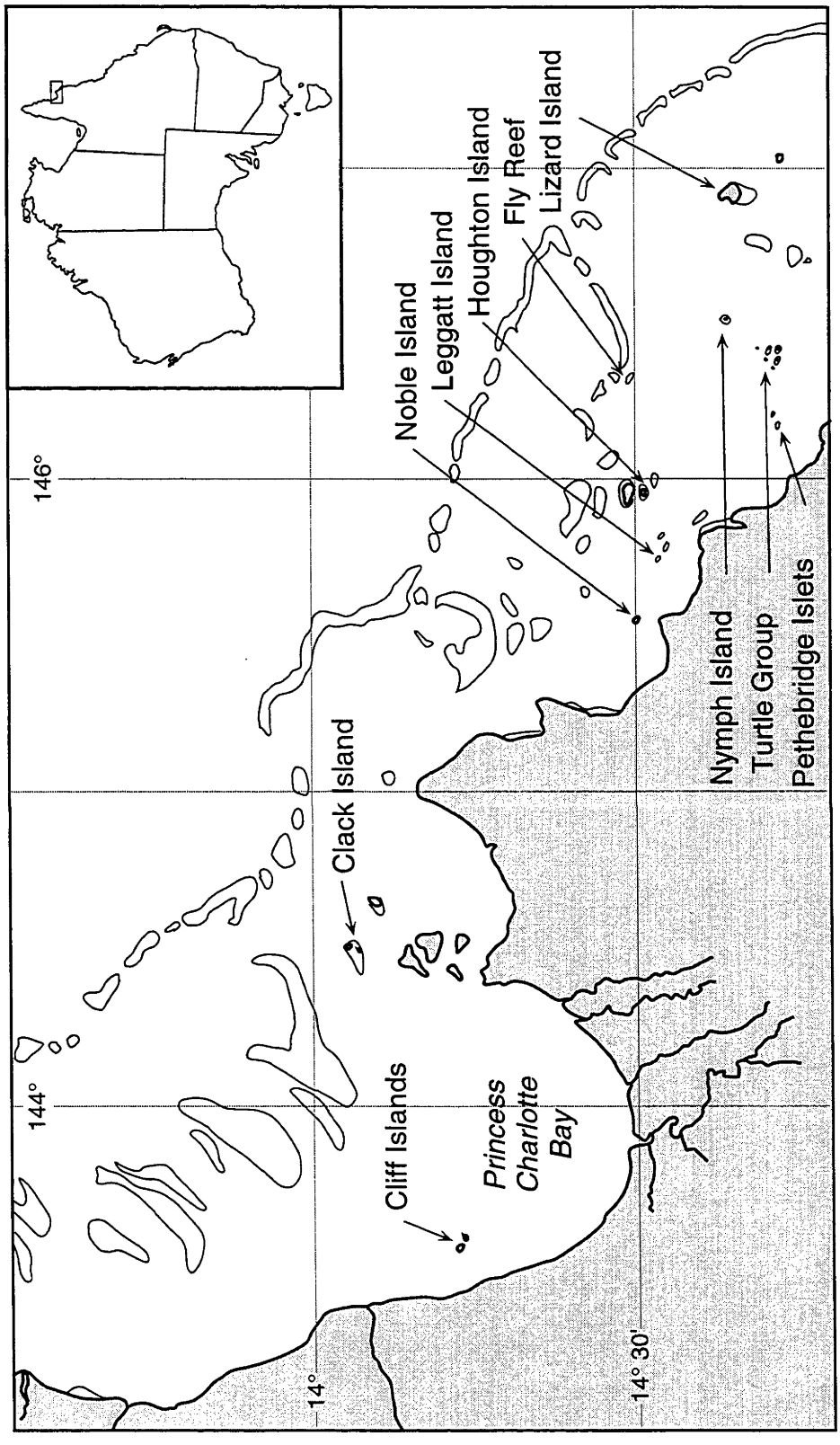

Figure 2.15 : Location map of the Lizard Island - Princess Charlotte Bay region, Great Barrier Reef, showing sample sites.

2.5.2 Sample collection

The sites from which samples were collected for this work are shown in Table 2.8 and Figure 2.15. These islands were visited over a two week period in November 1992, using the R.V. James Kirby, from James Cook University. When possible, sites were visited during the time of low tide, so that as much of the reef flat as possible could be studied. This timing also allowed the level of low tide to be observed. This level was then compared with the observations from the nearest tide gauge (data supplied by the National Tidal Facility, Flinders University) and the correction applied for the difference between that Standard Port and the nearest Secondary Place (Queensland Ministry of Transport 1992, Table 2). The site descriptions and samples collected are listed in Appendix A.

Table 2.8: Locations in the central and northern GBR which were studied, excluding Orpheus Island.

Site	S latitude	E longitude
Nymph Is.	14° 39'	145° 15'
Turtle I	14° 43'	145° 10'
Turtle II	14° 43'	145° 11'
West Pethebridge Is.	14° 43'	145° 04'
Fly Reef	14° 30'	145° 08'
Lizard Is.	14° 40'	145° 28'
Houghton Is.	14° 31'	144° 58'
Leggatt Is.	14° 33'	144° 40'
West Cliff Is.	14° 13'	143° 46'
Clack Is.	14° 04'	144° 15'
Noble Is.	14° 30'	144° 46'
Rykers Reef	16° 02'	145° 29'
Myall Reef	16° 05'	145° 30'

2.5.3 Results

Microatolls

Coral samples were selected and prepared for radiocarbon dating in the same way as for the Orpheus Island samples, described above. Radiocarbon ages were determined for thirty-two samples, shown in Table 2.9.

Table 2.9: Radiocarbon dates from samples in the central and northern GBR. All samples are coral microatolls except for LI 9202, which is an encrustation of rock-oyster shells and NO 9208 which is a large *Tridacna* clam.

Field code	ANU number	Height (MLWS)	conventional age (yr BP)	corrected age (yr BP)
NYMPH ISLAND				
NY 9203	9222	1.23 ± 0.2	3600 ± 70	3150 ± 78
NY 9206	8958	1.39 ± 0.2	3630 ± 70	3180 ± 78
NY 9211	8959	1.04 ± 0.2	5200 ± 60	4750 ± 69
TURTLE I				
T1 9204	8957	1.21 ± 0.2	1880 ± 70	1430 ± 78
T1 9201	8955	1.14 ± 0.2	2110 ± 60	1660 ± 69
T1 9202	8956	0.96 ± 0.2	1930 ± 70	1480 ± 78
TURTLE II				
T2 9201	9078	1.15 ± 0.2	1240 ± 70	790 ± 78
T2 9202	9077	0.86 ± 0.2	1390 ± 70	940 ± 78
T2 9207	9220	0.85 ± 0.2	1650 ± 60	1200 ± 69
T2 9203	9076	0.65 ± 0.2	2120 ± 70	1670 ± 78
WEST PETHEBRIDGE				
WP 9204	9080	1.07 ± 0.2	2210 ± 70	1760 ± 78
WP 9202	9081	0.90 ± 0.2	2800 ± 70	2350 ± 78
WP 9209	9079	0.55 ± 0.2	3190 ± 70	2740 ± 78
FLY REEF				
FR 9201	9211	0.11 ± 0.2	113 ± 1%M	0
FR 9202	9223	0.02 ± 0.2	116 ± 2%M	0
LIZARD ISLAND				
LI 9202	8687	2.16 ± 0.2	3480 ± 70	3030 ± 78
HOUGHTON ISLAND				
HO 9201	9180	1.18 ± 0.2	5040 ± 70	4590 ± 78
HO 9203	9210	1.04 ± 0.2	6180 ± 90	5730 ± 96
HO 9204	9181	0.84 ± 0.2	5600 ± 70	5150 ± 78
HO 9205	9182	0.56 ± 0.2	4350 ± 70	3900 ± 78
LEGGATT ISLAND				
LE 9201	9183	0.95 ± 0.2	5670 ± 70	5220 ± 78
LE 9203	9209	0.75 ± 0.2	4850 ± 80	4400 ± 87
LE 9204	9184	0.61 ± 0.2	5300 ± 80	4850 ± 87
CLACK ISLAND				
CK 9206	9187	0.87 ± 0.2	320 ± 70	-130 ± 78
CK 9205	9186	0.69 ± 0.2	420 ± 60	-30 ± 69
CK 9201	9185	0.21 ± 0.2	5370 ± 80	4920 ± 87
NOBLE ISLAND				
NO 9201	9188	0.99 ± 0.2	6030 ± 80	5580 ± 87
NO 9208	9221	0.91 ± 0.2	6110 ± 80	5660 ± 87
NO 9205	9189	0.76 ± 0.2	6250 ± 80	5800 ± 87
MYALL REEF				
MY 9302	9212	0.52 ± 0.2	5370 ± 80	4920 ± 87
MY 9303	9214	0.28 ± 0.2	6140 ± 90	5690 ± 96
MY 9305	9213	0.11 ± 0.2	4980 ± 80	4530 ± 87

When all microatoll data are plotted together (Figure 2.16), the result is not a uniform sea-level curve. The large vertical range seen in samples of similar age is probably due to a combination of moating and error in converting the tide observations from Cairns to local tides at each site. With such large errors, it is difficult to judge which samples might be reliable. Examining the results at each site (Figure 2.17) provides some guidance.

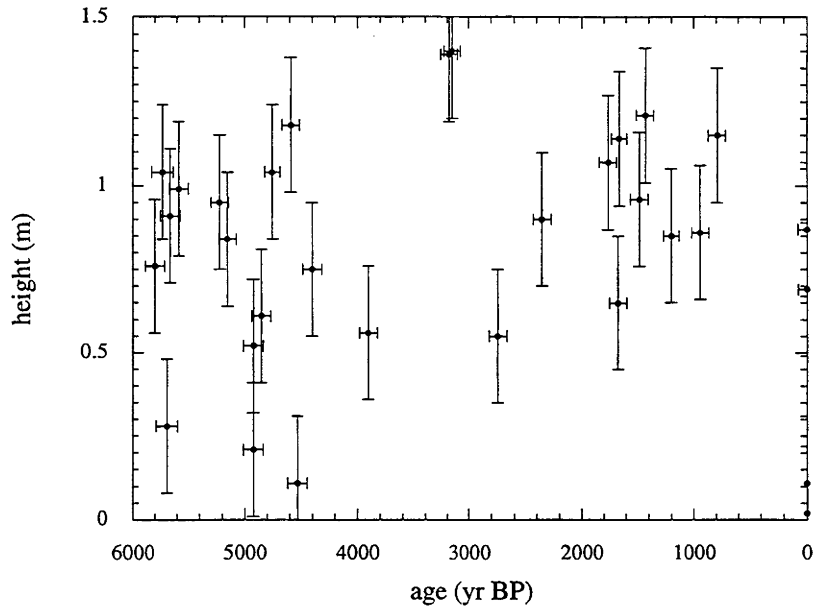

Figure 2.16 : All dated microatolls from the Lizard Island - Princess Charlotte Bay region, Great Barrier Reef. A marine reservoir correction of -450±35 yr has been applied (Gillespie and Polach 1979).

The data from Nymph Island, the Turtle Group, and West Pethebridge all indicate moating, apparent from patterns indicating rising sea-level in the late Holocene. While it is possible that the lowest sample at each of these sites is unmoated, and it is recognised that corals from close to 6 ka were unlikely to have been moated, there is no objective criterion for retaining some samples while discarding others, so all data from these sites must be discarded.

At Clack Island, two modern samples are clearly moated, but there is nothing to suggest that the third is suspect.

The samples from Leggatt, Houghton and Noble Islands all appear to be acceptable, although the highest sample at Houghton Island lies off the trend of the others. However, all of these samples were collected from a single well-exposed field of microatolls, and there was no evidence of moating, so there is no reason to discard this result.

At Myall Reef, the data appear anomalously low, but there is no reason to suspect moating at this site.

These new observations thus provide reliable new sea-level observations at four sites: Leggatt, Houghton and Noble Islands, and Myall Reef. The first three of these are located close together (Figure 2.15), so any variation in relative sea-level between them due to isostatic processes would be small. Myall Reef is further south, at Cape Tribulation, and is indicated on Figure 2.7. Although no spatial variation can be directly inferred from these new data alone, they can be combined with the existing body of sea-level observations from the GBR for statistical comparison with sea-level predictions, and this is done in Chapter 3.2.

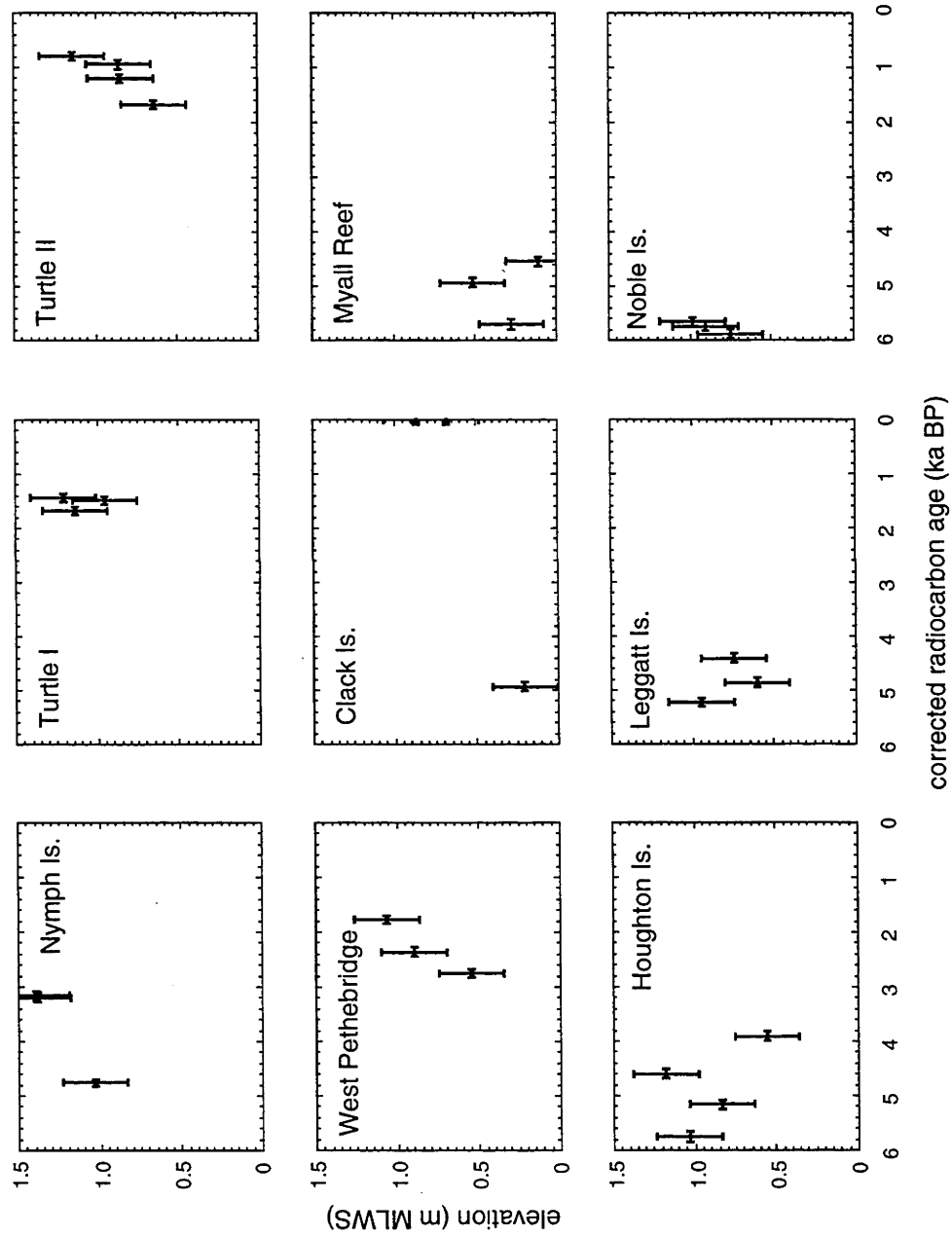

Figure 2.17 : Dated microatolls from the Lizard Island - Princess Charlotte Bay region, Great Barrier Reef, plotted by location. A marine reservoir correction of -450±35 yr has been applied (Gillespie and Polach 1979).

On Lizard Island, in a small bay on the rocky coast north of Watson's Bay, a deposit of oyster shells was found above their present growth limit (see Appendix A for a more detailed description of the sample site). The top of the shell bed is 0.83 ± 0.28 m above the upper limit of the modern band of oysters at that site, but only 0.56 ± 0.28 m above the observed limit of massive oyster growth in that region (Table 2.10)

Table 2.10: Comparison of elevations of modern and ancient oyster shell deposits in the central and northern GBR.

Elevation (m MSL)	corrected ^{14}C age (yr BP)	Reference
CENTRAL GBR		
0.2 - 0.3	modern	Endean and others (1956)
LIZARD ISLAND		
0.46 ± 0.2	modern	this work, exposed coast
0.53 ± 0.2	modern	this work, sheltered site
1.36 ± 0.2	3030 ± 78 (ANU 8687)	this work
WEST CLIFF ISLAND		
0.8 ± 0.2	modern	this work
MAGNETIC ISLAND		
0.4 ± 0.05	modern	Beaman and others (1994)
0.12 ± 0.1	modern	Kurt Lambeck, pers. comm.
2.07 ± 0.05	3590 ± 61 - 5210 ± 61	Beaman and others (1994)
~2.4 ± 0.2	4270 ± 69 (ANU 8001)	Kurt Lambeck, pers. comm.

The sea-level change indicated by the fossil oysters at Lizard Island, when compared to the modern limit of oysters at that site, is greater than the microatoll data suggest. This is also the case at Magnetic Island (Beaman and others 1994). For the reasons discussed in section 2.2.5, the discrepancy cannot be explained by changing tidal range, and the microatoll data are considered to be more accurate. If the anomalously high oyster deposits cannot be explained by their preservation in sheltered sites, then environmental conditions in the mid Holocene must have permitted oyster growth at a higher level than today. If the elevation of the highest modern oysters at West Cliff Island is used as a reference datum, the sea-level change implied by the fossil oysters is similar to the microatoll record.

2.5.4 Discussion

The problem posed by moating of microatolls is clearly significant. Extreme care needs to be taken in the field to ensure that samples are taken from sites that have not been moated, but this is not simple. Moats are commonly formed by shallow ramparts of cemented coral rubble which are later eroded.

The possibility of former ramparts can only be investigated by excavation of the reef flat (Chappell and others 1983)

Another method of discriminating between moated and unmoated microatolls may be to determine the water temperature in which the coral grew. This can be done by measuring either the oxygen-isotope or strontium/calcium ratios of the coral (McCulloch and others 1994). The water on a reef flat at high tide is considerably warmer than the open sea, due to heating by the sun where the water is shallow. Shallow moats on the reef flat retain this warm water after high tide. In such a moat, this heating is greater and more prolonged than at a site on the edge of the reef flat. The average water temperature difference between these sites amounts to several degrees, which is well within the precision of isotopic paleothermometry (McCulloch and others 1994). The effects of coral growth rate and sample position within the coral on the implied temperature have not been investigated, but this may prove to be a viable method of determining whether a microatoll grew in moated or open-water conditions. The possibility that sea surface temperatures may have varied throughout the late Holocene would also have to be considered.

2.6 Drillcore data

2.6.1 Introduction

Hopley (1983) reviewed evidence for Holocene sea-level change in north Queensland. Apart from a few notable studies, discussed above, dated samples from drill cores through reef flats provided most of the available evidence. As discussed earlier in this chapter, these data provide a lower limit for the sea-level curve. Treated individually, such cores are not sufficiently precise to constrain any spatial variation in Holocene sea-level change. Several cores from one location, if taken from different parts of the reef flat, may provide enough information to reliably constrain some aspects of the sea-level curve, such as the rate of sea-level rise and the time at which sea-level first reached its present level. These are both characteristics which are predicted to vary spatially, according to glacio-hydro-isostatic models: the rate of sea-level rise near the end of the postglacial transgression is sensitive to the relationship between the rates of eustatic sea-level rise and isostatic subsidence, and this determines the time at which present sea-level is first reached. With overall seaward tilting of the continental shelf, sea-level is predicted to reach its present level at inshore sites before shelf-edge sites (eg Thom and Chappell 1978, Nakada and Lambeck 1989).

This trend was noted by Hopley (1983) comparing borehole data from two fringing reefs on inshore islands (Orpheus and Rattlesnake Island) with that from two outer reefs (Wheeler and Grub Reefs) in the central GBR. In that study, however, he attributed the lag in the growth of the offshore reefs to "retardation of reef accretion rates" and suggested that the effect was not directly related to sea-level. In this section, borehole data from throughout the GBR are compiled, in an attempt to obtain a data set of sufficient size to examine the predictions of spatial variation of sea-level change. Comparison with model predictions will be made in Chapter 3.2.

2.6.2 Data sources

Core logs and associated radiocarbon dates were compiled from several sources, listed in Table 2.11. Many were found in published articles, and a large number of unpublished dates were supplied by David Hopley (James Cook University, Townsville) and John Marshall (AGSO, Canberra). Four unpublished theses from James Cook University also contained relevant information. A total of more than 650 values from 55 sites were compiled.

Where possible, the elevation of each sample was converted to MLWS, which represents the modern upper limit to coral growth. Neglecting the possibility that samples grew on a moated reef flat, this elevation thus represents the maximum sea-level change which can have occurred since the coral was alive. This assumption is justified, because sea-level was rising throughout much of the period under study, and reefs were unable to develop moated flats under these conditions. In many cases, sample elevations were only given with respect to the top of the core, which was at

the level of the reef flat. Reef flat levels usually range between MLWN (mean low water neap tide) and MLWS (D. Hopley, pers. comm.), which covers a range of up to 1 m (Queensland Ministry of Transport 1992). The upward error bar of these samples is thus increased by this amount.

2.6.3 Sites studied

The fifty-five sites for which drill core data have been compiled are shown in Table 2.11 and Figure 2.18. All are reef islands or fringing reefs, except for four boreholes on land near Townsville: Alva Beach bore, Barratta bore, Houghton bore and a hole at Pallarenda. As can be seen from Figure 2.18, the sites extend from 14.5° S to 24° S and cover most of the width of the GBR, and thus have the potential to demonstrate spatial variation in sea-level change.

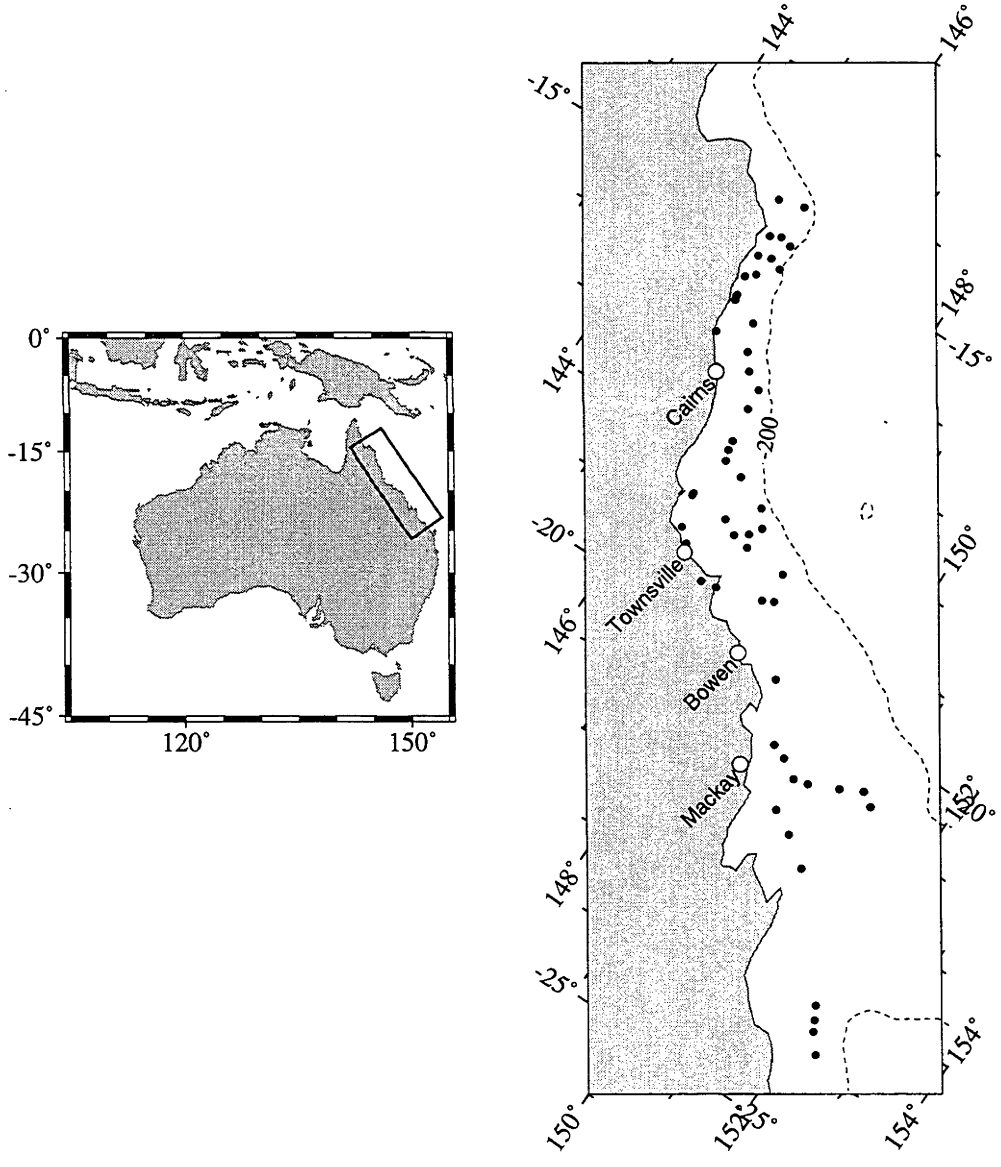

Figure 2.18 : Location map of the Great Barrier Reef, showing locations of reef cores. The 200 m isobath is a close approximation to the edge of the Reef.

Table 2.11: List of sites for which borehole data have been compiled, with their locations and the time at which present sea-level was first attained there. At some sites, the data were too sparse to estimate the first attainment time.

Location	South Latitude	East Longitude	Time (ka)	Reference
Carter	14° 33.0'	145° 36.0'	5.7	Hopley (1982)
Nymph	14° 39.0'	145° 15.0'	-	Hopley (1982)
Long	15° 3.0'	145° 34.2'	-	Hopley (1982)
Lark Pass	15° 4.8'	145° 43.8'	5.9	Hopley (1982)
Three Is.	15° 7.2'	145° 25.2'	-	Hopley (1982)
Williamson	15° 21.6'	145° 36.0'	6.2	Marshall (pers. comm)
Boulder	15° 25.2'	145° 25.8'	5.6	Marshall (pers. comm)
Ribbon 5	15° 25.2'	145° 46.8'	5.9	Marshall (pers. comm)
Cairns	15° 39.0'	145° 33.0'	-	Hopley (1982)
East Hope	15° 45.0'	145° 25.8'	-	Hopley (1982)
Emmagen	16° 1.2'	145° 28.8'	6.5	Partain (1992)
Rykers	16° 1.8'	145° 28.8'	6.5	Partain (1992)
South Myall	16° 4.8'	145° 30.0'	6.5	Partain (1992)
Opal	16° 13.2'	145° 52.8'	4.2	Hopley (1982)
Yule Point	16° 34.2'	145° 31.2'	-	Bird (1971)
Michaelmas	16° 34.8'	146° 1.8'	5.2	Hopley (1982)
Thetford	16° 48.0'	146° 12.0'	4.9	Hopley (1982)
Channel	16° 55.8'	146° 27.0'	1.8	Hopley (1982)
Hedley	17° 13.8'	146° 28.2'	1.8	Hopley (1982)
Potter	17° 42.0'	146° 31.8'	3.6	Kleypas (1991)
Taylor	17° 49.8'	146° 33.0'	5.2	Hopley (1982, pers comm.)
Moss	17° 58.2'	146° 36.0'	4.3	Hopley (1982, pers comm.)
Barnett	18° 3.0'	146° 54.0'	-	Hopley (1982)
Myrmidon	18° 15.0'	147° 22.8'	3.7	Marshall (pers. comm)
Bowl	18° 28.2'	147° 33.0'	3.3	Marshall, Hopley (pers. comm)
Iris Point	18° 34.2'	146° 28.8'	6.3	Barnes (1984)
Pioneer Bay	18° 36.0'	146° 28.8'	6.3	Slocombe (1981)
Grub	18° 37.8'	147° 25.8'	4.6	Hopley (pers comm.)
John Brewer	18° 37.8'	147° 3.0'	-	Walbran (1992)
Keeper	18° 45.0'	147° 16.2'	2.0	Hopley (1982)
Wheeler	18° 48.0'	147° 31.2'	4.4	Marshall (pers comm.), Hopley (1982)
Viper	18° 49.8'	148° 9.0'	4.6	Marshall (pers comm.), Hopley (1982)
Rattlesnake	19° 1.8'	146° 36.0'	6.3	Hopley (pers comm.)
Pallarenda	19° 10.8'	146° 46.8'	-	Belperio (1975)
Darley	19° 12.0'	148° 15.0'	6.0	Hopley (1982)
Stanley	19° 16.2'	148° 6.0'	6.3	Hopley, Marshall (pers comm.)
Alva Beach bore	19° 28.2'	147° 28.2'	4.1	Paine and others (1966)
Phillips Landing	19° 30.0'	147° 15.0'	-	Hopley (pers comm.)
Haughton bore	19° 30.0'	147° 15.0'	-	Hopley (pers comm.)
Barratta bore	19° 30.0'	147° 15.0'	3.6	Hopley (pers comm.)
Hayman Island	20° 3.0'	148° 52.8'	4.7	Hopley and others (1978)
Molar	20° 37.8'	150° 48.0'	-	Hopley (1982)
Cockatoo	20° 45.0'	151° 0.0'	4.7	Hopley (1982, pers comm.)
Gable	20° 46.8'	150° 30.0'	5.7	Hopley (pers comm.)
Cockermouth	20° 46.8'	149° 22.8'	6.0	Hopley (pers comm.)
Scawfell	20° 52.2'	149° 36.0'	3.3	Hopley (pers comm.)
Redbill	20° 58.2'	150° 4.8'	5.9	Hopley and others (1984)
Penrith	21° 1.2'	149° 52.8'	5.9	Hopley (pers comm.)
Digby	21° 28.8'	149° 55.2'	-	Hopley (pers comm.)
Percy	21° 40.2'	150° 16.2'	3.6	Hopley (pers comm.)
High Peak	21° 57.0'	150° 40.8'	5.5	Hopley (pers comm.)
Wreck	23° 19.8'	151° 58.2'	5.7	Marshall (pers comm.)
One Tree	23° 30.0'	152° 4.2'	5.4	Marshall (pers comm.)
Fitzroy	23° 37.8'	152° 9.0'	5.9	Marshall (pers comm.)
Fairfax	23° 52.2'	152° 22.2'	6.2	Marshall (pers comm.)

2.6.4 Results

The entire compiled data set is plotted in Figure 2.19. The result is very similar to the compilation of subtidal sea-level data from Larcombe and others (1995), and, indeed, comprises many of the same observations. Although grouping all data together obscures spatial variation between sites,

it does clearly indicate the general trend of sea-level rise in the GBR. There is no evidence for episodic sea-level rise, although the regression between 8.5 and 8.2 ka is not contradicted. A small number of points lie above the main cluster, and it is likely that these are erroneous, due to upward-reworking of corals during storm events. The processes which can introduce error into the age or depth of a sample are summarised in figure 2.20. Of these, the most likely on the GBR are those which move points younger and downwards. These errors are not apparent on Figure 2.19, since corals grow subtidally in any case.

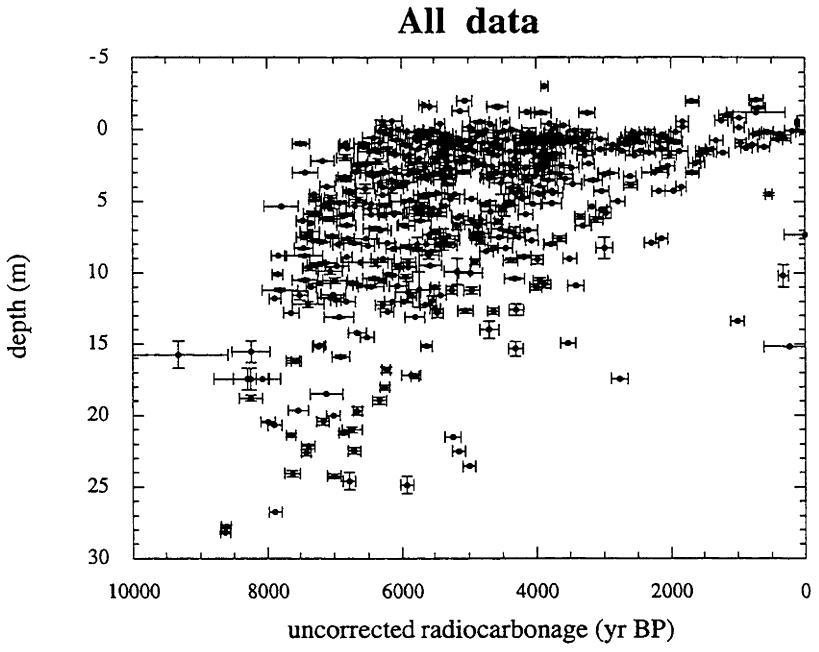

Figure 2.19 : All dated coral samples from reef cores in the Great Barrier Reef.

When the data from each site are plotted separately, they can be interpreted as records of reef growth. These cannot be used directly as local sea-level curves, since we cannot determine the water depth in which each coral grew. One parameter which can be measured is the time at which present sea-level was first reached at each site (the "first attainment time"). To estimate this, a line lying above all the points at each site was extrapolated to present sea-level. This time represent a minimum age for the first attainment of present sea-level. These data are examined in detail in Chapter 6.

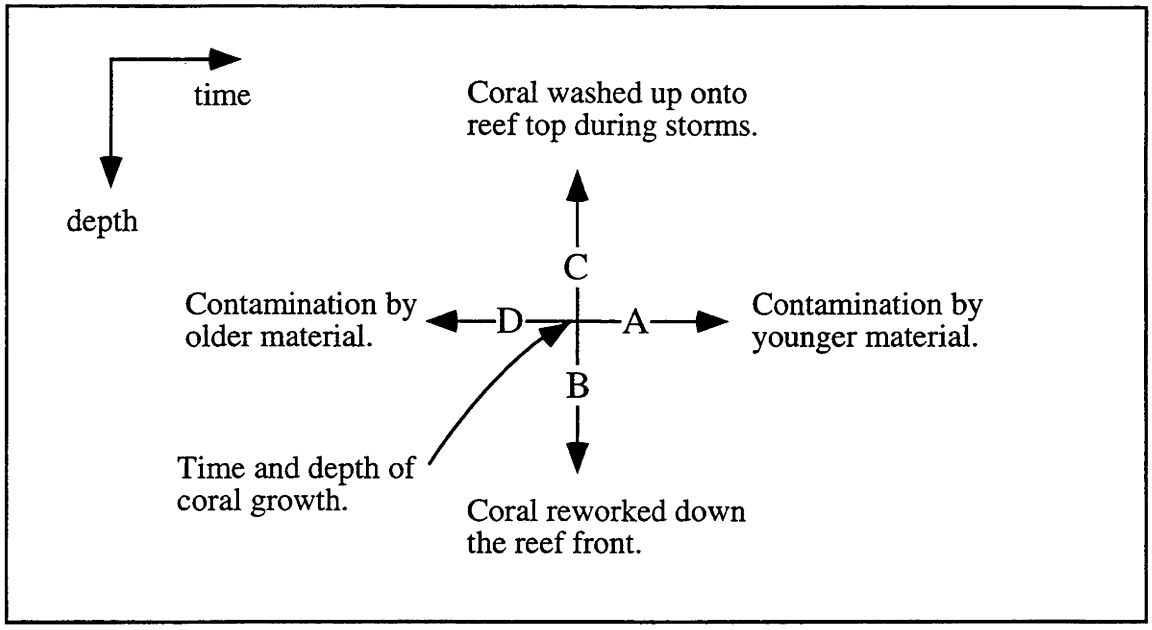

Figure 2.20 : Possible sources of error when inferring sea-level from a dated core sample. In the GBR, processes A and B are most likely. C is possible in high wave-energy environments, but D probably does not occur, as incorporation of Pleistocene material is unlikely there is no abundant source of radiocarbon-dead groundwaters.

Chapter 3

Sea-level Observations from Antarctica

3.1 Introduction

This chapter contains new results and a compilation of published Holocene sea-level observations from around Antarctica, which will be used in chapter 3 to constrain the distribution of ice on Antarctica at the LGM and during deglaciation. Most of the observations are compiled from the publications of geomorphologists and glaciologists working in Antarctica since the modern phase of exploration and study began in the late 1950's. In addition, the results of field work conducted in the Vestfold Hills in the summer of 1991-92 as part of the Australian National Antarctic Research Expedition (ANARE) are reported here. These observations constrain Holocene sea-level closely, compared to the published records from other Antarctic sites, which are reviewed here. Locations of sites discussed in this chapter are shown in Figure 3.1 and Table 3.1.

Table 3.1: Locations of Antarctic sites discussed in this chapter.

Location		
Vestfold Hills (Davis Station)	68° 35' S	77° 58' E
Windmill Islands (Casey Station)	66° 17' S	110° 32' E
Skarvsnes, Lützow-Holm Bay	69° 30' S	39° 35' E
Terra Nova Bay	74° 50' S	163° 30' E
Explorers Cove, McMurdo Sound	77° 30' S	163° 30' E
Bunger Hills	66° 10' S	101° E
King George Is (South Shetland Islands)	62° S	58° W

The sea-level record around Antarctica is poorly defined compared to any other continent, for several reasons. Most importantly, only 5% of the coastline consists of rock (Drewry and others 1982), and it is on these areas that former sea-levels can be recorded and preserved. In locations where the coastline does consist of rock, the unusual coastal environment, enclosed in sea-ice for most of the year, and the rarity of living organisms compared to warmer regions, mean that the sea-level record is difficult to interpret and difficult to date. The methods used to obtain sea-level records in the Antarctic will be discussed below before the record itself is presented.

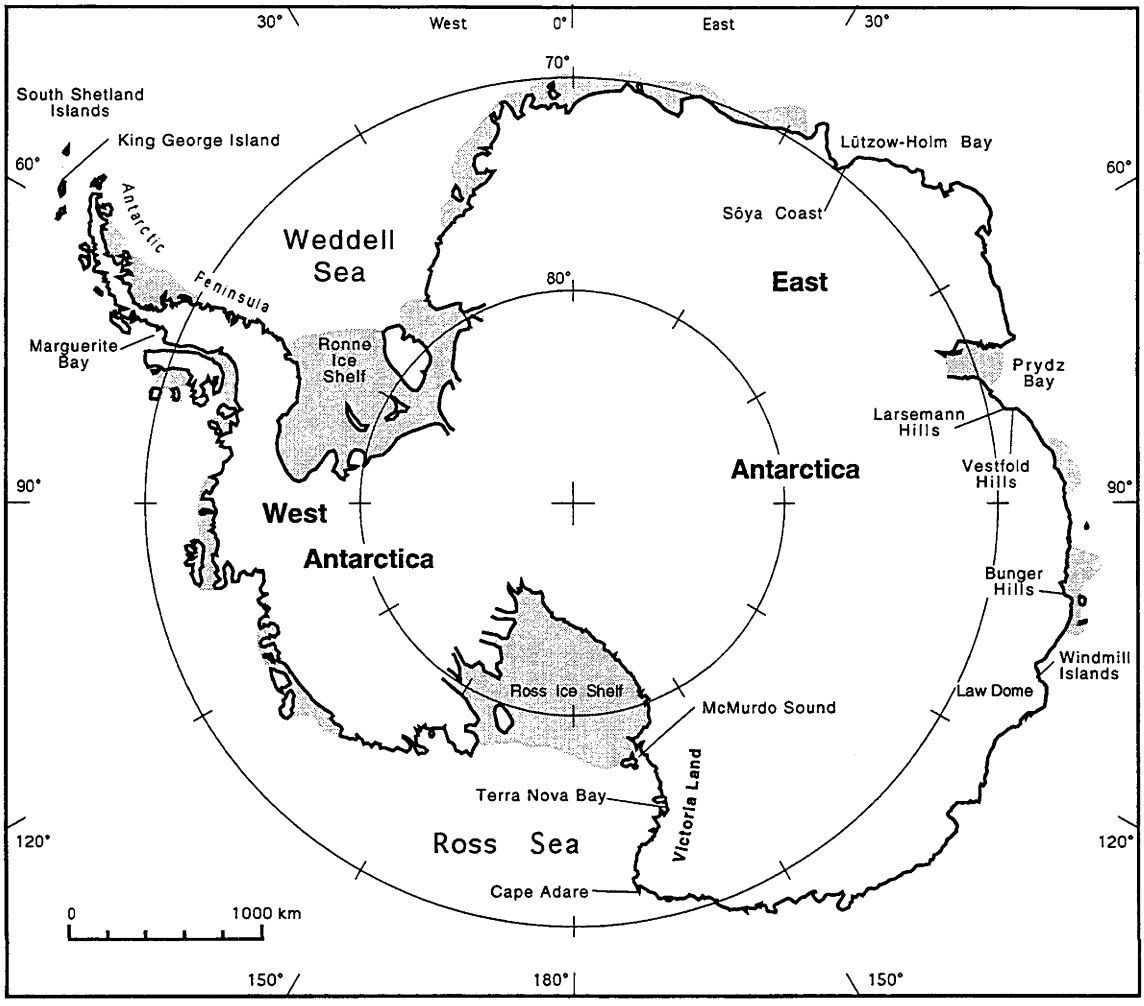

Figure 3.1 : Location map of Antarctica showing sites mentioned in this chapter.

3.2 Methods

3.2.1 Raised Beaches

Ancient beach deposits raised above their present-day counterparts are the most common evidence of past sea-level observed in Antarctica. This is because they are large landforms, easy to recognise, and exist in most coastal ice-free areas. However, their relationship to sea-level is not always clearly understood. Raised beaches have been used as a record of sea-level change in other parts of the world, and in general a modern beach ridge is needed at each location as a bench-mark from which relative sea-level changes can be measured. In Antarctica, processes capable of forming shore-parallel ridges include : wave action, when the coast is ice-free; "ice push", when sea ice is blown onshore; and removal of material frozen to the base of fast ice (ice which is frozen onto the shore). The features formed by these processes all bear a different relation to mean sea-level: wave action produces ridges above sea-level at a height dependant on the wave energy; ice-push may similarly produce a range of ridge heights, up to at least 1.75 m above sea-level (Colhoun and Adamson 1992); and removal of material by fast ice forms a "beach" terrace ~2 m below sea-level. In addition, persistent perennial snowbanks can trap wind-borne sand and form beach-like features which bear no relation at all to sea-level.

Beach ridges are commonly dated using fragments of marine shells incorporated in the beach material. Obviously, this material has been transported, and there is no guarantee that it was living at the same time as formation of the beach. The age of the shell fragments is therefore a maximum age for the formation of the beach. Better dating control is provided when shells can be found in growth position, such as the burrowing bivalve *Laternula elliptica*. This provides an accurate date for the marine status of the sediments in which the shell was found, but poorer control on the associated beach ridge, which may be some distance away. Due to the seasonal formation of fast ice, *Laternula* usually lives in at least 3 m water depth (Colhoun and Adamson 1992), so the link between the age of the surrounding sediments and a beach feature some distance away is tenuous at best. However, in regions of falling sea-level, such as the Antarctic coast during the Late Holocene, this correlation provides a minimum age for a feature known to have formed near sea-level.

3.2.2 Isolated Lakes

Another record of changing sea-level is found in sediments deposited in lakes near the coast. During a sea-level highstand, marine basins close to shore accumulate marine sediment (Figure 3.2). As sea-level falls, basins with submarine sills are cut off, and, if they have fresh water input, begin to accumulate fresh water lacustrine sediments. By recognising and dating the marine-lacustrine transitions in sediment cores from these basins, and measuring the elevation of the lakes' former outlet to the sea, a precise sea-level record can be obtained. If sea-level has oscillated, crossing the sill of a

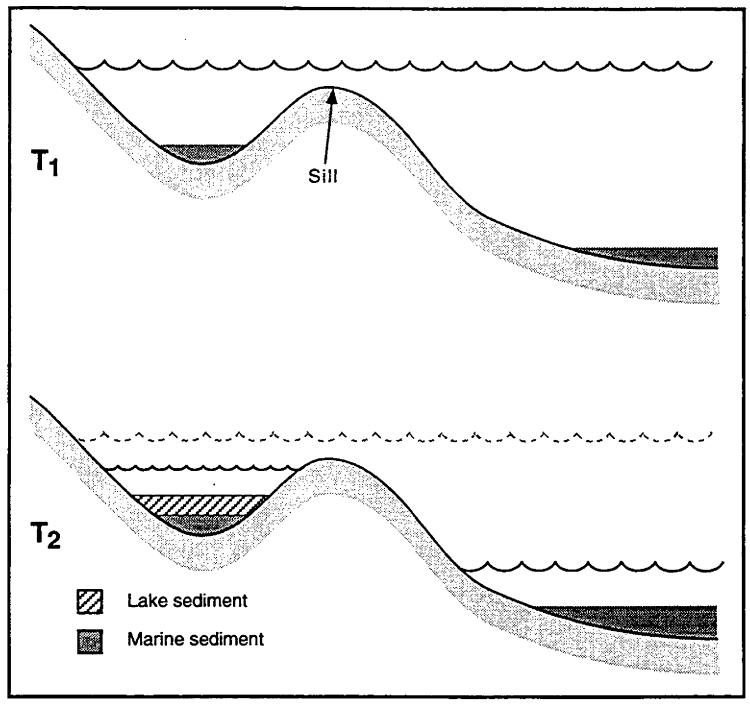

Figure 3.2 : Schematic representation of lake sedimentation in a changing sea-level environment. Sea-level changes may be recorded in lake sediments, if sea-level moves through the elevation of the basin's sill. In this simple example of sea-level fall, marine sediment is deposited in a nearshore basin at time T_1, when sea-level stands higher than the sill. At a later time T_2, sea-level has dropped below the sill and lake sediments are deposited in the basin on top of the older marine sediments.

lake several times, each transgression and isolation will be preserved in the sediment record (Figure 3.3). This method of determining past sea-levels has two major advantages over the use of beach ridges: by identifying the sill which represents the lake's last connection to the sea, the relationship between the dated transition and the sea-level is clear; and by dating the fresh-water material at the transition, the need to apply a reservoir correction to the radiocarbon date (discussed below) may be avoided.

Tidal range at the Vestfold Hills is presently ~1.75 m (Australian National Tidal Facility observations), which is significant compared to the sea-level change there over the Holocene. The transition from marine to lacustrine sedimentation in the lakes probably does not correspond to the same point in the tidal range at all sites, but depends on the fresh-water input to the lake. For example, a lake with significant fresh water inflow may maintain sufficiently low salinity to make the transition from marine to lacustrine sedimentation before the basin is completely isolated from the sea; a basin with low fresh water inflow, on the other hand, will become less saline only after the highest tides cease to overflow the sill. In this study, it is initially assumed that isolation occurred when mean sea-level was at the level of the lake's sill.

This method has been used extensively in Fennoscandia to measure the sea-level change due to glacial rebound there (eg Anundsen 1985, Svendsen and

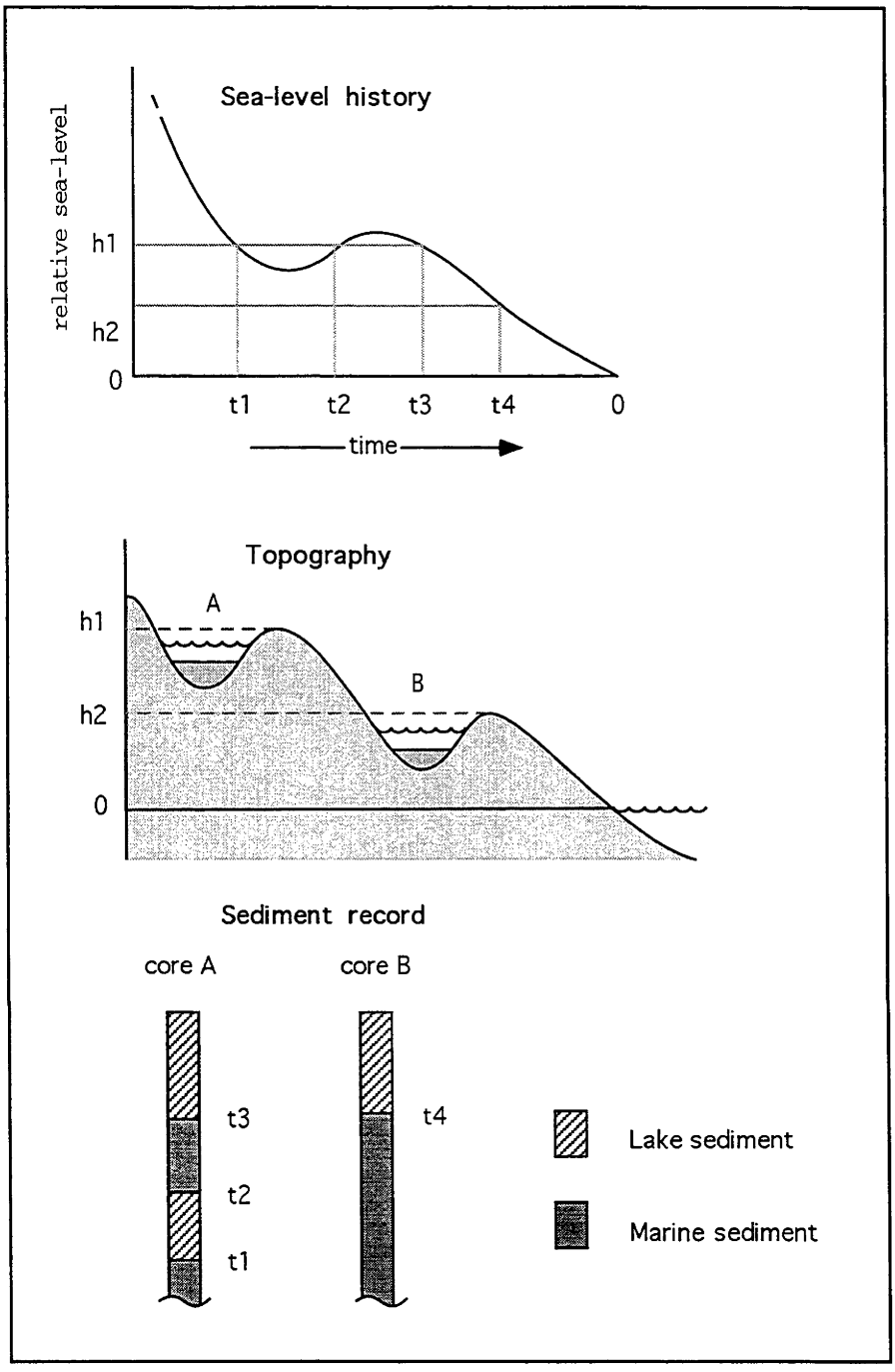

Figure 3.3 : The sediment record from lakes with different sill heights can be used to reconstruct complicated sea-level histories. In this example of oscillating sea-level, the elevations and ages of the sea-level highstand and lowstand are constrained by the dated sediment records from lakes A and B. Each marine-lacustrine transition in the sediment core corresponds to a point on the sea-level curve.

Mangerud 1987, Hafsten 1983), and also at some Antarctic sites (Mausbacher and others 1989 , Bird and others 1991).

3.2.3 Marine Limit

The marine limit is defined as the maximum height of a former transgression of the sea. In a formerly ice-covered area, the marine limit varies between locations due to different rebound rates and variations in the time at which sites became ice-free. The elevation of the marine limit gives a relation between the position of the ice margin and the amount of rebound since the time of retreat. Even when the age is unknown, this can provide a constraint in reconstructing former ice sheets and modelling glacial rebound, as in the case of the Fennoscandian ice sheet. Andrews (1975) showed that in some circumstances the trend of marine limits with respect to former ice flow direction may be an indicator of the relative rate of ice retreat. With a rapid retreat of grounded ice, the marine limit should rise towards the former ice centre, whereas the opposite pattern indicates slow retreat. This scheme was developed from observations in formerly glaciated regions in the northern hemisphere, where no ice remained after deglaciation, so that the geographic features which later would define the marine limit could begin forming immediately after retreat of the ice. This method is also only applicable over regions where the margin retreat is not controlling deglaciation. In Antarctica, the record is not so simple, since even after the disappearance of grounded ice from coastal regions, floating ice shelves may have persisted which prevented the formation of beach landforms. The assumption that deglaciation is not controlled by margin retreat may also not apply in Antarctica, as discussed further in Chapter 4. An undated marine limit in Antarctica, therefore, cannot constrain either the time of deglaciation or the relative sea-level history, unless one of these is already known. Nevertheless, Kirk (1991) uses the marine limits preserved in the western Ross Sea to estimate the former extent of ice there.

3.2.4 Limiting Observations

Well-constrained beach ridges and lake isolation events record the actual height of sea-level at a given time, albeit with an associated error. That is, they define a point on the relative sea-level curve. Other observations can constrain the sea-level history of a region in a more limited way, as being either above or below the observation site at a given time. Examples of lower limits to the sea-level curve include any *in situ* marine sediment or fossil organism. Upper limits can be obtained from any dateable deposit which can be shown to have formed above sea-level, such as terrestrial plants, penguin rookeries (eg Baroni and Orombelli 1991), and deposits of snow-petrel stomach-oil (eg Verkulich and Hiller 1994). A sufficiently large number of limiting observations from one site can be compiled to define an envelope within which the relative sea-level curve lies (eg Baroni and Orombelli 1991).

3.2.5 Radiocarbon dating

In order to obtain a relative sea-level record from geomorphic features, the features must be dateable. Over the time period since the last glacial maximum (LGM) around 18,000 years ago, the radiocarbon dating method is

the most practical technique available for determining the age of organic material. Several techniques for dating inorganic materials are being applied to the problems of former sea-levels and ice distribution in Antarctica, including Thermoluminescence (TL), Optically Stimulated Luminescence (OSL), and the accumulation of cosmogenic isotopes, but most geomorphic features are dated using the age of associated organic material, which can be reliably determined using the radiocarbon method.

Radiocarbon dates from all marine materials require a reservoir correction, to allow for the depletion of ^{14}C in sea water relative to the atmosphere. This depletion is due to the lag in carbon dioxide exchange between the atmosphere, where ^{14}C is produced, and the oceans, where most of the earth's ^{14}C inventory resides (Gordon and Harkness 1992). Because ocean circulation is comparatively slow, the distribution of radiocarbon in the oceans is not uniform, but varies both spatially and with time, depending on the movements of water masses. In Antarctic waters the radiocarbon deficit relative to the atmosphere is larger than in most oceans, due to the upwelling of old bottom water.

Radiocarbon assays of modern organisms can be used to determine the reservoir correction required for older samples. These measurements are only estimates, since the reservoir effect may have varied considerably with time, due to changes in the patterns of ocean circulation, and modern samples are also affected by "bomb carbon" produced by atmospheric nuclear weapons tests, which tends to counteract the reservoir effect. Stuiver and others (1981) estimate that the maximum reservoir correction required would be 1400 years, which is the radiocarbon "age" of deep circumpolar water uncontaminated by bomb carbon. If spatial variation in the reservoir effect is predominantly caused by ocean circulation patterns, and these have not changed significantly over time, then regional reservoir corrections for the locations where dates have been obtained from marine organisms may be estimated from the apparant age of equivalent modern (but pre-1950) organisms. Estimates for the reservoir correction obtained from a variety of marine organisms in the regions studied in this chapter are presented in Table 3.2.

Table 3.2: Estimates of the marine reservoir correction at some locations in East Antarctica.

Location	Reservoir correction	Reference
Ross Sea	1200 - 1400 yr	Stuiver and others (1981)
Vestfold Hills	950 - 1310 yr	Adamson and Pickard (1983)
Lützow-Holm Bay	860 - 1300 yr	Yoshida and Moriwaki (1979)

Another method of determining the reservoir correction was proposed by Stuiver and others (1986). They presented a method of calculating model radiocarbon ages for historical marine samples, using measured variation in radiocarbon production and a model for the mixing between the atmospheric and oceanic carbon reservoirs. A regional marine reservoir

correction, ΔR, can then be determined using a sample of known age, as the difference between the model age and the measured radiocarbon age. Stuiver and others (1986) suggest a value of 885±45 yr for coastal Antarctic waters, based on two shell samples from the Ross Sea. Using 12 published radiocarbon ages of samples of known age, mostly seal and penguins killed in the Terra Nova bay region early this century by Antarctic explorers, Baroni and Orombelli (1991) estimate ΔR = 779±60 years. The values of ΔR do not represent the entire reservoir correction, but rather the greater depletion of Antarctic waters in ^{14}C relative to the rest of the world.

Terrestrial materials incorporate ^{14}C in equilibrium with the atmosphere, so do not require a reservoir correction. The same applies to freshwater lakes, if they maintain a well-mixed carbon pool in equilibrium with the atmosphere. Old CO_2 trapped in pore spaces within the ice is a possible source of error in radiocarbon dates from lakes fed by meltwater from the Antarctic Ice Sheet. Radiocarbon ages of modern freshwater algae from several lakes which are immediately adjacent to the ice sheet in the Vestfold Hills indicate that this effect is negligible, and no correction is necessary (Table 3.3).

Table 3.3: Radiocarbon assays from modern algae in three lakes adjacent to the Antarctic ice sheet in the Vestfold Hills. The results indicate that old CO_2 from the ice sheet has no effect on the ^{14}C content of the lake. The atmospheric radiocarbon assay is from Cape Grim, Tasmania (Levin and others 1994).

Sample	^{14}C assay (% modern)	ANU number
Dec 1991 atmosphere	113 ± 0.5	-
Pauk Lake	112.8 ± 2.2	8156
Lake Bisernoye	113.4 ± 2.5	8164
Lake Druzhby	116.9 ± 0.9	8169

Ages to which no reservoir correction has been applied are described in subsequent sections as "conventional radiocarbon ages", measured in years before 1950 and written as ^{14}C-yr BP. When the reservoir correction has been applied, the ages are "corrected radiocarbon ages", measured in units of corr. ^{14}C-yr BP. No calibration has been included to allow for the systematic difference between the radiocarbon and siderial timescales, as determined using uranium-series dating (Bard and others 1990).

3.3 Vestfold Hills

The Vestfold Hills (Figure 3.4) lie on the eastern edge of Prydz Bay on the Ingrid Christiansen Coast, at 68°35' S, 78° E. They are bounded to the east by the East Antarctic Ice Sheet and to the south by the Sørsdal Glacier, an outlet glacier of the ice sheet. The ice-free region, consisting of long peninsulas, fjords and low hills, is approximately 20 km x 20 km, and covers an area of 410 km^2 (Pickard 1986). In summer most of the coast is exposed to the open sea. Raised beaches and saline lakes are found throughout the region, indicating a fall in relative sea-level during the Holocene.

3.3.1 Previous work

Zhang and Peterson (1984) obtained dates from shells within several terraces around 6 m a.s.l. in the Vestfold Hills, all of which fall near 6,000 ^{14}C-yr BP (see Table 3.4). They also note possible shoreline features up to 15 m a.s.l, which do not contain dateable material.

Adamson and Pickard (1986) claim a maximum emergence of 11 m at one site just to the south of Davis Station, though their highest dated sample comes from 5.5 m a.s.l.. From elevations of the highest marine terrace at locations throughout the Hills and radiocarbon dates obtained from marine algae and shells within these deposits (Table 3.4), they produced contour

Table 3.4 : Radiocarbon ages from marine organisms in emerged marine terraces in the Vestfold Hills. References: 1 = Zhang and Peterson (1984); 2 = Adamson and Pickard (1983); 3 = Pickard (1985); 4 = Pickard and Adamson (1983); 5 = Pickard and Seppelt (1984). The locations mentioned in this table are indicated on Figure 3.4.

† This sample is described as both algae and shells in Zhang and Peterson (1984). Provided the algae was marine, this does not affect the interpretation.

Location	Material	Elevation (m)	Uncorrected age	Sample code	Ref.
Mud Lake	shells	3.0	3325 ± 103	ZDL 66	1
Mud Lake	shells	3.0	3500 ± 86	ZDL 69	1
Watts Lake	shells	3.0	6100 ± 108	ZDL 70	1
Watts Lake	algae	3.0	3600 ± 95	ZDL 71	1
Triple Lake	shells	6.0	6141 ± 90	ZDL 78	1
Dingle Lake	shells	6.0	5600 ± 77	ZDL 79	1
Deep Lake	shells	6.0	6632 ± 118	ZDL 80	1
Platcha	algae†	6.0	5677 ± 94	ZDL 81	1
Watts Lake	algae	3.7	4760 ± 190	SUA 1828	2
Watts Lake	sediment	2.4	6225 ± 85	Beta 4761	2
Watts Lake	shells	5.5	7590 ± 80	SUA 2026	3
Laternula Lake	shells	2.0	2410 ± 90	SUA 1411	4
Death Valley	shells	2.6	4710 ± 70	ANU 1011	2
Death Valley	shells	2.6	5340 ± 90	SUA 1237	4
Calendar Lake	shells	1.8	6850 ± 160	SUA 2030	5
Lichen Valley	shells	2.0	6910 ± 150	SUA 2027	3
Partizan Island	shells	3.0	7370 ± 95	Beta 4767	2

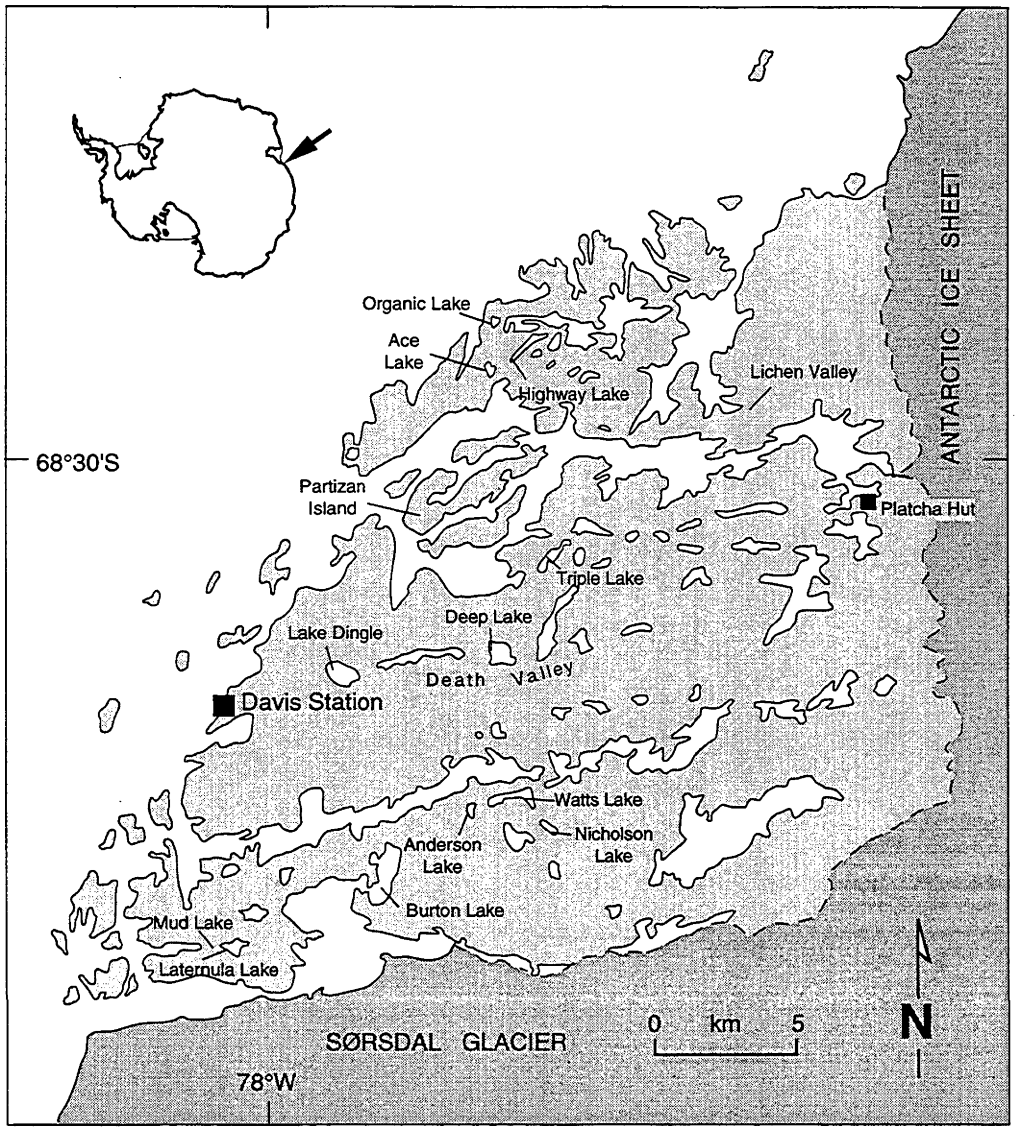

Figure 3.4 : Location map of the Vestfold Hills showing locations of published radiocarbon ages (Table 3.4).

maps of emergence and emergence rate for the area (Adamson and Pickard 1986, p84). The patterns indicated by these maps appear to be based purely on variable formation and/or preservation of marine features at the different sites, and do not represent actual rebound, as the contours of emergence and emergence rate are sometimes perpendicular (Figure 3.5). In addition, the emergence history of the region derived from these data show uplift accelerating from around 0.5 mm/yr 6000 years ago to 1.8 mm/yr 100 years ago and increasing asymptotically towards the present. The implausibility of this scenario supports the notion of incomplete preservation of the relative sea-level history in raised beach deposits.

The authors of the dates reported in Table 3.4 do not specify whether the samples were *in situ*. If it is assumed that they are, then these results constitute a lower bound for sea-level in the Vestfold Hills The lower bound for the relative sea-level curve which is defined by these data is shown on Figure 3.6. A minimum emergence rate of 1.5 - 2.0 mm/yr is defined, but the timing of former sea-levels above 6 m a.s.l. is not

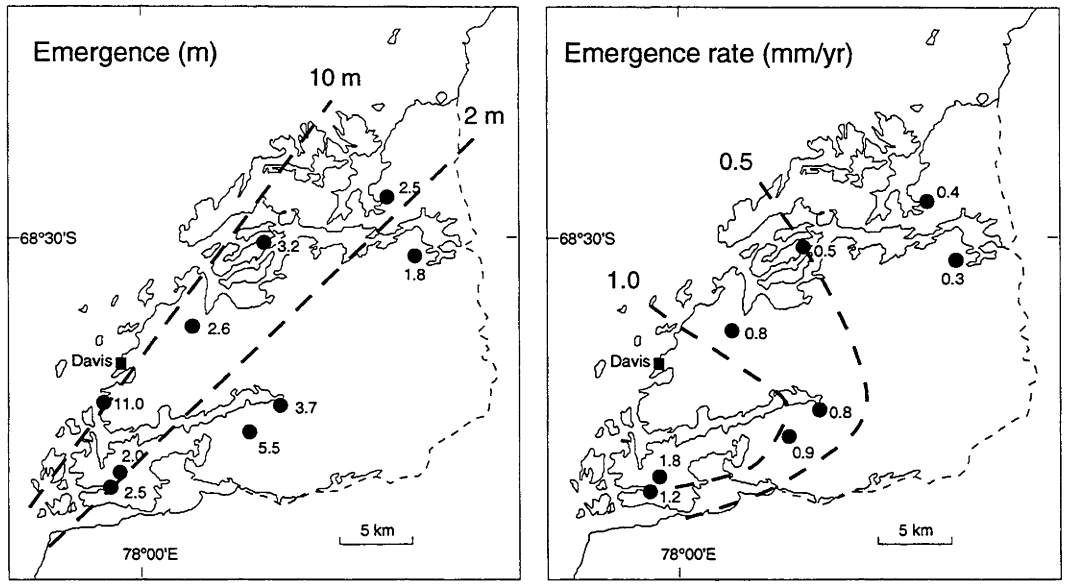

Figure 3.5 : Total emergence and inferred average emergence rate in the Vestfold Hills derived from dated marine sediments by Adamson and Pickard (1986). The contoured trends seem to bear no relation to each other, indicating that the observed patterns are probably due to inadequate sampling.

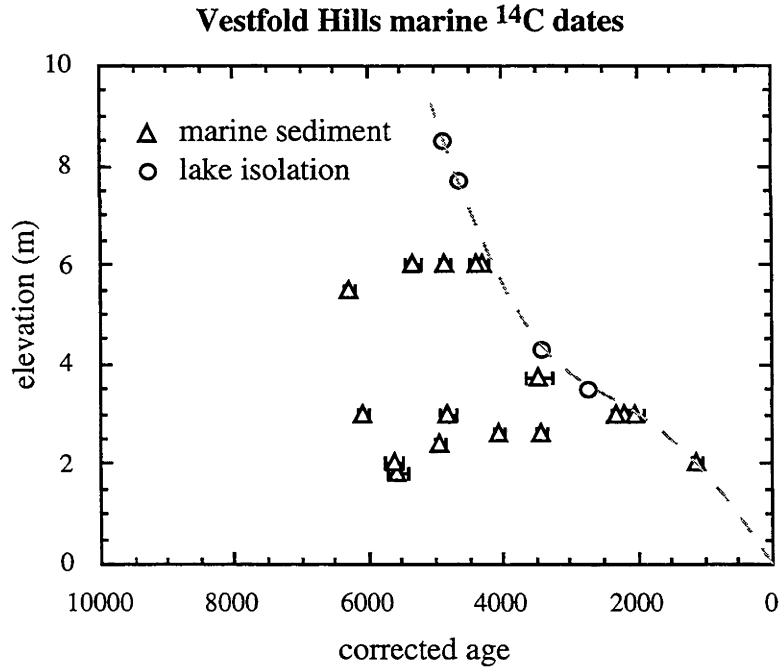

Figure 3.6 : Constraints on the sea-level curve for the Vestfold Hills based on the ages of published dated marine sediments and lake isolation events. The sources of the data are given in Table 3.4 and 3.5

constrained at all. The lakes of the Vestfold Hills contain the information necessary to fill in the remainder of the Holocene relative sea-level history.

In the Vestfold Hills, several lake isolation records have been collected. Pickard and others (1986) recognised a marine-lacustrine transition in sediments exposed on the shore of Watts Lake, in the southern Vestfold Hills. From the range of ages obtained from marine organisms in these

sediments, they dated the recession of sea-water below the sill at 4700 ^{14}C-yr BP (3400 corr. ^{14}C-yr BP). Bronge (1989) collected a sediment core from Nicholson Lake, a higher sub-basin of the former embayment now containing Watts, Nicholson and Anderson Lakes (Figures 3.7 and 3.8), and dated the marine-lacustrine there at 4650±200 corr. ^{14}C-yr BP. Pickard and others (1986) report sill heights of 3.8 m and 12.3 m for Watts and Nicholson Lakes respectively, however these elevations were estimated using a barometer, and are inaccurate. Both sills were re-levelled in the 1991-92 summer using a theodolite and electronic distance meter, with reference to bench marks installed by the Australian Division of National Mapping. The revised values are 4.3 m and 8.5 m a.s.l. respectively, which imply emergence rates of 3.4 mm/yr between the isolation of the lakes, and 1.3 mm/yr since.

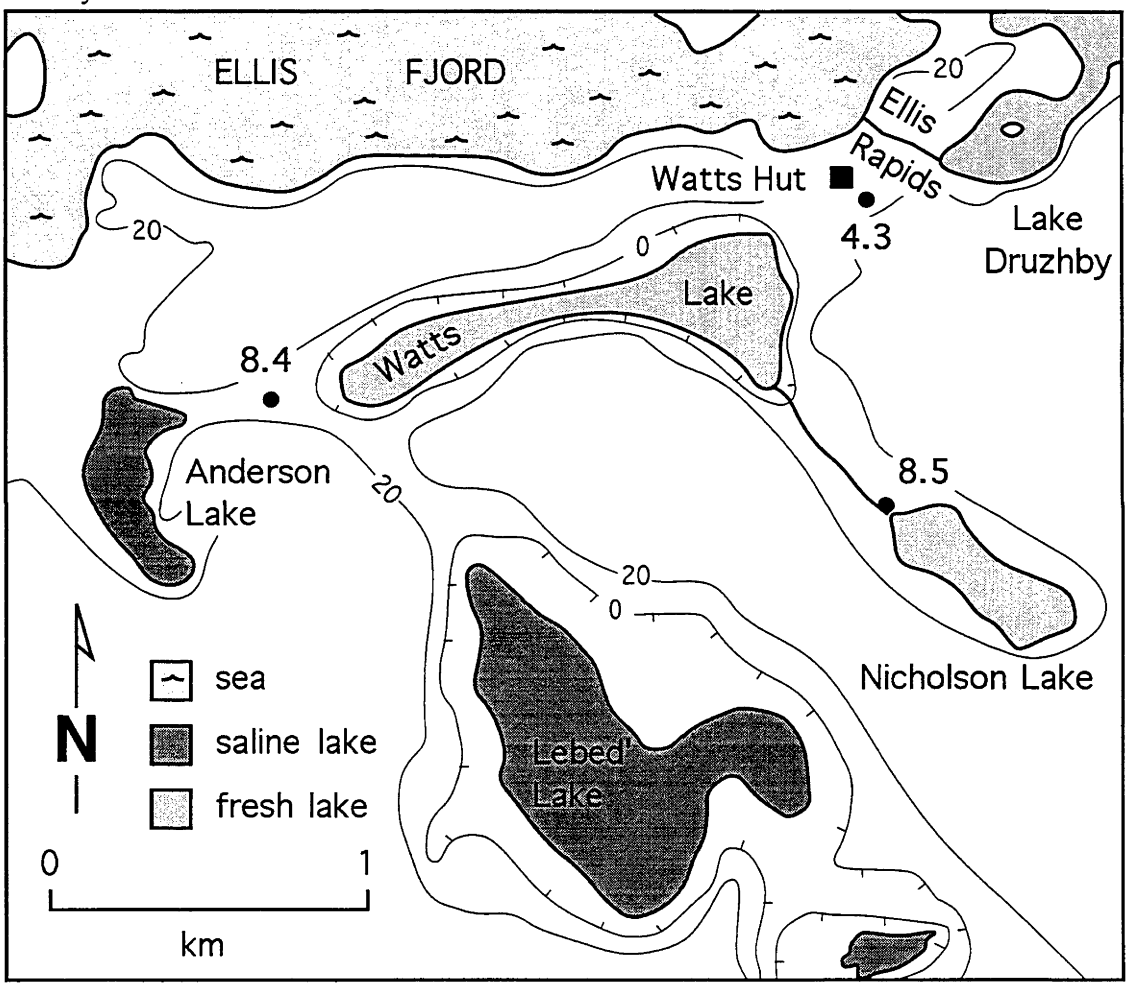

Figure 3.7 : Map of Watts/Nicholson/Anderson lake system. The sea formerly occupied an embayment which now contains the basins of Watts, Anderson, Nicholson and Lebed' lakes, as well as Oblong Lake to the south (not shown on map). The sill height of lakes from which sediment cores have been taken are indicated. Elevations are in metres, and contours above 20 m are not shown.

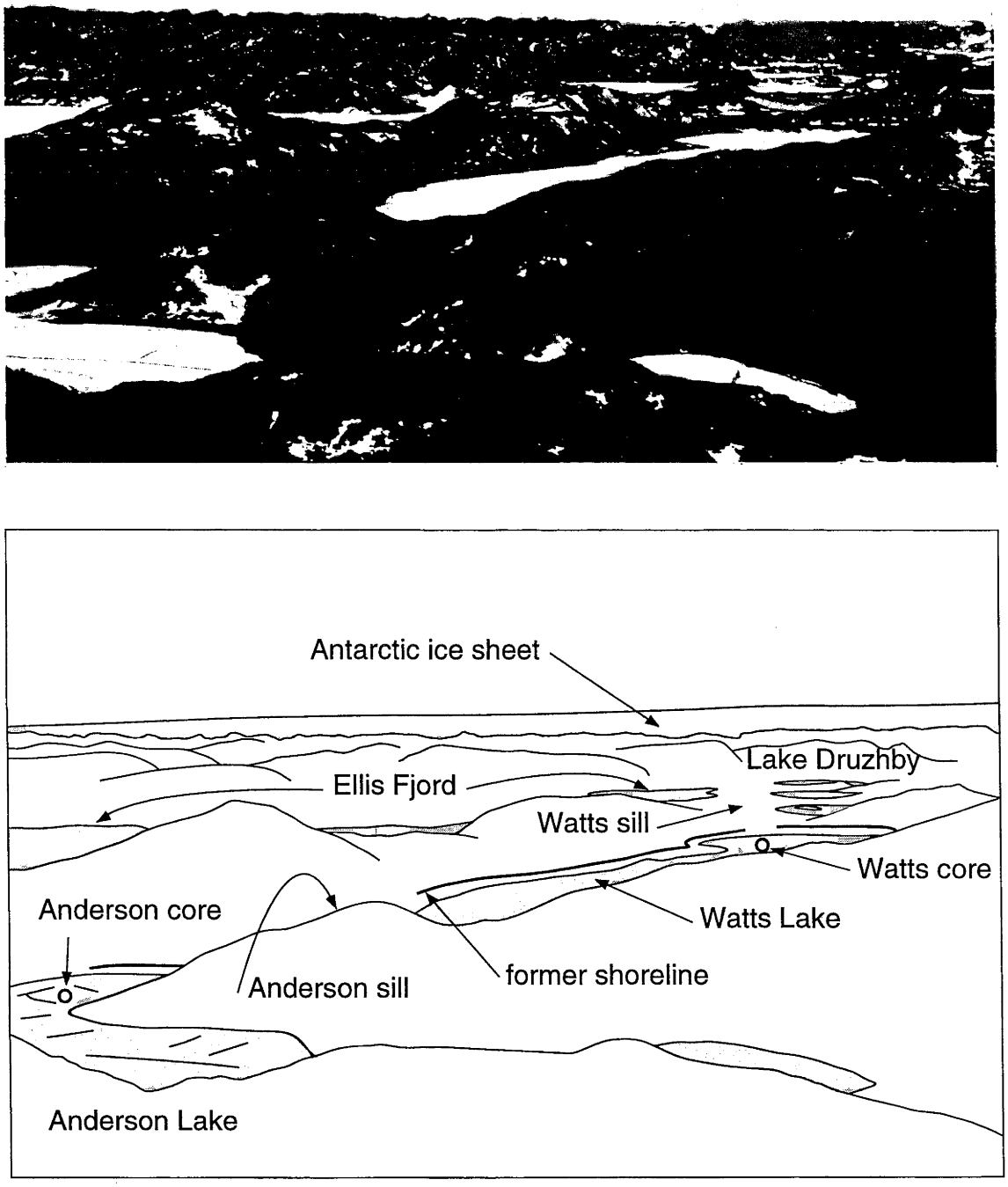

Figure 3.8 : Aerial view of Anderson Lake, Watts Lake and Ellis Fjord, looking north-northeast across the Vestfold Hills. A former shoreline is evident on the shore of Watts Lake. The patchy nature of the ice on Anderson Lake is due to its salinity. Width of foreground is ~1 km.

Bird and others (1991) identified marine-lacustrine transitions in cores from two lakes in the northern Vestfold Hills: Highway and Organic Lakes. The time at which relative sea-level fell below the sill connecting each lake to the sea was estimated by dating sediment samples from both the upper (fresh-water) and lower (marine) parts of the core. The sedimentation rate obtained from these dates was then extrapolated to the depth of the marine-lacustrine transition to obtain the time of transition. At least two dates were obtained from each section of core, and the ages obtained from extrapolations above and below the transition agree well, when a 1300 year reservoir correction is applied to the marine samples. Highway Lake, with a sill height of 7.7 m, was isolated from the sea about 4600 corr. ^{14}C-yr BP. Organic Lake, with a sill at 3.5 m, was isolated at 2700 corr. ^{14}C-yr BP. These points on the relative sea-level curve imply emergence rates of 2.2 mm/yr between 4600 and 2700 years ago, and 1.3 mm/yr since then. Although the rates differ slightly, this slowing of emergence rate is consistent with the result from Watts and Nicholson Lakes. A core from Ace Lake (sill 8.8 m) was also analysed by Bird and others (1991), but its relevance to sea-level change was not discussed, as the significance of the fresh-marine-fresh sediment sequence was not recognised. New analyses on this core are included in the present work.

Published sea-level estimates for the Vestfold Hills derived from lake isolation data are summarised in Table 3.5 and Figure 3.6. The results are consistent with the lower bound to the sea-level curve estimated from raised marine sediments, and show a noticeable decrease in the emergence rate around 3500 corr. ^{14}C-yr BP, if a sea-level curve is linearly interpolated. However, the points are poorly spaced in time and elevation, and do not constrain the maximum Holocene sea-level highstand.

Table 3.5 : Published former sea-levels derived from isolation of lakes in the Vestfold Hills. Error limits for the time of isolation were not generally provided by the original authors.

Lake	Sill height (m)	Isolation time (corr. age)	Reference
Organic Lake	3.5	2700	Bird and others (1991)
Watts Lake	4.3	3400	Pickard and others (1986)
Highway Lake	7.7	4600	Bird and others (1991)
Nicholson Lake	8.5	4650	Bronge (1989)

3.3.2 New observations

Collection of cores

In November and December 1991 several lakes in the Vestfold Hills were studied by a field party from the ANU Research School of Earth Sciences as part of the ANARE programme. Using a hammer-type piston corer, sediment cores were recovered from seventeen lakes (Figure 3.9) with sill heights ranging from just above sea-level to ~40 m a.s.l. (Table 3.6). Cores could only be taken from lakes with a solid ice cover, which provided the

platform from which to operate the corer. Lakes with salinity too high to form a solid ice cover were not sampled, eg the extremely hypersaline lakes in "Death Valley". On fresh-water lakes the ice was usually ~2 m thick, and a motor-driven auger was used to make a hole through which the corer was lowered. When possible, cores were taken from the centre of the lake basin, in an attempt to avoid cores with breaks in sedimentation. This sometimes resulted in very thin lacustrine sequences, since algal growth is often greatest close to shore, where a moat of open water often occurs in summer even if the lake does not become completely ice-free (D. Gillieson, pers. comm.). The apparatus was limited to ~35 m water depth, so cores from Watts, Scale, Druzhby and Clear Lakes were not taken from the deepest part of the basin. However, the cores from these lakes give no indication that sedimentation was interrupted. Cores were generally not examined in the field, but were sealed in the core barrel and frozen as soon as possible to prevent movement of sediment within the core during transportation. Unfortunately, on return to Australia, the cores were allowed by the courier to thaw during transport to Canberra, so some soft sediment may have been lost. However, the core stratigraphy appears to be intact in all cases, indicated by lamination of sediments. All cores were logged and refrozen before sampling. Samples were taken from the middle of the core, to avoid material which may have been contaminated by sediment movement during coring or transport.

Sill heights were measured using a theodolite and electronic distance meter (EDM), using the benchmarks installed in the Vestfold Hills by the Australian Division of National Mapping between 1979 and 1986. Two closed traverses between benchmarks indicate that surveyed heights are accurate to within 5 cm. Since sills were not usually on bedrock, the height could have changed slightly due to sediment movement since the sea was at that level. However, most lakes do not presently overflow their sills, and there is no evidence of significant sediment movement (stream deposits, deltas etc.) in the region of the sill. The change in sill height is probably only a few tens of centimetres at most. Sill heights are quoted to the nearest 10 cm.

Core stratigraphy and sediment characteristics

The stratigraphy of each core is given in Table 3.7. Three sediment types were observed in the cores, similar to those found in cores from other Antarctic oases such as the Larsemann Hills (Gillieson 1991), King George Island (Mausbacher and others 1989) and the Windmill Islands (Goodwin 1993):

1) Till:
The lowermost unit in many cores is a dark-grey, plastic, clay-rich sediment containing a variable amount of coarser sandy sediment and occasional pebbles up to several centimetres in diameter. It is characterised by both low water and low organic carbon content, although near the top of the unit it

may be interbedded with more organic-rich algal layers. The unit generally becomes more compact with depth, and usually limited the depth to which it was possible to drive the corer.
This sediment is considered to be reworked glacial till, washed into the lake basins from the drift deposits which would have covered the Vestfold Hills after the last retreat of ice cover. Deposition may have occurred at the time the lake basins were filling with early postglacial meltwater, so the boundary between 'till' and overlying lake sediment is sometimes transitional.

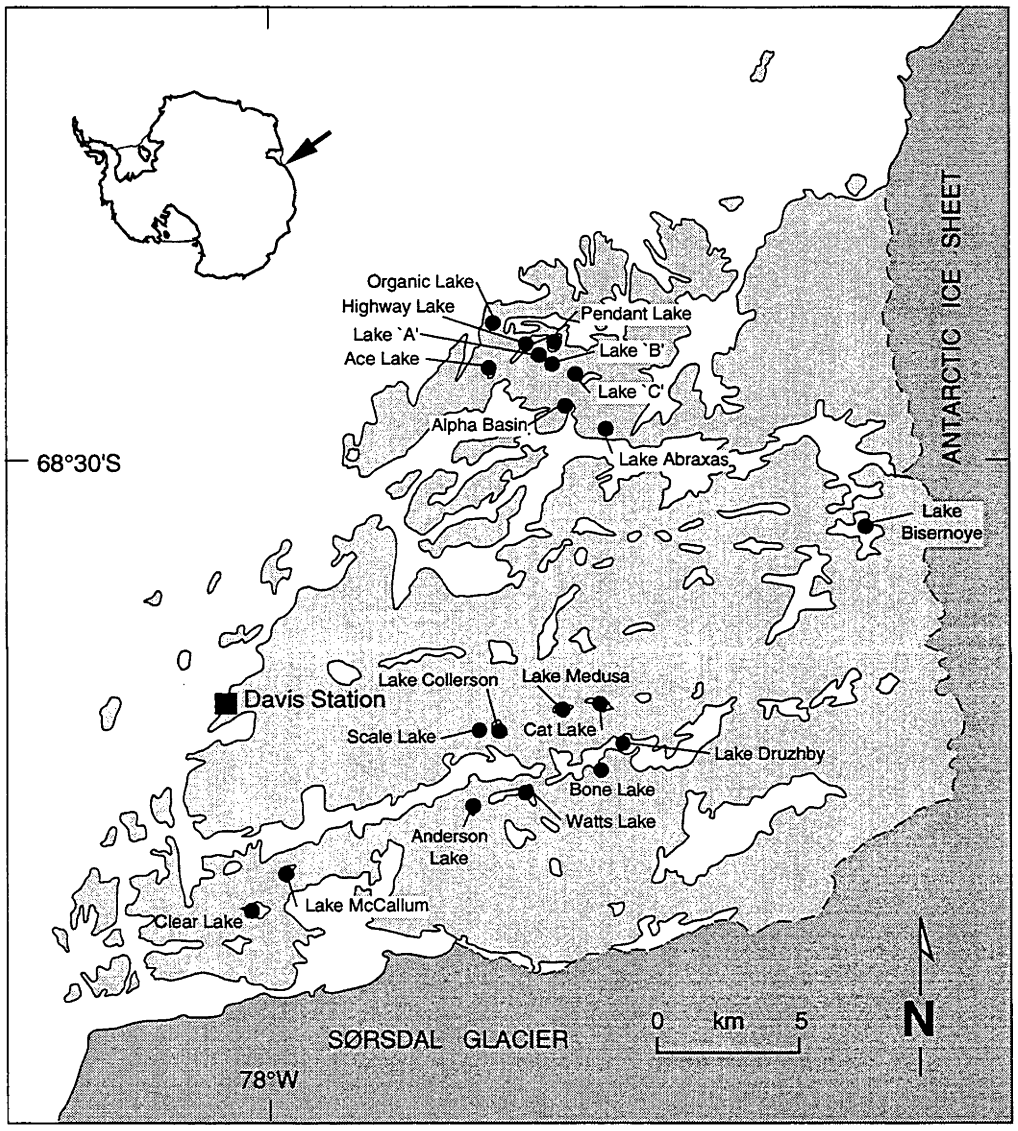

Figure 3.9 : Location map of the Vestfold Hills showing locations of lakes cored for this study (Table 3.6).

Table 3.6: Location and characteristics of lakes cored in the Vestfold Hills, November and December 1991. †Locations are given as grid references on the 1:50,000 map sheet "Vestfold Hills" published by the Australian Division of National Mapping, September 1982 (second edition). ‡ This is the water depth where the core was taken, not the maximum lake depth. §Where numerical values are given, salinity was determined by conductivity measurements (unpublished measurements compiled at Davis Station). Ranges apply where salinity is stratified within the lake. * From Bird and others (1991).

Lake	Location†	Sill height (m)	Water depth‡ (m)	Salinity§
Alpha Basin	875008	~0	8.5	saline
Pendant	870030	3.1	17	13.2 - 17.5 ‰
Organic*	848034	3.5	7.5	176 - 250 ‰
Watts	886873	4.3	33	slightly saline
Bisernoye	982970	4.9	15	fresh
Highway*	863026	7.7	15	8 - 10 ‰
Druzhby	889885	8.0	25	fresh
Anderson	849869	8.4	13	31.8 - 132.3 ‰
Ace*	847017	8.8	25	28 - 40 ‰
Bone	893880	~9	1.6	fresh
"B"	868022	12.4	6.2	fresh
Abraxas	889000	13.5	22.5	<20 ‰
McCallum	842788	13.9	32.5	<24 ‰
"C"	881015	14.5	5	fresh
Clear	776830	16.4	27	4.9 - 8.2 ‰
"A"	865024	19.2	4.3	fresh
Collerson	857895	26.9	10.5	6.5 - 7.8 ‰
Cat	891901	40+	17.8	slightly saline
Medusa	877902	40+	20.4	3.2 - 4.2 ‰
Scale	859892	40.2	12.5	saline

2) Algal lake sediment:
The unit found at the top of each core is characterised by high organic carbon (10 - 15%) and high water content, with a variable but generally small amount of clay- to sand-sized clastic inorganic material. In fresh to moderately saline lakes, the organic matter occurs as green and black laminated algal mats or masses of filamentous moss. These beds sometimes contain white flecks of biogenic carbonate, and may be interbedded with clay- to sand-sized clastic layers.
In hypersaline lakes, the organic-rich units tend to be diffusely laminated or structureless. These units vary in colour from green to black and may contain abundant authigenic mirabilite or gypsum.
This unit represents the current sedimentation in the lakes cored. The variation in style of sediment reflects the variation in salinity of the lakes, which range from completely fresh (eg Lake Druzhby) to hypersaline (eg Anderson Lake).

3) Marine sediment:
These units are generally homogeneous along their length, consisting of black, watery, diffusely banded organic-rich (1 - 5%) sediment with a low clastic content. The colour changes to light green on oxidation. Fine laminations were sometimes visible. These sediments are identical in character to those found in marine inlets in the Vestfold Hills (Bird and others 1991), and contain diagnostic marine diatoms (Lewis 1994).
These sediments are thought to have been deposited during times of higher relative sea-level, when the lake basins were occupied by the ocean as bays or fjords connected to the open sea by shallow sills in the same manner as Ellis Fjord is today.

The subdivision of marine and lacustrine sediments based on sediment characteristics, as described above, is supported by detailed diatom stratigraphy obtained for the Anderson Lake core (Lewis, 1994). Diatom populations determined for each 2 cm interval of the core show that below 105 cm the diatom assemblage is dominated by the freshwater genus *Pinnularia spp.*. Between 105 cm and 37 cm, freshwater varieties are absent and the assemblage is dominated by the cysts of the marine genus *Chaetoceros spp.* and the valves of the marine species *Nitzschia cylindrus, Nitzschia curta, Centrales* and *Eucampia antarctica.* Above 37 cm the most abundant diatom is the non-marine genus *Navicula spp.*. This matches closely the sedimentological interpretation shown in Table 3.7.

The base of the Ace Lake core was also examined for diatoms to ascertain whether a lower marine interval existed immediately above the till unit. Some abraded valves of marine/estuarine species were found (A. McMinn, pers. comm.) which is interpreted to indicate that the lake basin was not marine, but open marine conditions existed nearby, allowing some valves to be transported by wind into the lake basin.

Table 3.7 Descriptions of cores taken from lakes in the Vestfold Hills, November and December 1991. †Ace Lake core description from Bird and others (1991).

Lake	Interval (cm)	Sediment type	Description
Pendant	0 - 150	marine	Homogeneous, watery, diffusely-banded algal sediment with low clastic content. (note: top of core not recovered)
Watts	0 - 14	lacustrine	Green/black laminated algal mat material, lamination becoming less distinct towards base.
	14 - 269	marine	Structureless watery dark green algal sediment with low clastic content. Diffuse green/black bands occur from 140 to 212 cm, and sediments become more prominently banded below 254 cm.
Druzhby	0 - 30	lacustrine	Black/green laminated algal mat material, low clastic content.
	30 - 233	marine	Homogeneous, watery, green/black algal sediment, low organic content.
Anderson	0 - 20	lacustrine	Diffusely-banded watery clastic-poor green/black algal material.
	20 - 35	lacustrine	As above with ~5 mm gypsum crystals.
	35 - 43	transitional	Finely laminated grey-green algal sediment.
	43 - 103	marine	Structureless watery black/green algal material, low clastic content, laminated below 101 cm.
	103 - 111	lacustrine	Organic-rich laminated sediment with abundant filamentous algae and some carbonate.
	111 - 135	till	Structureless dark grey clay, becoming gritty and pebbly towards base.
Ace†	0 - 35	lacustrine	Black and reddish black laminated algal material with occasional light <0.5 mm carbonate-rich bands.
	35 - 130	marine	Watery, diffusely banded green sediment.
	130 - 185	lacustrine and till	Black in the upper portion, laminated algal material similar to unit 1, with occasional carbonate-rich bands. Changing gradually over ~15 cm to grey laminated algal material with progressively fewer algal laminations and more fine clastic material down the core. From 170 to 180 cm there is very little macroscopic algal material and the sediment is predominantly composed of grey silt-sized clastic material.
Abraxas	0 - 64	lacustrine	Alternating bands of green/black laminated algal mat material and lighter coloured carbonate-rich algal mat material. Abundance of carbonate decreasing towards base of unit.
	64 - 92	lacustrine	Structureless light to dark green algal-rich sediment becoming laminated and carbonate-flecked towards base.
	92 - 115	lacustrine	Green/grey mixed algal mat material and clay, occasionally gritty.
	115 - 137	lacustrine	Laminated green/grey clay with some algal mat laminations.
	137 - 179	lacustrine and till	Laminated grey clay, laminations becoming less distinct towards base. Becomes more gritty below 155 cm and abundant pebbles up to 3 cm diameter occur below 168 cm.

Table 3.7 (continued)

Lake	Interval (cm)	Sediment type	Description
McCallum	0 - 25	lacustrine	Structureless gelatinous green/black algal sediment.
	25 - 54	lacustrine	Diffusely laminated bands of green/black algal material and sandy to muddy clastic material.
	54 - 60	lacustrine	Grey sandy clay with some interbedded algal mat material.
	60 - 78	lacustrine	Green/black algal mat material with abundant lenses of grey clay.
	78 - 91	lacustrine	Grey sandy clay, with some possible algal fragments.
	91 - 100	lacustrine	Grading into finely laminated grey sandy clay.
	100 - 130	till	Structureless grey sandy clay with occasional pebbles.
Clear	0 - 55	lacustrine	Green/black laminated algal mat and filamentous algal material with occasional muddy or sandy bands and flecks of biogenic carbonate.
	55 - 88	lacustrine	Transition to mud containing strands and wads of filamentous algae.
	88 - 169	till	Structureless sandy grey clay with occasional pebbles up to 3 cm diameter. No visible organic matter, diffusely laminated from 105 to 110 cm.
"A"	0 - 96	lacustrine	Black/green laminated algal mat material, low clastic content, some biogenic carbonate towards bottom of interval.
	96 - 120	till	Dark grey clay becoming gritty and pebbly towards base.
Collerson	0 - 72	lacustrine	Green/black laminated algal mat sediment with filamentous algae below 45 cm, clastic-poor with some carbonate at 45 cm.
	72 - 74	lacustrine	transition to dark grey clay
	74 - 104	till	Grey clay, becoming gritty towards base with occasional pebbles. Abundant strands of filamentous algae down to 92 cm.
Cat	0 - 42	lacustrine	Watery green/black laminated algal mat and filamentous algal material. Occasional coarse clastic material.
	42 - 50	lacustrine	Muddy grey clay with fragments of filamentous algae.
	50 - 71	till	Plastic grey clay, gritty in places with occasional small pebbles. Diffuse laminations towards base.
Medusa	0 - 44	lacustrine	Strongly laminated green/black algal mat material, some carbonate towards base
	44 - 48	lacustrine	Light grey clay with layers of filamentous algae
	48 - 110	till	Light grey clay with occasional bands of algal material down to 70 cm, grading into dark organic-poor clay occasionally gritty with some pebbles near base.
Scale	0 - 89	lacustrine	Green/black laminated algal mat material, clastic-poor.
	89 - 93	lacustrine	Laminated dark grey algal-rich clay.
	93 - 140	till	Dark to light grey clay with occasional bands of filamentous algae in upper part. Becoming gritty with occasional pebbles towards base.

Interpretation

All cores show organic lacustrine sediment at the top, except Pendant (top of core not recovered), Alpha Basin (still connected to the sea) and Bisernoye (inorganic clastic sediment at top). Lakes can be subdivided according to the underlying sediment: one class (eg Watts, Druzhby) has a thick bed of marine sediment extending to the bottom of the core. These lakes have sills below 8.0 m. A second class (Anderson and Ace) penetrated marine sediment underlain by an older lacustrine sequence and till. Both these lakes have sills between 8 and 9 m. A third class of lakes, with sills above 13.5 m contain continuous sequences of lacustrine sediment underlain by till.

The presense of marine sediments in all cores from lakes with sills below ~9 m indicates that sea-level has been at least 9 m above its present level at some time in the period represented in the cores. Similarly, the absence of any marine sediment in cores from lakes with sills higher than 13.5 m indicates that sea-level has not stood this high in the period represented. Two lakes with sills between 9 m and 13.5 m (Lake "B" and Bone Lake) are too small to produce useful sedimentation records. Radiocarbon ages from the cores, presented and discussed below, indicate the duration of marine sedimentation in the various lakes.

In the core from Anderson Lake, the unit of marine sediment lies between two lacustrine layers, indicating that the lake existed before invasion by rising sea-level and was subsequently isolated when relative sea-level fell again (see Figure 3.3). This configuration is also seen in a core from Ace Lake (Bird and others 1991), which has a sill height of 8.8 m. This pattern of sea-level change is due to an oscillation in sea-level caused by the interaction between postglacial "eustatic" sea-level rise (ocean volume increase), and the isostatic response to changing ice and water loads (Figure 3.3). This interaction is discussed in Part 2 of this study.

The transition from marine to lacustrine sediment is commonly, though not always, gradational. The nature of the transition probably reflects the nature of the evolution of the lake water after isolation from the sea. In most cases, the process of isolation from the sea would have been gradual, with the lake basin progressing from being permanently linked to the sea, through periods as a tidal lagoon and as a low-lying lake intermittently connected to the ocean during the highest tides and storms, to eventually become a completely isolated body of water. The nature of the transition for each lake is dependent on the rate of emergence, the morphology of the connecting sill, the amount of fresh water input to the lake, and the environmental and climatic conditions at the time of isolation. Most of these factors are difficult to constrain, but the effect of fresh-water input can be seen in Lake Druzhby. Here, the large flow of fresh water from the Druzhby drainage system (Adamson and Pickard 1986) ensured that the transition to fresh water would have been made rapidly, and this is reflected

in the sharp sediment boundary. In most cases however, the transition is taken as the first occurrence of layered algal material.

Dating the marine-lacustrine transitions

Radiocarbon dates obtained from the cores from the Vestfold Hills lakes are presented in Table 3.8. All samples were processed by the ANU Quaternary Dating Research Centre. Samples labelled "AMS" were measured by accelerator mass spectrometry by the Nuclear Physics Department of the Research School of Physical Sciences and Engineering, at the ANU. Samples were chosen in order to determine the ages of marine-lacustrine and lacustrine-marine transitions, and the onset of organic sedimentation. The onset of sedimentation is not directly relevant to the relative sea-level record, and is discussed in more detail in the next chapter, where evidence regarding the history of the ice sheet is presented.

The simplest transition age to estimate is that of the lower, lacustrine-marine, transition, since the fresh-water material below the transition is uncontaminated by marine carbon and hence does not require a reservoir correction. Two or more age determinations made from this section allow the sedimentation rate to be estimated, and the age of the transition calculated by extrapolation.

The age of the upper, marine-lacustrine transition can be estimated by extrapolating the age of a dated lacustrine sample downwards to the transition. Several properties of the core must be assumed: sedimentation within the upper section must have been at a constant rate between dated samples, and without significant breaks. Compaction must be uniform, and material must not have been lost from the top of the section during coring if this part of the core is used to determine the sedimentation rate. Cores were taken from the deepest part of lake basins, where possible, to maximise the chance of constant sedimentation, and the water depth was sounded before each core was taken, in order to ensure that the uppermost sediment was sampled.

Even if a sample was taken adjacent to the transition, some extrapolation is required, since a length of core must be sampled in order to submit enough carbon for dating. The age obtained is assigned here to the mid-point of the dated interval. In principle, the "average" age does not apply to the middle of the interval but rather to a point slightly higher, since ^{14}C activity decreases exponentially with depth, but this effect is negligible. Non-uniform distribution of carbon within the sampled length will also alter the depth to which the age should apply. In this study, core-lengths required for dating varied from ~3 - 6 cm of organic-rich lacustrine sediment to 10 - 15 cm of marine sediment and ~20 cm of organic-poor till. There is a trade-off between errors when choosing the sample size, as decreasing the length of core dated reduces the errors due to extrapolation, but increases the uncertainty of the radiocarbon measurement.

Table 3.8: Conventional radiocarbon ages obtained from cores from lakes in the Vestfold Hills. †M = marine sediment; L = lacustrine sediment; T = "till"; l-m = marine→lacustrine transition; m-l = lacustrine→marine transition. ‡Dates from Bird and others (1991).

Lake	ANU No.	Age (^{14}C-yr BP)	Depth (cm)	Description†
Pendant	8392	3040 ± 200	0 - 10	M, top of core
Watts	AMS-334	3250 ± 340	13 - 14	L, above m-l transition
	8391	4540 ± 200	10 - 14	L, above m-l transition
	8146	4890 ± 300	254 - 269	M, base of core
Druzhby	8147	5240 ± 200	25 - 30	L, above m-l transition
	8148	7490 ± 230	213 - 233	M, base of core
Anderson	8446	6730 ± 200	38 - 43	at m-l transition
	8349	7110 ± 210	103 - 107	L, below l-m transition
	8145	8450 ± 210	107 - 111	L, lowest organic-rich
Ace	6414‡	5310 ± 90	20 - 35	L, above m-l transition
	6419‡	6110 ± 180	35 - 75	M, below l-m transition
	8263	6740 ± 230	135 - 140	L, below l-m transition
	8166	8380 ± 110	160 - 175	L, below l-m transition
"A"	8235	6710 ± 240	93 - 96	L, lowest algal-rich
Abraxas	8347	8030 ± 540	92 - 98	L, organic-rich
McCallum	8817	4970 ± 90	22 - 29	L, organic-rich
	8818	4610 ± 170	44 - 50	L, organic-rich
	8348	9620 ± 110	72 - 78	L, lowest organic-rich
	AMS-321	12570 ± 400	86 - 91	T, humic acid fraction
	8550	12850 ± 360	102 - 124	T, bulk sediment
	AMS-322	19700 ± 560	124 - 130	T, humic acid fraction
Clear	8346	7810 ± 210	50 - 55	L, lowest algal-rich
	AMS-324	20900 ± 540	130 - 141	T, near base of core
Collerson	8264	9210 ± 250	67 - 73	L, lowest algal-rich
Cat	8266	8170 ± 200	35 - 42	L, lowest algal mat
Medusa	8265	7780 ± 250	41 - 46	L, lowest organic-rich
Scale	8819	4100 ± 110	20 - 26	L, organic-rich
	8820	7180 ± 130	60 - 65	L, organic-rich
	8847	8840 ± 100	86 - 91	L, organic-rich
	8549	9290 ± 260	96 - 106	T, bulk sediment
	AMS-337	9500 ± 390	106 - 121	T, algae from till
	8549	13130 ± 280	106 - 121	T, bulk sediment
	8267	20870 ± 470	120 - 140	T, bulk sediment

Although no reservoir correction is required for modern algae from lakes in the Vestfold Hills, the lacustrine sediment immediately above the marine-lacustrine transition may have grown from a carbon pool which was largely marine in origin. These ages may therefore require a reservoir correction of up to 1300 years (Adamson and Pickard 1986), although this should decrease progressively above the transition as the marine carbon reservoir became exhausted and the lake achieved equilibrium with the atmosphere. In meromictic lakes (lakes with a basal layer which does not mix with the

upper part) the influence of marine carbon is expected to be significant for a longer period of time after isolation than if the lake is fully mixed. This is the case for several lakes from which cores were taken: Abraxas, Ace, Anderson, Clear, McCallum and Pendant Lakes are all meromictic.

The age of the transition can also be calculated from the marine section of the core if more than one age is measured, allowing the sedimentation rate to be estimated. This method has not been relied upon here since it is simpler to use dates from the lacustrine units, but the transition age estimates for Highway and Organic Lakes (Bird and others 1991) were, in part, calculated this way. Transition age estimates based on radiocarbon ages from marine sediment also have to include the reservoir correction. Dates from modern shells of *Laternula elliptica* (Adamson and Pickard 1986) and from the offset across the marine-lacustrine transition in lake cores (Bird and others 1991) indicate that this correction is 1000 - 1300 years (Table 3.2). Estimates based on the extrapolation of lacustrine and modern marine sediment ages to the top of the core (Bird and others 1991) suggest that the correction may be as high as 2500 years This is inconsistent with the maximum reservoir correction estimated by Stuiver and others (1981) and is probably due to the loss of sediment from the tops of these cores.

Using the principles outlined above, age ranges for the lacustrine-marine and marine-lacustrine transitions in lakes of the Vestfold Hills have been estimated, and these are presented in Table 3.9.

Table 3.9: Ages of marine-lacustrine transitions in lakes in the Vestfold Hills, including the reservoir correction and measurement errors. †M = estimated from ages of marine sediment; L = estimated from ages of lacustrine sediment; l→m = lacustrine to marine transition; m→l = marine to lacustrine transition. ‡Dates from Bird and others (1991).

Lake	Sill height (m)	Transition†	Lower bound (yr BP)	Upper bound (yr BP)
Organic‡	3.5	m→l (M)	3040	3890
		m→l (L)	2730	3060
Watts	4.3	m→l (L)	3430	3830
Highway‡	7.7	m→l (M)	4320	5190
		m→l (L)	4280	4520
Druzhby	8.0	m→l (L)	5500	5940
Anderson	8.4	l→m (L)	6020	6860
		m→l (M)	5090	5920
Ace	8.8	l→m (L)	6350	6860
		m→l (M)	4140	4960
		m→l (L)	5000	6870

Sea-level history of the Vestfold Hills

The relative sea-level history of the Vestfold Hills over the last ~7000 years is tightly constrained by the new lake isolation observations (Figure 3.10). In particular, the existence of a sea-level maximum during the Holocene is demonstrated for the first time in a sea-level record from Antarctica.

The sea-level curve for the Vestfold Hills shown in Figure 3.10 is consistent with all the lake isolation observations. It is noticeable, however, that the curve intersects the younger extremity of the possible period interpreted for the marine-lacustrine transitions in Watts and Druzhby Lakes; that is, these lakes appear to have been isolated earlier than expected for lakes at their respective altitudes. This can be explained by the observation that the largest fresh-water drainage in the Vestfold Hills currently enters Ellis Fjord via Lake Druzhby, and also flowed through Watts Lake at the time it was isolated from the sea (Pickard and others 1986). The flushing effect of this large fresh water input to the lake basins seems to have advanced the apparent marine-lacustrine transition in the sediments by 200-400 years.

In the last 4 kyr, the minimum transition ages for Watts and Organic Lakes indicate that some of the *Laternula elliptica* samples which are currently 2 - 3 m a.s.l. (Table 3.4) grew very close to sea-level. This is somewhat at odds with modern observations, which suggest that *Laternula* grows mainly below 3 m depth (Colhoun and Adamson 1992). Apart from this, the sea-level record derived from lake isolations is consistent with all earlier constraints (Table 3.4).

The marine - lacustrine transition ages from the higher lakes show a well-defined sea-level highstand at ~6200 yr BP. The absolute constraints on the elevation of this highstand are only that it was higher than 8.8 m (Ace Lake) and lower than 13.5 m (Lake Abraxas), but the shape of the sea-level curve suggests that the maximum was probably 9 - 9.5 m a.s.l.. Before ~7 ka, the relative sea-level curve is only constrained by limiting observations: basal ages from Anderson and Ace Lakes show that sea-level was below ~8.5 m for the period ~10 ka - 7 ka. There is no evidence that sea-level ever stood higher than ~9.5 m a.s.l. in the time since deglaciation.

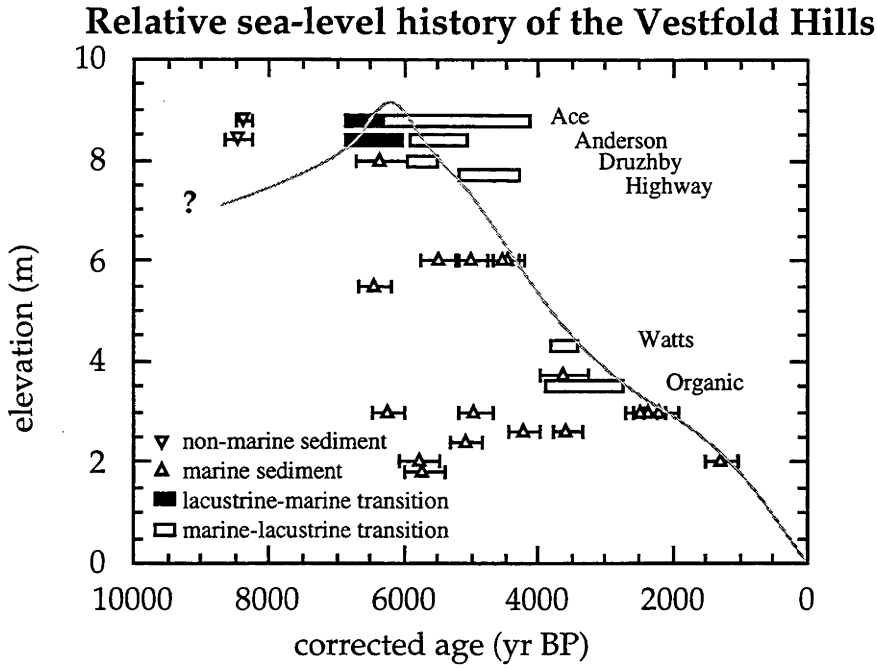

Figure 3.10 : The relative sea-level history of the Vestfold Hills, based on lake isolation observations. This is the best constrained sea-level record from Antarctica, and the first to observe a Holocene sea-level maximum.

3.4 Victoria Land

Victoria Land (Figure 3.11) borders the western side of the Ross Embayment, which is filled by the Ross Ice Shelf south of about 78° S. From McMurdo Sound (78°S 163°E) to Cape Adare (71°30'S 170°24'E), ~700 km of coast is exposed to the open sea during the summer months, allowing the development of coastal landforms on those parts of the coast which have exposed rock. Research has been concentrated in the McMurdo Sound region, which was the base for the British expeditions early this century and has hosted New Zealand and American bases in the modern era of research since 1957.

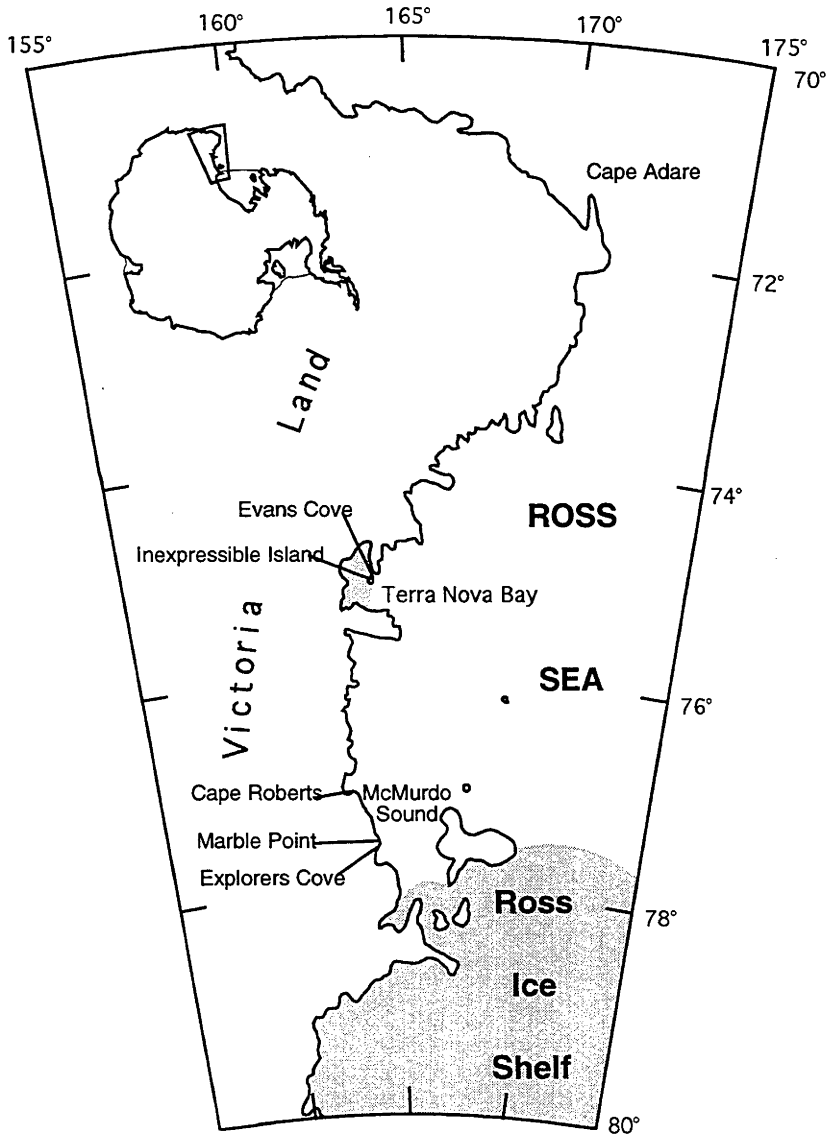

Figure 3.11 : Location map for Victoria Land, showing locations mentioned in the text.

3.4.1 McMurdo Sound region

Nichols (1968) recorded the elevations of beaches in the McMurdo Sound area, but did not obtain enough radiocarbon dates to infer a relative sea-level history. He noted that the marine limit was constant at ~20.4 m over the 48 km between Cape Roberts and Marble Point. He obtained an age of 4600±200 ^{14}C-yr BP (L-594, Lamont) from an elephant seal buried in a beach ~13.4 m a.s.l. at Marble Point, which provides a good estimate for the age of that beach, since the seal was presumably buried by wave action shortly after it died. This provides one point on the relative sea-level curve. If the seal died above sea-level and was subsequently buried by sediment movement, then this observation provides an upper limit for sea-level at that time.

Stuiver and others (1981) presented the evidence for deglaciation and sea-level change in the Ross Embayment. The elevation of drift deposits from the former ice sheet show that McMurdo Sound was filled with grounded ice up to 700 m thick. Isostatic rebound must have occurred due to removal of the ice, which would be recorded by raised beaches if environmental conditions were suitable. In southern McMurdo Sound, Holocene shells are present in sediments on the surface of the McMurdo Ice Shelf, which, together with algal deposits in the mouths of the Dry Valleys, show that grounded ice had retreated from that region by 6600±60 ^{14}C-yr BP (Stuiver and others 1981). The absence of raised beaches south of Explorers Cove reported by Stuiver and others (1981) must therefore be due to the lack of environmental conditions which would allow the formation of beaches.

Raised beaches from the Victoria Land coast north of Explorers Cove provide some evidence for higher shorelines in the past, although they have provided generally poor constraints on sea-level change so far. This is because dateable material from these deposits is restricted to marine material such as shell fragments incorporated into the ridge, and post-depositional, non-marine remains such as penguin rookeries. These materials only provide upper and lower limits to the age of the beach ridge itself, and a large number of radiocarbon ages are required to constrain sea-level change.

All but one of the radiocarbon ages obtained from raised marine sediments in McMurdo Sound at Explorers Cove and South Stream (Table 3.10) fall in the range 5000 - 6500 ^{14}C-yr BP (Stuiver and others 1981). These two sites are only ~15 km apart, and the data sets can be treated together since sea-level variation over this distance is expected to be smaller than the resolution of the available observations. Most of these ages are obtained from the unbroken and sometimes articulated shells of the free-swimming scallop *Adamussium colbecki*. Modern samples of this species have been dated at 850±50 and 990±50 ^{14}C-yr BP (samples QL-948 and QL-996, Stuiver and others 1981), which indicates a reservoir correction around 900 years, which is lower than the reservoir correction estimated from other marine organisms in the same region. Freshwater algae found in the marine sediments, which were presumably eroded by South Stream and deposited close to shore, were also dated, yielding younger ages (Table 3.10). The ages of these transported

algal deposits represent maximum ages for the beds which contain them. Modern freshwater algae were not dated by Stuiver and others (1981), so it is not clear whether a reservoir correction is required. However, dead algae returned ages as young as 350±80 years, providing a maximum limit for the correction. It is possible that no correction is required, as is the case for freshwater algae in the Vestfold Hills (see discussion at the beginning of this chapter).

Table 3.10: Radiocarbon ages from emerged marine sediments in McMurdo Sound. From Stuiver and others (1981).

Sample code	age (^{14}C-yr BP)	elevation (m)	description
Samples from emerged marine deposits near the mouth of South Stream			
QL-70	5930±200	6.6	algae
QL-71	6010±70	8.1	algae
QL-1041	5280±400	9.3	algae
QL-72	6430±70	6.0	*A. colbecki*
QL-96	6350±60	4.5	*A. colbecki*
QL-1042	6120±50	4.0	*A. colbecki*
Adamussium colbecki from emerged marine deposits at Explorers Cove			
QL-164	5760±60	0.5	
QL-160	5770±50	0.5	
QL-155	5310±60	1.0	
QL-153	5200±60	1.4	
QL-161	5500±70	1.7	
QL-159	5350±70	1.9	
QL-156	5090±50	2.2	
QL-165	4620±60	2.9	
QL-154	5630±60	3.3	
QL-158	5860±70	4.2	
QL-157	6150±80	4.5	
QL-139	5240±40	5.0	
QL-162	5970±70	5.3	
QL-137	6050±70	5.7	
QL-138	5800±70	7.5	
QL-163	5400±60	8.1	

It is not clear why all the marine sediments sampled, which are found at a range of elevations, produced similar ages in the range 5 - 6.5 ka. Possibly the region experienced a critical warming at that time, allowing significant fluvial erosion and hence deposition of a relatively large volume of sediment in a short period of time. If this is the case, it is still not clear why deposition rates have decreased, since there is an abundant supply of unconsolidated till in the catchment of South Stream. In any case, the temporal clustering of samples from emerged marine sediments in McMurdo Sound means that a full relative sea-level record cannot be

obtained. Rather, the data provide a lower bound for the sea-level curve for a period of ~1500 years in the mid-Holocene. The highest dated deposit is of algae, at 9.3 m a.s.l., although the bed which contains the sample collected at 8.1 m (QL-71) was traced to 10.4 m a.s.l. (Stuiver and others 1981). This implies a relative sea-level of more than 10.4 m at some time since 6010±70 ^{14}C-yr BP. The highest dated shell is from 8.1 m a.s.l. (QL-163), with an age of 5400±60 ^{14}C-yr BP (corrected age 4480±90 yr BP). This height also represents a lower limit to sea-level at that time, although it may have been much higher, depending on the depth at which the shellfish grew. Stuiver and others (1981) report that *Adamussium colbecki* currently lives on the floor of Explorers Cove at depths greater than 4 m, and is most common at 25 m. Using 4 m as the minimum depth at which sample QL-163 lived, and a reservoir correction for *A. colbecki* of 920±120 we conclude that sea-level at 4480±180 yr BP was more than 12.1 m above its present level. This minimum estimate is very close to the estimate from the dated elephant seal at Marble Point, the cape immediately north of South Stream (Nichols 1968), and these points constrain the upper limit of the sea-level envelope shown in Figure 3.12. The lower bound of the envelope is obtained by assuming that both the shell sample and the highest bed containing algae were deposited very close to sea-level.

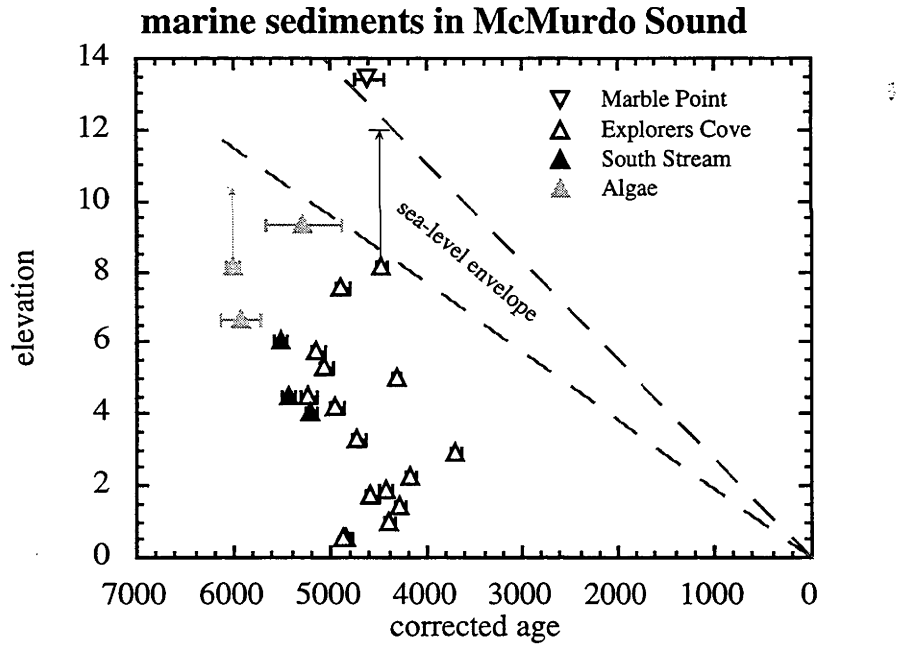

Figure 3.12 : Sea-level curve for McMurdo Sound, based on the dated samples of Stuiver and others (1981) and Nichols (1968). Upright triangles represent lower limits to sea-level; inverted triangles represent upper bounds. The estimated growth depth is indicated for the highest shell sample from Explorers Cove, as is the highest elevation of the bed which contained algal sediments. Because of the clustering of sample ages, the inferred sea-level curve is poorly constrained.

3.4.2 Terra Nova Bay

At Terra Nova Bay (74° 50' S 163° 30' E), in northern Victoria Land, Baroni and Orombelli (1991) determined more than 40 radiocarbon ages from marine shells and penguin remains collected from raised beaches, to obtain lower and upper bounds on the relative sea-level curve. As in the Vestfold Hills and McMurdo Sound, the elevation of dated *in situ* pelecypod shells, including *Laternula elliptica* and *Adamussium colbecki*, provide a lower limit for sea-level at that time. Shells collected from the surface of the beaches are thought to be transported, most likely by katabatic winds that transported shell fragments upslope from the surface of the adjacent Hells Gate ice shelf (Baroni 1990). Similar shell material is currently found on the surface of the ice shelf, where it is exposed by ablation of the ice after being incorporated in the basal layer of the ice at the grounding line. These reworked samples supply a minimum age for the beach on which they are found. Penguin remains and organic ornithogenic soils (guano) were also sampled and dated, providing an upper limit to the sea-level curve. Since the penguin rookeries must have been at least 1 - 2 m above sea-level when active, these samples were assigned the elevation of the first beach ridge below the sample site as an estimate of the maximum contemporary sea-level (Baroni and Orombelli 1991).

Following the radiocarbon calibration system of Stuiver and others (1986) described at the beginning of this chapter, Baroni and Orombelli (1991) estimate $\Delta R = 779 \pm 60$ years. This value is used to produce the calibrated ages shown in Table 3.11.

The sea-level envelope interpreted by Baroni and Orombelli (1991) from these data (Figure 3.13) has a decaying exponential form, and has been extrapolated beyond the constraints of the radiocarbon data until it intersects with the marine limit at ~30 m. Using this curve, they estimated the age of the beaches which form the marine limit. The lower limiting curve implies an age of about 7500 yr BP, which is close to that of the oldest dated material (sample GX-14069: calibrated age 7231 yr BP). The extrapolation of the upper limiting curve implies an age of about 6500 yr BP. On this basis, Baroni and Orombelli (1991) suggest that the real sea-level curve is close to the lower limit. However, this conclusion is not justified. The decaying exponential form is a reasonable description of the component of sea-level change due to isostatic rebound, but until at least 6 ka the melting of northern hemisphere ice sheets also made a significant contribution. The total sea-level change due to these, and other, components may have a more complicated form, and it is not obvious that the exponential form of the sea-level curve can be applied before 6 ka. Thus, it is possible that the marine limit in Terra Nova Bay is older than proposed by Baroni and Orombelli (1991).

Table 3.11: Radiocarbon ages from penguin remains and emerged marine sediments in Terra Nova Bay. From Baroni and Orombelli (1991).

Laboratory number	Conventional age (^{14}C-yr BP)	Calibrated age		Height (m)	Location
Shells collected at the surface of raised beaches					
GX-13626	2395 ± 60	1166	(+105,-91)	3.5	Evans Cove
GX-14101	2710 ± 135	1483	(+173,-157)	8.0	Evans Cove
GX-14073	3010 ± 150	1826	(+206,-193)	6.0	Evans Cove
GX-14065	3235 ± 155	2093	(+203,-216)	8.0	Evans Cove
GX-13628	3335 ± 90	2252	(+173,-77)	8.0	Evans Cove
GX-14071	3545 ± 150	2462	(+163,-257)	6.5	Evans Cove
GX-14068	4360 ± 175	3460	(+191,-229)	14.5	Evans Cove
GX-14077	4370 ± 170	3467	(+168,-222)	22.0	Evans Cove
GX-14619	4485 ± 300	3619	(+350,-410)	18.5	Evans Cove
GX-14067	4885 ± 155	4146	(+237,-253)	10.5	Evans Cove
Pelecypod shells found *in situ* in marine sediments					
GX-14825	6620 ± 190	6272	(+253,-187)	10.5	Evans Cove
GX-14627	6645 ± 95	6285	(+106,-114)	10.5	Evans Cove
GX-14824	6765 ± 355	6405	(+416,-404)	9.5	Evans Cove
GX-13627	6815 ± 90	6450	(+121,-159)	9.0	Evans Cove
GX-14628	6890 ± 100	6542	(+133,-137)	12.5	Evans Cove
GX-14066	6915 ± 230	6600	(+301,-239)	10.5	Evans Cove
GX-14823	6935 ± 100	6615	(+166,-114)	9.0	Evans Cove
GX-14070	7480 ± 260	7185	(+286,-234)	12.5	Evans Cove
GX-14069	7505 ± 230	7231	(+242,-188)	14.5	Evans Cove
Penguin remains and guano from ornithogenic soils on raised beaches					
GX-13613	3010 ± 220	1826	(+286,-273)	20.7	Inexpressible Island
GX-13616	3340 ± 85	2264	(+165,-65)	6.2	Inexpressible Island
GX-13617	3675 ± 90	2703	(+214,-56)	14.0	Inexpressible Island
GX-12757	4190 ± 80	3301	(+136,-80)	14.0	Inexpressible Island
GX-12758	4930 ± 85	4226	(+157,-163)	26.0	Inexpressible Island
GX-13609	5315 ± 100	4797	(+238,-52)	20.7	Inexpressible Island
GX-13608	5360 ± 90	4817	(+178,-52)	20.7	Inexpressible Island
GX-13610	5440 ± 85	4857	(+48,-132)	19.7	Inexpressible Island
GX-13611	5530 ± 100	4979	(+140,-240)	19.7	Inexpressible Island
GX-13614	5945 ± 340	5551	(+492,-348)	20.7	Inexpressible Island
GX-13612	6235 ± 110	5866	(+167,-83)	19.7	Inexpressible Island
GX-13615	6335 ± 110	5932	(+93,-157)	20.7	Inexpressible Island
GX-13620	4615 ± 85	3805	(+166,-104)	15.0	Gondwana Station
GX-12760	5770 ± 60	5307	(+53,-132)	18.0	Terra Nova Station

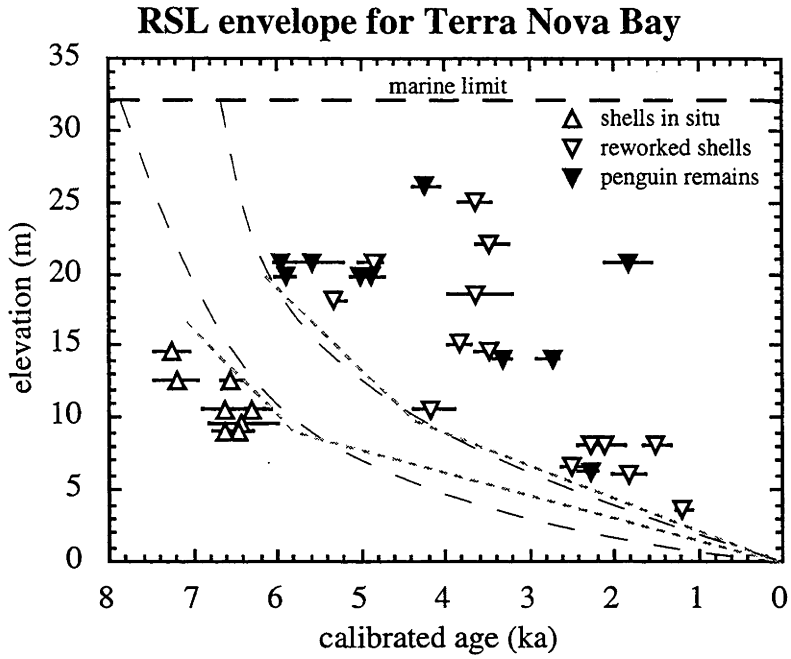

Figure 3.13 : Sea-level curve for Terra Nova Bay, based on the observations of Baroni and Orombelli (1991). Upright triangles represent lower limits to sea-level; inverted triangles represent upper bounds. The thin black dashed lines are the sea-level envelope proposed by Baroni and Orombelli (1991), who assumed a decaying exponential form. The grey dashed lines are the sea-level envelope that can be deduced without prior assumptions.

3.4.3 Marine limits

Mabin (1986), Kirk (1991) and Colhoun and others (1991) compiled observations of raised beaches along 700 km of central and northern Victoria Land coast, in the western Ross Sea, as shown in Figure 3.14. Very few dates are available from these sequences, so the marine limit was used by these authors as an indication of rebound due to deglaciation. As discussed earlier, this cannot lead to unambiguous conclusions, since the variation in beach heights could be due either to a) spatially variable emergence rates (due to the distribution of ice removed since the LGM), or b) differing lengths of exposure to open-sea conditions following deglaciation. An example of scenario b) has been demonstrated in the McMurdo Sound region by Stuiver and others (1981). Rejecting this interpretation of the McMurdo Sound observations and using the scenario a), Kirk (1991) concludes from the variation in the marine limit that there were two centres of ice removal on the Victoria Land coast. He places one centre of former ice thickening between Cape Ross and Terra Nova Bay, and another at Cape Adare, in the far north.

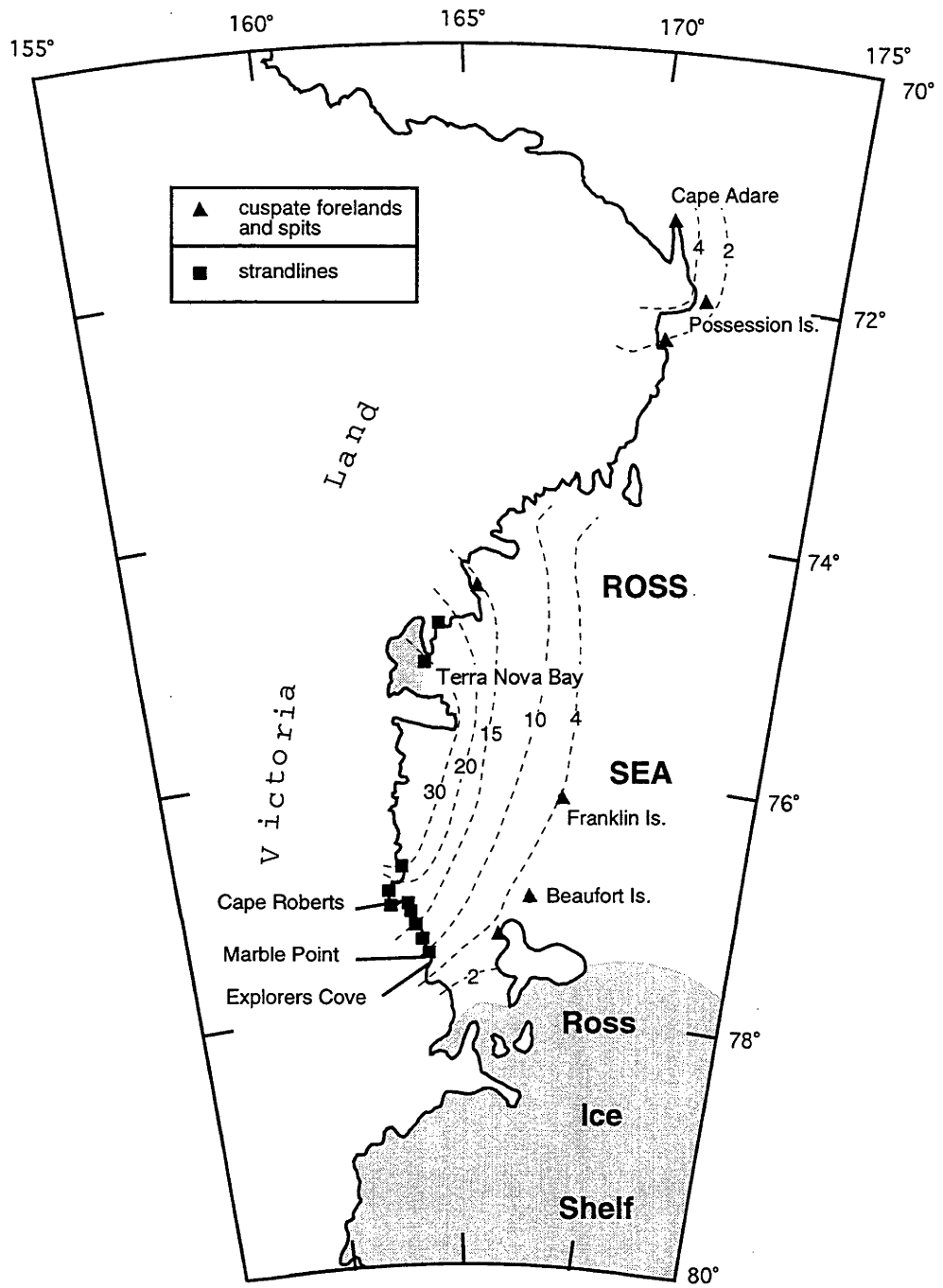

Figure 3.14 : Elevation of the marine limit in Victoria Land, from Kirk (1991).

3.4.4 Miscellaneous sea-level observations

The observations at McMurdo Sound and Terra Nova Bay provide sufficient information to constrain the sea-level curve for the late Holocene, at least. Isolated observations are available from a few other sites in the Ross Sea which cannot presently be used to infer a sea-level history, but may be useful later for testing the predictions of numerical models of deglaciation.

Colhoun and others (1991) present elevations and minimum ages for some raised beaches in the Ross Sea. On Franklin Island (~76° S) a beach 4 m above the modern shore has a minimum age of 3690±80 corr. ^{14}C-yr BP (NZ-6397, 1090 yr reservoir correction applied). Cape Adare, in the far northwestern Ross Sea, has a beach at 4.5 m a.s.l. with a minimum age of 2680±150 corr. ^{14}C-yr BP (NZ-6096, 1090 yr reservoir correction applied).

3.5 Windmill Islands

The Windmill Islands are a group of ice-free islands and peninsulas at the eastern edge of Vincennes Bay, around 110 ° E (Figures 3.1 and 3.15). They are due west of Law Dome, on the Budd Coast, and are the site of Australia's Casey Station (66°17' S, 110° 32' E).

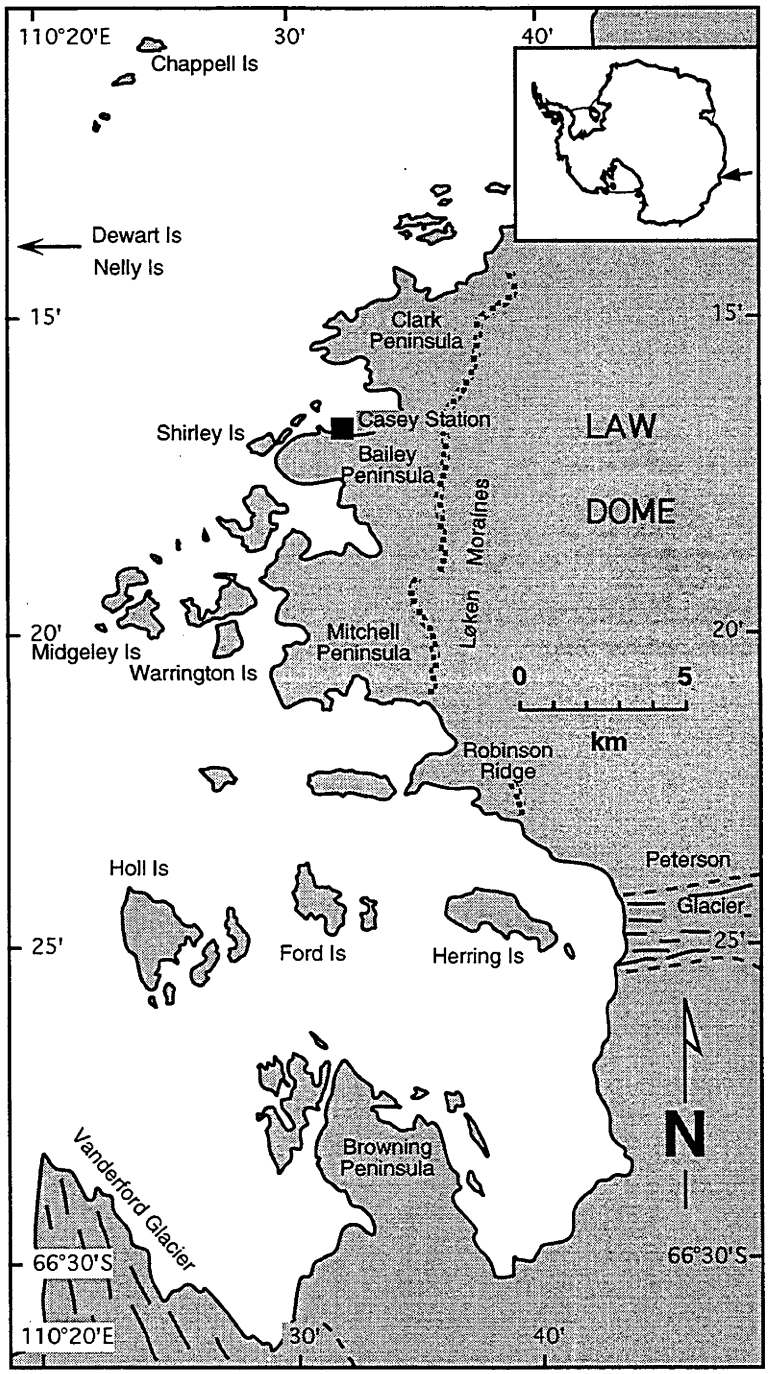

Figure 3.15 : Location map for Windmill Islands, showing locations mentioned in the text.

Published relative sea-level observations from this region prior to 1993 are restricted to one observation: a radiocarbon age of 6040±250 ^{14}C-yr BP (M-1052) from coraline algae on a beach 23 m a.s.l. (Cameron 1964). In this part of Antarctica the marine reservoir correction is ~1300 yr (Colhoun and Adamson 1992).

3.5.1 Marine limits

Goodwin (1993) collected and compiled observations of emerged beaches and wave-washed platforms throughout the Windmill Islands, and concluded that the marine limit increases by about 5 m over 30 km, from ~27 m in the north of the region to ~32 m in the south (Table 3.12). Radiocarbon ages from pond sediments in the south of the region returned maximum ages of around 8000 ^{14}C-yr BP (corrected), whereas those from the north have a maximum of around 5500 ^{14}C-yr BP.

Although only 5 ages were determined, Goodwin (1993) interprets these as ages of deglaciation, which qualitatively explains the trend in the marine limit, if sea-level was falling throughout that time period. If this is the case, then the emergence rate over the period of time between 8000 and 5500 ^{14}C-yr BP was ~2 mm/yr, significantly less than the rate of ~4.9 mm/yr since 5000 yr BP implied by the date from Cameron (1964) above. This is not a meaningful conclusion, however, since the sea-level curve over this period is unlikely to be linear, due to the complex interaction of isostatic rebound, ocean refilling, and water loading (see Chapter 5 for a discussion of these contributions).

An alternative explanation is that the variation in radiocarbon ages is due to poor sediment preservation or insufficient sample coverage of the region. The similarity in the elevation of the marine limit at sites throughout the region indicates that deglaciation was roughly contemporaneous at all sites (within ~1000 years), and application of the emergence rate of 4.9 mm/yr to

Table 3.12: Marine limit observations from the Windmill Islands. From Goodwin (1993).

Location	Elevation (m)	Feature	Source	Method
Chappell Is.	27.8±1.3	Beach	Løken, 1957	Optical level
N. Clark Pen.	26.7±0.5	Beach	Goodwin, 1987	Optical level
Nelly Is.	29.0±1.3	Wave-washed bedrock	Hollin, 1958	Hand level
Dewart Is.	29.0±1.3	Beach	Goodwin, 1987	Hand level
Baily Pen.	29.5±0.5	Ice-push ridge	Goodwin, 1987	Optical level
Shirley Is.	29.3±0.5	Beach	Goodwin, 1987	Optical level
Mitchell Pen.	28.1±1.0	Wave-washed bedrock	Løken, 1957	Optical level
Warrington Is.	27.5±1.0	Beach	Løken, 1957	Optical level
Midgeley Is.	28.1±1.0	Beach	Løken, 1957	Optical level
Robinson Ridge	28.5±1.0	Beach	Løken, 1957	Optical level
Ford Is.	28.9±1.0	Wave-washed bedrock	Løken, 1957	Optical level
Holl Is.	31.5±1.5	Wave-washed bedrock	Hollin, 1958	Optical level
Herring Is.	32.0±1.0	Beach	Hollin, 1958	Optical level
Browning Pen.	31.3±1.0	Wave-washed bedrock	Hollin, 1958	Optical level

the ~30 m marine limit suggests that this was about 6100 ^{14}C-yr BP. This is in good agreement with the result from the Vestfold Hills. Whether the trend in the marine limit is due to differential uplift or differing deglaciation time cannot be determined without better age control. However, assuming that the marine limit is contemporaneous throughout the region, the implied differential uplift of ~0.17 m/km is similar to those predicted by appropriate glacio-hydro-isostatic models (see Chapter 7).

3.5.2 Lake sediment cores

Goodwin (1993) collected sediment cores from three lakes below the marine limit. Two of these, Mitchell Pond B on Western Mitchell Peninsula, and Shirley Pond on Shirley Island, exist in depressions bounded by raised beach deposits. The radiocarbon dates obtained from the basal sediments in each pond, shown in Table 3.13, provide minimum ages for the beach ridges. A reservoir correction is not required if the lakes have never undergone a marine incursion.

Table 3.13: Radiocarbon ages from sediments in lakes in the Windmill Islands bounded by raised beach ridges. From Goodwin (1993).

Location	Elevation (m)	Radiocarbon age (^{14}C-yr BP)	Lab. number
Mitchell Pond B, Western Mitchell Peninsula	23.7	2410±70	ANU-6400
Shirley Pond, Shirley Island	25.5	2770±100	ANU-6398

The other pond, Holl Pond A on Holl Island, is bounded by a bedrock depression and lies at an elevation of 28 m (lake surface) in a location where the marine limit is 31.5±1.5 m. As the sill joining this lake to the sea lies at ~29 m (Goodwin 1993), this basin may contain sediments from a marine incursion. A 30 cm core taken from the shore of Holl Pond A ends in gravelly black mud. The basal 5 cm returned a radiocarbon age of 8160±300 ^{14}C-yr BP (ANU-6401). Goodwin (1993) applies a non-marine reservoir correction of 450-700 years, although several studies show that no correction is required, especially in shallow, well-mixed lakes such as Holl Pond A (this chapter, Adamson and Pickard 1986).

If these basal sediments are in fact non-marine and no correction is applied, then this date shows that deglaciation of Holl Island had taken place before 8160±300 ^{14}C-yr BP, and that relative sea-level, which once stood as high as 31.5±1.5 m a.s.l. (Goodwin 1993) had already fallen below 29 m. This interpretation is supported by the observation that similar sediments were found in a core from Holl Lake, also on Holl Island, which lies above the marine limit.

If, on the other hand, the basal sediments from Holl Pond A are marine, then a different relative sea-level history is implied. Applying the standard

marine reservoir correction of 1300 yr, the age of the basal sediments becomes 6860±300 corr. ^{14}C-yr BP, at which time sea-level must have been above 29 m.

Sea-level observations for the Windmill Islands are compiled in Figure 3.16. Neither of these cases contradicts the other relative sea-level observation from the Windmill Islands of >23 m at 4740±250 corr. ^{14}C-yr BP (Cameron 1964), although it is noted that using the latter case (ie. the sediments are marine) the two points are nearly collinear with the origin. The relative emergence rate, however, need not have remained constant, so this is not a constraint on the validity of this interpretation.

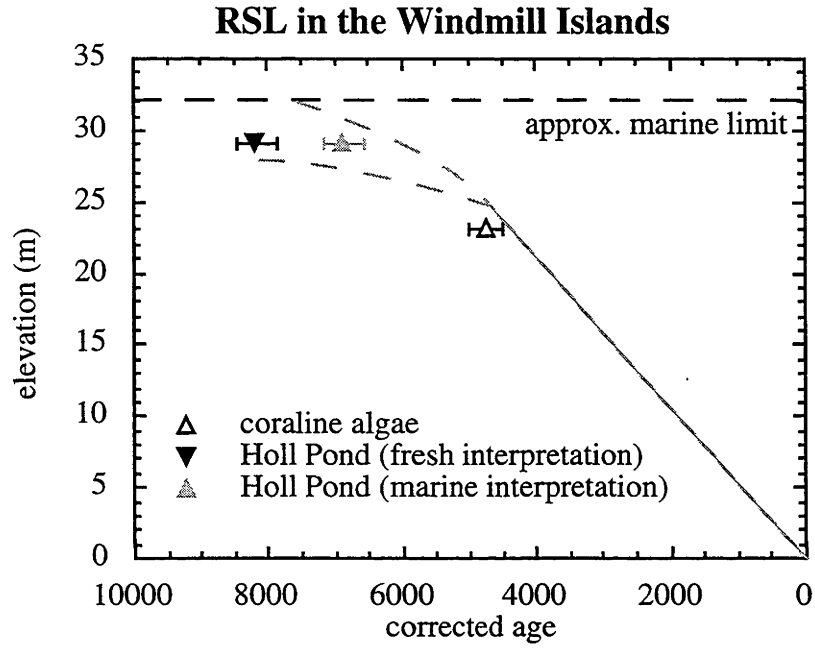

Figure 3.16 : Sea-level curve for Windmill Islands, constrained by the observations of Cameron (1964) and Goodwin (1993). Upright triangles represent lower limits to sea-level; inverted triangles represent upper bounds. The sample from Holl Pond may be either an upper or lower limit to sea-level, depending on whether it is freshwater or marine sediment, which has not been determined.

3.6 Bunger Hills

The Bunger Hills are the largest coastal Antarctic Oasis, situated at 66° 10' S, 101° E (Figure 3.1). Exposed parts of the low peninsulas and islands which form the oasis experience open-sea conditions for about two months during summer (Colhoun and Adamson 1992), but are isolated from the Antarctic Ocean by the Shackleton Ice Shelf, which is pinned on Mill Island and the Highjump Archipelago.

Bolshiyanov and others (1991) recorded terraces with marine sediments as high as 40 m. These sediments contained foraminifera and sponge spicules, but no radiometric or stratigraphic age determinations have been reported from the higher terraces. Valves of *Laternula elliptica* from sediments forming terraces at 5 - 7 m were dated at 5480±40 ^{14}C-yr BP (LU-2292). The sample height is not given, but is presumably below the level of the terraces themselves. This sample thus constrains sea-level to have been at or above 5 m at 4180±40 corr. ^{14}C-yr-BP (1300 yr reservoir correction applied).

Colhoun and Adamson (1992) surveyed the elevations of raised beaches throughout the Bunger Hills, and concluded that the "best estimate of higher relative sea-level for the region is 7.5±1 m, although they record beach and ice-push features up to 10.5 m a.s.l.. Ice-pushed boulder ridges attributed to present-day sea-level were found to at least 1.75 m above the modern high water mark (which was used as the datum for all observations), so the actual sea-level represented by the higher features may be this much less than their reported elevation. They also note that Lake Polest, which has a surface elevation of 6 m and is linked to the sea by a sill at 12 m, has saline water (Kaup and others 1989) consistent with marine incursion followed by isolation from the sea due to isostatic uplift. Beaches occur above Lake Polest at 20 m and 23 m a.s.l., but these may be due either to higher sea-levels or glacial damming of the lake. In the absence of other unequivocal marine beaches at such altitude in the Bunger Hills, Colhoun and Adamson (1992) suggest the latter interpretation.

Shell fragments in raised beach sands and *in situ* valves of *Laternula elliptica* from emerged marine sediments at several locations were dated in an attempt to constrain the age of the marine limit (Colhoun and Adamson 1992). While the *in situ* shells provide a reliable lower limit to sea-level, the shell fragments are all from beaches at or below 3 m a.s.l., and may include material from shells which grew either above or below their present position which has become incorporated in beaches either by erosion of formerly submarine sediments as sea-level fell or raised by basal freezing of sediments onto sea ice which was then driven onto land. Thus the ages of these shell fragments do not constrain the relative sea-level curve, except in that they indicate that the coast was free of grounded ice at that time. Furthermore, the fragments dated may be mixtures of shells of different ages, though this is unimportant, as other evidence indicates that the region was ice-free throughout the Holocene (see Chapter 4).

The four ages from *in situ* marine shells (three from Colhoun and Adamson 1992, and one from Bolshiyanov and others 1991) can be used to constrain the relative sea-level curve. The sample elevation is a lower bound for sea-level at the time it grew, although *Laternula* usually grows in more than 3 m of water, which implies a lower limit this far above the sample position. These limits are indicated on Figure 3.17. The authors also recorded the highest beach elevation found near each dated sample of *in situ* shells. This is not necessarily related to the sea-level curve: sea-level at the time the shells grew could have been higher or lower than the highest preserved beach nearby. In any case, the curve obtained using these observations is roughly the same as the lower limit derived from the assumption that the shells grew in at least 3 m of water (Figure 3.17).

A useful upper limit to the relative sea-level curve has not been obtained for the Bunger Hills, as there are no reported radiocarbon ages on terrestrial material at relevant elevations.

Table 3.14: Radiocarbon ages from shells of the marine bivalve *Laternula elliptica* in emerged marine terraces in the Bunger Hills. References: 1 = Colhoun and Adamson (1992); 2 = Bolshiyanov and others (1991).

Material	Sample height (m)	Beach height (m)	Conventional age (^{14}C-yr BP)	Laboratory number	Ref.
Shell fragments	2.8	6.8	8950 ± 490	Beta 15828	1
Shell fragments	3.0	6.9	4960 ± 120	Beta 17526	1
Shells *in situ*	4.0	10.5	5630 ± 90	Beta 15830	1
Shell fragments	2.6	6.0	6010 ± 100	Beta 17525	1
Shell fragments	1.3	7.0	6210 ± 100	Beta 17524	1
Shell fragments	2.0	3.0	6880 ± 160	Beta 15831	1
Shell fragments	2.2	8.5	6500 ± 130	Beta 17527	1
Shells *in situ*	3.5	8.0	6900 ± 120	Beta 15829	1
Shells *in situ*	5.2	8.6	6250 ± 140	Beta 15832	1
Shells *in situ*	~5.0	7.0	5480 ± 40	LU - 2292	2

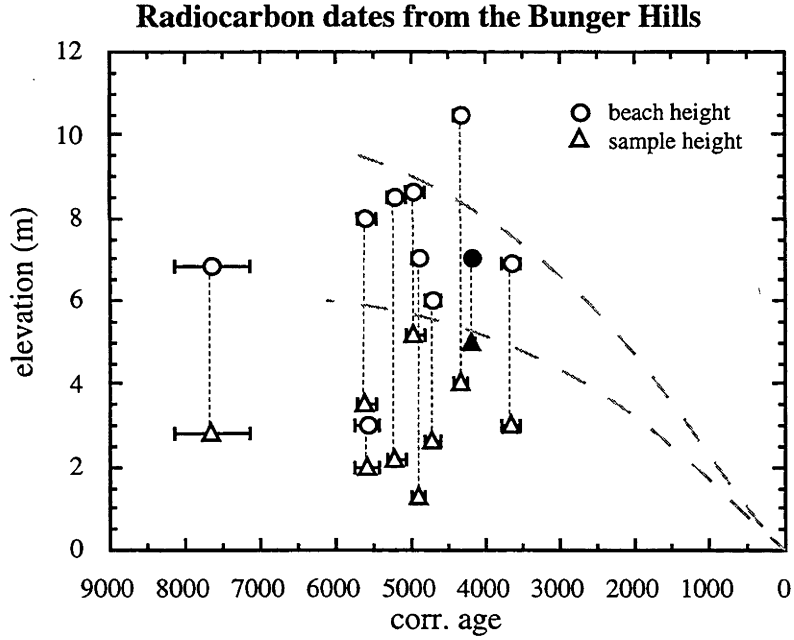

Figure 3.17 : Sea-level curve for the Bunger Hills, using the measurements of Colhoun and Adamson (1992) (open symbols) and Bolshiyanov and others (1991) (filled symbols). The sample height is indicated by an upright triangle, representing a lower limit to sea-level. The circles indicate the elevation of the beach associated with each sample, identified in the field by the respective authors. The dashed lines are estimates for the upper and lower bounds to the sea-level curve, assuming that the beach at 10.5 m has been incorrectly associated with the sample dated at that locality.

3.7 Larsemann Hills

The Larsemann Hills lie on the Eastern edge of Prydz Bay, about 100 km south of the Vestfold Hills (Figure 3.1). They extend along only ~10 km of coastline, and consist of numerous peninsula and low islands.

Diatom stratigraphy of sediment cores from two lakes in the Larsemann Hills (Gillieson and others 1990, Gillieson 1991) have been interpreted as a history of marine incursion and regression. In the core from Kirisjes Pond, which currently lies at less than 5 m a.s.l., a layer of marine sediment ~10 cm thick is sandwiched between two freshwater layers, with an increase in the number of marine species towards the top of the core in the upper freshwater unit. A radiocarbon age from the lower freshwater unit shows that the marine incursion occurred after 9410±180 ^{14}C-yr BP (SUA-2749). An age within the marine layer shows that marine conditions persisted until at least 4030±330 ^{14}C-yr BP (Beta-22253). Assuming a marine reservoir correction of 1000 - 1300 years, the inferred relative sea-level history of the Larsemann Hills is compatible with that of the Vestfold Hills, showing sea-level rise before 9 ka and sea-level fall in the late Holocene. However, the core is very short, with the lower dated sample coming from ~45 cm down the core, and the "marine" section extending only from ~20 to ~30 cm. This is inconsistent with observed marine sedimentation rates from the Vestfold Hills, which are about 0.5 m/kyr. Therefore it seems likely that the marine diatoms in the core represent periods of contamination due to inwashing of sea water and salt spray, and possibly episodic surges due to iceberg calving, which are mechanisms suggested by Gillieson (1991) explaining the presence of marine diatoms in the uppermost part of the core.

A similar core from Pup Lagoon, which lies virtually at sea-level, shows a freshwater unit overlain by a marine one. Since under present conditions salt water only enters Pup Lagoon as spray or in surges due to iceberg calving, presumably the marine layers in Kirisjes Pond can be explained in the same way.

3.8 Sôya Coast

The Sôya Coast lies along the eastern edge of Lützow-Holm Bay, around 69° S, 39°E (Figure 3.1). There are several small oases of rocky islands and peninsulas (Figure 3.18) where raised beachs with associated marine sediments and shell fragments preserve a record of postglacial sea-level change.

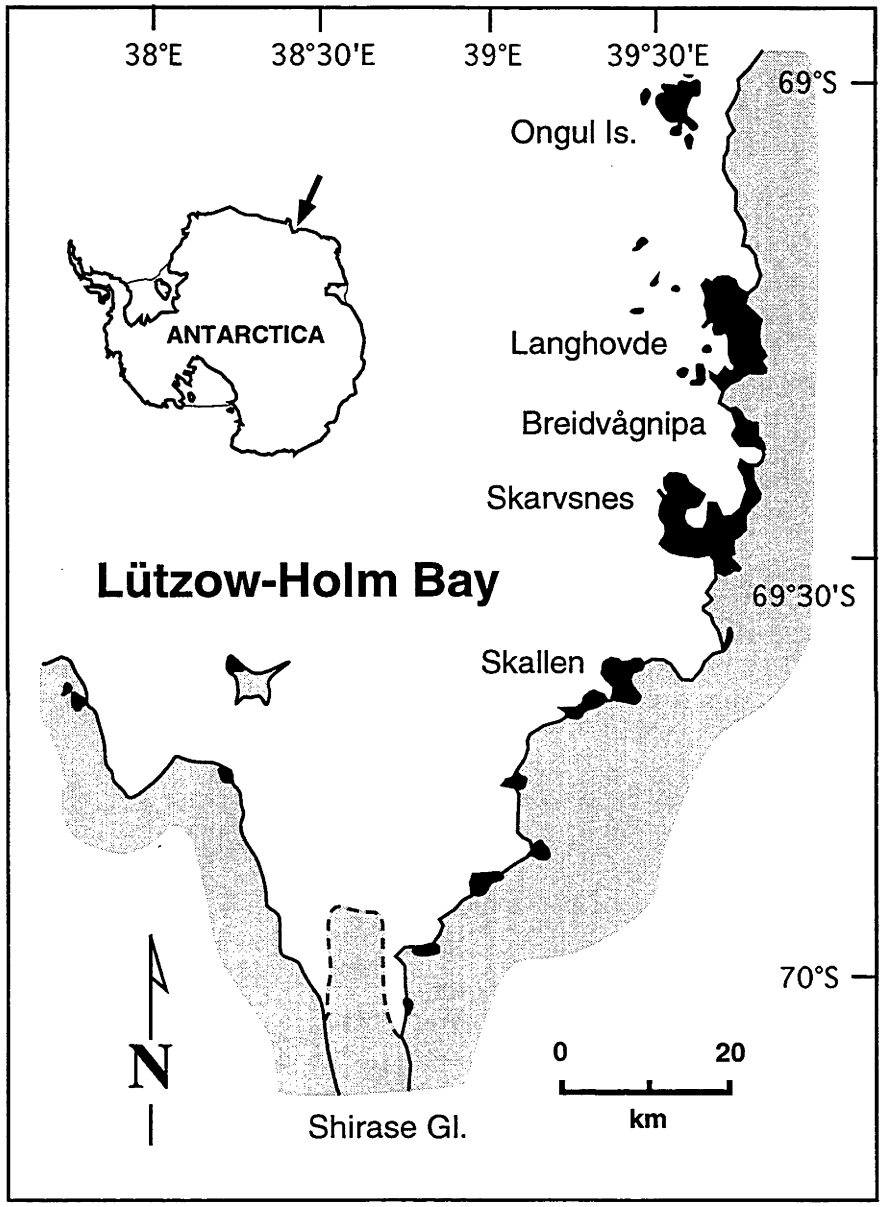

Figure 3.18 : Location map for Lützow-Holm Bay, showing locations mentioned in the text.

Meguro and others (1963) dated molluscan shell fragments from East Ongul Island, and found most samples older than the range of reliable radiocarbon dating. One sample of *Adamussium colbecki*, however, from 3 - 4 m a.s.l., returned an age of 3840±110 ^{14}C-yr BP.

Studying raised beaches at several sites in Lützow-Holm Bay, Yoshida and Moriwaki (1979) dated enough samples of emerged marine shells and worm tubes in growth position to produce a useful lower bound to the sea-level curve, showing a sea-level highstand of at least 16 m between 6000-7000 radiocarbon years ago, falling monotonically to the present. The presence of material older than 7000 years, but none higher than the 16 m highstand, suggests that this was in fact the maximum emergence, with lower sea-levels beforehand, though this is not conclusive. An upper bound to the sea-level curve can be derived from marine-lacustrine transitions in two lakes from the Skarvsnes area. Only initial results have been reported, without detailed stratigraphy or chronology (Hayashi 1994), which indicate that Lakes Suribati and Hunazoko, both with sill heights slightly over 10 m a.s.l., were isolated from the sea before 4000 and 1000 corr. ^{14}C-yr BP respectively. The relative sea-level curve for Skarvsnes based on these lower and upper bounds, is shown in Figure 3.19. The lake isolation data are compatible with the dates from emerged shells, although the date from Lake Hunazoko does not add a useful constraint.

Hayashi (1994) also presents marine limits for the oases of the Sôya Coast: Ongul Islands, 16 m; northern Langhovde, 20 m; southern Langhovde, 22 m; Skarvsnes, 23 m; and Skallen, 12 m. Except for Skallen, these increase towards the south, with a gradient of ~14 cm/km. However, there is no reason to believe that the marine limit should be contemporaneous between these sites, and the varying height of the marine limit probably reflects both varying uplift rates and times of ice sheet retreat.

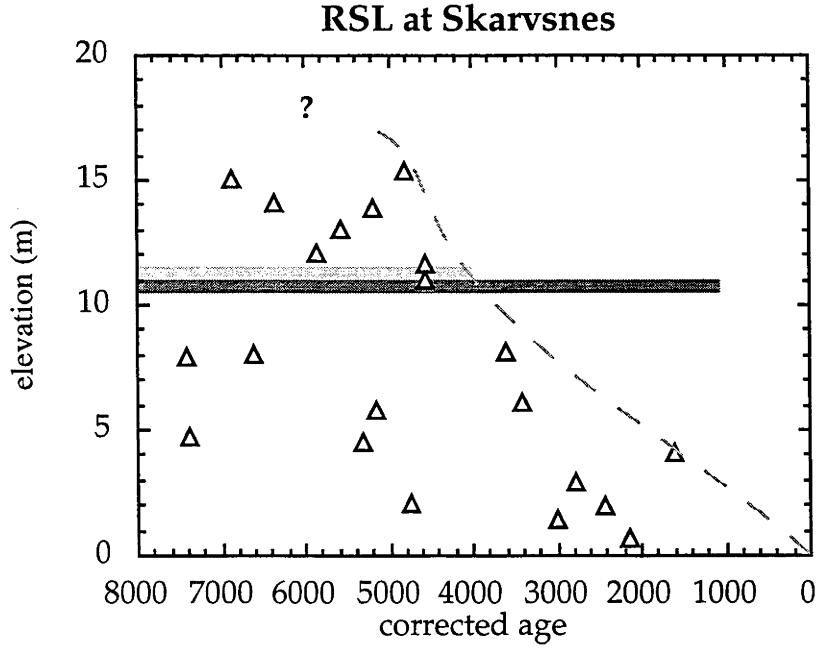

Figure 3.19 : Sea-level curve for Skarvsnes, in Lützow-Holm Bay. Samples are in situ marine shells and worm shells, dated by Yoshida and Moriwaki (1979). The shaded bars represent the possible age range of marine sediment in Lakes Suribati (dark grey)and Hunazoko (light grey), both with sill heights slightly over 10 m a.s.l. (Hayashi 1994). The dashed line is a reasonably well constrained estimate of the sea-level history of this location.

Other estimates of sea-level change from the Sôya Coast seem to have no relevance to the Holocene record. Odamaki and others (1991) measured sea-level at Syowa Station in the Ongul Islands over three decades from 1966 using tide gauges, and observed a trend showing sea-level fall at the rate of about 1 cm/yr from 1981 to 1987. This rate is too high to represent the average Holocene rate, and may be due to relatively short-term fluctuations or instrumental drift.

Similarly, measurements of ground tilt using a borehole tiltmeter over a nine month period showed an average tilt rate of ~8 μrad/yr towards the southwest, although the data seemed to be seriously affected by temperature variations (Kaminuma and others 1983). Extrapolated to the time of the mid-Holocene sea-level highstand, this tilt rate would result in ~50 m difference in the amount of uplift at sites 1 km apart. Clearly this is not realistic, and the measured rates are not representative of Holocene emergence.

3.9 Antarctic Peninsula

Adie (1963) recorded many wave-cut platforms and raised beaches in Graham Land on the Antarctic Peninsula (Figure 3.1), and on several sub-antarctic islands in that region. However, none of these sites are dated. In Graham Land he records several flights of raised beaches up to 50 m a.s.l., and possibly as high as 300 m. In the South Shetland Islands, too, he notes beaches up to at least 50 m a.s.l, though he only attributes those up to 30 m as due to "late isostatic phenomena related to deglaciation". In the South Orkneys and South Sandwich Islands he records maximum beach levels of 45 m and 20 m, respectively. On South Georgia, beach ridges occur up to 8 m, and wave-cut platforms up to 50 m a.s.l.

Nichols (1966) observed raised beaches up to 27 m a.s.l. in Marguerite Bay, but reported no ages for these features. Similarly, a marine limit of 18.6 m has been reported on Livingston Island in the South Shetland Islands (Lopez-Martinez and others 1992). Clearly, the Antarctic Peninsula region has experienced many changes in relative sea-level which are preserved in the geomorphology, but without age determinations these observations cannot provide useful constraints on the former glaciation and deglaciation of the region.

Useful constraints on the relative sea-level history of the region have been provided by Mäusbacher and others (1989), who collected sediment cores from four lakes on King George Island (62° S, 58° W) in the South Shetland Islands. Only one, Kiteschsee, 16 m a.s.l., contains a marine-lacustrine transition. Radiocarbon dates from above and below the transition both suggest that the transition occurred around 6200±200 yr BP (corrected age). A sediment core from another lake, Tiefersee, at 17.5 m, contained only fresh water sediment. Basal sediment from this core returned an age of 5380±165 ^{14}C-yr BP (HD 11420-11161) indicating that relative sea-level has been below that level since that time. The remaining lakes, Jurasee, at 47 m a.s.l. and Mondsee at 47.5 m, also contained no marine sediments, and portions were dated at 8700±300 ^{14}C-yr BP and 7200 years BP respectively, providing maximum limits for sea-level at those times. A lower bound on the relative sea-level history of King George Island comes from marine sediments at 16 m a.s.l which have been dated at 5900±90 yr BP (corrected age). The interpreted relative sea-level curve is shown in Figure 3.20. Although the maximum highstand is only constrained by limits at 18 m and 47 m, the absence of marine features above 19 m suggests that the actual sea-level highstand lies close to the lower limit (Mäusbacher and others 1989).

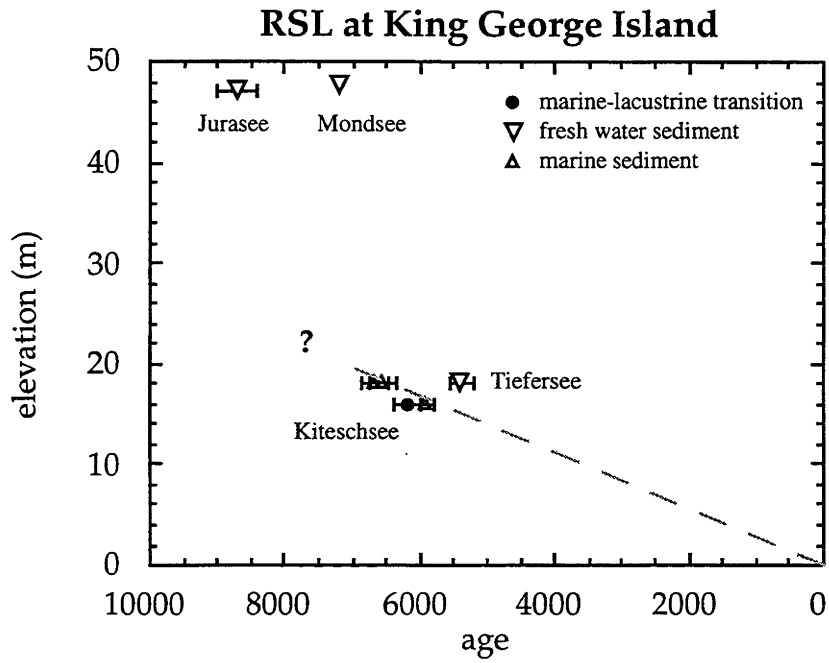

Figure 3.20 : Sea-level observations from King George Island (South Shetland Islands). Sea-level is well constrained by marine sediments and a lake isolation around 6 ka, but is otherwise unconstrained.

3.10 Summary

Summary diagrams of the relative sea-level histories of several Antarctic locations (Table 3.1) are compiled in Figure 3.21. The sea-level records around Antarctica all show the same general pattern of monotonic fall throughout the middle and late Holocene, presumably because of isostatic rebound of the land in response to deglaciation. In Part Two of this thesis we will examine the predicted response of the earth to changing ice loads, and used the observed sea-level records to constrain the size, distribution and melting history of the former ice sheet. Additional constraints will be provided by observations of the ice sheet itself, summarised in the next chapter.

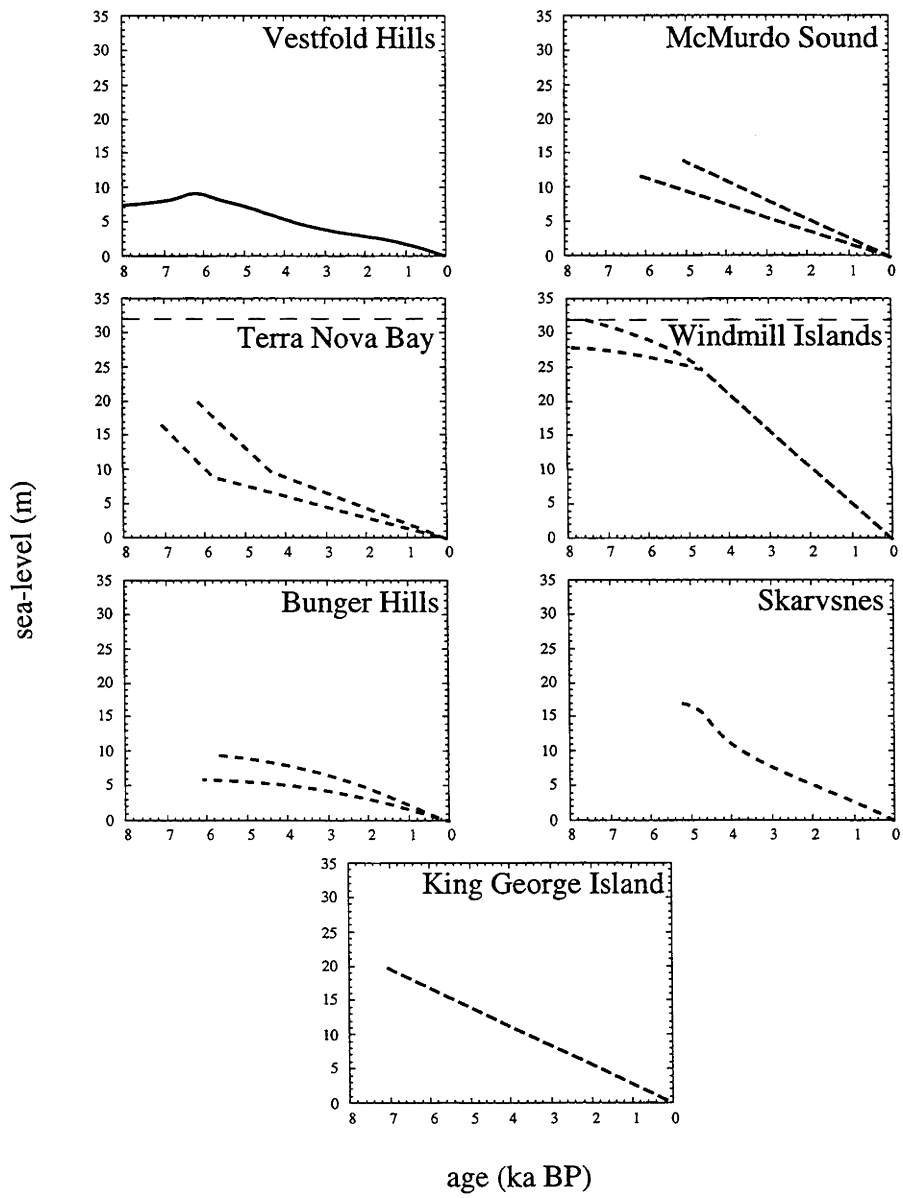

Figure 3.21 : Summary of sea-level observations for Antarctic sites discussed in this chapter.

Chapter 4

The Antarctic Ice Sheet

4.1 Introduction

In modelling the glacial rebound and sea-level change associated with the melting of an ice sheet, an essential requirement is a knowledge of the spatial and temporal evolution of the ice sheet over the time period of interest. For some of the former ice sheets located on continents, the ice sheet's history is often reasonably well constrained by a range of markers left as the ice retreated. This is the case, for example, for the southern margins of the Fennoscandian and Laurentian ice sheets. But where the ice formerly extended beyond the presently exposed continent, the evidence for the position of the former ice sheet margins is frequently much less satisfactory. This is the case in the Barents and Kara Seas in arctic Europe.

Likewise, the thicknesses of the former ice sheets can rarely be determined from direct observation. In some instances, mountains stood out through the ice as nunataks, and trim lines formed which indicate the former ice height. But for most of the larger ice sheets such information does not exist.

Reconstruction of the former ice sheets is therefore not usually based upon direct observation, but on reconstruction from proxy records subject to many considerations and inferences, including models of ice flow, models of ice sheet growth and decay, and models of glacial rebound.

This is particularly the case for Antarctica, where ice covering the continent persists at the present day and little direct evidence is preserved for either the extent or thickness of the former ice sheet. In consequence, estimates of the dimensions of this ice sheet during the last glacial maximum cover a wide range, dependant upon the assumptions made. For example, Hughes and others (1981) proposed a maximum ice sheet whose volume was ~45 % greater than the present ice volume, whereas Colhoun and others (1992) propose a maximum change of only ~3 %. This section reviews published estimates and presents new observations in an attempt to determine approximate bounds on ice sheet dimensions in latest Pleistocene and Holocene time.

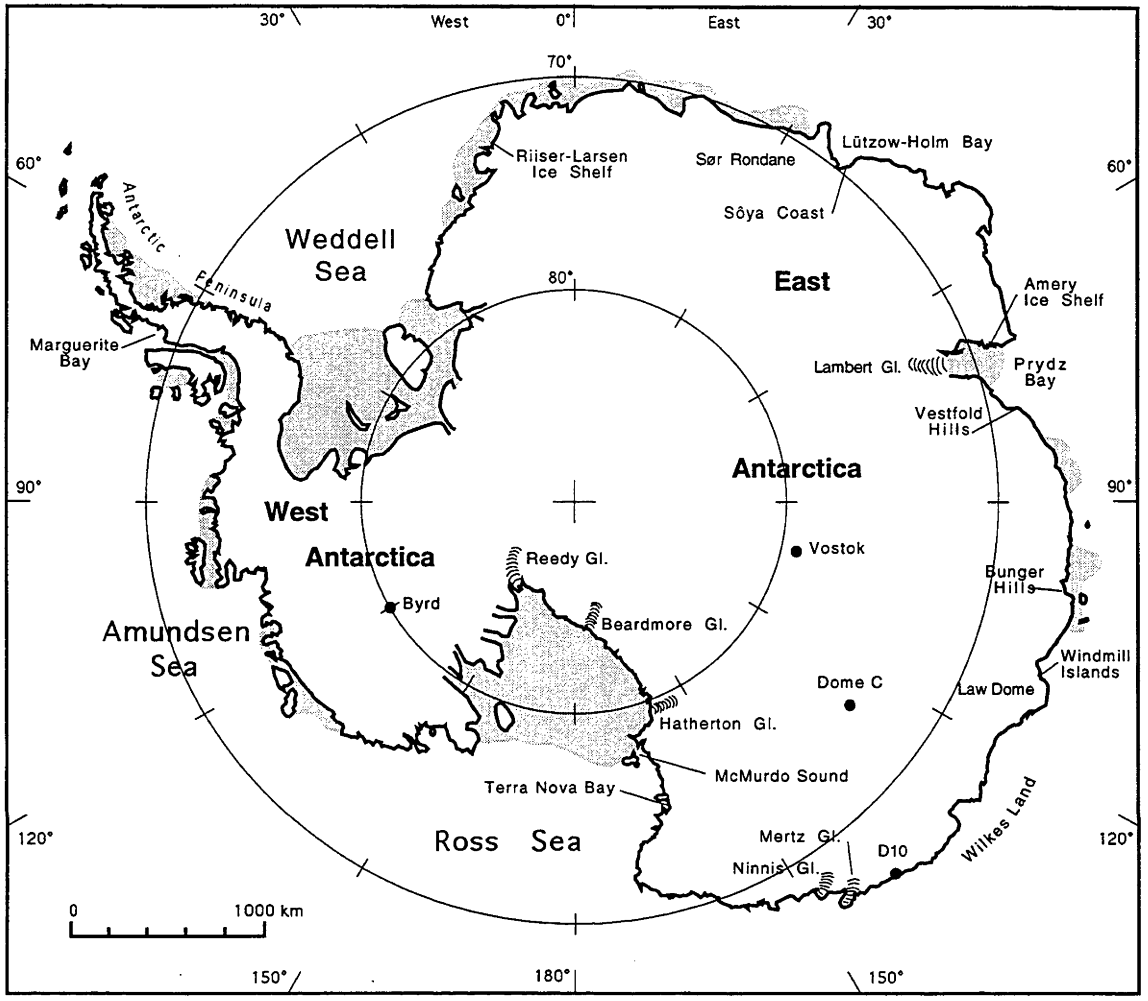

Figure 4.1 : Map of Antarctica, showing sites mentioned in this chapter.

4.2 Glacial Geology

Only about 2% of Antarctica's surface consists of exposed rock, and most of this is in the Transantarctic Mountains and the Antarctic Peninsula region, so geological constraints on the ice sheets' history are sparse outside these areas. Observations from rock outcrops around the Antarctic coast and from isolated exposed mountain ranges and nunataks provide some information on the former extent and timing of retreat of the LGM ice sheets. Figure 4.1 shows the location of sites mentioned in the text.

Ice-free "oases" exist in a few places on the Antarctic coastline. Glacial trimlines are not found at any of these sites, so they do not directly indicate the former thickness of the ice sheet there. Moraine deposits and dated biological material can, however, constrain the retreat history of the ice sheet margin. Determining the regional ice thickness history from the sea-level records obtained from some of these oases (already presented in Chapter 3) will be discussed in the next chapter.

4.2.1 Vestfold Hills

Initial estimates of the ice retreat history in the Vestfold Hills (Adamson and Pickard 1983, 1986) were based on ~50 radiocarbon dates from marine sediments and terrestrial plant remains. The inferred ice retreat history placed the ice sheet margin approximately 10 km from its present position at 8 ka, ~ 5 km at 5 ka, and ~2 km at 1 ka, although the retreat shows no clear spatial pattern. Retreat rates calculated at each dated site show an inverse relationship between rate and age (Adamson and Pickard 1986), which is incompatible with physical processes and is probably due to inadequate sampling.

Lake sediment ages

Age determinations from the lowest organic-rich sediments in lakes cored during the 1991-92 summer (see Chapter 3) yield uniform ages of 8 - 10 ka (Table 4.1), although no sites within 5 km of the present ice margin were dated. The uniformity in these ages, and the lack of any systematic spatial trend, suggest that the onset of highly organic sedimentation in these lakes was not controlled by their emergence from beneath the retreating ice sheet, but rather by a change in climatic conditions permitting a rapid increase in biological productivity. The isotopic temperature record from the Vostok ice core indicates that rapid warming peaked around 9500 - 10000 calendar years ago (Jouzel and others 1987). This temperature rise could have initiated seasonal melting of the lakes, allowing biological productivity to increase substantially. The roughly simultaneous initiation of organic sedimentation in all lakes implies that the lake basins existed on an ice-free Vestfold Hills prior to that time, and that, if the ice sheet did cover the Hills at the LGM, it had retreated to within 5 km of its present position by 10 ka.

Table 4.1 : Age of lowest organic-rich lacustrine sediments in lakes of the Vestfold Hills. These ages have been determined by extrapolating the sedimentation rate determined from radiocarbon dates higher in the core (Table 3.8).

Lake	age (^{14}C years)
`A'	6820 ± 240
Abraxas	8280 ± 560
Ace	8760 ± 120
Anderson	8610 ± 210
Cat	8910 ± 220
Clear	8180 ± 220
Collerson	9600 ± 260
McCallum	10010 ± 120
Medusa	8230 ± 260
Scale	9090 ± 100

Underlying the organic-rich sediments are poorly sorted, largely inorganic sediments, probably till or reworked glacial drift deposits. The till deposits from Scale Lake and Lake McCallum were examined in detail. Conventional and Accelerator Mass Spectrometry (AMS) radiocarbon ages were obtained from bulk sediment samples and from extracted organic fractions (Table 4.2). The only macroscopic organic material found in the till, moss fragments from Scale Lake, yielded an age of 9500±390 yrs (AMS-337), whereas bulk sediments from the same core interval were ~3000 years older (ANU-8549), and the ages of bulk sediment and humic acid fractions ranged between ~9 and ~21 ka. This indicates the presence of more than one source of carbon in the sediments: material which was alive shortly before deposition in the lake (represented by the moss fragments) and older material, presumably derived from the drift deposits. The similarity between the age of bulk sediment from Lake McCallum and the age of humic acids extracted from sediments adjacent in the core (ANU-8550 and AMS-322), Table 4.2) suggests that the old component is dominantly organic, and not lithogenic graphite or carbonate. If significant lithogenic carbon was present, sampling of the humic acid fraction would exclude this component, and the ages obtained would differ from the bulk sediment ages. Chromic acid treatment of the sediments also indicates that no graphite is present.

Table 4.2: Radiocarbon ages from till in cores from the Vestfold Hills

Lake	Depth (cm)	ANU No.	Age	Fraction
Clear	130-141	AMS-324	20900±540	AMS on bulk sediment
Scale	96-106	8548	9290±260	conventional date on bulk sediment
Scale	106-121	8549	13130±280	conventional date on bulk sediment
Scale	106-121	AMS-337	9500±390	AMS on moss fragments
Scale	120-140	8267	20870±470	conventional date on bulk sediment
McCallum	86-91	AMS-321	12570±400	AMS on humic acid fraction
McCallum	102-124	8550	12850±360	conventional date on bulk sediment
McCallum	124-130	AMS-322	19700±560	AMS on humic acid fraction

Carbon analyses

The existence of two sources of organic carbon in the till is supported by carbon isotope analyses. Negative correlation between the sediments' total organic carbon content and their $\delta^{13}C$ (Figure 4.2) suggests that the old carbon source has a fairly constant $\delta^{13}C$ of ~-23‰, whereas the young carbon, whose concentration increases up the core, has a value as low as -29‰. Implications for the ice exposure history of the Vestfold Hills depend on the age of the old carbon component. If we can estimate the proportions of various components of the organic carbon, then it is possible to calculate the ages of these components and thus constrain the exposure history of the area.

On one hand, if the Vestfold Hills were to some extent ice-free during the LGM, the old organic component could be composed of hardy organisms which were living on the rock oasis during the glaciation and which were washed into the lake basins when deposition began about 10 ka. Marine organisms from the LGM are unlikely to have blown onto the Vestfold Hills, as permanent sea ice probably extended ~1500 km further north than it does at present (Hats 1978). In this scenario, the "old" component would be derived from material with a wide range of ages, since life would have been present in the Vestfold Hills throughout the last glacial period. The observed radiocarbon ages could result from various mixtures of material of different ages.

On the other hand, if the Vestfold Hills were completely covered by the ice sheet during the LGM, the old component of organic carbon must be derived from some source which could be incorporated with the drift deposits before or during the ice retreat. One possibility is organic material deposited on the Hills during the last interglacial period, previous interglacials, or even during the Pliocene. When overrun by the ice sheet, these deposits could become finely divided so that no macroscopic organic material remained, and be incorporated into the till. The presence of undisturbed Pliocene sediments on Marine Plain, in the southern Vestfold Hills, indicates that this process would not necessarily remove sedimentary deposits from the region, so some would be available for redeposition when sedimentation began in the lakes ~10,000 years ago. Reworked macroscopic moss fragments found in former shoreline deposits of Lake Stinear (Hirvas and others, 1993) have a radiocarbon age of 37,520±1390 years. As this date is at the limit of meaningful radiocarbon ages, this material probably dates from the Last Interglacial or earlier, and demonstrates that organic material of this age does exist in postglacial sediments in the Vestfold Hills. In this case, the old carbon fraction would contain no ^{14}C, so that 20 ka ages would result from a 70:30 mix of old carbon and 10 ka material, and the 13 ka ages from a 30:70 combination.

The relative proportions of the "old" and "young" sources of carbon present can be estimated from the total organic carbon (TOC) content of the core. To

do this, the "background" proportion of the old component present in the till is determined, and it is assumed that this remains roughly constant. The young fraction is then calculated from the TOC. The background proportion of the "old" component has been estimated in two ways. One method uses the TOC at the base of the core as an estimate of the background, since this represents a period early in the lake's depositional history, when drift material was available in large quantities for reworking and redeposition. Later, when the supply of drift material was depleted and biological productivity increased, the sediment became progressively diluted by contemporary organic carbon.

TOC determinations from Scale Lake and Lake McCallum (Figure 4.2), suggest that the background proportion of "old" carbon is 0.4 - 0.5 %. These values are supported by the uniformity of the TOC contents at the base of both cores. An alternative estimate comes from the TOC content of modern sediment in Lake Bisernoye, directly adjacent to the present margin of the ice sheet in the eastern Vestfold Hills. Although algae grow in the lake, there appears to be a strong water current flowing from beneath the ice sheet, and the sediment core taken here consists purely of "till" with a TOC of 0.1 %. Using these values, and the estimated proportions of "old" and "young" carbon, the ages of one component can be calculated from the measured radiocarbon ages, if we assume an age for the other component. It seems reasonable, from the oldest ages of the organic-rich sediments, to assume that the young component has an actual age of 10 ka. Using the range of estimates from 0.1 - 0.5 %, the age of the old component is found to be between 13 ka and "radiocarbon-dead". The higher estimates of the old fraction (0.4 - 0.5 %), obtained from the cores which were dated, imply a postglacial age for the old component, ie that some life existed in the Vestfold Hills before the onset of significant biogenic sedimentation in the lakes. This could indicate that the Hills were not ice covered before this time, although the question cannot be resolved without knowing the nature of the organisms.

Most of the variation in the age estimates above is due to uncertainty in the background concentration of the old component. If this can be better constrained, perhaps using biochemical markers, a more precise estimate of the age of former biological activity in the Vestfold Hills may be obtained.

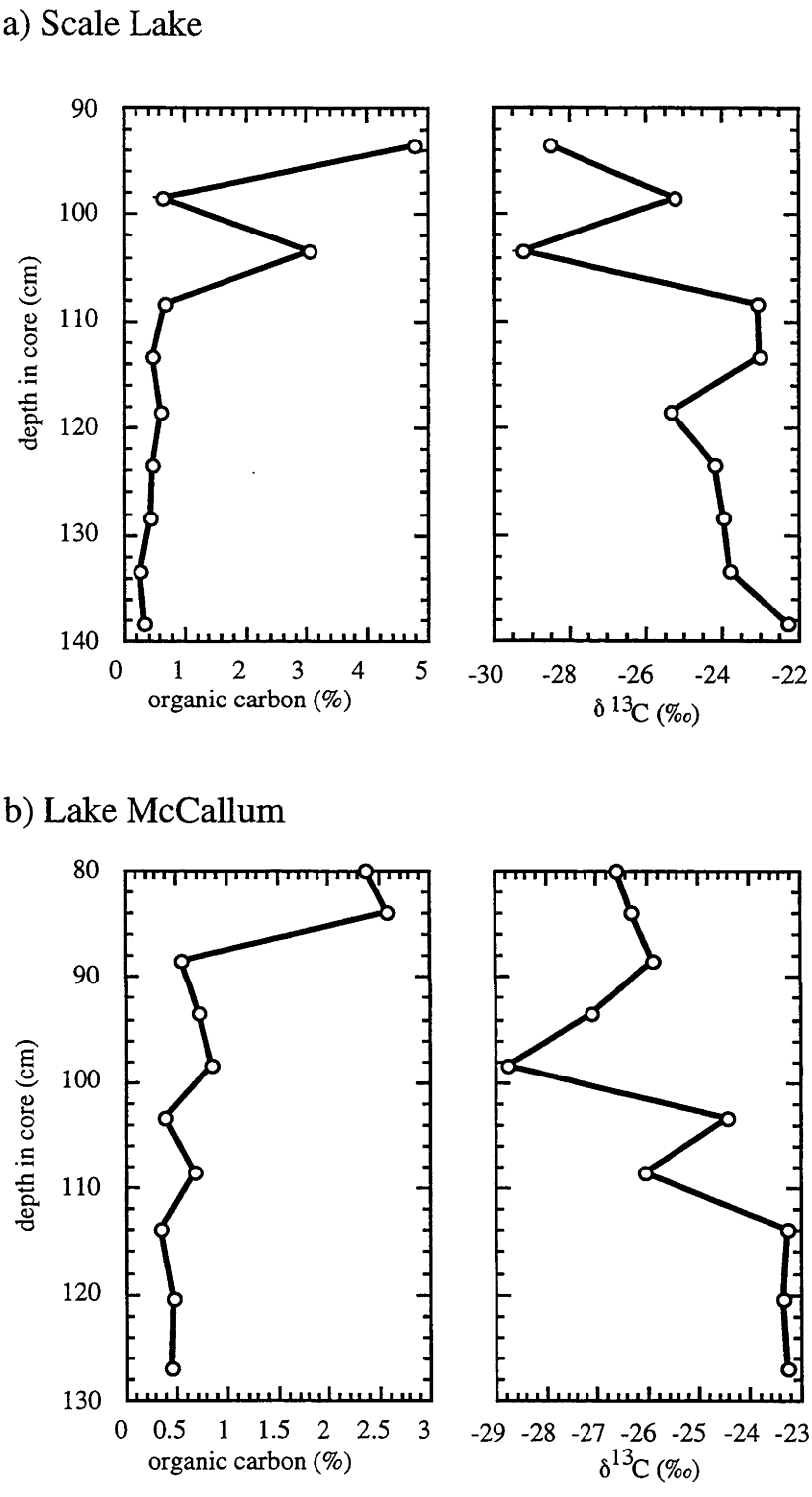

Figure 4.2 Total organic carbon content (TOC) and $\delta^{13}C$ profiles of the till layer at the base of the cores from Scale Lake and Lake McCallum. The negative correlation between TOC and $\delta^{13}C$ in both cores suggests that mixing is taking place between a component in the till with a high $\delta^{13}C$, and a younger component, with a lower $\delta^{13}C$, which becomes more abundant up the core.

Cosmogenic isotope measurements

An attempt to constrain the retreat of ice from the Vestfold Hills has also been made using measurements of cosmogenic isotopes. These are produced *in-situ* in the uppermost few metres of the Earth by high-energy reactions initiated by cosmic ray particles. If there is negligible erosion, unstable isotopes produced in this way accumulate in response to their production rate and decay rate. If the ice sheet eroded more than a few metres of material during its last advance across the Vestfold Hills, thus removing previously exposed rock, then the abundance of cosmogenic isotopes in rocks should be simply related to the length of time since the ice sheet retreated from that location (Cerling and Craig, 1994). To deduce exposure ages from isotope abundances, it is necessary to know the isotope's production rate, which depends on the cosmic ray flux through time, and the chemical composition of the rock. Suitable isotopes include ^{36}Cl, ^{26}Al and ^{10}Be, which are produced in common rock-forming minerals in sufficient abundance to permit their measurement in suitable rock types using accelerator mass spectrometry.

The exposure history of sites adjacent to the ice sheet may not be as simple as the scenario described above. For example, if a site is covered again by the ice sheet without erosion, then production of the cosmogenic isotopes ceases due to the shielding effect of the ice. Unstable isotopes will continue to decay, however, resulting in abundances which do not represent the true exposure time of the site. Measurement of multiple cosmogenic isotopes with different decay rates allows the interpretation of more complex exposure histories.

^{36}Cl (half-life 300 ka) ages from striated and polished rock surfaces throughout the Vestfold Hills (J. Stone, pers. comm.) indicate unexpectedly long exposure ages ranging from 25 to 100 ka (Figure 4.3) These show no spatial trend, although a group of sites from the eastern part of the Hills produce uniform ages of 25 - 27 ka. A likely interpretation of these results is that the last advance of the ice sheet eroded an insufficient depth to remove all previously exposed rock. In this case, the ages reflect a combination of the complex exposure history and the degree of erosion, which almost certainly varied throughout the Hills. Thus, these ages do not constrain the most recent retreat of the ice sheet. Alternatively, assuming a single exposure period, the ice margin history inferred from these ages is one of irregular retreat at a time when ice sheets were expanding in the rest of the world. This is considered unlikely.

To test whether multiple exposures were responsible for the old ^{36}Cl ages, sites within a few tens of metres of the original samples were dated using ^{26}Al (half-life 710 ka), where suitable rock types could be found. If multiple exposure with negligible erosion is the cause of old ^{36}Cl ages, we would expect the apparant ^{26}Al ages at the same sites to be uniformly older, since less ^{26}Al than ^{36}Cl would decay during the periods of burial. In fact, most

age pairs do not agree (Figure 4.3), and there is no consistent relationship between the ^{36}Cl and ^{26}Al ages. This is indicative of uneven erosion on an outcrop scale. In this case, the youngest ages are most likely to represent the time of the last deglaciation. ^{26}Al ages of 10±3 ka and 14±4 ka support the notion that the Vestfold Hills were ice-covered at the LGM, but these two ages are both from the southern part of the Hills, and it cannot yet be determined whether the ice sheet completely covered the Hills.

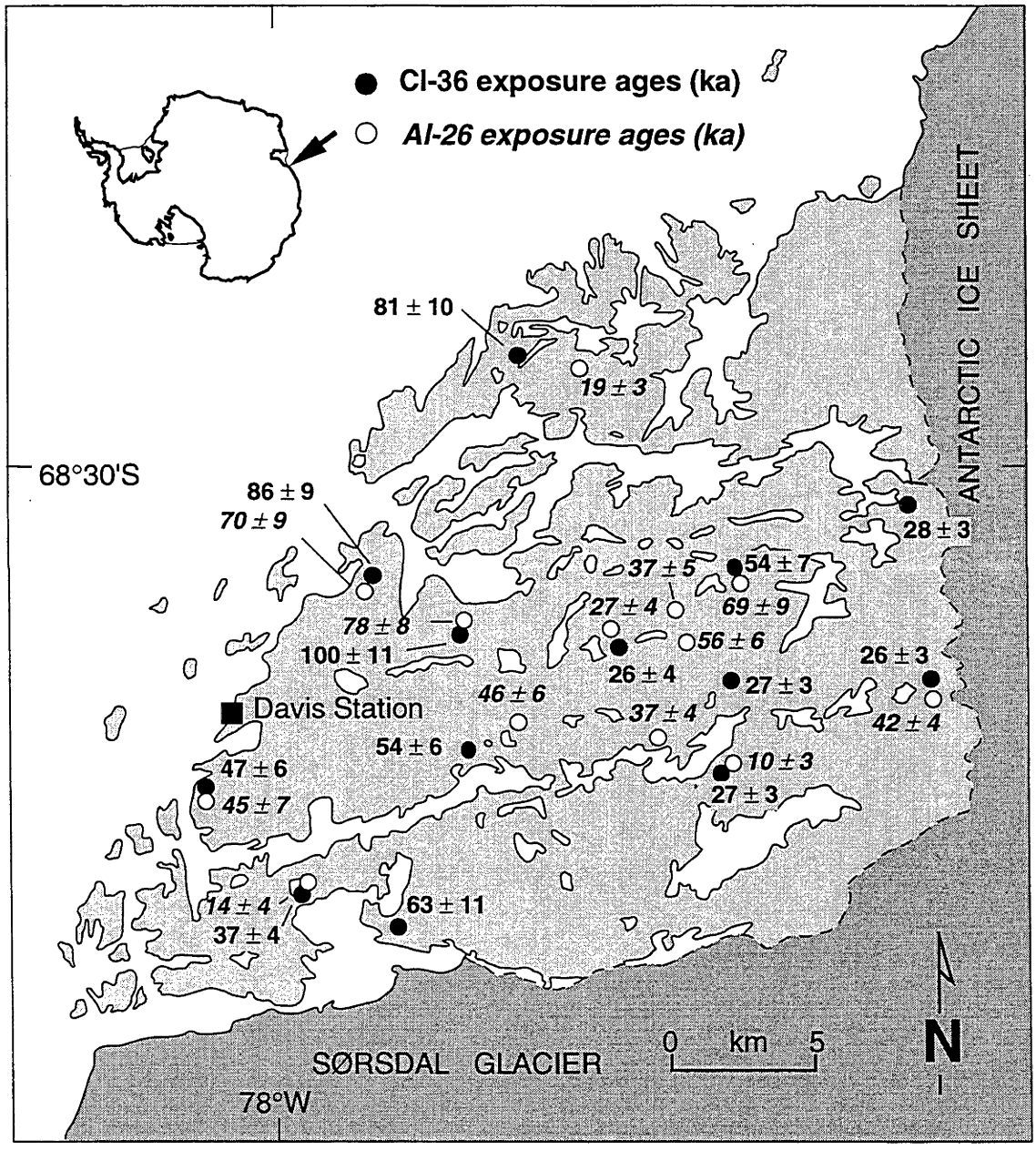

Figure 4.3 : Apparent cosmogenic isotope exposure ages from the Vestfold Hills.

The problem of pre-exposure may be reduced by dating the exposure of selected moraine boulders. If lithologies are chosen which are not found in the Vestfold Hills, then exposure is unlikely to have occurred prior to deposition, since there are no nunataks upstream of the Vestfold Hills. Moraine boulders are susceptible to mobility after deposition, which might reduce the measured exposure ages by burial or erosion of the sampled boulders, but this problem can be avoided by sampling large boulders which retain glacial surface features. The problem of pre-exposure also exists with these samples, since moraine boulders may be derived from pre-exposed rock, and boulders deposited by previous glaciations may have remained in the Vestfold Hills throughout the last glaciation which covered the region. Such boulders are unlikely to preserve the surface characteristics of freshly-transported moraine boulders, so can be avoided during sampling. Even if pre-exposed samples cannot be avoided, the youngest ages obtained should represent the last retreat of ice from the region. Samples have been collected for this work during the 1994-95 summer, but analyses have yet to be performed on these samples (pers. comm J. Stone (ANU) and D. Fabel (University of Melbourne)).

Discussion

Radiocarbon ages of lake sediments show that the Vestfold Hills were ice-free by ~10 ka. Whether they were covered by ice before this time and during the LGM is unclear. Glacio-hydro-isostatic modelling can be used to provide an indication of the former extent of ice on a regional scale (and this is done in Chapter 7), but even if the ice sheet margin was generally far beyond its present position at the LGM it is possible that the Hills were anomalously ice-free, as they are today. Using simplistic rebound arguments which indicate only minor ice sheet retreat, and the location of moraines on Broad Peninsula, Pickard (1986) proposed a LGM ice sheet that extended about 10 km beyond its present position, halfway across the Hills. However, the former margin in this reconstruction was chosen so that it lies inland of all the moraines on the seaward end of Broad Peninsula, which implies that the moraines were formed during an ice advance prior to the LGM. If this were the case, it seems unlikely that they would have survived until the present, as erosion and weathering are quite active in the western Vestfold Hills. On the other hand, these processes are highly dependant on temperature and the position of the coastline, which control the amount of liquid water available for weathering processes. The histories of these environmental variables are virtually unknown, so arguments based on weathering rates cannot be conclusive.

The presence of the Pliocene Marine Plain deposits also raises the possibility that lake sediments from the last interglacial may remain in some lake basins, below a layer of till which our sediment corer was unable to penetrate. A more robust and longer coring device might allow these sediments, if they exist, to be sampled. Interpreted in the same way as the

Holocene sediments from the same lakes, these sediments could provide valuable information on sea-levels during the last interglacial.

4.2.2 Other coastal oases

Larsemann Hills

Fewer radiocarbon ages have been obtained from the Larsemann Hills than from the Vestfolds, but in general the pattern appears to be similar, with biological productivity becoming significant around ~10 ka (Gillieson 1991). One significantly different age has been obtained from an *in situ* moss sample found at the bottom of a 2.5 m sediment core taken on the shore of Lake Nella (Burgess and others 1994). This material has been dated at 24,950 ^{14}C-yr BP (ANU-8826). As it is not derived from marine material, no reservoir correction need be applied to this age. Burgess and others (1994) suggest that this date "casts very serious doubt" on ice sheet reconstructions such as that of Gillieson (1991) in which the Larsemann Hills are ice-covered at the LGM. This age, however, is considerably older than the LGM, and it is also possible that the moss grew before ice advanced over the region, or in an interstadial period in which the Larsemann Hills were briefly uncovered.

Although this age does not constrain the position of the ice sheet margin at the LGM, nevertheless it raises fascinating questions regarding the evolution of environmental conditions in the coastal oases. If the age is correct, then the Larsemann Hills were warm enough to support the growth of mosses shortly before the LGM. If this was the case, then it seems strange that, since the region persisted this long as an ice-free "heat island", significant biological activity seems to have ceased during the LGM and did not resume until 10 ka.

Bunger Hills

The Bunger Hills have not been studied as intensively as the Vestfold Hills, and the history of the ice sheet in that region in consequently less well constrained. Early work (Shumskiy 1957, Wisniewski 1983) suggests deglaciation of the region between 15 and 6 ka, with a probable date of about 10 ka. In a study of raised beach ridges, Colhoun and Adamson (1992) obtained radiocarbon ages of shells in growth position within marine sediments, and from shell fragments associated with raised beach deposits. The oldest age obtained was 7700±490 ^{14}C-yr BP (Beta-15828, corrected for the marine reservoir effect), from fragments of *Laternula elliptica* found in "beach sand amongst morainic boulders", and they regard this as the minimum age for the deglaciation of the region. A similar sample from close to the present ice sheet margin indicates that the ice sheet had retreated to approximately its present position by ~5600 corr. ^{14}C-yr BP (reservoir corrected). Radiocarbon ages obtained from basal lake sediments and petrel nest material (Bolshiyanov and others 1991) indicate that this estimate of deglaciation may be too young. The oldest age obtained was 10,070±80 ^{14}C-yr BP, from "organic sediments in nests". Assuming that this material is

derived from the petrels themselves, this date probably requires a marine reservoir correction of ~1300 years (Colhoun and Adamson 1992) since the birds obtain all their food from the sea. This age is supported by ages of 9850±600 ^{14}C-yr BP (Bolshiyanov and others 1991) and 9510±90 ^{14}C-yr BP (OxA-3940, Melles and others 1994) from freshwater algal lake sediments. Also, another lake sediment age of 8310±80 years BP from a lake ~1.5 km from the present margin of the ice sheet indicates that the margin has been stable through most of the Holocene.

The deglaciation history of the Bunger Hills seems to be similar to that of the Vestfold Hills, with organic sedimentation beginning at ~10 ka throughout the region. Whether this represents the age of deglaciation, or simply the time at which climatic conditions allowed sedimentation to begin in an area that was already ice-free cannot be determined from the information available.

Windmill Islands

Lake sediments from the Windmill Islands, west of Law Dome, have been used to constrain the timing and pattern of deglaciation there (Goodwin 1993). Maximum ages are around 8 ka in the south of the region, and 5.5 ka in the north (ages corrected for reservoir effects). The difference in these ages may be due to insufficient sampling, but their validity is supported by the presence of a higher observed marine limit in the south (see section 2.3).

Using isostatic rebound arguments, Goodwin (1993) estimates that during the LGM the Windmill Islands were covered by ~200 m of ice, and that the ice sheet advanced to the location of the present 200 m isobath, which lies 8 - 15 km to the west, and ~50 km offshore to the north.

Sôya Coast

Raised beaches occur at several coastal ice-free areas on the Sôya Coast in Lützow-Holm Bay (Figure 4.4). Conventional radiocarbon ages obtained from the marine sediments associated with the beaches can be divided into younger (2 - 10 ka) and older (20 - 35 ka) groups (Yoshida and Moriwaki 1979). AMS ages of *in situ* samples from the Ongul Islands and Langhovde fall between 33 ka and 38 ka (Moriwaki, pers. comm.). These latter dates are at the limit of the radiocarbon method, and must be treated cautiously, but if they are correct and marine sediments were deposited in these regions around 35 ka, then the area must have been ice-free at that time, and probably since then, since beach deposits would probably not survive being over-ridden by the expanding ice sheet (Moriwaki, pers. comm.). The ice sheet may not have covered these locations, but regionally there must have been significant expansion of the ice sheet, causing isostatic depression which lowered the region so that marine sediments could be deposited at a time when global sea-level was 75 - 100 m lower (Shackleton 1987). The beach ridges from which these old samples were taken are separated from the ice sheet by a deep channel (Ongul Islands) or mountains (Langhovde)

(Moriwaki pers. comm.), so it is possible that the ice sheet advanced beyond these areas on either side but did not cover them. Alternatively, the older dates could result from the contamination of samples which grew during the last interglacial period, when sea-levels were similar to their present position. This interpretation also implies that the ice sheet did not cover these regions at the LGM.

Cosmogenic ^{36}Cl concentrations from Breidvågnipa (Figure 4.4) indicate exposure of 10 - 12 kyr (J. Stone and J. Evans pers. comm.). Assuming that these apparent ages are the result of a simple exposure history, they indicate that this location was ice-covered at the LGM. However, as coastal rock outcrops are generally unrepresentative of the Antarctic coast, this may not represent a regional advance of the ice sheet at that time.

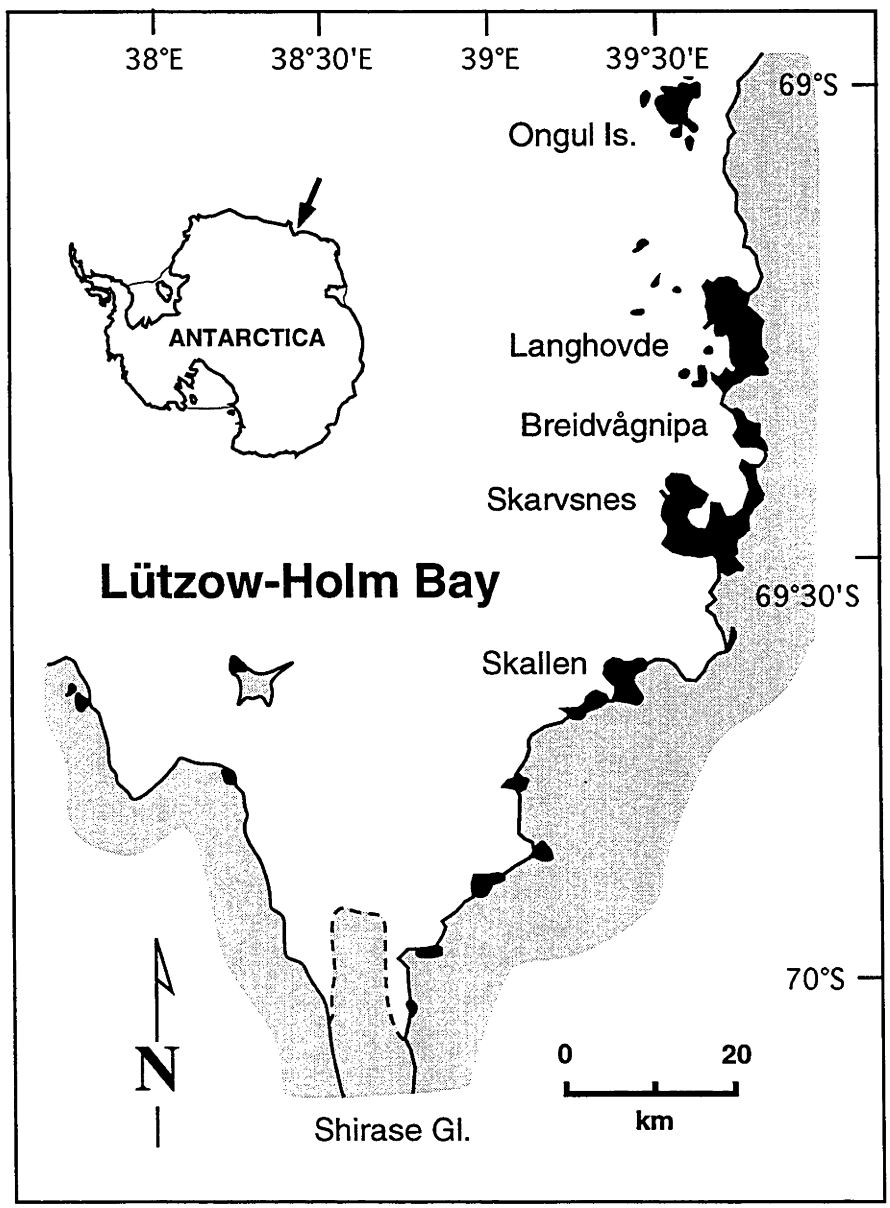

Figure 4.4 : Location map for Lützow-Holm Bay, showing locations mentioned in the text.

4.2.3 Ross Sea Region

Geological constraints on the former extent of the Antarctic ice sheets consist largely of moraines and lateral drift sheets. However, these features are usually difficult to date, as they are generally not deposited with any contemporaneous organic material, and, especially in Antarctica, exist in hostile environments that are not readily colonised by plants or animals. Denton and others (1989b) examined the longitudinal profiles of the drifts of several large outlet glaciers which drain the East Antarctic ice sheet through the Transantarctic mountains, and correlated them stratigraphically with the Ross sea drift in McMurdo Sound, which, being at lower altitude and beside the sea, contains dateable organic remains.

The LGM drift sheets studied were deposited by the Beardmore, Hatherton and Reedy Glaciers (Figure 4.1). The profiles of these drift sheets (Figure 4.5) are similar, showing substantial thickening (500 - 1100 m) at the glacier mouths near the Ross Ice Shelf, contemporaneous with only slight thickening (30 - 100 m) at glacier heads near the polar plateau (Denton and others 1989b). Similar former glacier profiles have been deduced from drift deposits above the Reeves and Campbell Glaciers, which flow into Terra Nova Bay (Central Victoria Land), and both have former elevations of ~400 m at the present coast (Orombelli and others 1990).

This style of glacier enlargement could be achieved in two ways. One is increased ice flow due to higher precipitation on the polar plateau. This is not plausible, as measurements of meteoric ^{10}Be in the Vostok ice core (Yiou and others 1985) and observed relationships between precipitation rate and atmospheric temperature (Robin 1977, Lorius and others 1985) indicate that the precipitation rate on the polar plateau during the LGM was only 50 - 60 % of its present value. The more plausible explanation is that the increased glacier heights resulted from ice shelf grounding in the southwestern and southern Ross Embayment (Denton and others 1989b). This explanation is supported by the flow history of the Taylor Glacier, an outlet glacier which drains Taylor Dome (a peripheral dome of the East Antarctic Ice Sheet) and terminates in the ice-free region of southern Victoria Land. This glacier fluctuates out of phase with the outlet glaciers which drain into the Ross Sea (Marchant and others 1994). This is consistent with a scenario in which the Taylor glacier expands due to increased precipitation when the Ross Sea is open during interglacial periods, whereas the other outlet glaciers expand due to increased grounding of the Ross Ice Shelf when it advances across the Ross Embayment due to sea-level fall in glacial periods.

From these observed profiles, it is not possible to reconstruct the elevation of the polar plateau at the LGM, although it seems unlikely to have been significantly higher than present. It is possible that the plateau was lower than present (see Section 4.4), and that the elevation change at the glacier heads was due to ice sheet grounding near their mouths. In any case, elevation change of the polar plateau since the LGM appears to have been small. Denton and others (1989b) use the profiles to produce two possible

reconstructions of ice in the Ross Sea at the LGM (Figure 4.6). Both models propose grounded ice in the entire inner Ross Embayment, and the elevations of the interior East and West Antarctic ice sheets do not differ from their present configuration. The minimum reconstruction, based on the assumption that the fast-flowing West Antarctic ice streams existed then as they do today, has the grounding line of the Ross Ice Shelf extending only ~200 km beyond its present position. If, however, the ice shelf advanced to near the edge of the continental shelf, it would have grounded on submarine banks, and ice inflow from the West Antarctic ice sheet and outlet glaciers in the Transantarctic mountains would have led to a grounded ice sheet over the entire Ross Embayment. This is the maximum model of Denton and others (1989b), in which the grounded slab of ice thickens gradually from the continental shelf edge to about 1200 m in the inner Ross Embayment. The volume change of the maximum model is ~1.9 m ESL. The reconstruction of Hughes and others (1981) which was used as the basis for the ANT3 model of Nakada and Lambeck (1988), is about twice as large as the maximum model of Denton and others (1989b).

4.2.4 Lambert Glacier

The Lambert Glacier system (figure 4.1) drains about 13.5 % of the East Antarctic ice sheet into Prydz Bay via the Amery ice shelf. Measurements of the LGM conditions near the mouth of the Lambert Glacier therefore provide useful constraints on the history of the East Antarctic ice sheet as a whole. Unlike the outlet glaciers which pass through the Transantarctic Mountains (Denton and others 1989a,b, Bockheim and others 1989), the Lambert does not have continuous flanking ranges where moraines and drift sheets can accumulate which allow the reconstruction of former glacier elevation profiles. However, at Fisher Massif and Mount Meredith, Mabin (1992) observed three generations of drift sheets associated with former elevations of the glacier. These lateral moraines lie 700 m, 500 m, and 100 m above the present surface of the glacier, which is at ~100 m asl. in that region and grounded in a trough several hundred metres below sea-level. No radiocarbon ages have been obtained for these moraines, but by direct correlation with dates obtained from ice-cored moraines in other parts of Antarctica (Stuiver and others 1981, Bockheim and others 1989) the lowest ice-cored moraines have been assigned a LGM age by Mabin (1992). *In situ* cosmogenic ^{36}-Cl exposure ages of 16.8±1.1 and 13.3±1.0 ka from boulders on this moraine (samples FM-5 and FM-6, J. Stone pers. comm.) lend some support to this correlation. The implied postglacial ice thinning is 100-170 m, due to uncertainty in reconstructing the surface topography of the glacier, which is currently tens of metres higher in the middle than at the margin adjacent to the moraines. In any case, this is significantly less than those observed at glacier mouths in the Ross Embayment (Denton and others 1989a,b, Bockheim and others 1989), implying that the grounding line of the Amery ice shelf has not retreated significantly from its position during the LGM. This, in turn, implies that the Lambert Glacier ice drainage and the Amery ice shelf did not contribute significantly to global postglacial sea-level

rise, and also that the isostatic response to ice removal in the region would have been small.

However, the correlation of the lowest Lambert Glacier moraine with the LGM glacier position may be incorrect. Denton and others (1989a) also record three drift sheets deposited by the Beardmore Glacier (Figure 4.5). The lowest (Plunket drift sheet), 7 - 30 m above the present ice surface, is thought to be Holocene in age, recording ice-surface lowering due to increased surface ablation, decreased ice flow, or grounding-line recession. The intermediate (Beardmore) drift sheet, ranging from 30 - 1100 m above

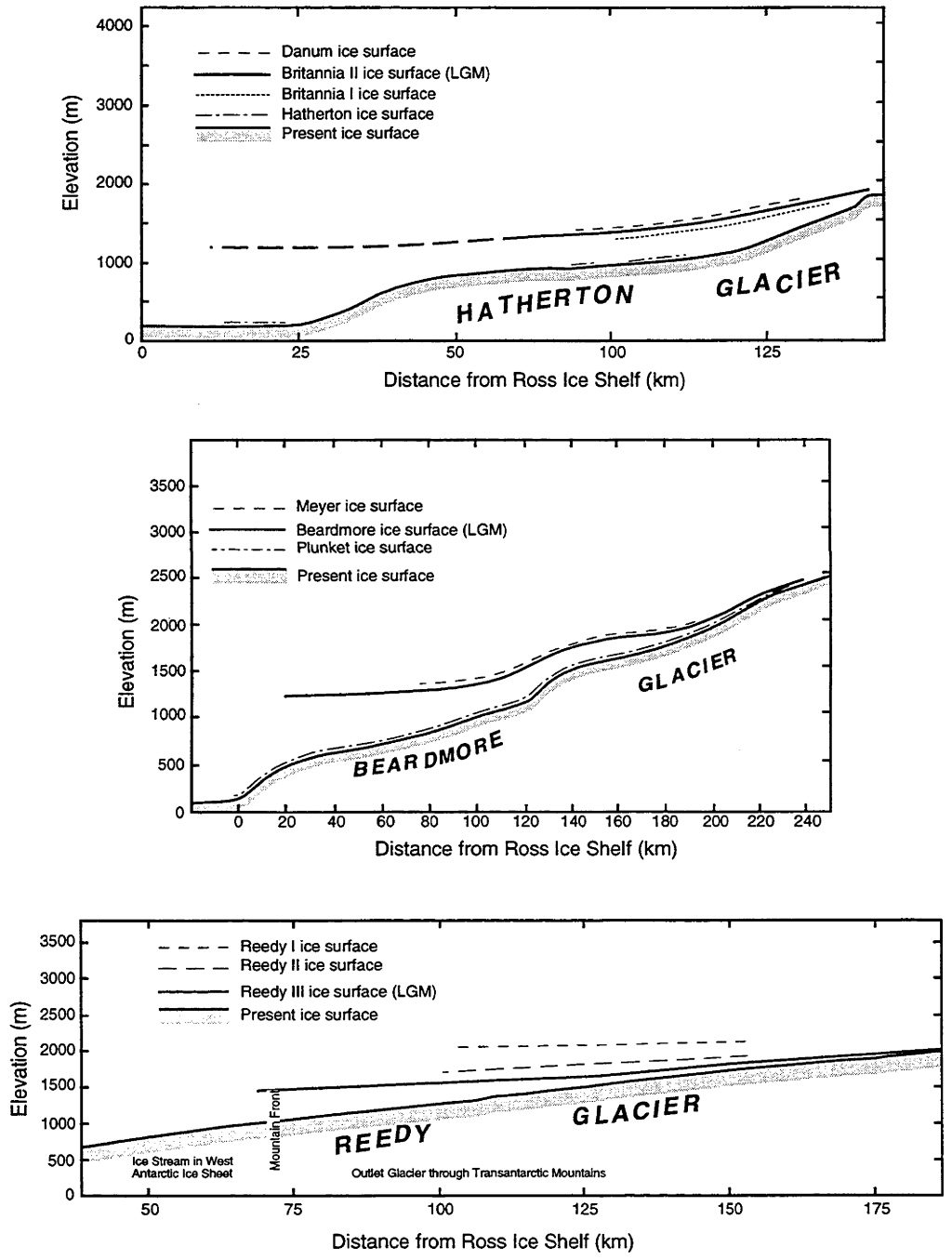

Figure 4.5 : Profiles of drift sheets adjacent to outlet glaciers in the Transantarctic Mountains (from Denton and others 1989b).

a)

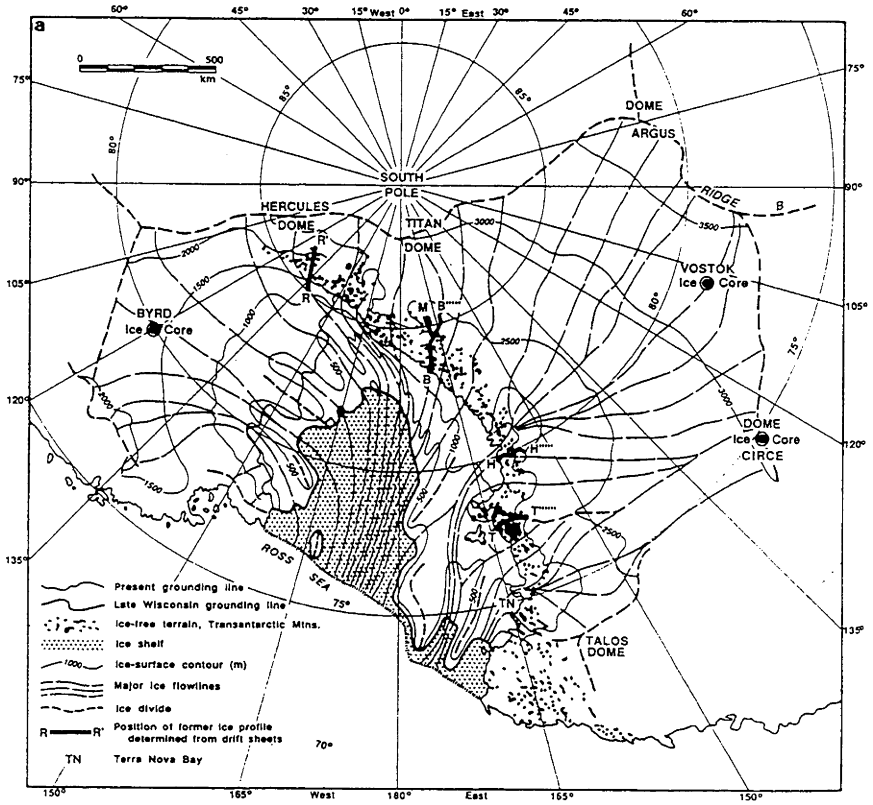

b)

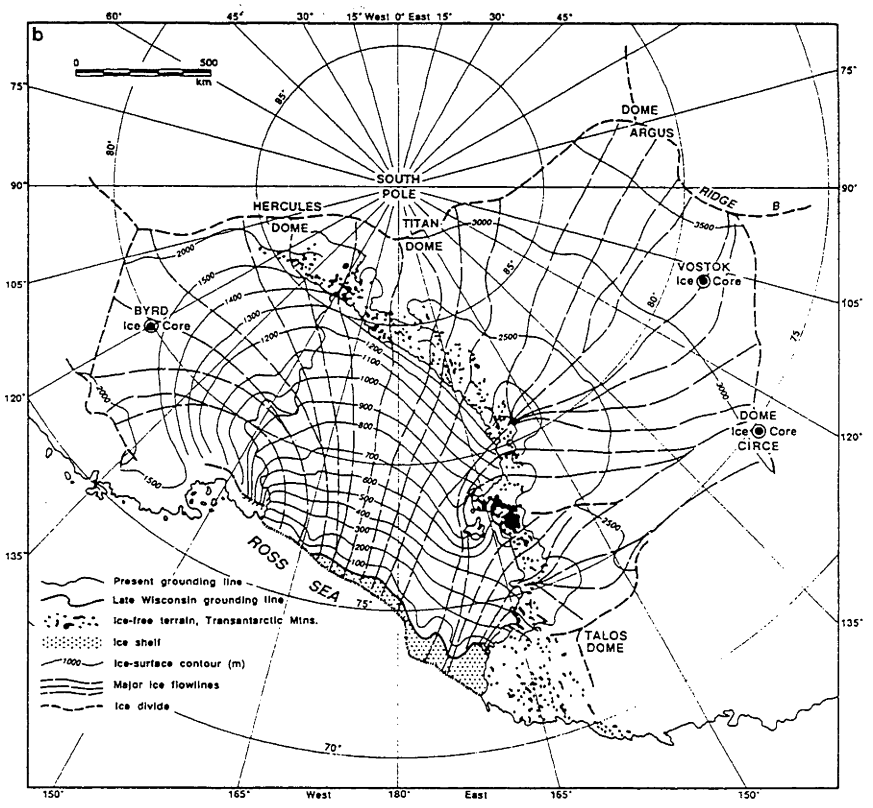

Figure 4.6 : Minimum (a) and maximum (b) reconstructions of the Ross Ice Sheet at the LGM (from Denton and others 1989b).

the glacier's present elevation, as described above, is correlated with the LGM, and the highest (Meyer drift sheet), 30 - 50 m above the Beardmore drift sheet, is thought to represent the penultimate glacial period (Denton and others 1989a). A similar situation occurs at the Hatherton Glacier, except that there are two drift sheets (Britannia I and II), separated by 50 - 100 m vertically, which are thought to represent the LGM, in addition to the Holocene and penultimate glacial drifts (Bockheim and others 1989). If one of the as-yet-undated higher Lambert Glacier drift sheets represents the glacier elevation during the LGM, then the ice thickening is comparable to, if slightly less than, that which occurred in the Ross Embayment. The grounding line of the Amery ice shelf would thus have been considerably northward of its present position, and the Amery/Lambert system would have contributed significantly to global and regional sea-levels. Evidence for the advance of the Amery ice shelf is discussed below, in the section on marine geology.

4.2.5 Sør Rondane Mountains

In the Sør Rondane Mountains (figure 4.1), which are 200 km from the present coastline, Hirakawa and Moriwaki (1990) found that the ice sheet was formerly about 400 m higher than its present elevation there. The age of this former elevation is not known, as the till deposits have not been dated, although a relative chronology based on weathering has been constructed by Moriwaki and others (1994).

4.2.6 Antarctic Peninsula

Hjort and others (1992) reviewed research on the last deglaciation in the Antarctic Peninsula region, but did not draw conclusions on the amount of ice formerly present. They conclude that deglaciation occurred in two phases, separated by a significant glacial readvance around 7 ka.

4.3 Marine Geology

4.3.1 Weddell Sea

From sedimentological analysis of marine sediment cores in the eastern Weddell Sea (Figure 4.1), Grobe and others (1993) conclude that the Antarctic ice sheet there (the Riiser-Larsen, Maudheim and Ekström ice shelves) advanced to the edge of the continental shelf in water depths of ~500 m at the LGM. Assuming that sea-level was ~120 m lower at that time and allowing for local isostatic equilibrium, this implies a former ice thickness of 500 - 600 m at the edge of the continental shelf. The same conclusion has been reached in the case of the Ronne-Filchner Ice Shelf (Elverhoi 1981) which occupies the Weddell Sea, and ice seems to have grounded in the Filchner Trough to a depth of 1000 m, indicating considerable ice thickness (Melles 1991).

4.3.2 Prydz Bay

In Prydz Bay, compact sediments in sediment cores from the Four Ladies Bank near the edge of the continental shelf are interpreted as subglacial till (O'Brien 1994). This implies that the Amery ice shelf grounded in (current) water depths of ~500 m. The continental shelf is mostly deeper than this, but grounding on banks at the outer margin could have caused grounding across the entire shelf, as proposed for the Ross ice shelf by Denton and others (1989).

In eastern Prydz Bay, at ODP site 740, Domack and others (1991) estimated the time of onset of open marine conditions during deglaciation as 10,700±70 years BP (AA-3935, uncorrected age). This represents the time at which biogenic sediments first became more abundant than terrigenous material. Since permanent sea ice cover also inhibits bioproductivity, this is not necessarily the time that the ice shelf ceased to be grounded there. The Amery ice shelf probably remained grounded in eastern Prydz Bay longer than in the west, due to shallower water depths in the former region.

4.3.3 Ross Sea

Anderson and others (1992) studied the sedimentology and composition of diamictons from piston cores on the Ross Sea continental shelf. They differentiated between subglacial till deposits and glacio-marine sediments on the basis of petrologic provinces. The petrologic composition of terrigenous sediment in the Ross Sea is determined by the source of glacial debris. Distinct compositional provinces, related to the source region of the sediment, are preserved by ice sheet flow but become mixed on the sea-floor if sediment is deposited from floating ice beyond the grounding line. The former grounding line of the Ross ice shelf reconstructed on this basis extends to the edge of the continental shelf, in close agreement with the maximum reconstruction of Denton and others (1989).

4.3.4 Wilkes Coast

The regions discussed so far in this section have been the major ice shelves, which are fed by convergent ice drainages. Reconstructions based on evidence from such localities may not generally applicable, as most of the Antarctic coast is fed by divergent ice drainages. Domack and others (1991) studied sediment cores from the Wilkes Land continental shelf, which includes the outlets of the Mertz and Ninnis Glaciers, as well as large stretches of coast where the East Antarctic ice sheet flows directly into the sea. Two shelf transects combined with detailed bathymetry indicate that grounded ice advanced to the edge of the continental shelf during the last glacial maximum, but only within the confines of depressions and troughs. Regions which now lie in ~300 m of water apparently were not glaciated. Their reconstructions show ~200 km of recession since the LGM in front of the Mertz Glacier, but only ~20 km on the adjacent Adélie Coast.

The Adélie Coast transect was close to the onshore site of ice core D-10 (see Section 4.2) where the elevation change of the ice sheet was estimated as 1300 m near the coast (Grootes and Stuiver 1987) and 400 m 250 km inland (Raynaud and others 1979). A 20 km advance of the ice margin seems insufficient to cause this ice elevation change, since the present ice sheet only reaches 1300 m asl at a distance of ~150 km from the coast.

4.3.5 Antarctic Peninsula

A coring programme on the continental shelf to the west of the Antarctic Peninsula indicates that a grounded marine ice sheet extended at least over the inner continental shelf and that grounded ice streams extended further across the shelf (Pope and Anderson 1992). Grounded ice may have covered the outer shelf as well, but sediments of glacial age were not cored there, due to the thick deposits of postglacial material. Radiocarbon ages indicate that the grounded ice shelf retreated from the inner shelf at Marguerite Bay some time after 12,430 years BP (corrected age). It has been suggested that the presence of subglacial deltas at the edge of the continental shelf is consistent with the hypothesis that grounded ice in this region was low profile and fast flowing (Larter and Vanneste 1995). This hypothesis attempts to reconcile the ice sheet reconstructions based on marine observations with others. The marine-derived models generally propose a greater expansion than those based on onshore data and numerical glaciological models.

4.4 Ice Cores

Unlike the great ice sheets of the northern hemisphere, which exist only during glacial periods, permanent ice has been present on the Antarctic continent for at least several million years (Denton and others 1991). The movement of this ice under the influence of changing temperature and precipitation patterns and topography is very complicated, but ice deposited several hundred thousand years ago probably exists on East Antarctica. This ice contains a record of the conditions under which it formed, and several long cores have been drilled to examine this record. Cores have been obtained from Vostok and Dome C on the East Antarctic ice sheet, Byrd Station in West Antarctica, and site J-9 on the Ross ice shelf (Figure 4.1). All these records span a period of at least 30,000 years, with the Vostok record extending back beyond the last interglacial period to ~160 ka (Jouzel and others 1987).

The records obtained from these ice cores include the isotopic compositions of oxygen and hydrogen in the ice, the amount and composition of atmospheric gases sealed within the ice, the temperature of the ice, the abundance of particulate impurities, and of isotopes such as meteoric Be-10. Some of these can be used directly to infer the ice thickness or elevation history. Others indicate the conditions of formation of the ice, and can be combined with ice-flow models to date the core and hence provide an environmental history of the region. Since the conditions of snow formation are sensitive to elevation, reconstructions of the ice sheet are a vital part of paleoclimatic interpretations of the environmental data. Conversely, if assumptions are made regarding the response of the ice sheet to climate changes, the paleoenvironmental record derived from an ice core can be used to constrain the former size of the ice sheet.

4.4.1 Total gas content

Following the observation that the total gas content in ice could be used as an indicator of the elevation at which the ice was formed (Raynaud and Lorius 1973, 1977), Raynaud and Lebel (1979) derived an equation relating this volume to the atmospheric temperature and pressure at the time of ice formation. The amount of gas trapped in pore spaces within ice is dependant on the initial pore volume, and the atmospheric temperature and pressure at the time of pore closure. These can be related to the volume of gas measured at standard temperature and pressure using Boyle's Law:

$$V = V_C \cdot \frac{P_C \cdot T}{T_C \cdot P} \qquad (4.1)$$

where V is the volume of gas measured at standard temperature T and Pressure P, and V_C (per gram of ice) is the pore volume when pores are finally closed off in the firn temperature T_C and atmospheric pressure P_C. In order to determine how V_C depends on T_C and P_C, Raynaud and Lebel (1979) measured V for samples of recently formed ice from six locations in

Antarctica and Greenland and obtained the following relation between V, T_C, and P_C:

$$V=\left[7.4 \times 10^{-4} P_C - 0.057\frac{P_C}{T_C}\right] \frac{T}{P} \qquad (4.2)$$

where the temperatures are expressed in degrees Kelvin, and the pressures in millibars.

This relationship has been used to derive elevation histories for the East and West Antarctic ice sheet, and the Greenland ice sheet, using gas content profiles measured from ice cores (eg Raynaud and Whillans 1981, 1982, Lorius and others 1984, Herron and Langway 1987, Raynaud and others 1987, Jouzel and others 1989).

This method rests on the assumption that the dependance of gas content on elevation was the same in the past as it is today. This assumption is thought to be dubious by Paterson and Hammer (1987), who note that gas content depends on pore volume, which in turn depends on the grain size of the ice crystals; this was reduced during the glaciations as a result of reduced temperature and increased atmospheric dust concentration. Paterson (1981, p343) also notes that the seasonal variation in gas content corresponds to an elevation difference of nearly 600 m according to the formula of Raynaud and Lebel (1979). This represents a possible error margin if sampling is inadequate.

The total gas content determinations from the upper part of the Vostok core are shown in Figure 4.7. Lorius and others (1984) suggest that the LGM ice appears to have formed at an elevation ~30 m below the youngest ice, but the scatter in the data is significant, and they conclude that the elevation was close to the current Vostok altitude. From measured ice velocities and the present topography of the ice sheet, Lorius and others (1984) estimate that the LGM ice formed a few tens of kilometres from the drilling site, where the ice sheet is currently ~100 m higher than at Vostok. This implies that the elevation of the ice sheet in this region has increased by ~100 m since the LGM, although this value is significantly smaller than the uncertainty of ±600 m noted above.

Similar treatment of the Byrd core in West Antarctica indicates 200 - 350 m elevation increase since the LGM (Raynaud and Whillans 1982, Jenssen 1983).

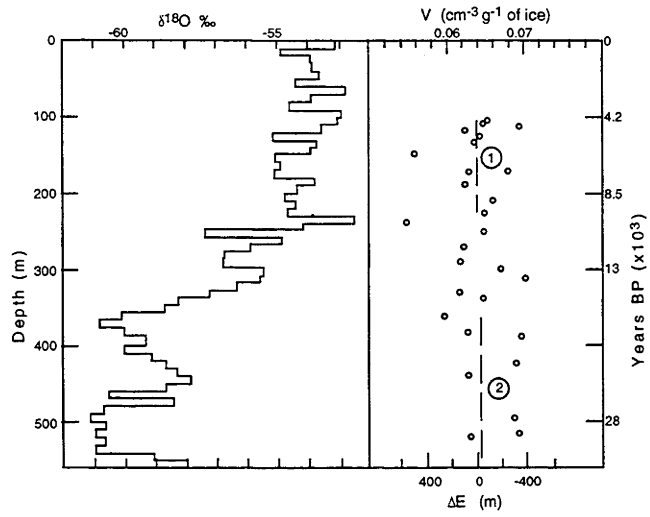

Figure 4.7 : Total gas volume measurements in the Vostok ice core, showing that LGM ice formed at a similar elevation to the present Vostok site. Since the source of this ice is several tens of kilometres from the Vostok site, this implies that the ice sheet was ~100 m lower at the time (Lorius and others 1984). The oxygen isotope profile is also presented, showing the lighter values associated with colder temperatures during the last glaciation.

4.4.2 Isotopic records

The oxygen- and hydrogen-isotopic composition of water and ice are measured by the abundance of ^{18}O and deuterium (D or ^{2}H) in the sample relative to the abundance of the more common isotopes ^{16}O and ^{1}H respectively. This ratio is expressed relative to the ratio in Standard Mean Ocean Water (SMOW), for example:

$$\delta^{18}O = \frac{[^{18}O/^{16}O]_{sample} - [^{18}O/^{16}O]_{SMOW}}{[^{18}O/^{16}O]_{SMOW}} \qquad (4.3)$$

This delta value is usually multiplied by 1000 and the result expressed in parts-per-thousand (‰). The isotopic ratios of oxygen and hydrogen in Antarctic precipitation depend on a) the isotopic composition of the source region in the ocean, b) the temperature and humidity at which evaporation occurred, c) the degree of precipitation which occurs between the source and the site of deposition, and d) the temperature at which precipitation occurs. The variation in a) is known from marine stable isotope records obtained from deep-sea cores: at the LGM, the $\delta^{18}O$ of the oceans was ~+1.1‰ relative to SMOW (Chappell and Shackleton 1986). The effect of this difference on the isotopic composition of Antarctic precipitation at the time has been included in published interpretations of the stable isotope record from ice cores. The effect of b) is difficult to reconstruct for past climates, but is thought to be small (Robin, 1977); alternatively, the temperature of evaporation may have remained the same if the main source moves closer to the equator during glacial periods. The effects of c) and d) have been successfully modelled as a process of Rayleigh condensation, with

continuous removal of the condensate (Jouzel and Merlivat 1984), and the relationships between the isotopic ratios of oxygen and hydrogen and the temperature at which precipitation occurs is the basis for interpreting paleotemperatures from the ice core record.

The present snow accumulation rate at Vostok is 2.2 - 2.5 g cm^{-2} yr^{-1} (Lorius and others 1985), which is much less than the scale of surface roughness caused by wind scouring of the ice ("sastrugi"). Because of the low accumulation rates, and diffusion processes during firnification (the sintering of snow into ice), seasonal variation in the isotopic composition of snowfall is not preserved at depth in the ice sheet (Johnsen and others 1972), and the temperature inferred from $\delta^{18}O$ or δD represents the mean annual temperature. At the present, the mean annual temperature varies over the ice sheet mainly as a function of altitude, so an estimate of the formation height of the ice at a given depth in the core is required before paleoclimate can be inferred from the paleotemperatures. This is done using flow models for the ice sheet (Lorius and others 1985), which calculate the age and formation position of ice in the core, assuming that the ice sheet was not significantly different from its present configuration.

Observations of current snow accumulation rates in Antarctica show a positive correlation with mean annual temperature (Robin 1977), due to the fact that cold air can carry less moisture. The temperature record from Vostok, which indicates that LGM conditions were ~6°C colder than present, therefore implies that precipitation rates may have been generally lower at that time. This result is supported by measurements of meteoric ^{10}Be in the same core. Production of ^{10}Be is thought to have remained roughly constant, but ice which formed at the LGM contains substantially higher concentrations than modern ice (Yiou and others 1985). This indicates that precipitation at that time was about half the present value. The same record shows that precipitation rates during the last interglacial were similar to those during the Holocene.

The isotope record from the Vostok core indicates that temperatures during the last interglacial period were ~2 °C warmer than present conditions (Jouzel and others 1987). This was originally interpreted as a regional, if not global, paleotemperature, but this interpretation is dependant on the assumption that the ice sheet has not changed significantly. An alternative explanation, advanced by Robin (1985) is that this warmer temperature is due to ice sheet elevations 300 - 350 m lower than present. This suggestion is reasonable because the snow accumulation rate in the Antarctic interior is very low, so the response time of ice thickness to climate change is probably tens of millenia, compared to a few millenia in coastal regions (Robin 1985). Lower elevations of the ice sheet during the last interglacial would therefore be due to the lower precipitation rates during the penultimate glaciation, which is thought to have been relatively colder and more prolonged than the last glaciation (Shackleton and Opdyke 1973). This argument is supported when the beginning of the last glaciation is considered (116-106 ka, isotope stage F in Lorius and others 1985). The Vostok stable isotope

record indicates colder temperatures for this period than are implied by the ice-volume record from deep-marine cores. Robin (1985) suggests that these colder temperatures at Vostok represent a higher ice sheet at that time, in response to the high precipitation rates of the preceding 20 kyr of interglacial conditions. Applying a similar argument to the LGM, after ~100 kyr of glacial period conditions, suggests that the ice sheet may have been 200 - 300 m thinner than present. If this is the case, then the LGM-to-present temperature rise of ~6 °C (Lorius and others 1984), calculated assuming negligible change in ice sheet elevation, must be increased by 2 - 3 °C.

4.4.3 Cores from coastal regions

Ice cores from coastal regions of the East Antarctic ice sheet indicate an elevation history very different from that of the interior. Budd and Morgan (1977) obtained stable isotope ratios and total gas content measurements from several cores from Law Dome, and observed changes attributed to postglacial climate change, though the relative importance of climate, ice flow and ice thickness were not separated. Based on the geomorphological observations of Cameron (1964) and the assumption that the ice sheet formerly extended as far as the shelf edge, they estimated that the ice sheet at the LGM extended ~60 km beyond its present position, with ~1200 m more ice at the present coastline, decreasing to ~500 m 400 km inland. Grootes and Stuiver (1987) re-analysed the oxygen isotope profiles from three coastal cores, and estimated a maximum decrease in elevation of the ice since the LGM of around 530 m.

At another coastal site, D-10 in Terre Adélie, Grootes and Stuiver (1987) estimate that about 1300 m of surface lowering occurred in the glacial-interglacial transition. Studying a flow line passing through this site, Raynaud and others (1979) estimated 400 m of postglacial surface lowering 250 km inland. The estimated decrease in excess ice at the LGM with increasing distance from the coast is consistent with the estimates of static or increasing ice thickness in the interior of the ice sheet.

4.4.4 Ice temperature profile

Analysis of a temperature profile from a core taken at Dome C, combined with ice sheet flow modelling, led Ritz and others (1982) to conclude that the East Antarctic ice sheet has thickened by 200 - 280 m in the last 10 kyr. This estimate depends on the snow accumulation rate measured over a few years, and the estimate, the vertical component of ice flow derived from the flow model, and the surface temperature history inferred from oxygen isotope measurements.

4.4.5 Discussion

It is important to realise that the measurements obtained from ice cores do not all measure the same property of the ice sheet. The total gas content measurements record the elevation of the ice sheet, that is, the height of the

ice sheet surface above sea-level. This is analogous to a record of relative sea-level, with the ice sheet thickness forming an extra variable compared to observations made from a location on rock. The former ice sheet elevations derived from the isotopic records also fall into this category, so require some interpretation before a change in the ice load can be inferred. This is discussed in detail in Chapter 7. The temperature-profile study, on the other hand, measures the change in thickness of the ice sheet, but cannot detect elevation change due to vertical movements of the underlying bedrock.

4.5 Theoretical Models

Theoretical models of the Antarctic ice sheet also provide estimates of the ice volume and distribution at the LGM. Hughes and others (1981) produced a comprehensive reconstruction of the entire Antarctic Ice Sheet based on the assumptions that a) the ice sheet expanded to the edge of the continental shelf (the 500 m bathymetric contour), and b) the ice sheet reached equilibrium. Theoretical profiles were then calculated along many flowlines to produce the model reconstruction (Figure 4.8). This model ice sheet contains an excess ice volume, compared to the present ice sheet, equivalent to 24.7 - 29.2 m of sea-level change, depending on the rock-to-ice density ratio used. This reconstruction has been used as the basis for the Antarctic contribution to global models of glacio-hydro-isostasy (Nakada and Lambeck 1988, Tushingham and Peltier 1992). The authors of this model have revised portion of it in the light of new geologic evidence (Denton and others 1989b) but have not constructed a new model based on glaciological principles.

A time-dependant, thermomechanical model for the entire Antarctic ice sheet constructed by Huybrechts (1990, 1992) takes into account the dynamics of ice sheets and shelves, and is forced by sea-level changes, temperature, and precipitation. The resulting reconstruction for the LGM shows general agreement with some observed constraints on the ice sheet at that time, such as the negligible elevation change of the central East Antarctic ice sheet, and the sensitivity of the West Antarctic ice sheet to sea-level change. The volume difference between the LGM reconstruction and the present ice sheet equates to 12 - 16 m equivalent sea-level. The model predicts grounding of the Ross and Filchner-Ronne ice shelves, although in the Ross Sea a longer period of glacial conditions is required.

Alley and Whillans (1984) modelled the response of the ice sheet to sea-level change, assuming that deglaciation was initiated by sea-level rise due to melting of northern hemisphere ice sheets (Denton and others 1986). The model suggests that ice sheet retreat leads to over-steepening of the margin, which causes draw-down of the interior regions which propagates inland over thousands of years. Although this work overestimates the amount of sea-level change which actually occurred during deglaciation, since isostasy was not taken into account, it demonstrates how removing ice from the margin only, which is a readily explicable physical mechanism for deglaciation, eventually results in ice removal from further inland as well, as the ice sheet responds to preserve its height/width relationship. This model does not aid reconstructions of the LGM ice sheet, but it does provide a mechanism for the thinning of the ice sheet during deglaciation. One implication of this model is that the excess ice is not removed from all locations at the same rate: coastal ice is removed before thinning occurs further inland. This may explain the observed stabilisation of the ice sheet margin by ~10 ka, as observed at several coastal oases, while the global sea-level record indicates that significant melting continued until at least 6 ka.

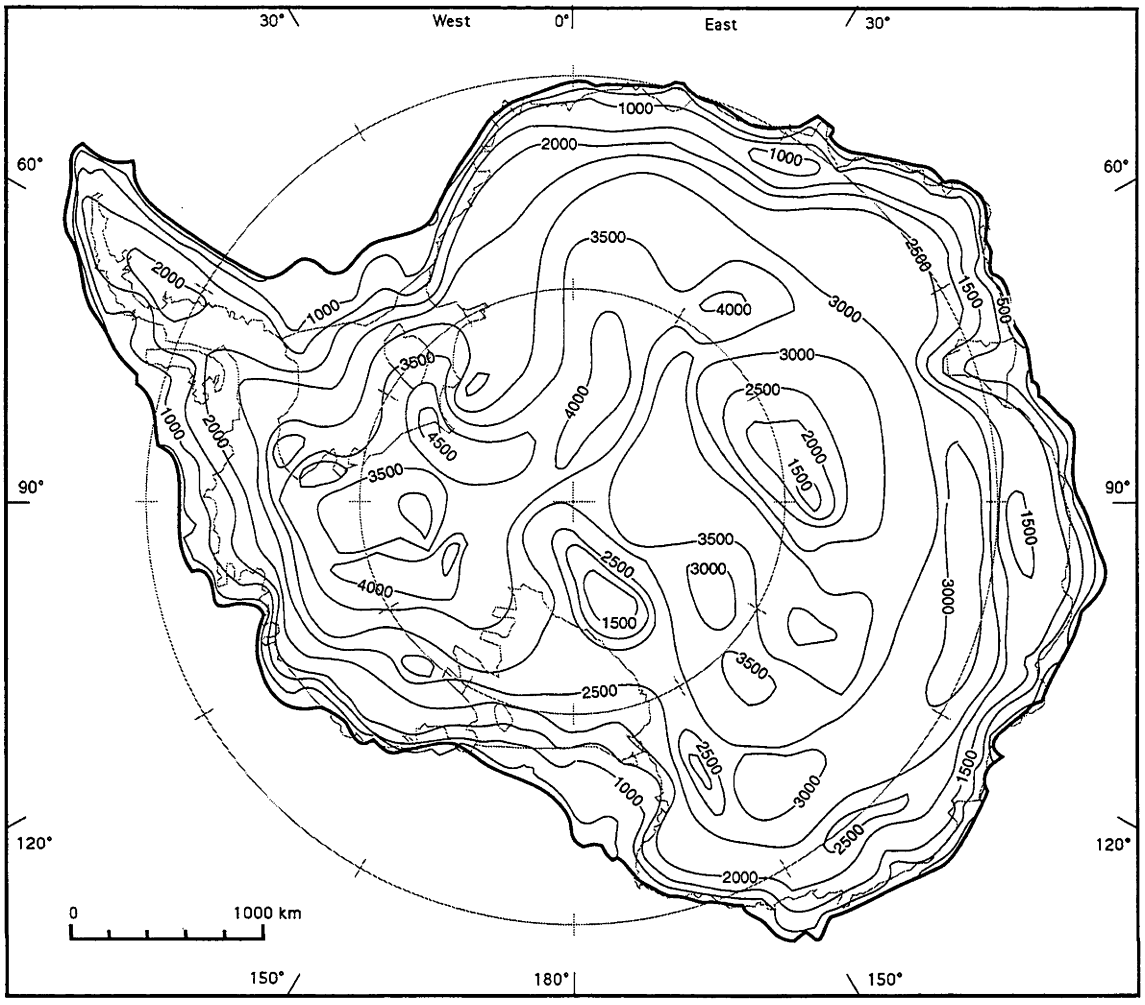

Figure 4.8 : Ice-thickness contours in 500 m intervals for the maximum reconstruction of the LGM Antarctic Ice Sheet by Stuiver and others (1981, fig 6-16).

The ice sheet of the Antarctic Peninsula has been modelled separately by Payne and others (1989). Using a model forced chiefly by sea-level change, they derive a reconstruction for the LGM which has an ice dome 3.5 km high over the Peninsula, which contributed ~1.9 m equivalent sea-level during deglaciation. This contrasts with Huybrechts' (1990) model which has ice only 1.5 km high. One reason for this discrepancy could be the fact that Payne and others assume that precipitation did not vary from its present value over the last glacial cycle. Estimates of paleo-precipitation from that region are not available, but data from the interior of the East Antarctic ice sheet (Jouzel and others 1989) show that precipitation rates there were ~50 % of their present value. Tests by Payne and others (1989) indicate that if this was the case in the Antarctic Peninsula region, the ice sheet there would not have expanded at all. This model indicates rapid deglaciation of the Peninsula region, mostly between 10 ka and 6.5 ka.

4.6 Estimates of Modern Mass Balance

Major melting of the Antarctic ice sheet ceased ~6 ka, as shown by the general stability of global sea-levels since then, and the stability of the ice sheet margin. However, the discrepancy between predicted and observed sea-level highstands in eastern Australia and other far-field sites (Nakada and Lambeck, 1988) indicates that water has been added to the world's oceans in the last 6,000 years equivalent to about three metres of sea-level, ie. an equivalent sea-level rise of 0.5 mm/year. Similarly, sea-level observations from Great Britain indicate melting of 1.7±1 m esl since 6 ka. As the largest reservoir of grounded ice, the Antarctic ice sheet is a likely source for the majority of this water, although alpine glaciers and small ice caps may also have contributed. Since this degree of melting would have caused negligible margin retreat (although it may have caused significant but unobservable grounding line retreat), the best estimate of its magnitude probably comes from calculations of the modern mass balance, although these may be affected by both short-term variation in mass balance, and by anthropogenic changes, and so may not be representative of the late Holocene as a whole.

Unfortunately, opinion is divided over whether the ice sheet is gaining or losing mass. A summary of glaciological measurements (Bentley and Giovinetto 1992) concludes that the ice sheet is growing at a rate equivalent to a sea-level fall of about 0.5 mm/year. This conflicts with the conclusion from oceanographic estimates of iceberg flux, which indicate a mass loss (sea-level rise) of several times this rate (Orheim 1993). The difference may be due to non-equilibrium retreat of the ice shelves during the period of observation, but this has not been ascertained.

4.7 Summary

Glaciological data from the East and West Antarctic ice sheets suggest that the elevation of their interiors has not changed dramatically since the LGM, and may even have been ~200 m lower than at present as a result of lower accumulation rates during the glacial period, caused by lower temperatures and increased distance from the open sea.

The margin of the ice sheet away from major ice shelves and outlet glaciers seems to have advanced to the shelf edge in some places but may not have done so everywhere. This advance was probably in response to the exposure of the continental shelf as sea-level fell, so the amount of advance was dependant on the bathymetry at each site. This expansion of the ice sheet margins is documented in coastal ice cores and glacial deposits in the Sør Rondane Mountains, which indicate ~1000 m thicker ice at the coast, thinning inland to ~400 m 200-250 km inland. An average advance of ~50 km is probably reasonable in East Antarctica. The continental shelf of West Antarctica in the Amundsen Sea is generally wider that around East Antarctica, but also deeper, so it is difficult to estimate the former position of the ice sheet margin at these locations. An advance of 50 km around the entire Antarctic coast, with an ice thickness of 1000 m, constitutes an ice volume of ~4.5 m ESL.

The Ross, Filchner-Ronne and Amery ice shelves probably all advanced to the continental shelf edge, in ~500 m water depth, causing thickening inland of 1000 - 1500 m in the inner Ross Embayment and up to 700 m in the lower Lambert Glacier. Thickening in the inner Ronne-Filchner Ice Shelves was probably slightly more than in the Ross Sea, since the extent of grounded ice would have been greater.

The timing and pattern of postglacial melting can be estimated from the marine and terrestrial organisms which recolonise land or sea-floor exhumed from under the ice sheet. Ages determined in this way represent minimum exposure ages, since conditions may not have been suitable for life immediately after the retreat of the ice. Radiocarbon ages from several rocky oases on the East Antarctic coast indicate that retreat was complete by ~10 ka. This is in general agreement with radiocarbon dates from marine sediments offshore. Marine sediments offshore from some coastal glaciers, and terrestrial sediments in the Antarctic Peninsula region suggest a minor readvance of some glaciers in the early Holocene.

Some theoretical models, forced by global sea-level change, indicate that most Antarctic melting occurred between 10 ka and 6 ka.

The present mass balance of the Antarctic ice sheet is not known well enough to constrain its melting during the late Holocene.

Part II

Modelling sea-level change

Chapter 5 : Basics of glacio-hydro-isostasy 139

Chapter 6 : Modelling sea-level change in north Queensland 159

Chapter 7 : The Antarctic Ice Sheet and sea-level change 185

Chapter 5

Basics of glacio-hydro-isostasy

5.1 Introduction

The formation of a large ice sheet has several effects on global sea-level. A large amount of water is removed from the oceans, causing a sea-level fall; isostatic compensation to the altered ice and water loads causes a relative sea-level rise close to the ice sheet where subsidence occurs, and a relative fall in the region of the "peripheral bulge"; and the redistribution of mass from the oceans onto the land causes the geoid, which defines sea-level, to rise near the ice sheet and fall elsewhere. These effects are summarised in Figure 5.1 a) and b). When an ice sheet melts, the sea-level changes described above are reversed as melt-water returns to the ocean basins.

The sea-level changes at a continental margin far from the ice sheet are shown in Figure 5.1 c). The earth takes time to adjust to the altered loads, and sea-level change in the late Pleistocene and Holocene due to these processes is highly complex, because of the existence of several ice sheets, the irregular shape and bathymetry of the oceans, and probable spatial variation in the rheological properties of the earth. Clearly, if we are to interpret the sea-level histories which we observe in different parts of the world, we must be able to model the glacio-hydro-isostatic effects of a given ice-sheet reconstruction.

Early studies in this field (Walcott 1972, 1973, Chappell 1974, Cathles 1975) recognised the relationship between ice loads and deformation of the earth, and used global sea-level records to infer the rheological parameters of the earth, assuming a three-layer visco-elastic model. Farrell and Clark (1976) presented an exact method for calculating the sea-level change due to the movement of ice and water masses on the surface of a viscoelastic earth, including the effects of the changes in the Earth's gravitational field. In this method, Green's functions are used to calculate the deformation due to a point load, and this response is convolved with the model load. Point loads, however, cause singularities in the computation, and this method was adapted by Peltier and others (1978) to a finite-element form, with the ice and water loads represented by a number of disc loads of varying sizes. Nakada and Lambeck (1987) reformulated the problem, expressing the irregular ice and water loads over the entire surface of the earth as the sum of a spherical harmonic series. The sea-level change at any location can then be calculated by the combination of surface deformation and potential changes caused by each degree of the spherical harmonic expansion.

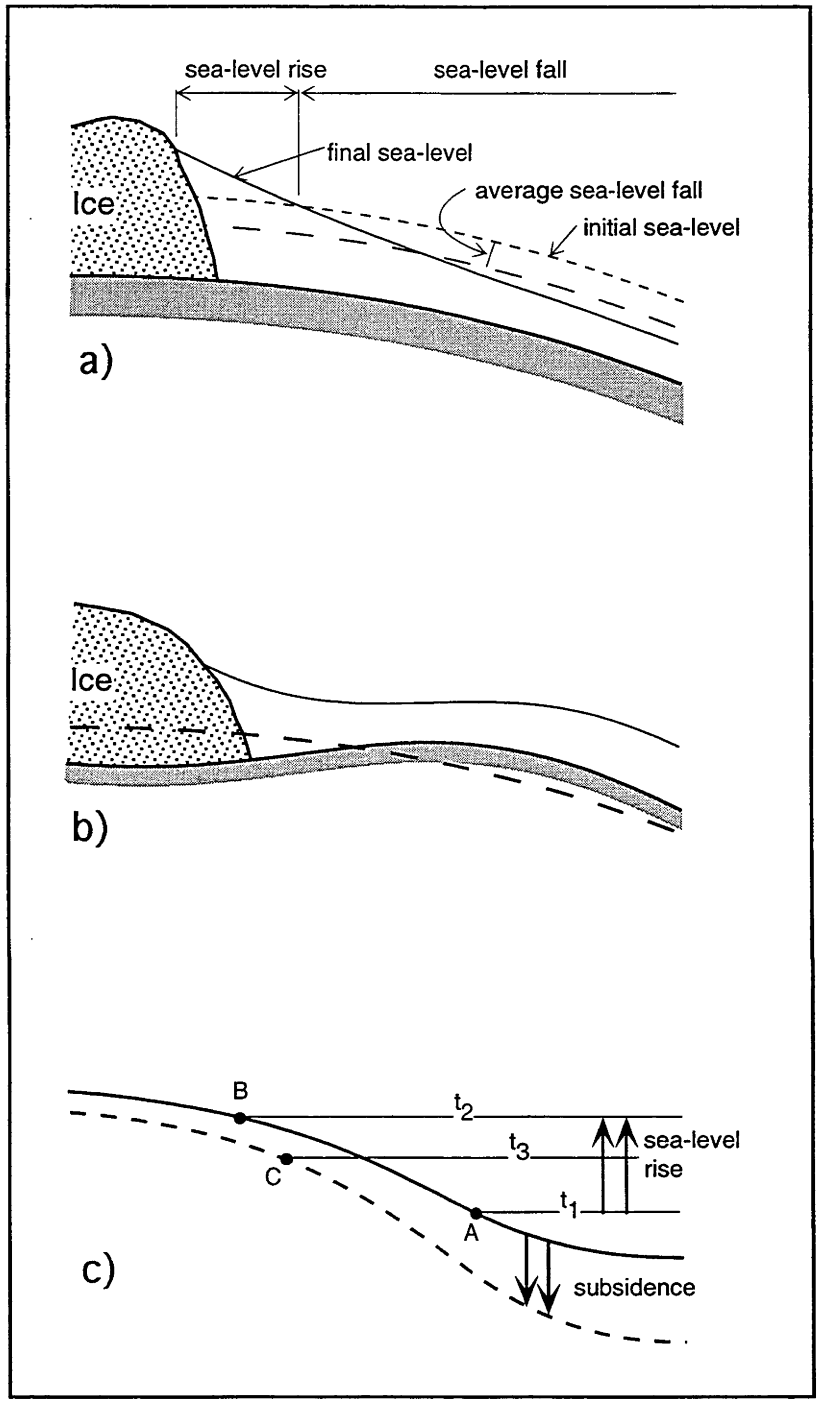

Figure 5.1 : Schematic illustration of the sea-level changes which occur in response to the formation of an ice sheet. a) near the edge of an ice sheet on a rigid planet, sea-level may rise due to the gravitational attraction of the ice; b) on a deformable earth, subsidence near the ice sheet contributes to a sea-level rise there, while the emergence of a peripheral bulge causes sea-level fall further from the ice sheet. c) at a continental coastline far from the ice sheet, rapid sea-level rise from time t_1 to t_2 causes the shoreline to move from point A to B. The crust responds to the increased water load by subsiding beneath the oceans and rising beneath the continent, producing a tilting of the margin. Thus at time $t_3 > t_2$, sea-level appears to drop (point C).. Figure from Lambeck (1990).

The accuracy of the spherical harmonic calculation depends on the degree to which the expansion is made, and also on the resolution of the ice models and ocean description which are used as input for the calculation. The degree of the expansion corresponds to the number of half-wavelengths in 180°, so that the expansion to degree 90, for example, cannot model loads or deformation to a resolution finer than 180°/90, or approximately 220 km. Similarly, if the loads are only described at coarse resolution, high-resolution sea-level predictions cannot be calculated.

Both of these factors have been serious limitations to early calculations of sea-level change. Cathles (1975) was restricted to degree 36, and Mitrovica and Peltier (1991) truncated the series at degree 30. A slightly different theoretical approach allowed Nakada and Lambeck (1987) to extend calculations to beyond degree 180, and more recently degree 256 has become routinely attainable using the method of Mitrovica and Peltier (1991). This should be sufficient for all future sea-level calculations, since the rigidity of the lithosphere ensures that short-wavelength loads are distributed over a wider area.

The resolution to which the ice load was known was also very poorly known initially. Wu and Peltier (1983) used a 5° grid, which corresponds to degree 18. Higher degree calculations based on this model were nevertheless warranted, since the water load, which produces most of the sea-level change far from the ice sheet, could be accurately described. However, this ice model produced deformation with significant power at high degrees (>30) which meant that an earth model with a thick lithosphere was required in order to obtain agreement with sea-level observations. Nakada and Lambeck (1987) interpolated the 5° model to 1° resolution, which provided satisfactory sea-level predictions using a reasonable lithospheric thickness.

5.2 The sea-level equation

Sea-level change due to changing ice sheets can be described as the sum of three components which vary over the earth's surface and with time. This description is called the sea-level equation, as formulated in Farrell & Clark (1976) and Nakada & Lambeck (1987):

$$\Delta\zeta(\lambda,\phi,t) = \Delta\zeta^{e}(t) + \Delta\zeta^{i}(\lambda,\phi,t) + \Delta\zeta^{w}(\lambda,\phi,t) \qquad (5.1)$$

where $\Delta\zeta(\lambda,\phi,t)$ is the sea-level relative to its present value, at time t, latitude λ, and longitude ϕ. The first term is the equivalent sea-level (ESL), defined as

$$\Delta\zeta^{e} = \frac{\text{change in ocean volume}}{\text{ocean surface area}} \qquad (5.2)$$

The change in ocean volume is equal to the change in the volume of ice on land, multiplied by the ratio of the densities of ice and water. The ocean surface area may change slightly through time, as sea-level changes cause low-lying land to be inundated or shallow seas to become exposed. On the earth in the Late Pleistocene and Holocene, the ocean surface area has always been close to 70 % of the earth's surface.

The second term in equation (5.1) is the ice-load component of sea-level change, which includes the delayed isostatic effects of earlier changes in the ice load, and the effect of changes in the earth's gravity field caused by the redistribution of ice on the surface and material within the earth.

The third term is the water-load component, which incorporates the isostatic and gravity effects due to sea-level change. This term is a function of the total sea-level change and of the change in ocean geometry, and must be determined iteratively. For the first iteration, the sea-level change is taken to be the equivalent sea-level. This is a reasonable approximation in the far-field. Near the ice sheet, however, where the rate of isostatic rebound is greater than that of ESL rise, the first estimate of the water-load component will actually have the wrong sign, so at least two iterations are necessary. For higher iterations, the sum of the ESL, ice-load and water-load components of sea-level change are used to define the water load.

The relationship between the influence of the ice-load and water-load components allows us to define zones of sea-level change according to their distance from the ice sheet. For regions within or close to the margins of the ice sheet, $|\Delta\zeta^{i}| >> |\Delta\zeta^{w}|$, and this region forms the *near field*. Far from the ice sheet, $|\Delta\zeta^{w}| > |\Delta\zeta^{i}|$, and this region forms the *far field*. In the *intermediate field*, between these two zones, the two terms are of roughly equal importance.

5.3 Axisymmetric models

If we model an ice-earth-ocean system that is symmetric about the pole, then the sea-level calculations become much simpler, and high resolutions can be obtained relatively easily. Using this simple model, the processes which cause sea-level change can be investigated without the complicated effects of ice sheet and ocean geometry. The computer programmes used to implement this model were developed by Johnston (1993). As described above, numerical calculations of sea-level change due to glacio-hydro-isostasy require ice sheet, ocean and Earth rheology models as input, and these are discussed below.

5.3.1 Axisymmetric ice sheet models

The ice sheets used in this series of models are circular, and have a profile which approximates that of real ice sheets. Assuming perfectly plastic flow within the ice, Paterson (1969) derives a parabolic profile for an ice sheet in equilibrium on an flat surface:

$$\left(\frac{h}{H}\right)^2 = 1 - \frac{x}{L} \tag{5.3}$$

where h is the height of the ice sheet surface at a distance x from the centre, and H and L are the maximum height and radius of the ice sheet. The values of H and L are related by the basal shear stress of the ice sheet, τ_b, in the following way:

$$H^2 = \frac{2\,\tau_b\,L}{\rho\,g} \tag{5.4}$$

where ρ is the density of ice, and g is the acceleration due to gravity. Observations of real ice sheets suggest that τ_b usually lies in the range 0 - 100 kPa (Paterson 1994), and Figure 5.2 shows an ice sheet profile using $\tau_b = 50$ kPa, with a radius of 1000 km. This approximately the size of the Fennoscandian ice sheet at the LGM, and contains an ice volume of 14.2 m ESL.

The parabolic model matches observed ice sheet profiles reasonably well, and is adopted here. However, it does predict a non-zero slope at $x = 0$, which would result in a cusp at the centre of the ice sheet. If the actual flow law of ice is used to calculate the surface profile, instead of assuming perfect plasticity, then a smooth profile results, described by the following equation (Paterson 1969):

$$\left(\frac{h}{H}\right)^{2.5} = 1 - \left(\frac{x}{L}\right)^{1.5} \tag{5.5}$$

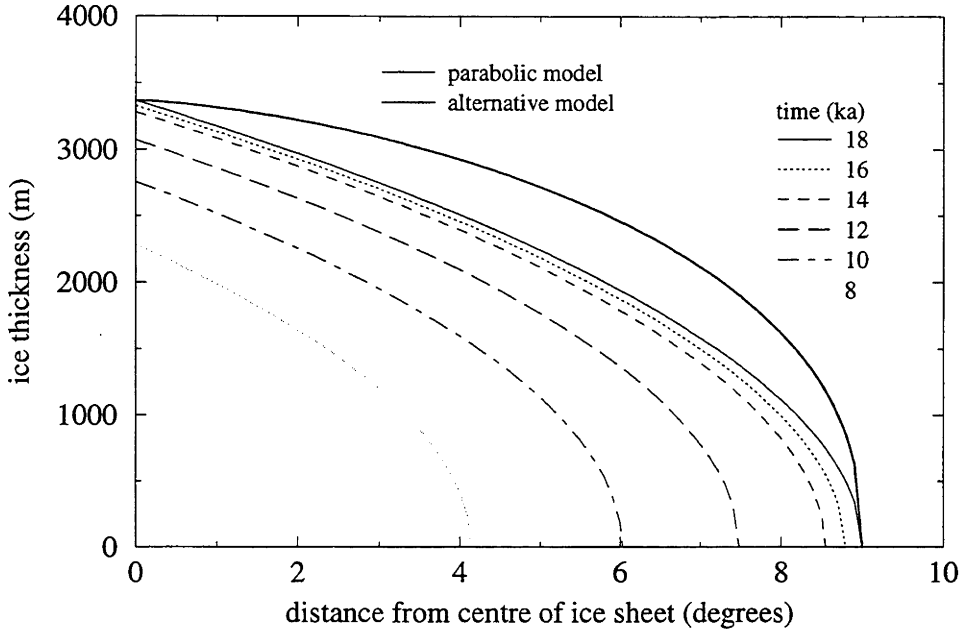

Figure 5.2 : Profiles of axisymmetric ice sheet models. The thin lines show the parabolic profile, shown in equation 5.3. This is the model adopted for the calculations in this chapter, and the profiles of the ice sheet as it melts are also shown on the figure. Melting is complete at 6 ka. The thick line shows an alternative model ice sheet profile, defined in equation 5.5.

This form has been used in some realistic ice sheet modelling (Lambeck 1993), and an example is shown in Figure 5.2, for comparison with the parabolic model. The two models have similar distribution of ice within a circular ice sheet, and are probably equally good for these simple axisymmetric models. Note the vertical exaggeration in Figure 5.2, and that the cusp at the centre of the parabolic ice sheet is in fact very small.

The melting history of this model is proportional to that of the northern hemisphere ice sheets since the last glacial maximum (LGM) 18,000 years ago, as described by the ESL curve ARC3 in Lambeck (1990). Most of the melt occurs between 16 ka and 8 ka, and melting is complete at 6 ka. It is assumed that the ice sheet remains in equilibrium at all times, and that the basal shear stress, τ_b, does not change as the ice sheet melts. This results in the ratio H^2/L remaining constant. Figure 5.2 shows the profile of the ice sheet at several stages of melting. Alternative models, in which the ice sheet does not maintain constant proportions, but shrinks by losing height, width, or some combination of these, will be discussed in Chapter 7.

5.3.2 Ocean models

The ocean models used in this section have one land mass at the 'north' pole, where the ice sheet is, which is the same size as the ice sheet before

melting begins (1000 km, or 9°). A second circular land mass exists at the opposite pole, which has a radius of ~7300 km (~65°). This size is chosen so that the surface area of the ocean is the same as on the real earth, ensuring that the ESL rise caused by melting an ice sheet on the model earth is the same as that caused by melting an ice sheet of the same volume on the real earth.

Almost all sea-level observations come from coastlines, so it is important to understand the glacio-hydro-isostatic processes taking place in these regions and model them correctly. The simplest ocean basin model is box-shaped in cross-section, with high vertical edges so that the shape of ocean being loaded does not change as sea-level rises. In a more realistic model the far-field coastline has a sloping continental shelf, so that the loading effects of an ocean which transgresses over the continent as sea-level rises can be investigated. The slope of the continental shelf in the latter model was chosen so that the coastline advances 110 km, similar to the advance which has occurred in many some of the world, such as parts of northern Queensland, Australia..

5.3.3 Earth rheological model

The rheological description of the earth is highly dependant on the time-scale under investigation. For rapidly changing loads and short time-scales, eg earthquakes, the earth behaves as an elastic body, apart from the outer core, which is liquid. Over millions of years, the earth responds to external forces in a fluid manner. Examples include the compensation below thickened continental crust, and the flattening of the earth due to its rotation. On the intermediate time-scales on which glaciations occur, neither description is applicable. For these problems, it is most appropriate to treat the earth as a visco-elastic (Maxwell) body, though this cannot be derived from the material properties of its constituent materials. Use of the Maxwell rheology is largely a matter of convenience, since it allows a simple numerical solution and reproduces the observed behaviour of the earth satisfactorily. The parameters of the models are thus "effective" parameters, that describe the average rheology for a particular time scale (10^3 - 10^4 years) and range of stresses.

The rheological models of the earth used in these glacio-hydro-isostatic calculations are radially symmetric, that is, the earth is described as a set of spherical shells which have internally uniform viscosity. Three-layered models are used in these calculations: a rigid lithosphere overlying a two-layer mantle. The boundary between the upper and lower mantle is assumed to be at 670 km depth, as indicated by seismic studies such as PREM (Dziewonski and Anderson, 1981). The variables under consideration, then, are the viscosities of the upper and lower mantle, and the thickness of the crust. To calculate the response of a visco-elastic body when loaded, we also need to define density, and the elastic (K) and shear (μ) moduli throughout the body. The values used here are obtained from the seismic velocity model PREM (Dziewonski and Anderson, 1981).

Initial estimates of the viscosity of the mantle were obtained from early work on postglacial rebound (Walcott 1972, Cathles 1975), and subsequent studies involving searches through a wide range of plausible models have refined these estimates (eg Nakada and Lambeck 1989, Tushingham and Peltier 1992, Fjeldskaar and Cathles 1992, Lambeck 1993b), although agreement has not been reached on the most appropriate model. In this chapter, the rheology used is based on the optimal model determined by Nakada and Lambeck (1989) for the Australasian region. The lithospheric thickness is 100 km, and the upper and lower mantle viscosities are 2×10^{20} Pa.s and 10^{22} Pa.s respectively.

5.4 Sea-level predictions for axisymmetric models

When the earth is loaded by a circular ice sheet with a parabolic profile, the profile of the earth's surface when regional isostatic equilibrium has been reached will consist of a depression which almost matches the profile of the ice sheet, surrounded by a small peripheral bulge in the crust. The depression in the crust at the centre of the load is equal to the thickness of the ice load multiplied by the ratio of the densities of ice and the mantle (ρ_i/ρ_m), which is about 0.25. Far from the ice sheet there is almost no deformation. When the ice load is removed, the depressed crust beneath the load will rise, causing sea-level fall at the centre of the load. Measured relative to present sea-level there, past sea-levels were higher, so the point on the crest of the bulge appears as a maximum on the relative sea-level curve. Conversely, the peripheral bulge, where subsidence has occurred, appears as a minimum on the sea-level curve.

To obtain the sea-level calculations presented in this section, the spherical harmonic expansions of the ice and water loads were truncated at degree 180. Johnston (1993) determined that at degree 90, the sea-level predictions had converged to within 5 cm for this particular earth model, so the precision of these calculations is certainly adequate.

5.4.1 Near field sea-level change

Sea-level change in the near field is dominated by the ice load contribution. This can be divided into an instantaneous component, due to the elastic response of the earth and the change in the gravitational field, and a delayed component due to the earth's viscous response. In practice, it is not useful to separate these contributions, since the melting occurs continuously and over the same time-scale as the viscous response. However, we can determine the instantaneous contribution by removing the model load instantaneously and observing the resulting sea-level change.

Ice-load component

Figure 5.3 a) shows the ice-load component of sea-level change caused by melting the ice sheet instantaneously at 18 ka. There is an immediate fall in sea-level within 49° of the load due to elastic rebound and the loss of gravitational attraction. The effect is greatest in the centre of the ice sheet, where there is a fall of 180 m. This elastic rebound causes the peripheral bulge to increase in size initally. After this initial sea-level fall, viscous rebound continues and the peripheral bulge subsides and moves outwards. After 18,000 years rebound is virtually complete. In the centre of the ice sheet, where the load was 3400 m thick, a total of 830 m (3400 m x ρ_i/ρ_m) of rebound has occurred. The magnitude of the peripheral bulge was about 1/30 of the maximum rebound, with 27 m of subsidence occurring in 18,000 years.

a)

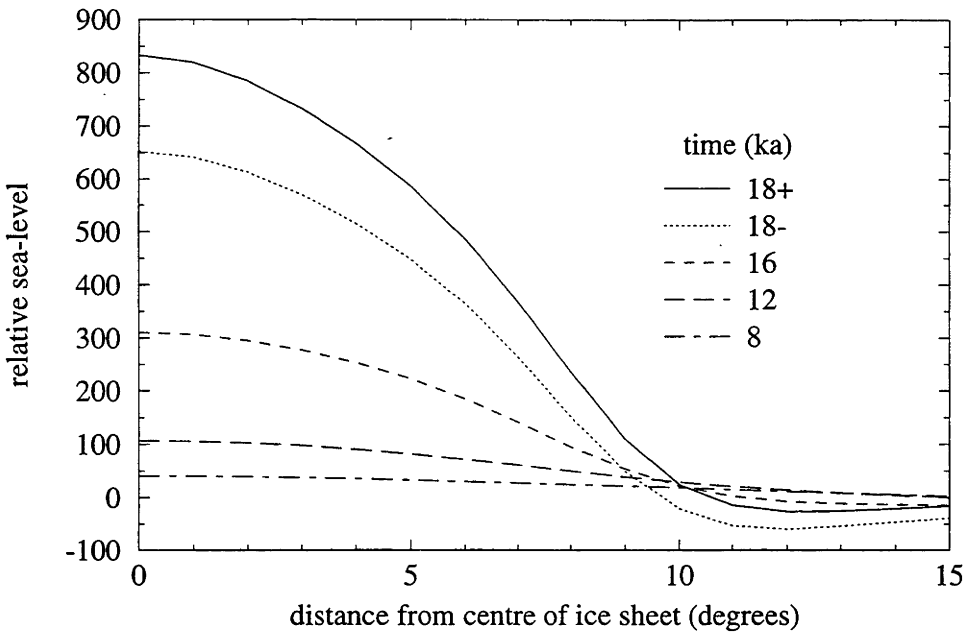

b)

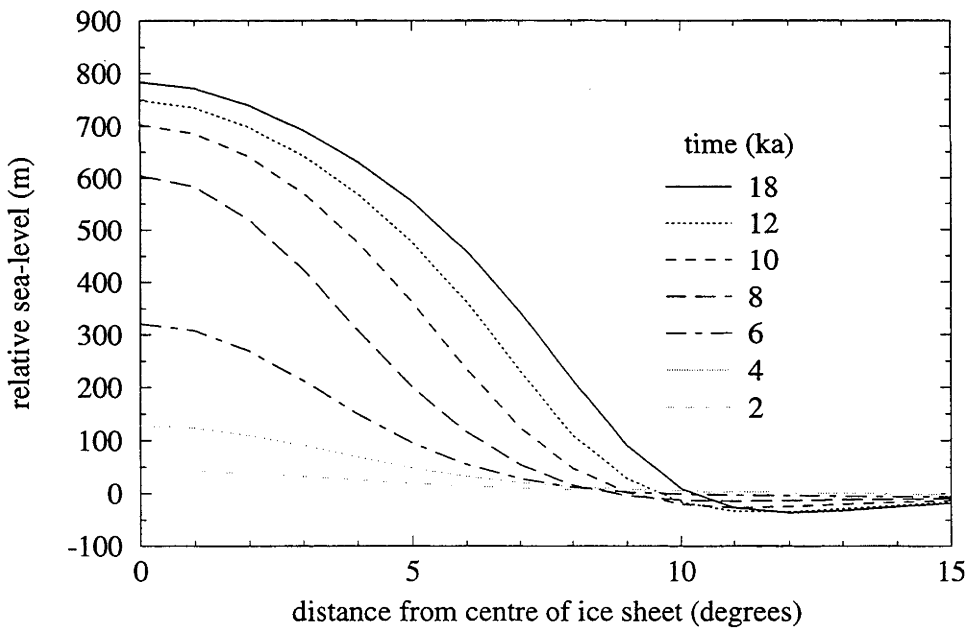

Figure 5.3 : The ice-load component of sea-level change in the near field, caused by removing a circular ice sheet 9 degrees in radius. a) instantaneous melting at 18 ka; b) continuous melting between 18 ka and 6 ka, proportional to the melting of model ARC3 of Lambeck (1990).

The origin of the peripheral bulge is a common source of misunderstanding. A clear distinction must be drawn between the phenomenon of crustal flexure, and that of mantle flow. Crustal flexure causes the peripheral uplift around a load that is mainly supported by the rigidity of the crust, such as seamounts (eg Lambeck 1981). In these cases loading occurs on long (10^6 - 10^7) time scales, so that the mantle can be treated as a fluid and the flexural bulge is controlled by the effective flexural rigidity of the lithosphere. On shorter time scales, loads such as ice sheets are initially supported isostatically by the mantle, and the peripheral bulge is due to outward flow of mantle material in response to subsidence of the earth's surface beneath the load. The magnitude of this bulge is primarily a function of the mantle iscosity, particularly if the lithosphere is thin compared to the viscous layers. When the load is removed, the isostatic rebound causes mantle return flow, which causes the peripheral bulge to collapse. The rigidity of the crust controls the shape of the peripheral bulge to some extent, but the peripheral subsidence discussed here, and later in Chapter 7, is essentially due to mantle flow.

When a continuous melting model is used (Figure 5.3 b), the elastic and viscous contributions cannot be separated, since they occur simultaneously. Rebound in the centre of the ice sheet occurs more slowly than in the case of instantaneous melting, so a smaller amount of compensation is accomplished after 18,000 years. The peripheral bulge moves inwards during melting, following the ice sheet margin, then moves out again as it does in the instantaneous-melting scenario.

Water-load component

The water load component of sea-level change in the near field, shown in Figure 5.4, is much smaller than the ice load component, and is almost negligible as far as the pattern of predicted sea-level change is concerned. The first iteration (Figure 5.4 a) shows the response to a uniform water load of 14.2 m (the equivalent sea-level of the ice sheet) applied over the oceans. No deformation would result if the entire surface of the earth was uniformly loaded, and the middle of the ocean is a close approximation to this, since there is no nearby change in load. At the near field coastline, however, the ocean receives a meltwater load while the adjacent continent does not. This is a situation analogous to removing a disc load from the surface of the continent, causing uplift on land and slight subsidence offshore.

The water load for the second iteration is the sum of the ESL and the ice-load component of sea-level change, restricted to the ocean. As Figure 5.4 b) shows, the second iteration water load correction in the near field is dominated by the ice load component, with the subsidence of the peripheral bulge causing a large increase in the water load in that region. In this model, the near field coastline is fixed at the position of the former ice sheet margin. If the ocean covered the region formerly below the ice sheet, the uplift would cause a large negative water load, causing further uplift in that

region. The effect of moving coastlines in the near field is treated in more detail in Chapter 7.

a)

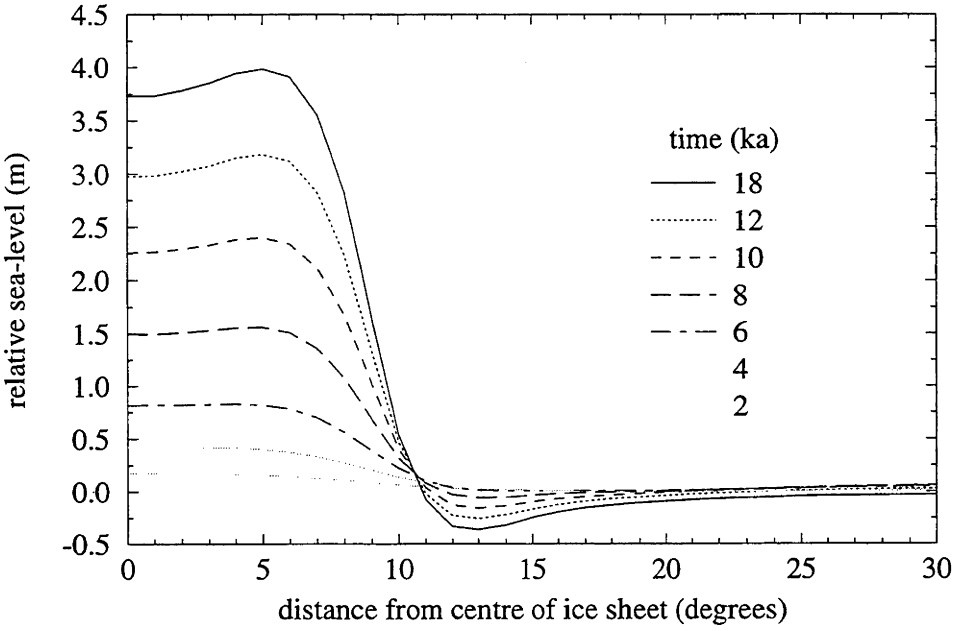

b)

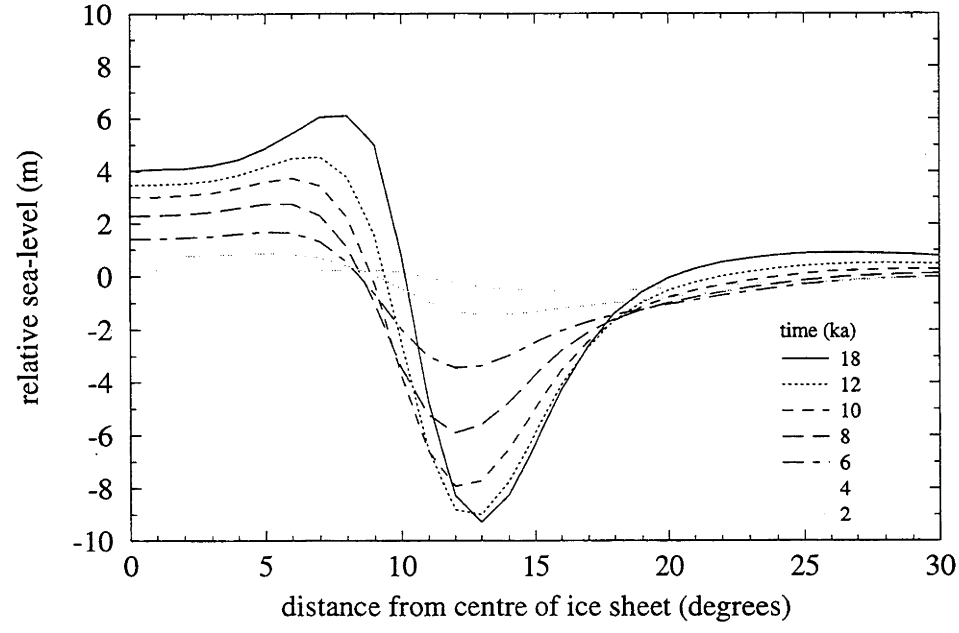

Figure 5.4 : The water-load component of sea-level change in the near field, for the continuous melting model. The coastline is static, 9 degrees from the centre of the ice sheet. a) first iteration; b) second iteration. Note the difference in vertical scale between the two plots.

Total sea-level change

The sum of the ESL and the water-and ice-load components constitutes the total relative sea-level change at a given site. Figure 5.5 shows the sea-level history for the continuous-melting model at three near field sites: the centre of the ice sheet (a,d), the coastline, 9° from the centre (b,e), and a point on the peripheral bulge, 12° from the centre (c,f).

At the centre of the ice sheet, $\Delta\zeta^i > \Delta\zeta^e$, and sea-level change is completely dominated by the ice-load component. In the case of instant deglaciation, the ice-load component, and hence the relative sea-level, would have a decaying exponential form. With continuous melting, the sea-level curve is the sum of a set of exponential curves, offset from each other in time and of

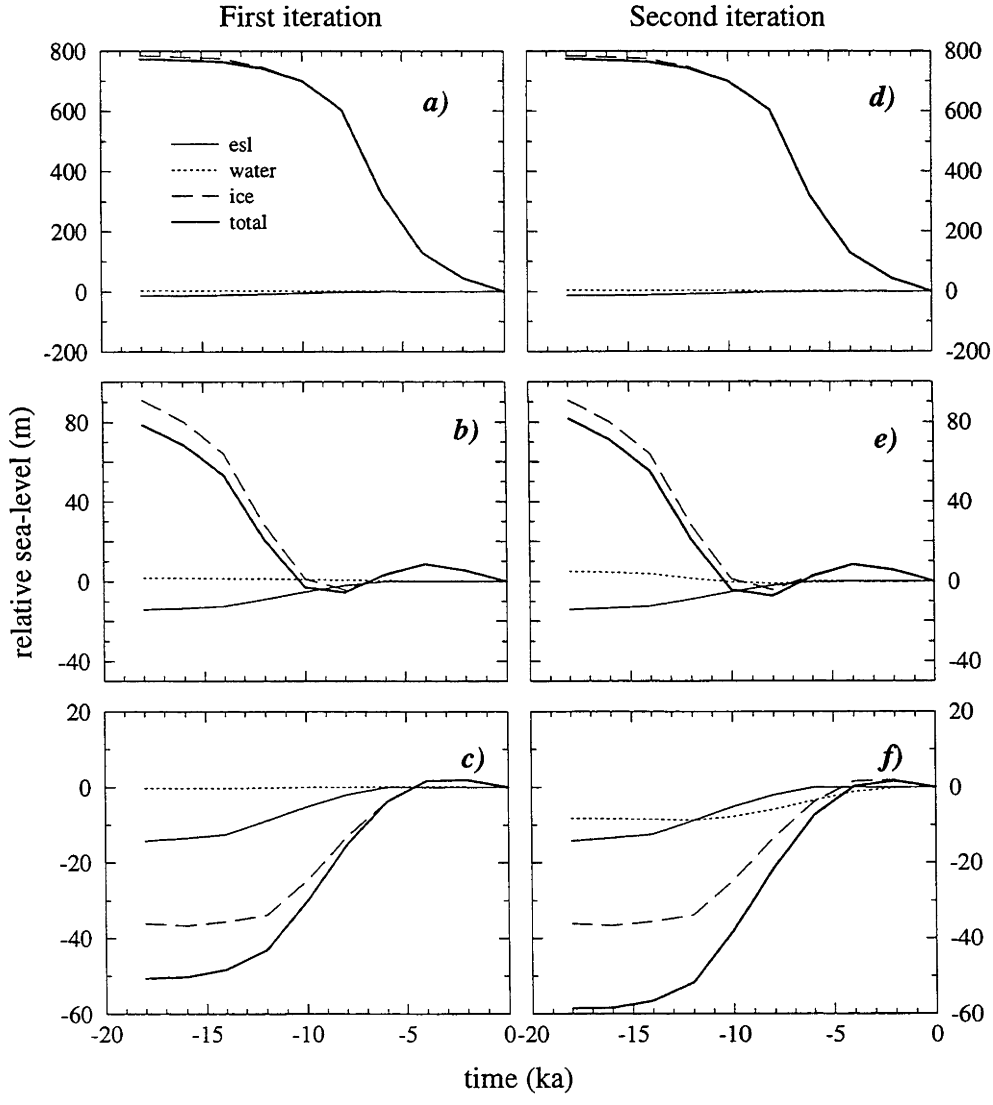

Figure 5.5 : Components of predicted sea-level change for one and two iterations of the water load, at three near field sites: the centre of the ice sheet (a and d); the coastline, 9 degrees from the centre (b and e); and the crest of the peripheral bulge, 12 degrees from the centre (c and f). The effect of the second iteration of the water load is greatest at the bulge site.

magnitude proportional to the rate of melting at that time. The relative sea-level curve is thus strongly influenced by the ESL curve. After melting ceases, sea-level falls exponentially. Because this site is far from the coastline, the second iteration of the water-load component (Figure 5.5 d) is not significantly different from the first iteration.

The migration of the peripheral bulge causes complex sea-level changes at the near field coastline (Figure 5.5 b,e). Again, the sea-level history is dominated by the ice-load component. However, the total amount of rebound is smaller than at the centre of the ice sheet, so the ESL contribution of 14.2 m noticeably reduces the amount of sea-level fall. Initially, sea-level falls due to isostatic rebound, but at 8 ka the bulge has moved over the coast. Collapse of the bulge, and its migration away from the pole again cause subsidence until 4 ka. From then until the present, uplift occurs. As at the centre of the ice sheet, the effect of the second iteration of the water load is small.

At a point on the crest of the peripheral bulge at its initial state, 12° from the centre of the ice sheet, the ESL and ice-load terms are of similar magnitude (Figure 5.5 c,f). Here, the ESL rise is reinforced by the subsidence of the bulge, causing monotonic sea-level rise until 4 ka. During this time, the bulge has migrated towards the centre of the ice sheet and back out again, but this is not detectable in the pattern of subsidence. After 4 ka, the bulge lies further out from the ice sheet than its initial position, and that site experiences uplift (relative sea-level fall) associated with the main isostatic rebound. At this location, the effect of the second iteration of the water load is large, as the subsidence of the bulge causes a continually increasing load. As Figure 5.5 f) shows, the subsidence of 50 m in the first iteration causes a further subsidence of ~10 m in the second. This increase is still of the same order of magnitude as the first iteration sea-level change, which suggests that three or more iterations of the sea-level equation are required to obtain convergence in this region.

Sea-level changes in the near field have only been calculated here for the case of a static coastline. In the next section, I will investigate sea-level change in the far field, including the effect of moving coastlines. Because of the large second iteration water loads, and the correction which must be applied to the ice load if it is grounded below sea-level, a complete analysis of the effects of moving coastlines in the near field is not made here. In Chapter 7, the appropriate scenario for the Antarctic ice sheet is investigated.

5.4.2 Far field sea-level change

Sea-level change in the far field is dominated by the ESL term: the rise in sea-level due the addition of meltwater to the oceans. The ice-load and water-load terms are of similar magnitude, and appear as small perturbations on the sea-level curve. Although they are of similar magnitude, the importance of the water-load term is of much greater

importance in explaining spatial variation in sea-level histories, since it is strongly influenced by the presence of coastlines, whereas the ice-load term is almost the same throughout the far field.

Ice-load component

Beyond about 60° from the centre of the ice load, there is almost no spatial variation in the ice-load component of sea-level change (Figure 5.6), and this region will be referred to as the far field. 18,000 years after the start of melting, there has been almost no net sea-level change in the far field due to the ice-load component, but in that period of time there has been a component of sea-level rise of ~1 m by 10 ka, followed by a similar amount of fall. The rise is due to the change in the earth's gravitational field: water that was formerly attracted to the ice sheet is redistributed over the earth when the ice sheet melts. The subsidence is due to mantle flow towards the formerly glaciated region.

The collapse of the peripheral bulge contributes to the ice-load component of sea-level change in the far field. As the bulge collapses, water flows in to fill the space, causing slight sea-level fall in the far-field. This has been discussed by Johnston (1993) and Mitrovica and Peltier (1991), who called this effect "equatorial ocean siphoning", since on the real earth water is drawn from the equatorial regions to compensate for the subsidence of the peripheral bulges at both poles.

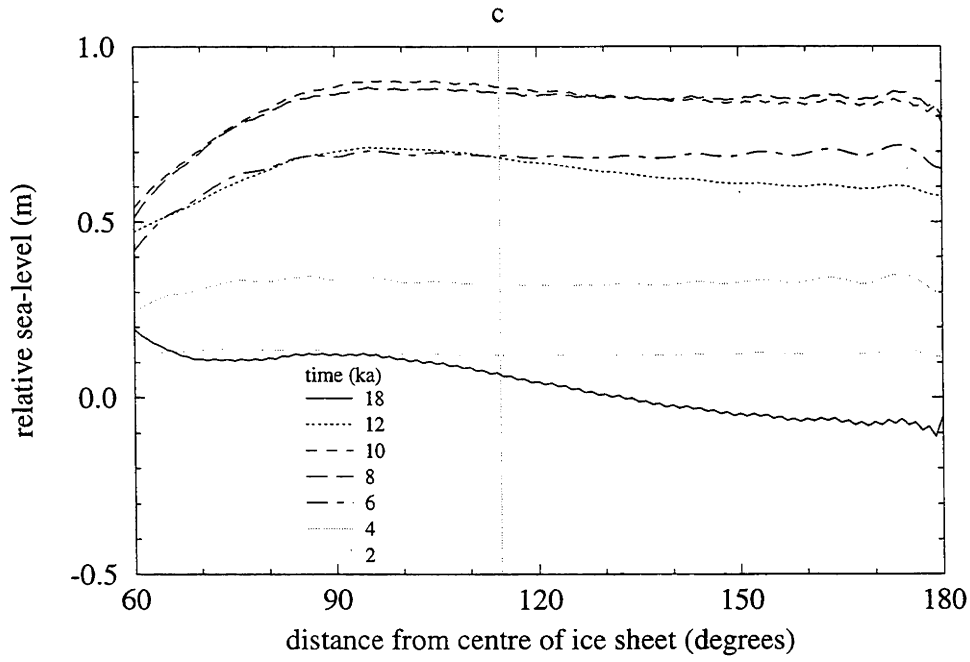

Figure 5.6 : The ice-load component of sea-level change in the far-field, for the continuous melting model. There is almost no spatial variation. The position of the far field coastline is indicated by the vertical line marked "c". The wiggle in the lines is caused by the truncation of the spherical harmonic expansion at degree 180, and has an amplitude of about 2 cm, indicating the degree of convergence achieved.

Water-load component

A long distance from a coastline, the water-load component of sea-level change in the far field is similar in form to the ice-load component, but only ~5 cm in magnitude. At a far-field coastline, the second iteration of the water load component (Figure 5.7) is similar to the first iteration at a near-field coastline (Figure 5.4 a), and can be envisaged as the result of removing a load of uniform thickness from the continent. The uplift caused by this contributes ~2 m to sea-level fall at the coastline in 18,000 years, although the amount of uplift varies rapidly with position at the edge of the load. At the centre of the far field continent, 180° from the centre of the ice load, the amount of uplift is 4 m in 18,000 years.

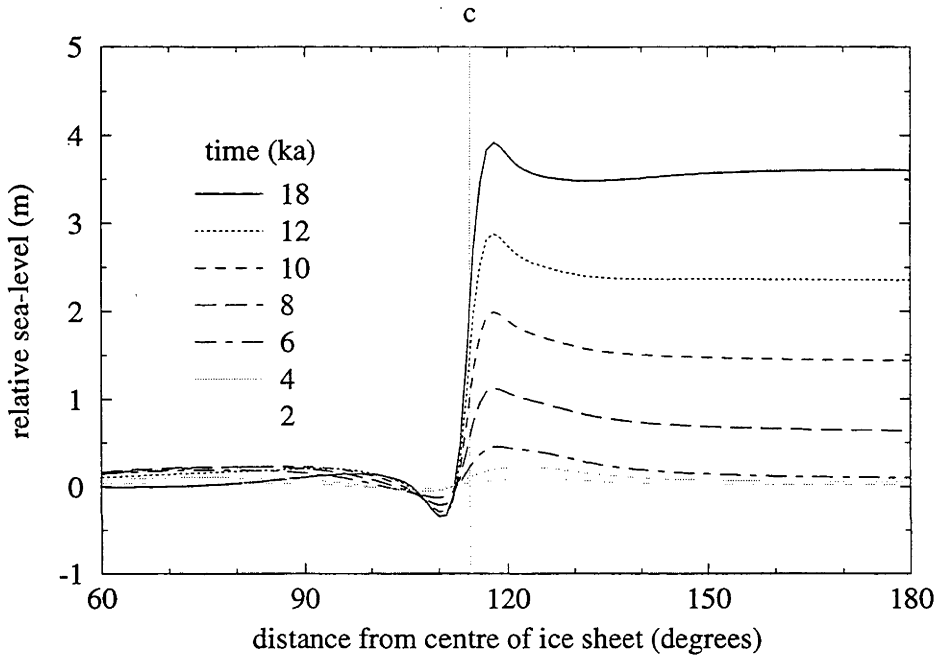

Figure 5.7 : The second iteration of the water load in the far field, for the continuous melting model. The effect of the coastline is evident, with uplift occurring on the continent where there is no water load. The position of the coastline is indicated by the vertical line marked "c".

Total sea-level change

The small magnitude of the ice-load and water-load components compared to the ESL contribution mean that they have no significant effect on the shape of the sea-level curve while the rate of melting is high. The contribution to sea-level fall from both the ice-load and water-load terms mean that the total sea-level curve lies above the ESL curve at all times since melting began. After 6 ka, when melting has ceased, the sea-level fall due to the ice- and water-load components forms a sea-level highstand at 6 ka. This is a feature of all far-field sea-level histories predicted by this model (Figure 5.8). The magnitude of the 6 ka highstand tends to increase landwards, from 0.85 m in the open ocean, to 0.9 m at the coastline, and 1.14 m slightly inland. These are the values for an ESL rise of 14.2 m, and the

predicted values for the actual ESL rise since the LGM, ~125 m (Fairbanks 1989, Nakada and Lambeck 1988), would be proportionately larger, assuming that the shape of the ESL curve is roughly the same. While not as great as the sea-level changes which occur in the near field, these differences in elevation are within the resolution of Holocene sea-level observations, allowing the model parameters to be determined from field data. However, the sensitivity of the predicted sea-level change to position in the coastal region, where most observations are made, means that the errors which result from using a static coastline model are significant, and the model must be made more sophisticated in this region.

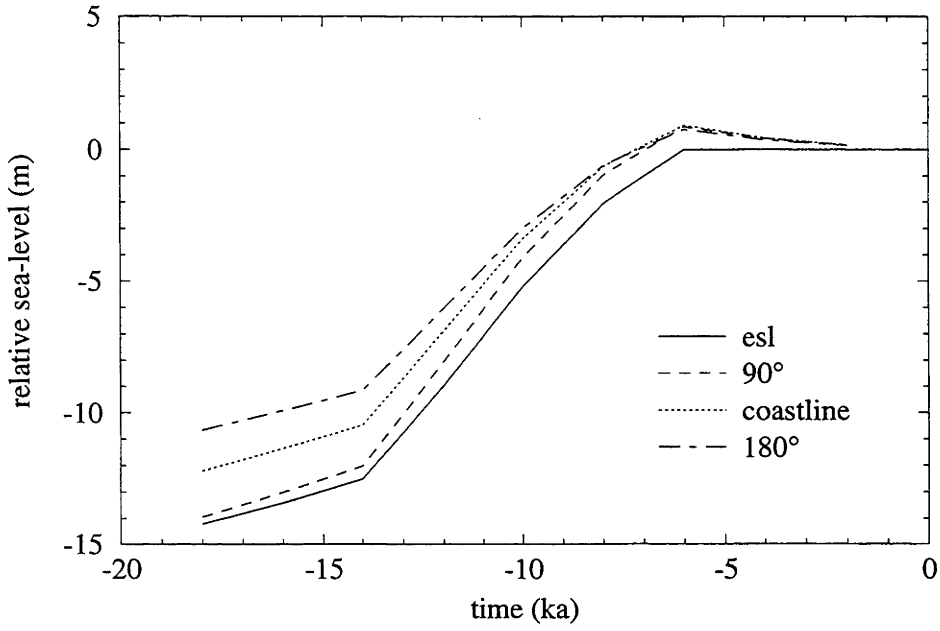

Figure 5.8 : Total predicted sea-level change at three far field sites. All curves lie above the ESL curve, and show a sea-level highstand at 6 ka.

5.4.3 Moving coastlines in the far field

On the real earth, the coastline is formed where the sea surface intersects the seaward-sloping surface of a continental margin. As sea-level rises and falls according to the influences of glacio-hydro-isostasy, as well as the short time-scale effects of tides and waves, the position of the coastline moves. To investigate the effect this has on sea-level change in the coastal region, a bathymetry model was constructed which slopes seaward so that the coastline advances 1° of latitude (~110 km) in the 18,000 years after the onset of deglaciation. This bathymetric profile, and that of the static coastline model, are shown in Figure 5.9.

For the sea-level predictions using the continuous melting ice model and two iterations of the water load, the bathymetry models are constructed so that the final position of the coastline is the same for both. Since the predicted sea-level curve does not rise monotonically, but falls over the last 6,000 years, the coastline actually advances from 113.35 degrees as far as

114.42 degrees before retreating back to 114.35 degrees, the position of the static coastline. This amount of advance is a realistic estimate of the coastline movement in many parts of the world, which is mostly influenced by the width of the shallow part of the continental shelf. Actual coastline migration ranges from as much as 1000 km in the Gulf of Carpentaria, Australia, and in the Persian Gulf, to around 800 km in the North Sea, and less than 10 km in regions of steep topography such as New Guinea and New Zealand.

The ESL and ice-load components are not affected by the moving coastline. The water-load component of sea-level predictions of the moving- and static coastline models are compared in Figure 5.10. At all times, the moving coastline model predicts higher sea-level than the static model. This can be qualitatively explained by considering the average position of the coastline over time, which lies offshore from its present position. The water-load component of sea-level change is therefore comparable to that of a site further inland when the static model is used. Because the water-load component increases landwards in the coastal region, the moving-coastline model thus predicts consistently higher sea-level.

In practice, the difference between the two models is best observed as the elevation of the 6 ka highstand, since sea-level observations from the period of rapidly rising sea-level typically have poor depth precision. In the scenario modelled here, with ~110 km of coastline movement and 14.2 m ESL rise, the difference in the elevation of the 6 ka highstand at the present coastline is only 3 cm. The effect of the ~125 m of late Pleistocene and Holocene sea-level rise would therefore be 20 - 30 cm, which is probably detectable by the most precise sea-level observations. At sites where the coastline migration is greater, the effect will be more important.

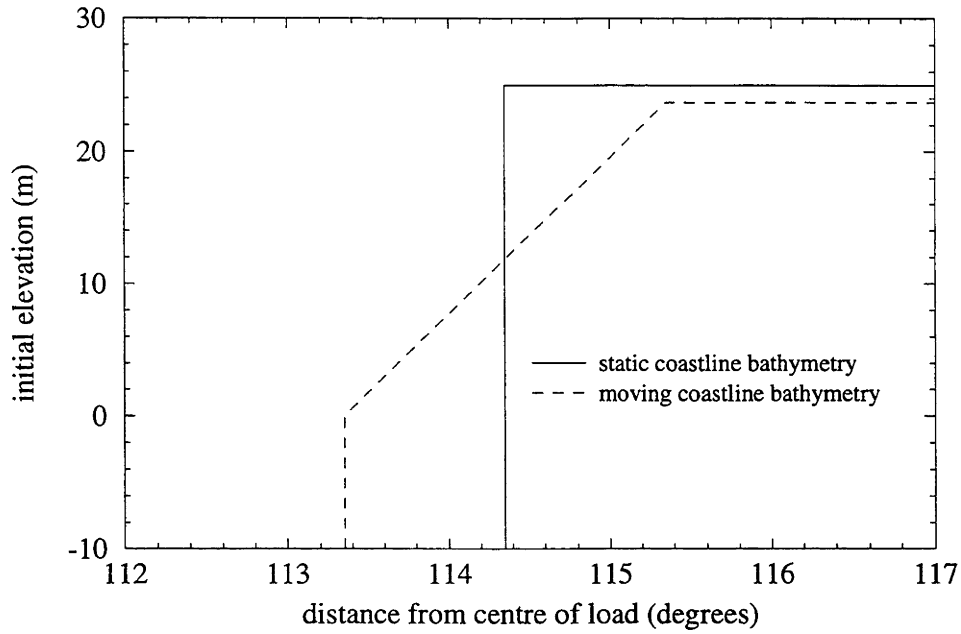

Figure 5.9 : Bathymetric profiles of the far field coastline for the static and moving coastline models. The models begin with sea-level at 0 m, and a rise of about 12 m takes place at the coastline. In the case of the sloping bathymetry, this rise causes the coastline to migrate inland.

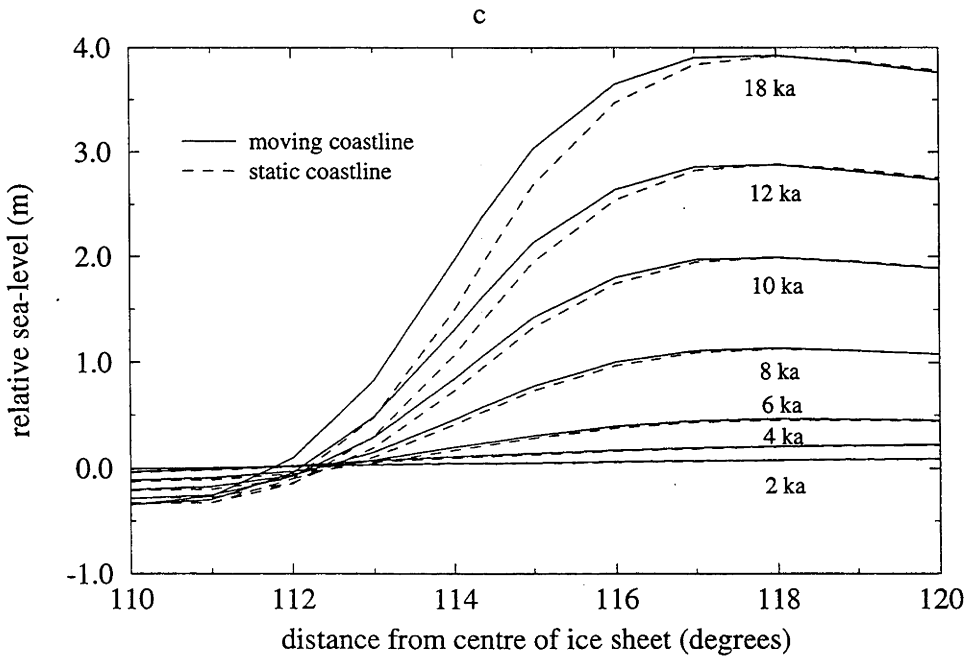

Figure 5.10 : The second iteration of the water-load component of sea-level change at the far field coastline, for the static and moving coastline models. The effect of the moving coastline is to move the sea-level profiles seawards, causing higher predicted sea-levels at all sites.

5.5 Realistic models

The processes which control the changes in sea-level due to deglaciation on the real earth are the same as those presented so far in this chapter, although the complex interaction between the effects of the irregular and changing geometries of the ice sheets and ocean basins mean that it is often difficult to determine the dominant influence on the pattern of predicted sea-level change. Nevertheless, the good fit obtained between model predictions and observed data in several studies (eg Nakada and Lambeck 1989, Tushingham and Peltier 1992, Lambeck 1993a) indicate that not only does the theory accurately represent the real-earth processes, but also that the ice-sheet reconstructions used in these studies are realistic.

The rheological models of the earth used in these glacio-hydro-isostatic calculations are radially symmetric, that is, the earth is described as a set of spherical shells which have internally uniform viscosity. As this is not the case for the real earth, whose properties vary considerably laterally, the rheological properties determined using data from any region will be effective local values. Most sea-level observations are made at continental margins, where there is strong lateral variation in the thickness of the crust and possibly the viscosity of the mantle. The earth models used here do not account for this, so the model values obtained by comparison of model predictions with sea-level observations are effective average values. Sea-level observations from several regions may therefore indirectly describe laterally varying properties of the crust and mantle on a global scale. Nakada and Lambeck (1991) compared the optimum rheological models for Pacific Ocean islands, Australasia, Hudson Bay, and northwestern Europe, and found that some variation is mantle viscosity is suggested, in agreement with observations of lateral variation in seismic shear wave velocities. In the Pacific, where S-wave velocities are anomalously low, the viscosity of the upper mantle is also inferred to be low ($<10^{20}$ Pa.s.). At the other sites, inferred upper mantle viscosity ranges from 10^{20} - 10^{21} Pa.s.

Chapter 6

Modelling sea-level change in North Queensland

6.1 Introduction

Since relative sea-level (RSL) change at any site depends on several variables, all of which are unknown to a greater or lesser degree, we need some method of separating them if we are to invert our observed RSL records to constrain the components of the sea-level equation. To do this, we need a property of the observational record which is independent of one of the parameters, or at least is negligibly affected. One example of this is the original determination of the earth rheology from rebound observations in Hudson Bay (eg Walcott 1972). In this case the ice load is assumed to be known, and the effect of the changing water load in the vicinity of Hudson Bay is considered negligible compared to the rebound due to deglaciation. This method was sufficient for preliminary estimation of the earth's rheological parameters, but if the ice load is also considered to be not sufficiently well known, another approach must be made.

In the far field, differential sea-level change between two sites is dependent on the water load only. The ice-load contribution is small in this region and spatially quite uniform, and eustatic sea-level is the same at all sites, so spatial variation in sea-level is mainly due to the shape of the ocean in the region of each site. For example, we expect differences between coastal and island sites, or inland vs offshore sites. If sufficiently detailed sea-level records can be found, we can compare the observed and predicted differences between sea-level at pairs of sites for a range of rheological models to find the optimum earth model. The earth rheology parameters obtained in this way represent effective values over the region and timescale sampled by the observed data. This was done for sites in the Australian region by Nakada and Lambeck (1989), using 3-layer rheological models similar to those used in Chapter 5, with the upper/lower mantle boundary at 670 km depth. That study assumed a lithospheric thickness of 50 - 100 km, and found that optimum effective upper and lower mantle viscosities were (1-2) x 10^{20} Pa.s and ~10^{22} Pa.s respectively. These values form the standard model used in this chapter. Eight rheological models close to this model were used to investigate the dependance of sea-level change on the various parameters. These models are listed in Table 6.1. The ice distribution model used in that study (ARC3 + ANT3, Nakada and Lambeck 1988) is also used throughout this chapter. This ice model covers the period of time since the LGM, and sea-level predictions are presented on the assumption that isostatic equilibrium was attained at that time.

Table 6.1: Rheological models used in this chapter. H_{lith} = lithospheric thickness; η_{um}=upper mantle viscosity; η_{lm}=lower mantle viscosity.

Name	H_{lith} (km)	η_{um} (Pa.s.)	η_{lm} (Pa.s.)
510	50	2×10^{20}	5×10^{21}
513	50	1×10^{20}	1×10^{22}
514	50	2×10^{20}	1×10^{22}
515	50	5×10^{20}	1×10^{22}
610	100	2×10^{20}	5×10^{21}
613	100	1×10^{20}	1×10^{22}
614	100	2×10^{20}	1×10^{22}
615	100	5×10^{20}	1×10^{22}

With the rheological model constrained, the difference between predicted and observed relative sea-level changes at far field sites can be attributed to errors in the eustatic sea-level curve. In particular, with adequate observations three aspects of this curve can be constrained: the total postglacial sea-level rise, the existence or otherwise of episodic sea-level rise, and the degree of eustatic sea-level change which has occurred in the late Holocene. These three problems are addressed in this chapter.

6.2 Sea-level at the Last Glacial Maximuum (LGM)

Knowledge of sea-level at the LGM, especially at far field sites, allows us to estimate the total volume of ice which was stored on land in the form of ice sheets at that time. The level of LGM sea-level varies spatially, due to the glacio-hydro-isostatic adjustment of the earth to the melting of the ice sheets and the refilling of the oceans. Figure 6.1 shows a calculation of sea-level at the LGM using the standard ice and rheological models outlined above. The eustatic sea-level rise due to this ice model is 126 m. The influence of the Laurentide, Fennoscandian and Antarctic ice sheets is evident where isostatic rebound has raised the LGM sea-level hundreds of metres above present sea-level. In the far field, spatial variation in the LGM sea-level is mostly due to the effect of the asymmetry of the water load at coastlines, causing tilting of the continental shelf which results in higher (shallower) LGM sea-levels at sites on the inner continental shelf than at offshore and oceanic locations. Depths of 110 - 140 m are predicted at most far field sites.

Nakada and Lambeck (1989) compiled observations of LGM sea-level in the Australian region, and compared them with numerical predictions. They used the same ice and rheological models as have been used here, but computational resources available then only allowed calculation of the first iteration of the sea-level equation (see Chapter 5), and the effect of moving coastlines was not included. As Table 6.2 shows, including these effects and performing the calculations at a higher resolution does not have a great effect around most of the Australian coastline. The greatest difference occurs in the Arafura Sea, where the marine transgression over the Gulf of Carpentaria causes the contours of the second iteration predictions to be moved seawards with respect to the first iteration (Figure 6.2). The revised prediction for the site in the Arafura sea is thus lower than that of Nakada and Lambeck (1989). Calculating the third iteration of the sea-level equation has a negligible effect on the predictions.

At most sites, agreement between predictions and observations is reasonable, although the depths of over 150 m cannot be obtained with the present model. On this evidence, there is no reason to propose a total postglacial eustatic sea-level different to that represented by the ice models ARC3 and ANT3.

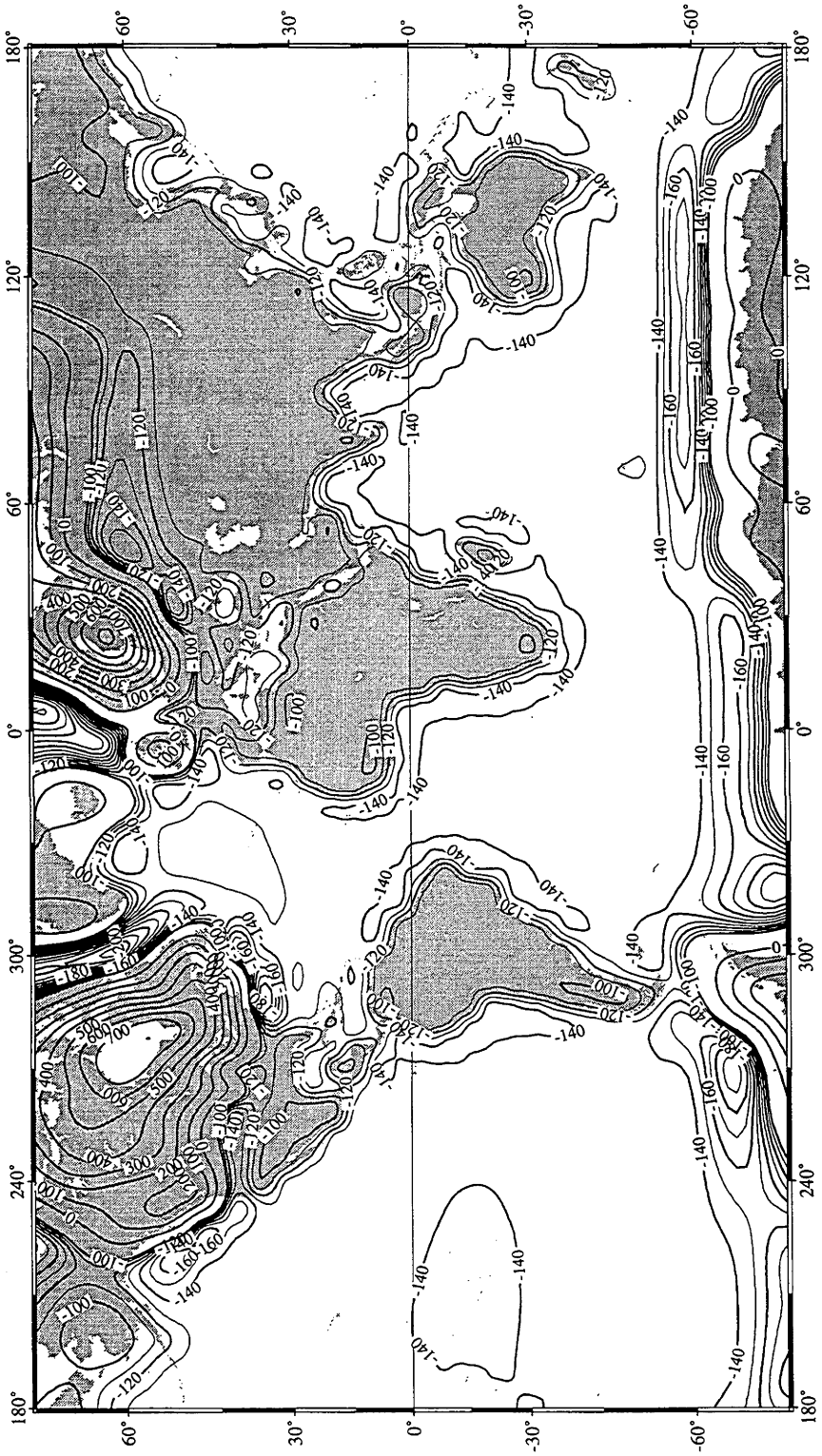

Figure 6.1 : Predicted sea-level at the LGM, 18 000 years ago, using the ice models ARC3 and ANT3 (Nakada and Lambeck 1988) and the standard earth rheological model described in this chapter. Two iterations of the sea-level equation were calculated to degree 256. Contour interval is 10 m below -100 m, and 100 m above.

Table 6.2: Observations and predictions of relative sea-level at the LGM at some far field sites. The latitudes and longitudes given were used to calculate the predictions, estimated from the observation publications. Prediction in column (1) are from Nakada and Lambeck (1989); those in column (2) were made for this study.

Location	Reference	Observed depth (m)	Predicted depth (m) (1)	(2)
Barbados 13°N 59.5°W	Fairbanks (1989)	116 - 126	-	139
Northern GBR 17°S 146.5°E	Carter and Johnson (1986)	114 - 133	129	130
Timor Sea 11.96°S 123.84°E	van Andel and Veevers (1967)	120 - 130	136	137
Huon Peninsula 6.04°S 147.39°E	Chappell and Shackleton (1986)	130	126	126
Central GBR 23.5°S 152.25°E	Veeh and Veevers (1970)	150 - 175	130	125
Arafura Sea 9.12°S 133.87°E	Jongsma (1970)	150 - 175	138	130

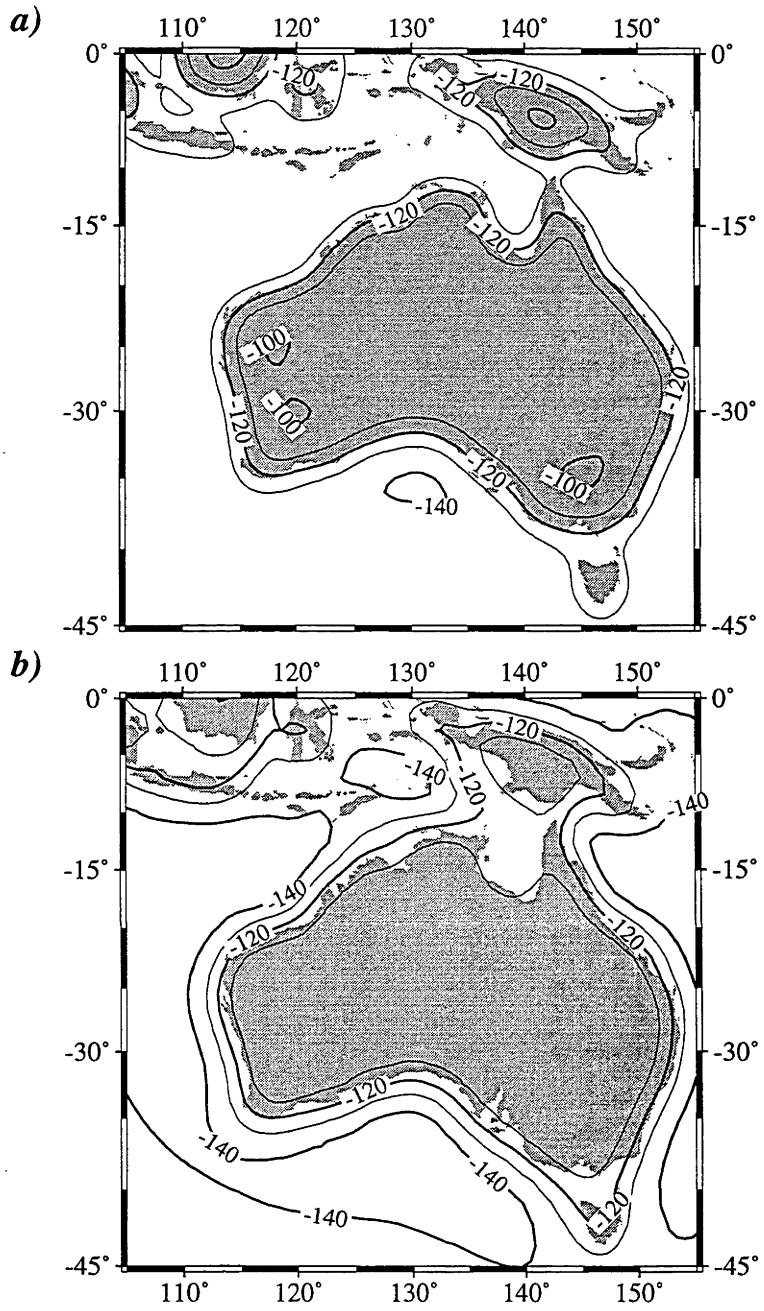

Figure 6.2 : Predicted sea-level at the LGM in the Australian region using a) 1, and b) 2 iterations of the sea-level equation. The effect of the advance of the coastline over the Gulf of Carpentaria is evident: in (a) the Gulf of Carpentaria is treated as sea throughout and isobases tend to follow the present coastline. In (b) the Gulf of Carpentaric is above sea-level at the LGM and is flooded at ~11 ka, and the isobases tend to follow the LGM coastline. Contour interval is 10 m.

6.3 The post-glacial transgression

6.3.1 Introduction

The period of sea-level rise at far field sites between the LGM and the cessation of significant melting at ~ 6 ka is referred to here as the post-glacial transgression. Although the total sea-level rise is not known accurately, as discussed above in Section 6.2, the average rate of rise over this period was probably about 10 mm/yr. The ESL models of Nakada and Lambeck (1988) and Peltier (1994), which rise monotonically, indicate a maximum rate faster than 15 mm/yr during this period. Reconstructions of episodic sea-level rise based on field observations suggest considerably faster peak rates of rise, up to 30 mm/yr (Larcombe and others 1995) or >45 mm/yr (Blanchon and Shaw 1995), although these estimates are not tightly constrained. It is very difficult to obtain accurate sea-level records from this time, because the rapid rate of rise prevented the formation of many precise sea-level indicators, and because the uncertainty in radiometric ages corresponds to a greater uncertainty in elevation than it does during times of slowly-changing sea-level. Most observations from this time period are either sub-tidal corals or intertidal mangrove sediments, both of which have considerable uncertainty, as discussed in Chapter 2.

Because precise sea-level records during the postglacial transgression are rare, it is difficult to observe spatial variation which might be used to constrain the parameters of glacio-hydro-isostatic models. The rate of sea-level rise during this time is insensitive to the rheology of the earth, as eustatic change is much greater than the contributions from isostatic effects. Two potentially useful features of the sea-level record in this time are discussed in this section: the time at which sea-level first reached its present level, and the records of episodicity, if it occurred.

6.3.2 Time at which present sea-level first attained

Model predictions

Predictions of sea-level in the GBR region (Thom and Chappell 1978, Nakada and Lambeck 1989) show seaward tilting of the continental shelf, so that sea-level at inshore sites reaches its present sea-level before offshore and oceanic sites. In a simplistic consideration, in which ice melting ceases at 6 ka, uplift on the inner part of the shelf would result in sea-level reaching its present level before this time, rising to a highstand at 6 ka, and falling from then until the present. On the edge of a wide shelf, subsidence means that even after the addition of water to the ocean has stopped, relative sea-level keeps rising, so that present-day sea-level is not reached until the present (Figure 6.3). In fact, there are at least two other significant processes which alter this pattern. First, any continued addition of meltwater to the oceans throughout the late Holocene tends to lower the sea-level curves described above, so that the time present sea-level is first reached (henceforth called "first attainment time") becomes later. Second,

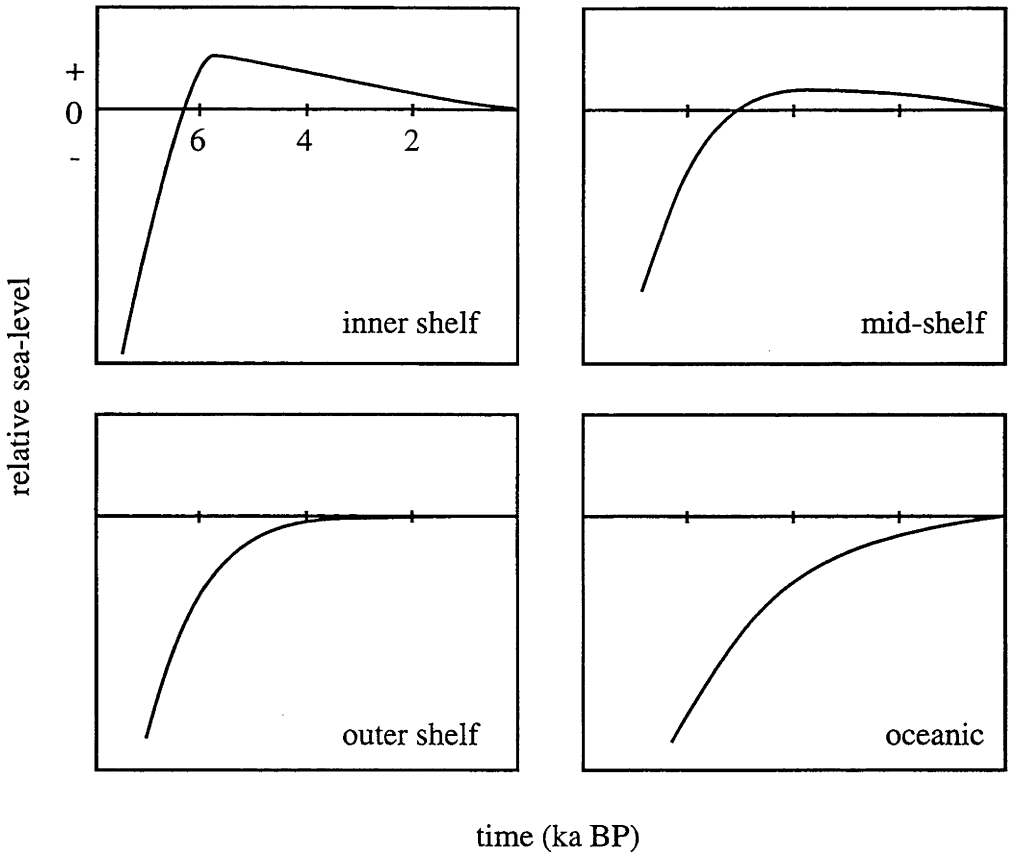

Figure 6.3 : Predicted sea-level curves at sites on a transect of the GBR. Predictions were made using the standard ice and earth models, and only one iteration of the sea-level equation. (From Nakada and Lambeck 1989).

the subsidence of the ice sheets' peripheral bulges results in sea-level fall in the far field, increasing the height of the mid-Holocene highstand and causing present sea-level to be reached earlier. This is the process referred to as "equatorial ocean siphoning" (Mitrovica and Peltier 1991, Johnston 1993).

In the predictions used here, late Holocene melting is not initially included, but equatorial ocean siphoning is, so the predicted first attainment times can be expected to be earlier than the observed times at each site. Although the late Holocene melting is a eustatic contribution and has no spatial variation, the effect which it has on the first attainment time may vary considerably, according to the relative size of the isostatic and eustatic components. This is demonstrated in Figure 6.4, using the standard earth model and late Holocene melting of 3 m, proportional to the melting proposed by Lambeck (1993b). At inshore sites (Figure 6.4 b), the isostatic highstand is greater than the amount of late melting, so the first attainment time remains in the steeply-rising part of the sea-level curve, and is only delayed by a few hundred years. At the shelf edge, the predicted isostatic highstand is roughly equal in magnitude to the late melting (Figure 6.4 c), so the first attainment time moves to the part of the sea-level curve with low gradient, where it is highly sensitive to small changes in the eustatic component. At mid-ocean sites, where the predicted highstand is small, due solely to equatorial ocean siphoning (Figure 6.4 d), late Holocene melting may cause

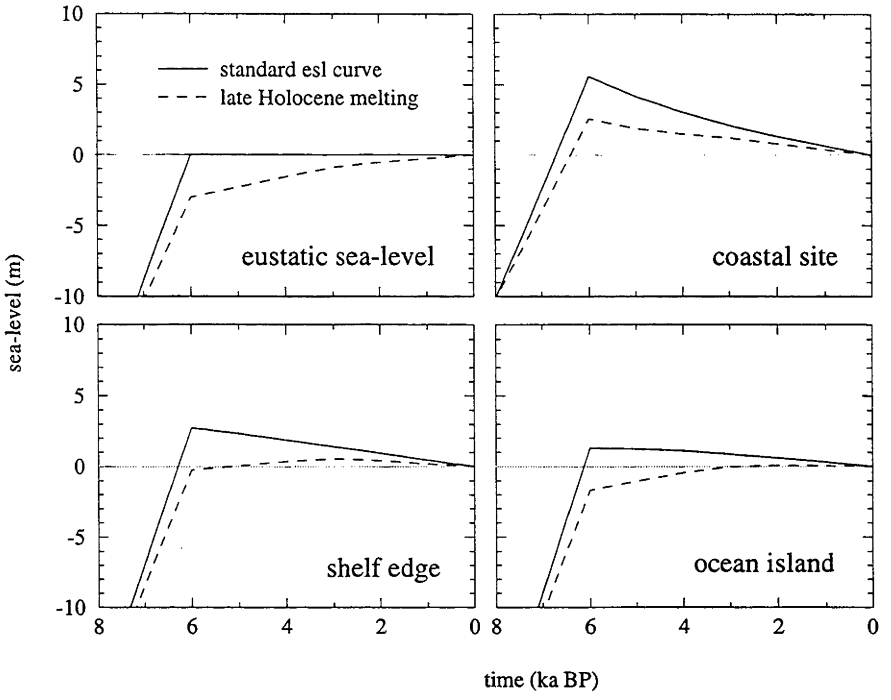

Figure 6.4 : Predicted sea-level histories on a transect of the north Queensland coast, using two eustatic sea-level models. The "standard" model is ARC3+ANT3 (Nakada and Lambeck 1988). The late Holocene melting in the other model is based on the results of Lambeck (1993b) scaled to 3 m at 6 ka.

sea-level to rise continuously through the Holocene. The effect of late Holocene melting on the magnitude and timing of the Holocene sea-level highstand is discussed in the next section.

The first attainment time at each site has been determined here using the numerical model described in the introduction to this chapter (Section 6.1). Relative sea-level was calculated at 100 year intervals through the mid Holocene, and the time at which present sea-level is first reached was estimated by linear interpolation.

Figure 6.5 shows the predicted first attainment time contoured over the Australian region. Two features are evident: first, inland sites reach present sea-level earlier than offshore sites, due to isostatic tilting at the continental margin. The contour lines are unaffected by the smaller islands, which are effectively loaded equally on all sides. Second, at oceanic sites, sea-level is reached later in the south than in the north. This is because the southern end of the region shown is affected by the subsidence of the peripheral bulge around Antarctica, causing sea-level rise up to the present.

Contour maps of the predicted first attainment time in the Great Barrier Reef region (Figures 6.6 and 6.7) show the influence of lithospheric thickness and upper and lower mantle viscosity. A thinner lithosphere (Figure 6.7) can deform at shorter wavelengths, so the contours of

deformation produced by the ocean load follow the coastline more closely than when a thicker lithosphere is present (Figure 6.6). Increasing the viscosity of the upper mantle increases the gradient of tilting across the continental shelf, because much of the relaxation is already completed by this time for models with a lower viscosity upper mantle. This causes the first attainment time to vary more rapidly across this region, as shown by the closer spaced contours in Figures 6.6 d) and 6.7 d) compared to Figures 6.6 b) and 6.7 b). The viscosity of the lower mantle has a negligible effect, indicated by the similarity between the pairs of maps Figures 6.6 a) and c), and Figures 6.7 a) and c).

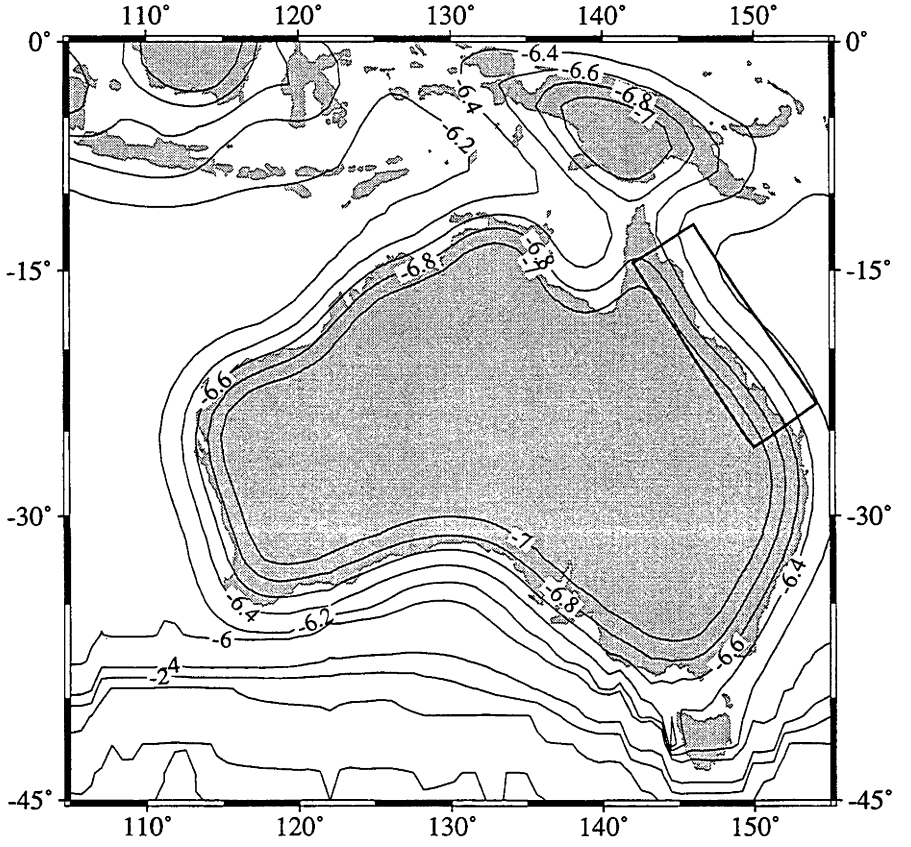

Figure 6.5 : Predicted time at which sea-level first reached its present level in the Australian region. Two iterations of the sea-level equation were performed to degree 256, using the standard ice and earth models. Contour interval is 200 years, labelled in thousands of years. Box indicates the study region on the Great Barrier Reef.

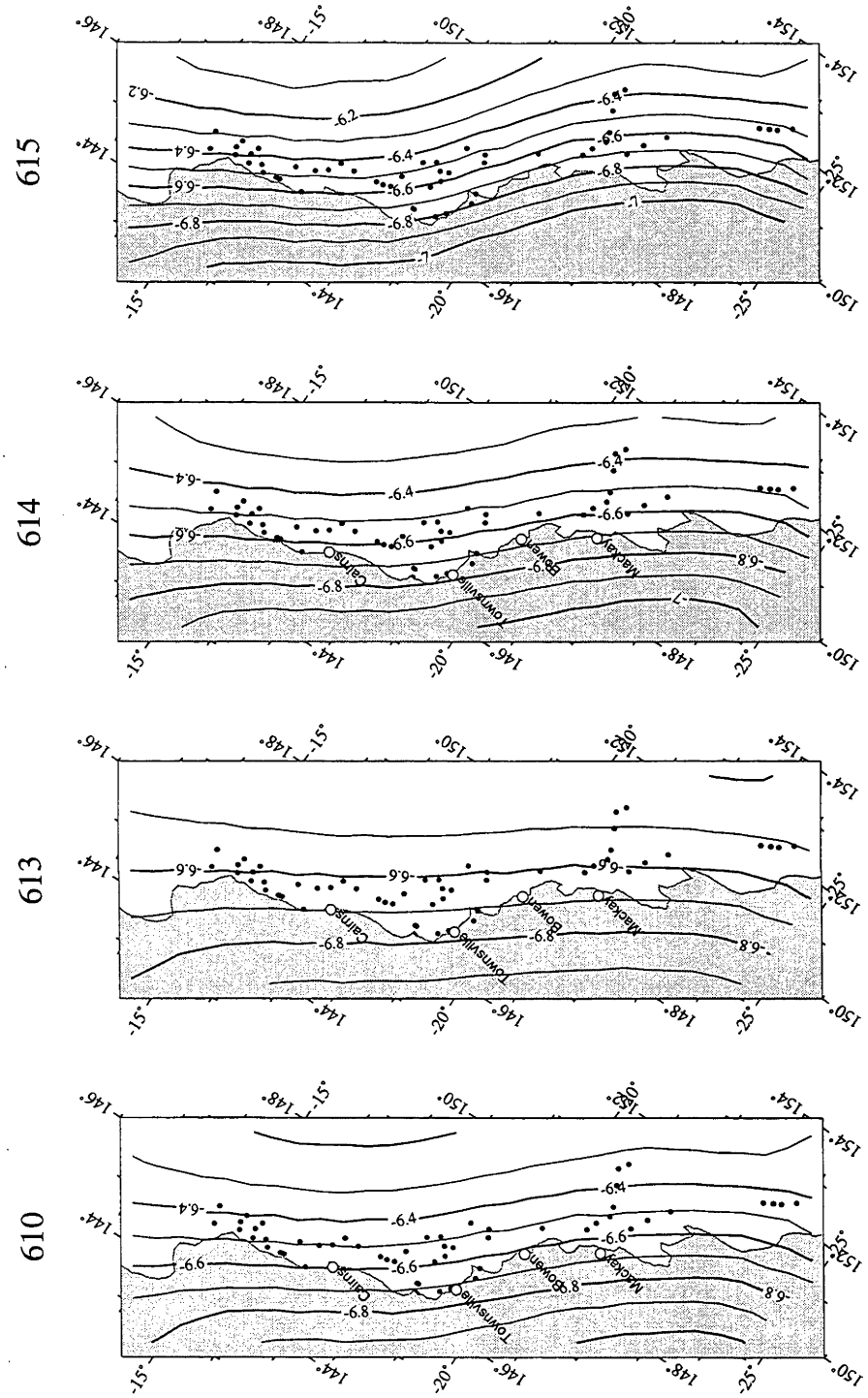

Figure 6.6 : Predicted first attainment time in the study area on the GBR, for the standard ice model and a range of earth models with a 100 km lithosphere. The earth model parameters are listed in Table 6.1. Sites from which reef cores have been collected are indicated.

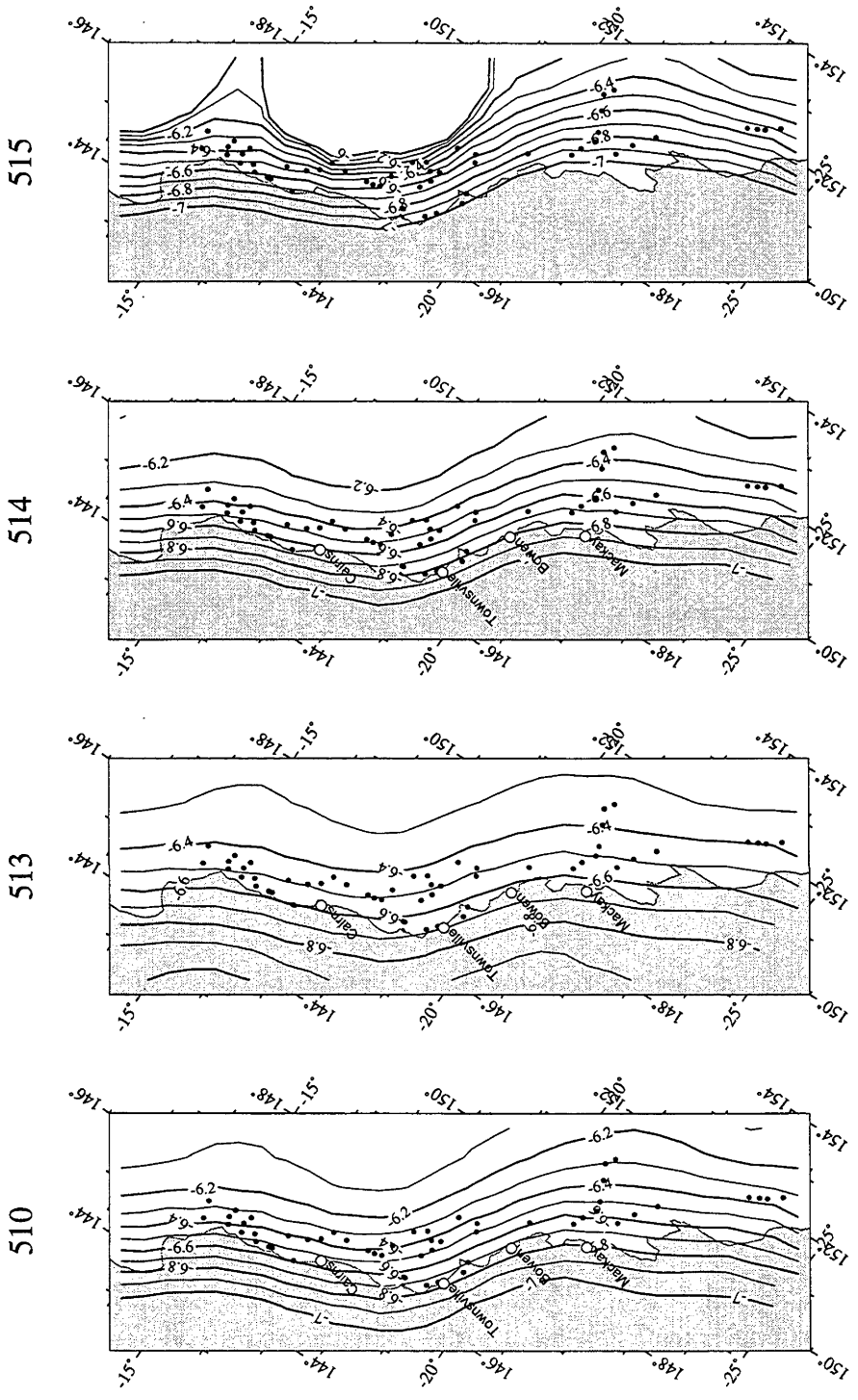

Figure 6.7 : Same as Figure 6.6, but for models with a 50 km lithosphere.

Comparison with observations

To compare the predictions and observations, the observed first attainment times shown in Table 2.11 were plotted as shore-perpendicular transects. The offshore distance was defined for each model as the shortest distance to the predicted 6.6 ka contour, which runs through the middle of the study area in most cases. The predicted contours are almost parallel throughout the region, so choosing another contour has no significant effect on the appearance of the results.

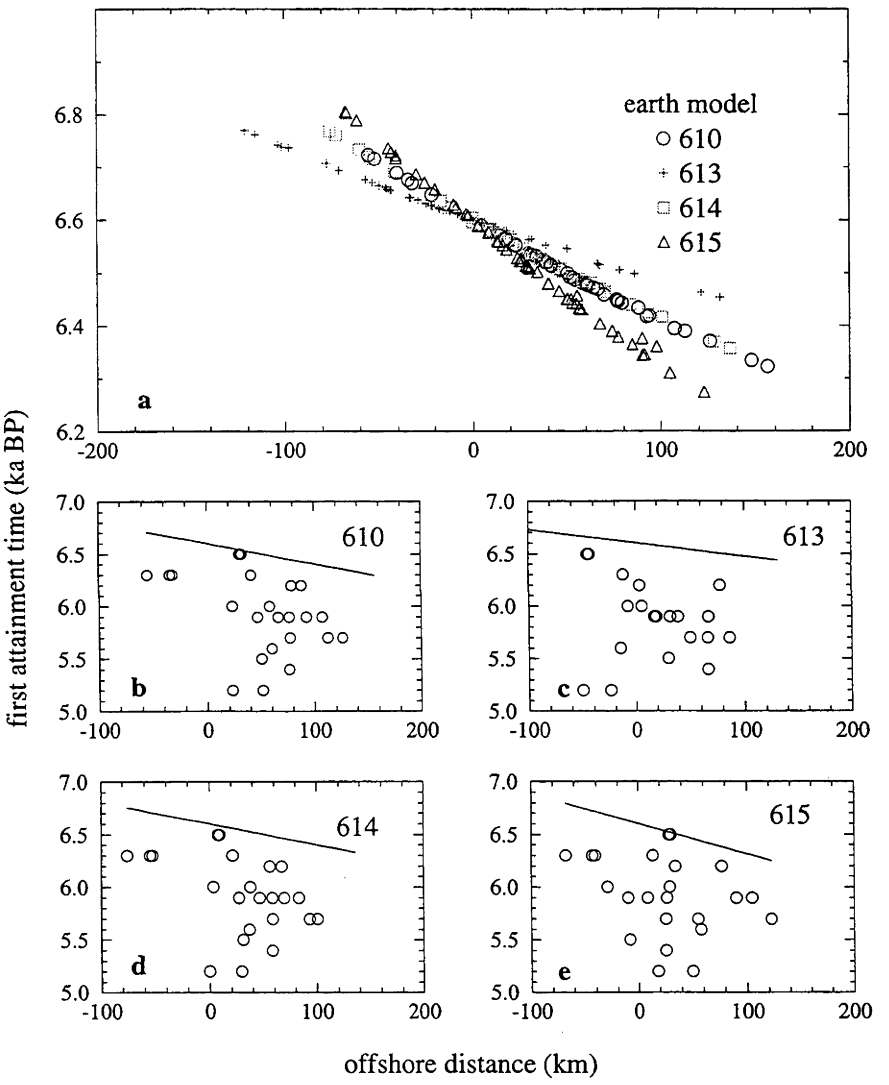

Figure 6.8 : Predicted and observed spatial gradients in the first attainment time, for the standard ice model and earth models with a 100 km lithosphere. Offshore distance is defined as the shortest distance to the 6.6 ka contour on the appropriate model in Figure 6.6. Graph a) shows the dependance of the onshore-offshore gradient on upper mantle viscosity, and indicates that the effect of varying the lower mantle viscosity is negligible. Graphs b) to e) compare the observations (circles) with the predicted gradients (lines) for each earth model.

The predicted and observed first attainment times are compared in Figures 6.8 and 6.9. Although the data are sparse, the upper limit to the observations seems to confirm the predicted decrease seawards in the age of the first attainment of present sea-level. Because the slope of this upper bound is usually constrained by only three of four sites, it it not possible to determine which rheological model is most appropriate.

One of the predicted effects of late Holocene melting, described above, is the sensitivity of the first attainment time at offshore sites to the magnitude of melting. If late Holocene melting causes sea-level rise greater than the fall due to equatorial ocean siphoning, then the first attainment time occurs during the late Holocene, instead of during the period of rapid sea-level rise, which ended around 6 ka. On the transects shown in Figures 6.8 and 6.9, this would appear as a steepening of the gradient at the seaward end of the transect. In the models using an upper mantle viscosity of 2 x 10^{20} Pa.s, the value considered most appropriate for the Australian region (Nakada and Lambeck 1989), there is some suggestion of this steepening in the observed

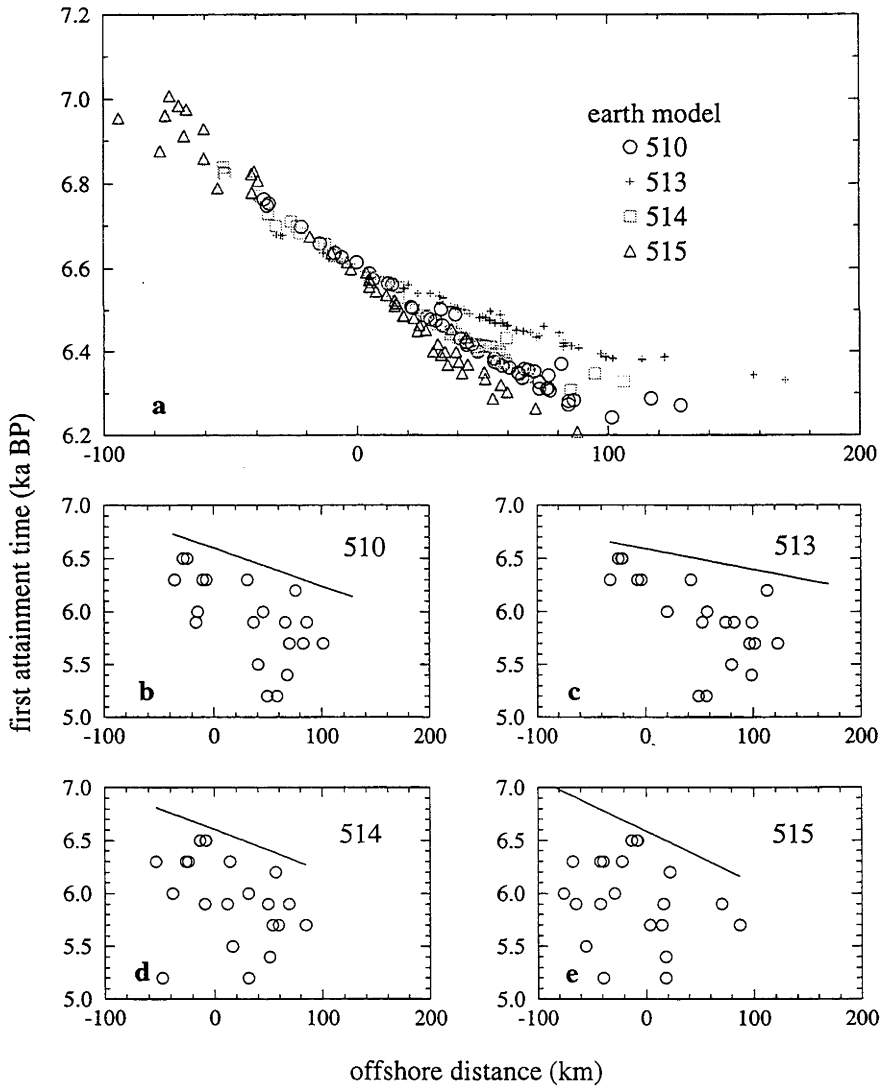

Figure 6.9 : Same as Figure 6.8, for models with a 50 km lithosphere.

first attainment times (Figures 6.8 a & c, and 6.9 a & c), but the data are too sparse for this to conclude that it exists.

Predictions of the first attainment time were also made using two models of late Holocene melting. The first is based on that of Lambeck (1993b), derived from observations in the British Isles, but restricted to the last 8 000 years. This model allows 1.7 m of eustatic sea-level rise since 6 ka. The second is proportional to the first model, but scaled so that 3 m of ESL rise occurs since 6 ka, which is in closer agreement with previous estimates from the Australian region (Nakada and Lambeck 1989). Both these models are within the uncertainties of previous estimates of the late Holocene melting.

Model 1 (Figures 6.10 and 6.11) reduces the predicted age of the first attainment of present sea-level by about 200 years. The predictions remain a plausible upper bound to the observations, except for the Cape Tribulation sites, which are estimated to have reached present sea-level about 100 years before the predicted time.

Model 2 (Figures 6.12 and 6.13) predicts even later first attainment times, about 300 years younger than the standard model. For some mantle rheologies, this late melting model causes the predicted first attainment time at some outer shelf sites to be delayed until 4 ka (using the 100 km lithosphere model) or even removes the Holocene highstand altogether, causing the first attainment time to be the present (Figure 6.12 a & d). The predictions of this model are not an upper bound to the observations, with several sites reaching sea-level before the model predicts. These results, therefore, suggest that late Holocene melting is unlikely to have been as much as 3 m, if the rheological models used are representative of the region.

The lag time of coral growth behind sea-level change remains an unknown factor in the relationship between eustasy, isostasy and the reef growth record. However, the predicted first attainment times using the ESL model 1 form a close upper bound to the observations, suggesting that this lag time is negligible.

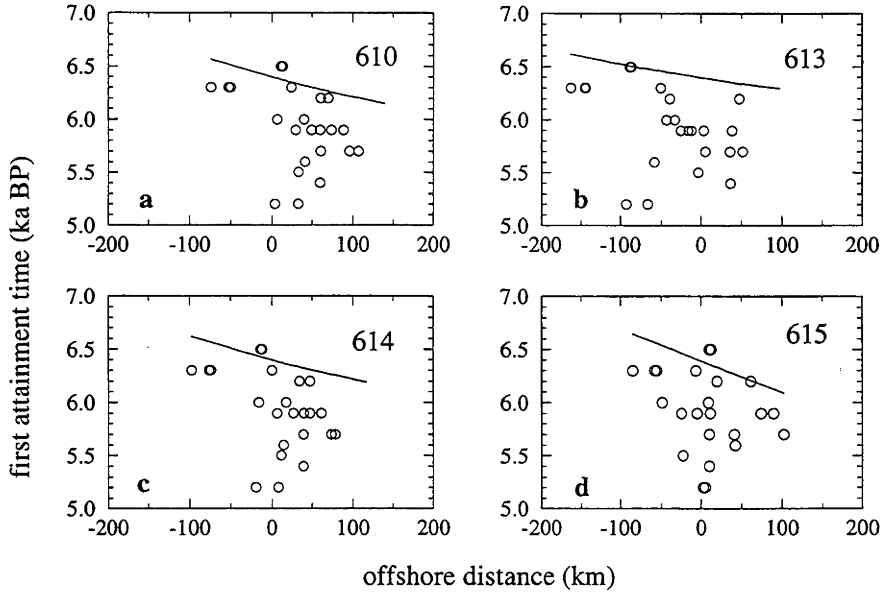

Figure 6.10 : Same as Figure 6.8, but including 1.7 m of late Holocene melting.

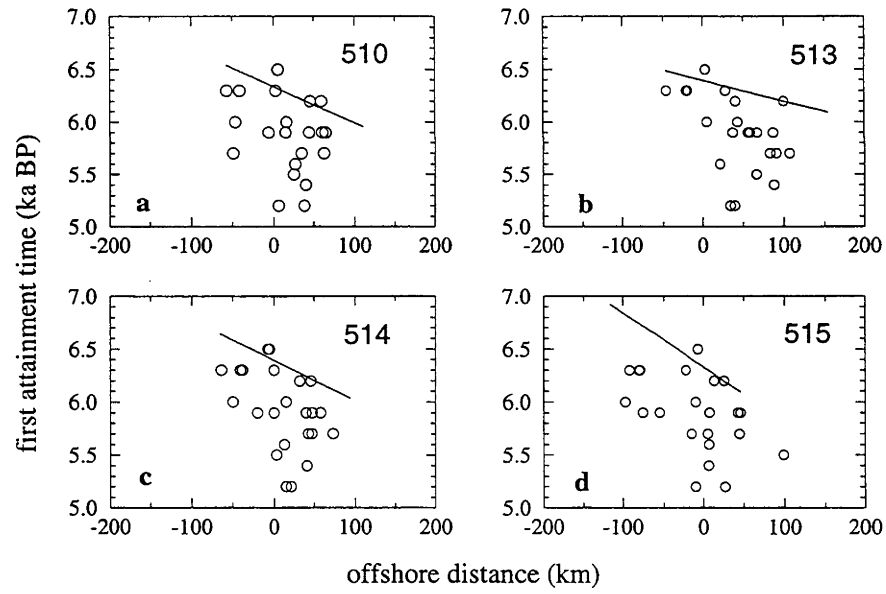

Figure 6.11 : Same as Figure 6.9, but including 1.7 m of late Holocene melting.

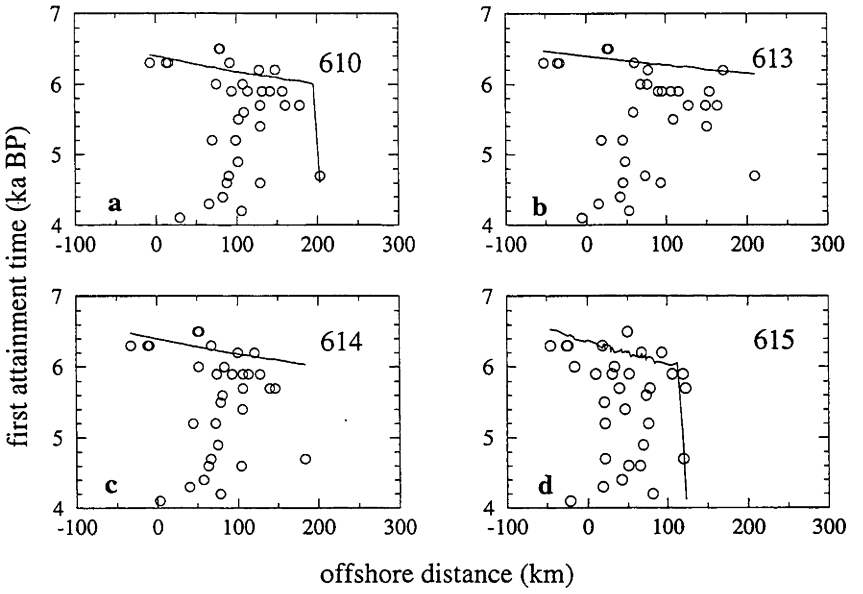

Figure 6.12 : Same as Figure 6.8, but including 3 m of late Holocene melting. The rapid decrease in the age of the first attainment time at far offshore sites indicates that the transition between the scenarios of Figures 6.4 c) and 6.4 d) has been reached, which does not occur with smaller amounts of Holocene melting.

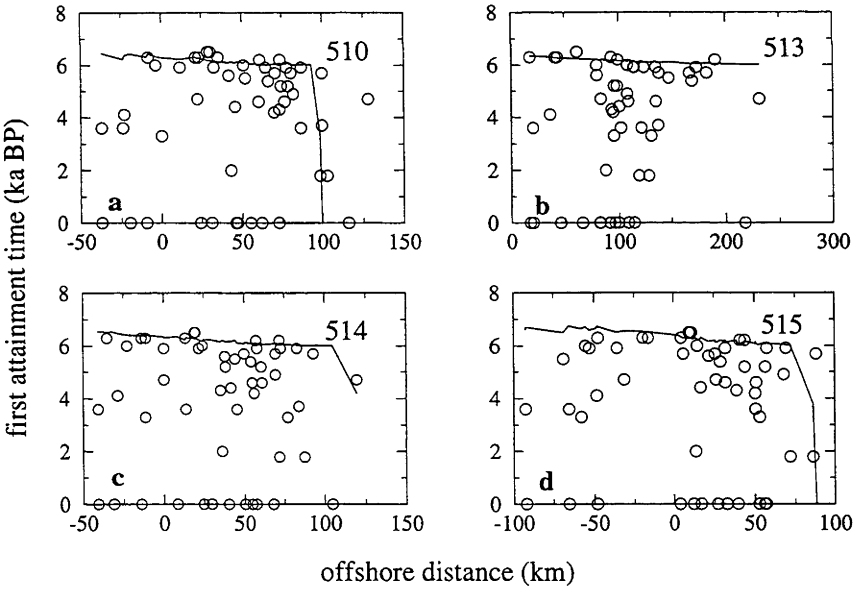

Figure 6.13 : Same as Figure 6.9, but including 3 m of late Holocene melting. The rapid decrease in the age of the first attainment time at far offshore sites indicates that the transition between the scenarios of Figures 6.4 c) and 6.4 d) has been reached, which does not occur with smaller amounts of Holocene melting.

6.3.3 Sea-level stillstands and regressions

As discussed in Section 2.3.2, the issue of whether postglacial sea-level rise was continuous or episodic has not been resolved. No resolution will be possible until a sufficiently accurate and precise record can be found, which is beyond the scope of this study. In this section, however, the spatial variation in the predicted effects of episodic sea-level rise are discussed, which may assist in choosing a location likely to preserve such a record.

Two of the best sites for studying the postglacial sea-level rise are the Great Barrier Reef and the Caribbean. Records from Barbados in the Caribbean and Halifax Bay on the GBR have been interpreted as evidence of episodic sea-level rise (Blanchon and Shaw 1995, Larcombe and others 1995), although the timing of the sea-level stillstands is different at each site. This indicates that either the interpretations are unreliable or incomplete, or that local factors such as episodic tectonism are significant at one or both sites.

From a glacio-hydro-isostatic perspective, the sites occupy fundamentally different locations. Both are in the far field with respect to the late Pleistocene ice sheets, but Barbados is surrounded by ocean whereas Halifax Bay is a typical coastal site. The difference in the RSL history of these sites is mainly due to the water load component. When the eustatic component is removed, sea-level change at Barbados is dominated by slow rise caused by subsidence of the ocean floor under the increased water load, while Halifax Bay undergoes sea-level fall caused by the tilting of the continental margin due to the asymmetry of the water load at that site (Figure 6.14).

A consequence of this difference in the water-load component of sea-level change is the behaviour of the RSL curve if eustatic sea-level rise is episodic. If no eustatic rise occurs between 11 and 10 ka, as proposed by Peltier (1994), then sea-level at Barbados will continue at about 1/30 of the preceding rate, rising ~0.5 m during that time. This amount is smaller than the uncertainty in sea-level observations at that time, and could not be distinguished from a eustatic contribution. In Halifax Bay, however, under the same eustatic regime, ~1.5 m of sea-level fall would occur in the thousand years of eustatic stillstand. This amount is probably also beyond the resolution of sea-level records at that time, which, though rare, consist of either corals, with only a limiting constraint on sea-level, or intertidal mangrove sediments, which currently have a vertical range of ~ 4 m.

Stillstands shorter than 1000 years would produce proportionally smaller differences between the two sites. If stillstands occurred, it is unlikely that the spatial variation in their signature is observable, given the uncertainty in sea-level observations and the probability that a "stillstand" would likely contain a eustatic signal similar in magnitude to the isostatic one.

The spatial variation in sea-level change during the postglacial transgression is most likely to be observed if the eustatic sea-level curve includes not only stillstands, but also regressions. By the same processes

described above, the magnitude of such a regression would be accentuated at coastal sites, such as Halifax Bay, and diminished at mid-ocean sites such as Barbados. In the right environment, a sea-level regression would be preserved as an alternation of subaerial/freshwater and marine sediments. No such record exists, but if one is found it will probably be at an inshore coastal site, where the magnitude of the regression would be greatest.

a)

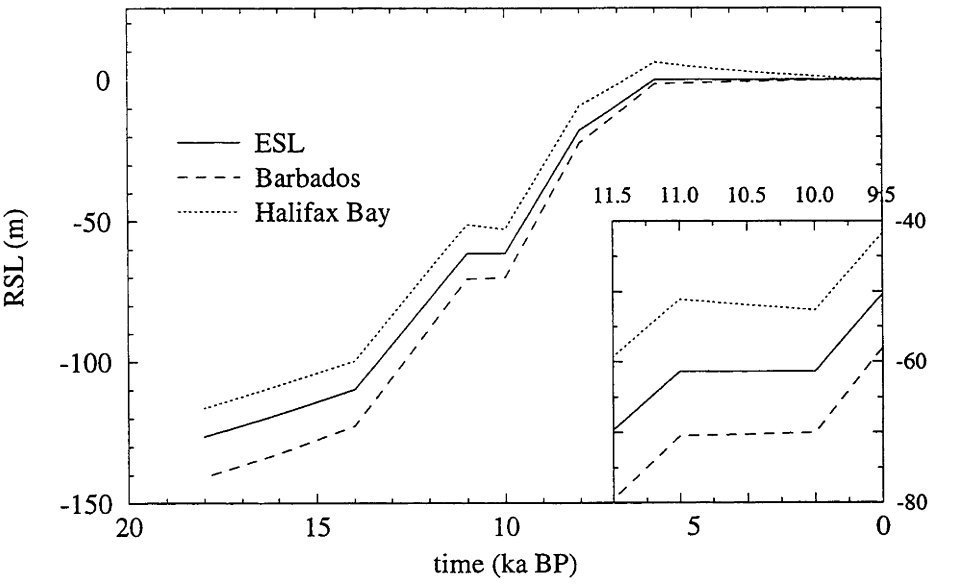

b)

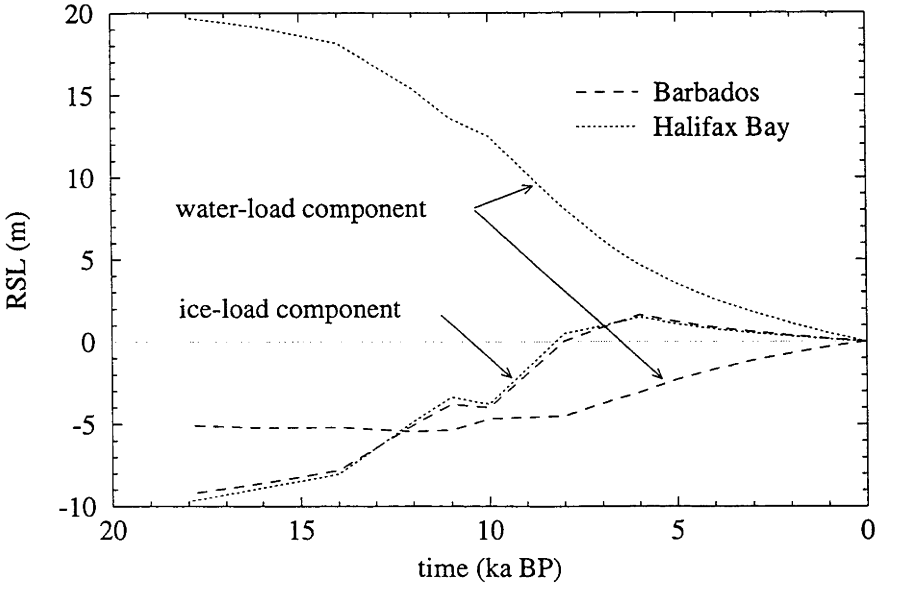

Figure 6.14 : Predicted relative sea-level curves at Barbados and Halifax Bay for a melting model including a stillstand from 11 to 10 ka BP. Graph a) shows total relative sea-level; b) shows the ice- and water-load components.

6.4 Mid-late Holocene sea-level

6.4.1 Introduction

Thom and Chappell (1978) used early models of glacio-hydro-isostasy (Walcott 1972, Chappell 1974) to make predictions for sea-level change in the GBR region. They made three important observations, illustrated in Figure 6.15: 1) sites on the inner margin will tend to exhibit a mid Holocene highstand, whereas sites on the outer margin will not; 2) models with a wider continental shelf and a thinner lithosphere predict greater differences between the inner and outer shelf sites; and 3) if eustatic sea-level rise has continued throughout the Holocene, then the predicted mid Holocene sea-level highstand is lower than would otherwise occur. Insufficient sea-level observations were available to evaluate these models.

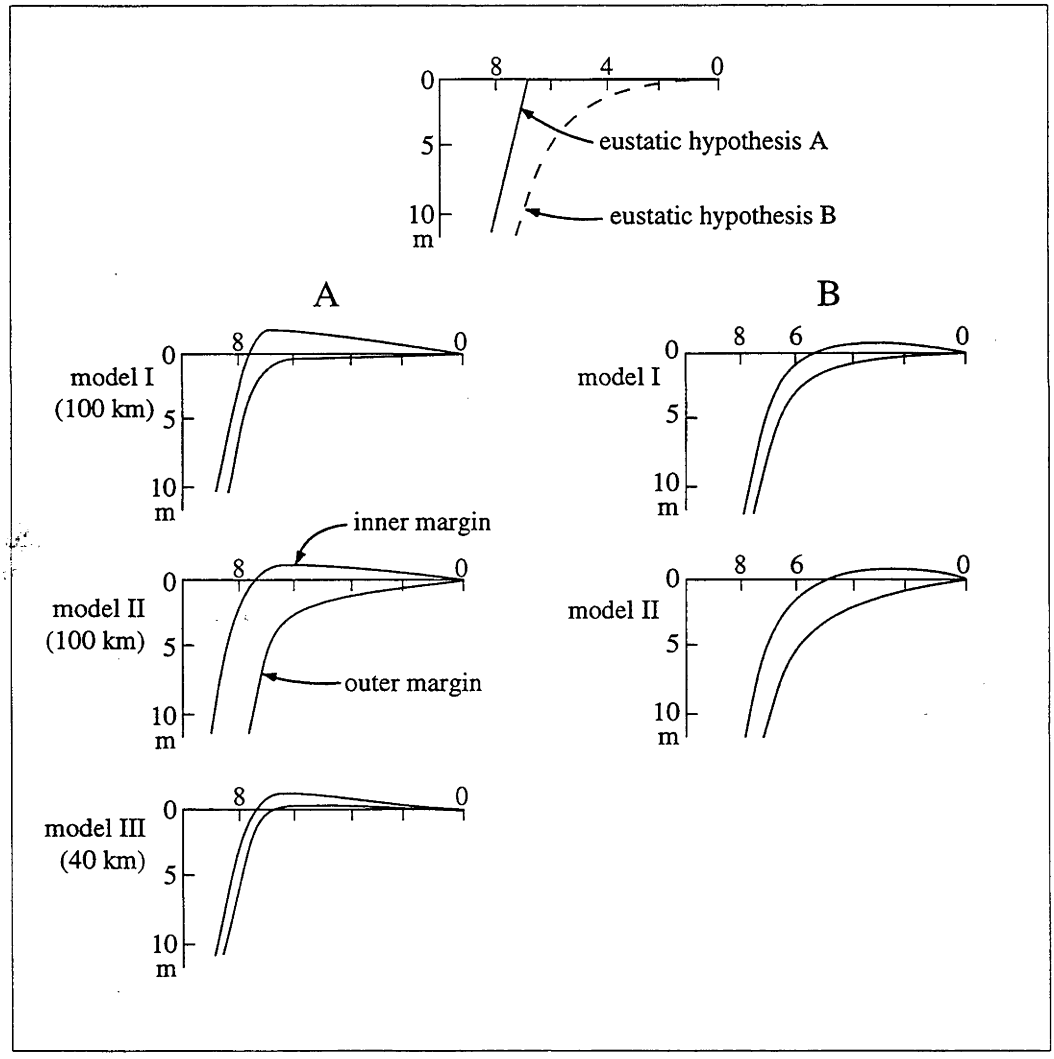

Figure 6.15 : Predicted relative sea-level curves for inner and outer margins of continental shelves, for two ice-melt (eustatic) hypotheses. Three rheological models are depicted: I continental (thick) lithosphere; II oceanic (thin) lithosphere; III continental-oceanic transitional lithosphere. Curves are derived for continental shelf widths of 100 km in the case of models I and II, and 40 km in the case of model III. (From Thom and Chappell 1978).

As discussed in the introduction to this chapter, Nakada and Lambeck (1989) compiled Holocene sea-level observations in the Australian region, and used differential relative sea-level between pairs of sites to constrain the earth rheological model. Using the range of rheological parameters suggested by that study, and an expanded data set including the new observations reported in Chapter 2, this section aims to evaluate the rheological model and obtain an estimate for late Holocene eustatic sea-level change.

6.4.2 Late Holocene eustatic sea-level change

The ice model used to calculate sea-level predictions in this chapter, ARC3+ANT3 (Nakada and Lambeck 1988), has no eustatic sea-level change since 6 ka. When the most appropriate earth model is used, and the numerical calculation of sea-level change includes all significant glacio-hydro-isostatic terms, such as the effect of moving coastlines and multiple iterations of the sea-level equation, the predictions are consistently higher than the observations throughout the late Holocene. This discrepancy may be due either to errors in the model, or else local effects such as tectonism and changes in tidal range.

The observed-predicted residual is shown in Figure 6.16 for a range of plausible earth models, and the sea-level data presented in Chapter 2. The scatter in these data, shown in Table 6.3, can be used as a measure of how well the predictions explain the spatial variation in the observations. On this criterion, the models with a higher viscosity upper mantle (Figure 6.16 d & h) and those with a less viscous lower mantle (Figure 6.16 a & e) are less suitable. There is little difference between the models with 50 km or 100 km lithospheres, or with upper mantle viscosities in the range (1-2) x 10^{20} Pa.s, although perhaps the lower viscosity is preferred. These results are in close agreement with those of Nakada and Lambeck (1989). Another rheological model, with a lithospheric thickness of 100 km and a uniform mantle viscosity of 10^{21} Pa.s. was also investigated, similar to the global rheological model proposed by Tushingham and Peltier (1992). The observed - predicted residuals of this model are lower than for the others (Figure 6.17), but the scatter in the data is much greater (Table 6.3), and it is not considered to be a viable rheological model for north Queensland.

Although the amount of scatter in the residual plot does not vary significantly for models of different lithospheric thickness, the magnitude of the residual at 6 ka is about 4 - 6 m for the 100 km lithosphere, but only 3 - 5 m for the 50 km lithosphere. However, this does not necessarily imply that the thinner lithosphere model is more appropriate for that region, as there is no reason to assume that 4 m rather than 5 m of melting has occurred. The correct values for both the rheological parameters and late Holocene melting will only be obtained by better regional constraints on the rheology, and global constraints on the melting curve.

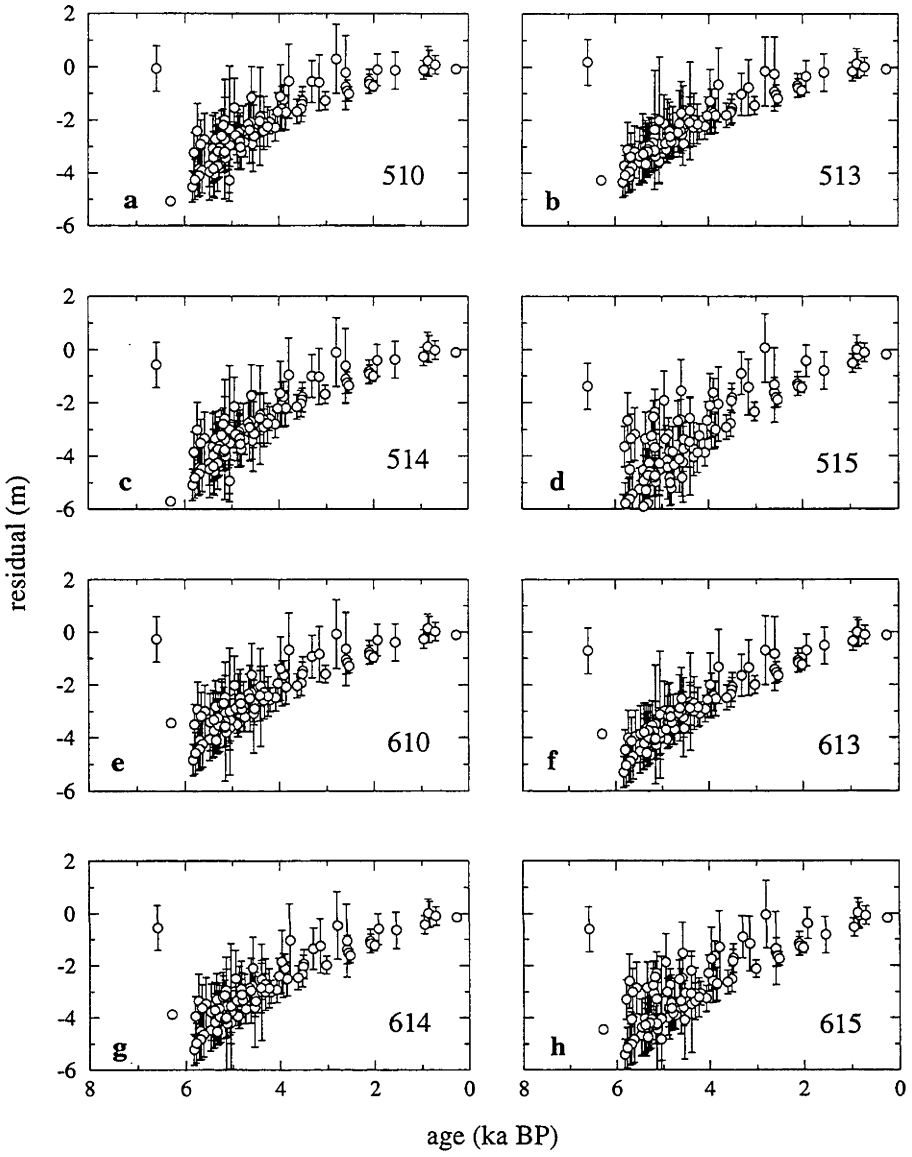

Figure 6.16 : Observed - predicted sea-level residuals for mid-late Holocene observations in north Queensland. Predictions were obtained using the standard ice model, calculated to degree 256 for 2 iterations of the sea-level equation. The parameters of the earth models are listed in Table 6.1.

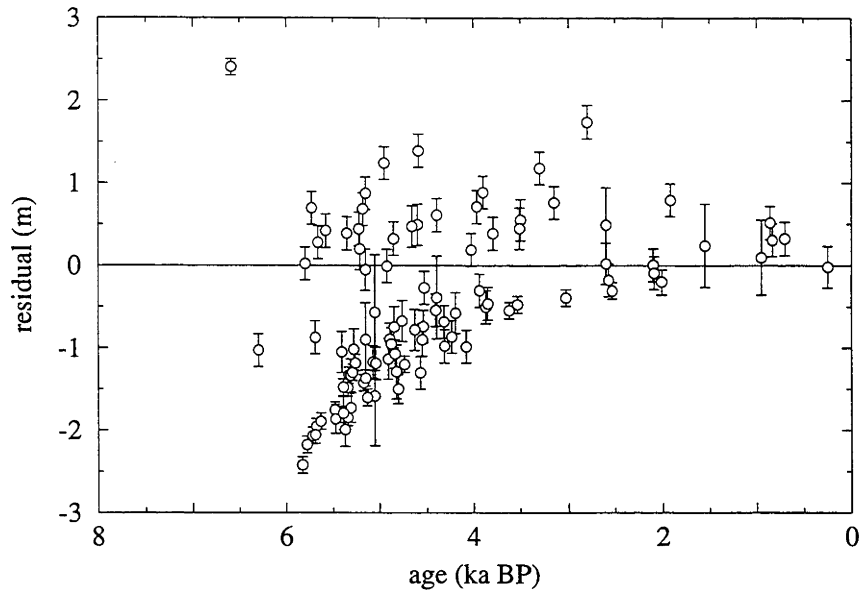

Figure 6.17 : Same as for Figure 6.16, but for an earth model with 100 km lithosphere and a uniform mantle viscosity of 10^{21} Pa.s. The residuals are smaller than for the models shown in Figure 6.16, but the scatter is much greater, indicating that this model does not explain the observed sea-levels well.

Table 6.3: Correlation coefficient between the observed-predicted sea-level residuals shown in Figures 6.16 and 6.17 and the best fit quadratic curve. High correlation coefficients indicate less spread in the data, suggesting that sea-level is well modelled using that rheological model. The quadratic form was chosen because it allows for some curvature in the trend of the residuals, but is not intended to describe the form of the late Holocene eustatic sea-level curve. The parameters of the rheological models are given in Table 6.1, except for model 604, which has a lithospheric thickness of 100 km and a uniform mantle viscosity of 10^{21} Pa.s.

Rheological model	Correlation coefficient
510	0.719
513	0.748
514	0.758
515	0.643
610	0.735
613	0.797
614	0.756
615	0.654
604	0.186

Lambeck (1993b) used sea-level observations from the British Isles to propose that about 1.7±1 m of melting has occurred since 6 ka. This is considerably smaller than the values estimated here from the North Queensland data, although the shape of the melting curve between 6 ka and the present is similar (Figure 6.18). Comparison of observations and

predictions from the French coast (Kurt Lambeck, pers. comm.) indicate about 4±2.5 m of late Holocene melting. The British and French sites are close to, or within, formerly glaciated regions, where the glacio-isostatic component of sea-level change is much more significant than in Queensland, and small refinements of the optimum rheological models may reduce the discrepancy between these estimates.

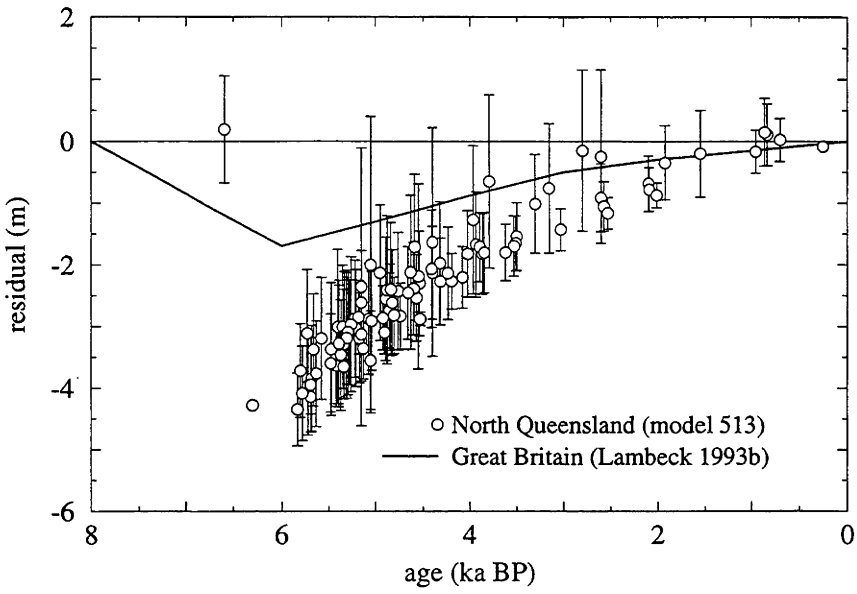

Figure 6.18 : The observed - predicted sea-level residual for mid-late Holocene data from north Queensland, using the predictions of earth model 513, which produces the lowest scatter in the data. The result of Lambeck (1993b) obtained from sea-level observations in Great Britain is shown for comparison.

The observed-predicted sea-level residual could represent the combined effects of eustasy and tectonics. One possible scenario is that the British estimate of 1.7±1 m of late Holocene melting is correct, and the remaining 2 - 3 m of the Queensland residual is caused by tectonic subsidence. This would imply a subsidence rate of 0.3 - 0.5 mm/yr over the late Holocene, which would result in 40 - 60 m of subsidence since the last interglacial period. This is excessive, since the Pleistocene surface (commonly taken to be the level of last interglacial reefs) is only 5 - 30 m below present sea-level (Hopley 1982, Marshall in prep). If last interglacial sea-level was similar to present, then subsidence rates of 0.05 - 0.25 mm/yr are indicated, implying 0.3 - 1.5 m of subsidence in the last 6000 years. Using the residuals from the 100 km lithosphere models, this in turn implies a eustatic rise of 2.5 - 5.7 m over the same time. Clearly, a range of values for the tectonic and eustatic components can explain the observed residuals, but the notion of subsidence is supported by the observed absence of emergent last interglacial shorelines in north Queensland, while they are seen in many other Australian locations (Murray-Wallace and Belperio 1991).

The amount of water required to cause 3 - 5 m of sea-level rise represents a significant amount of ice on land, larger than the entire British ice sheet at

the LGM. In the period since 6 ka, this eustatic sea-level rise cannot have been derived from the Fennoscandia or Laurentide ice sheets, since these had both completely melted by that time. The contribution must be from the melting of the Antarctic ice sheet, alpine glaciers & small ice caps, or other reservoirs such as vegetation, lakes, and groundwater. The relevance of this correction to the Antarctic melting history and sea-level change is examined in Chapter 7. Estimates of the modern rate of sea-level rise due to mountain glacier melting are around 0.4±0.26 mm/yr (Lambeck 1980, Meier 1984, Nakiboglu and Lambeck 1991). These estimates are based on glacier observations in this century, but if the rate can be extrapolated to cover the mid-late Holocene, the total contribution since 6 ka would be 2.4 ± 1.6 m, which is a significant proportion of the inferred rise.

Spatial variation

The data set of late Holocene sea-level observations from north Queensland consists of about 100 points. These can be divided roughly in half by a line at 18.5°S, and the residuals for each section compared. Although there is considerable overlap (Figure 6.19), the southern data consistently indicate up to 0.5 m more late Holocene melting than the northern sites. Possible reasons for this difference include lateral variation in the lithospheric thickness or mantle viscosity, tectonic movement, and error in the ice model for the Antarctic ice sheet.

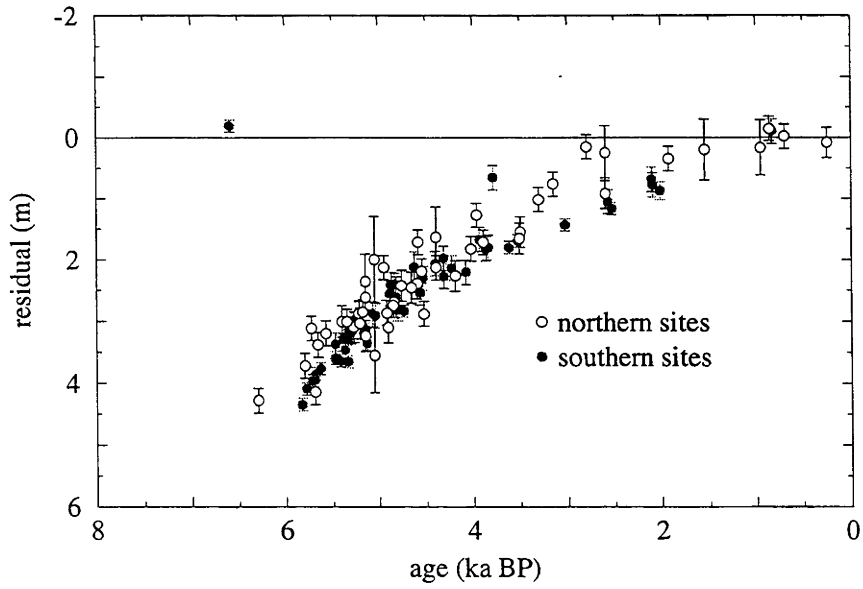

Figure 6.19 : Comparison of the observed - predicted sea-level residuals in the study area, north and south of a line at 18.5°S. Predictions were obtained using the standard ice model and earth model 513, calculated to degree 256 for 2 iterations of the sea-level equation. The residuals at southern sites tend to lie below those at the northen sites.

It is probably impossible to prove that the difference is due to differential tectonic movement, since the rate is only ~0.5 m in 6000 years, or less than

0.1 mm/yr, and this is not likely to be observable using a datum which is not linked to sea-level.

Lateral variations in lithospheric thickness or mantle viscosity cannot currently be demonstrated, but accumulation of a better database of sea-level observations may make this possible in the future. Lambeck and Nakada (1990) suggested that apparent lateral variation in earth rheology in north Queensland could be linked to variation in the width of the continental shelf, which is much narrower in the far north.

The chosen ice model for the Antarctic ice sheet also has a small influence on sea-level change in North Queensland. The crest of the peripheral bulge to the Antarctic ice sheet lies in the Antarctic ocean south of Australia, and subsidence of the bulge following deglaciation causes sea-level to rise there. The rate of subsidence decreases northwards on the flank of the bulge, so that the predicted differential sea-level since 6 ka due to this effect is about 1 m over the north-south extent of the Australian continent. This is discussed in detail in Chapter 7. The consequence of this contribution is that higher 6 ka highstands are predicted in the north of Australia than in the south (see Section 7.8). The observed-predicted sea-level residuals from north Queensland (Figure 6.19) indicate that, using current models, sea-level is overestimated more in the south than in the north. This could be due to an underestimation of the contribution from the peripheral bulge, which would imply that the amount of ice removed from this sector of the Antarctic ice sheet is underestimated in the ANT3 model.

Chapter 7

The Antarctic ice sheet and sea-level change

7.1 Objectives of this chapter

In Chapter 5, I discussed the principles of isostasy applied on a global scale to the redistribution of large masses of ice and water, and demonstrated the calculation of changes in relative sea-level due to the melting of a simple axisymmetric ice sheet. Reconstructions of former ice sheets and their melting histories can therefore be made, based on comparison between predicted and observed sea-level curves, if the parameters defining the Earth's response are known and if adequate observational data exist. Changes in sea-level near to an ice sheet are sensitive to the spatial distribution of the ice, whereas in the far-field the change is mainly a function of the total volume of ice melted. Thus, with the bulk of sea-level observations coming from locations in Europe and North America, relatively detailed reconstructions of the northern hemisphere ice sheets have been made using this method. In contrast, models of the Antarctic Ice Sheet were almost unconstrained and were adjusted in order to make up the total ice volume indicated by far-field observations (Nakada and Lambeck 1988, Tushingham and Peltier 1992, Peltier 1994).

In this chapter, I first discuss the relevance of using simple axisymmetric models to represent the Antarctic Ice Sheet. Next I calculate the sea-level changes caused by these models, and investigate their dependence on the rheological parameters of the earth model used. The sea-level observations from Chapter 3 are then used to constrain the volume of the former Antarctic Ice Sheet and its melting history. Finally, the conclusions of this section and previous reconstructions are combined to obtain constraints on the configuration of the Antarctic Ice Sheet at the last glacial maximum (LGM) and its deglaciation.

7.2 Previous work

The aim of the modelling in this section is first to determine the total contribution of the Antarctic ice sheet to sea-level fall at the LGM, and, if possible, to describe its geographical distribution and melting history. An optimum rheological model for the Antarctic region will also be determined. Previous approaches to constraining the history of the ice sheet have mostly been based on glacial geomorphology, ice cores, and physical models of ice sheet dynamics (see Chapter 4) but sea-level and isostatic arguments have also been used before.

7.2.1 The former Antarctic Ice Sheet

Lingle and Clark (1979) used the Antarctic ice sheet reconstruction of Hughes and others (1981) to predict global sea-level changes. Since there are insufficient data constraining the retreat of the ice sheet, several styles were modelled, including a model with linear retreat complete by 6 ka, and an exponential model in which early melting is faster and some melting continues until the present. It was found that in the far-field, the sea-level curve is a close approximation to the equivalent sea-level function, and that isostatic effects are more important close to the ice sheet. Although insufficient observational data were available to draw detailed conclusions, they found general support for an ESL contribution of ~25 m at the time of the last glacial maximum. In addition, they noted that continued melting of the ice sheet in the last 5000 years would greatly reduce the Holocene highstands found worldwide. Comparison with observed highstands led them to suggest less than 0.7 m ESL contribution during this time, while acknowledging that more observations were required. These general conclusions are valid, but the work was handicapped by the inadequate resolution of the models, due to the limited computing resources of the time. Recent calculations (Mitrovica and Peltier (1991), Johnston (1993)) show that the effect of a second iteration of the sea-level equation (see Chapter 5) is to accentuate the Holocene highstand in the far-field. This increases the amount of late Holocene melting required to match observations.

The equivalent sea-level curve for the Antarctic ice sheet was studied by Nakada and Lambeck (1988), without detailed consideration of the actual distribution of ice. They used a total melt volume of 37 m ESL, based on the reconstruction of Hughes and others (1981), and estimates of the amount of "missing" ice required by sea-level records in addition to the relatively well-constrained northern hemisphere ice sheets. They formulated a melting history (ANT3a) roughly in phase with northern hemisphere melting until ~12 ka, after which Antarctic melting is retarded (Figure 7.1). In this model, melting of 3 m ESL occurs after 6 ka, based on the sea-level observations from the Gulf of Carpentaria, the north Queensland coast and Spencer Gulf, in Australia. Melting histories in phase with the northern hemisphere ice sheets, or with early melting (similar to Clark and Lingle's (1979)

exponential model) were rejected, as they predict sea-level rise between 9 ka and 6 ka which is faster than observations indicate.

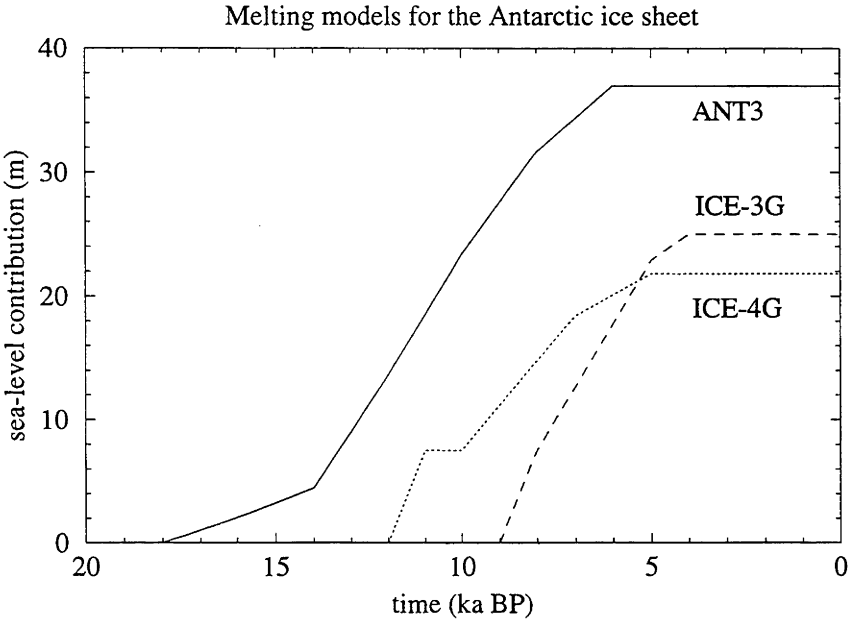

Figure 7.1 : Previous models for the Antarctic meltwater contribution estimated from sea-level records. ANT3 and ANT3a: Nakada and Lambeck (1988); ICE-3G: Tushingham and Peltier (1992); ICE-4G: Peltier (1994).

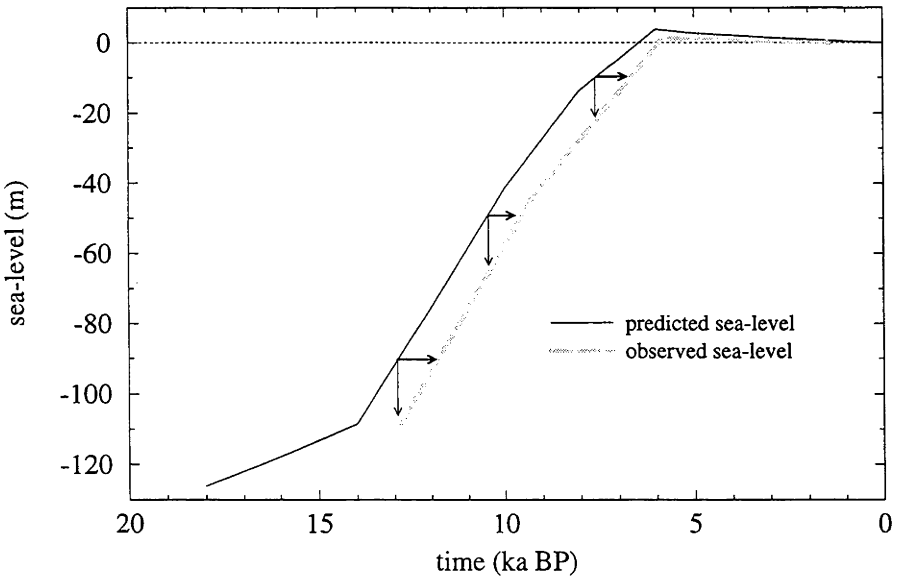

Figure 7.2 : Example predicted and observed far-field sea-level curves for the late-glacial period, indicating the trade-off between ice volume and time of melting. In this example, the predicted curve lies above the observed. The prediction could be made to agree with the observations either by increasing the total esl rise, or by delaying the melting.

Tushingham and Peltier (1991) proposed a different style of melting for the Antarctic ice sheet, in which melting does not begin until the northern hemisphere ice sheets are at their maximum rate of deglaciation, 9000 years ago. In this model, ICE-3G, the Antarctic ice sheets contribute only 25 m to global sea-level rise (Figure 7.1). The most recent model, ICE-4G, is smaller still, with 21.8 m ESL coming from Antarctica (Peltier 1994). The 12 m ESL difference between ANT3 and ICE-3G is not distributed to other ice sheets - Tushingham and Peltier (1991) propose a total postglacial ESL rise of 115 m, compared to Nakada and Lambeck's 126 m. The few observations of relative sea-level from the time of the last glacial maximum, 18-20 ka, are generally compatible with a total sea-level fall of 120 - 130 m relative to the present (see Chapter 6), but the maximum volume and time of melting of the models cannot be independently constrained by far-field observations, since a discrepancy between predicted and observed sea-level curves can be accommodated by adjusting either of these parameters (Figure 7.2). Around the Antarctic coastline, however, the isostatic response to these models is significantly different, so sea-level observations can be used to constrain the ice sheet history.

Colhoun and others (1992) compiled raised beach altitudes from several sites around the East Antarctic ice sheet, and estimated a former ice thickness at each site. To do this, it was assumed that the rebound at each site is entirely due to the removal of local ice, and that Airy isostatic equilibrium was attained during the LGM and has been attained again now. The total rebound was defined as the sum of the maximum beach ridge height and the total global eustatic sea-level rise of 121 m (Fairbanks, 1989). This rebound was multiplied by the ratio of mantle density to ice density to obtain the ice height. At the six sites used, the estimated former ice height was close to 500 m. This value was then used by Colhoun and others (1992) to model the profile of the ice sheet at the LGM. Using the present-day profile of Hollin (1962) as a guide, the LGM profile need only be 30 km wider in order to model 500 m of ice removal at the present-day coastline. Colhoun and others (1992) therefore suggest that the LGM ice sheet margin was 30 km beyond the present one, with the difference between the LGM and present profiles decreasing inland to 0 m at the 2000 m elevation contour. The cross-sectional area of this extra ice is multiplied by the length of the Antarctic coastline between 170°E and 30°W to obtain the total ice volume change due to coastal ice movements. To estimate the total ESL contribution of the Antarctic ice sheets since the LGM, Colhoun and others assume an average of 150 m of ice accumulation in regions above 2000 m, based on interpretations of isotopic measurements from ice cores (Robin 1985, Jouzel, 1989). Estimates for other regions of Antarctica were drawn from several sources, leading to the conclusion that the total Antarctic ESL contribution was 0.5-2.5 m (Table 7.1). Clearly the isostatic arguments used in producing this model are over-simplified, and the assumption that the marine limit at the sites studied was formed at the LGM is invalid, leading to an underestimate of the ice volume change. The results from several sites presented in Chapter 3 indicate that an age of 6000 - 7000 yr BP is more likely for the marine limit. Later in this chapter a deglaciation model similar to that of Colhoun and others (1992) is discussed using more realistic

rheological calculations combined with reinterpreted and new sea-level observations.

Table 7.1 - Regional contributions to postglacial sea-level rise from the Antarctic Ice Sheet, according to Colhoun and others (1992).

region	ESL (m)
coastal East Ant. ice sheet	0.73
Lambert Glacier	0.13
interior East Ant. ice sheet	-1.5 - 0.0
Ross Sea	0.3 - 0.45
Weddell Sea	0.35 - 0.55
West Ant., and Peninsula	0.48
total	0.49 - 2.34

7.2.2 Rheological models of the Earth

As described in Chapter 5, the rheological model of the earth is defined by the variation in density, elasticity and viscosity as a function of radius. In all models used here, the density and elasticity functions are defined using standard published models with realistic depth distributions of density and elastic moduli. The mantle is divided into two layers by a boundary at 670 km depth, and is overlain by an elastic lithosphere. The model is parameterised by the effective thickness of the lithosphere H_l, and the effective viscosities of the upper and lower mantle (η_{um} and η_{lm}).

Previous studies have produced a range of estimates for the Earth's rheological parameters on the time scale of postglacial rebound (10^3 - 10^4 years), although none have been obtained specifically for the Antarctic region. Tushingham and Peltier (1992) use the elastic structure model 1066B (Gilbert and Dziewonski 1975), which they show to be not significantly different from the PREM model (Dziewonski and Anderson 1981) when calculating sea-level changes on glacial timescales. They use a "standard" model with H_l = 120 km, $\eta_{um} = 10^{21}$ Pa.s, and $\eta_{lm} = 2 \times 10^{21}$ Pa.s, and examine the performance of a range of models in which only one of the three parameters at any one time differs from the standard values. These tests therefore do not represent a complete examination of "rheology-space", but are limited to a set of mutually perpendicular axes within it. Tests of the sensitivity of sea-level predictions to lithospheric thickness indicate that a value of H_l = 71 km produces the best fit to the sea-level observations from the Antarctic region, within the margin of the former ice sheet. This may be due to a poor ice model or inaccurate observed sea-level records for the Antarctic region. The latter possibility is likely, since the interpreted sea-level record for McMurdo Sound presented by Tushingham and Peltier (1992) differs significantly from that presented earlier in this work, in Chapter 3. Varying η_{lm} while keeping the other parameters constant, Tushingham and Peltier (1992) found that the sea-level observations from

the Atlantic, Indian and Southern Oceans (treated together) indicate that η_{lm} is 1 to 3 orders of magnitude greater than η_{um}. This contrasts strongly with the "standard" model, which provides good fits for sites in Europe and North America. The "standard" model is also strongly preferred over one with a sub-lithospheric low-viscosity zone. It should be noted that the ice model used in these sensitivity tests (ICE-3G) was created using the "standard" rheological model, so it is perhaps inevitable that the fit of sea-level predictions produced using these models is good in regions where there are many observed records, and poorer elsewhere. The same sites were not used for creating and testing the ice model, but nevertheless some circularity in the argument is evident.

Lambeck and Nakada (1990) compared sea-level observations from around Australia with predictions based on the ice model ARC3+ANT3 and a range of earth models. Models in the range H_l = 50 - 150 km, $\eta_{um} = 10^{20} - 10^{21}$ Pa.s, and $\eta_{lm} = 10^{21} - 10^{23}$ Pa.s were considered, and it was found that the optimum fit occurs for H_l = 70 - 80 km, η_{um} = (2-3) x 10^{20} Pa.s, and $\eta_{lm} = 10^{22}$ Pa.s, although some lateral variation in these parameters is indicated. This variation is probably partly due to the fact that these are effective parameters only, and the lithospheric thickness is known to vary across this region, between continental and oceanic values.

Lambeck (1993) found that the optimum rheological models fitting sea-level observations from Great Britain and northwestern Europe are similar to the Australasian model, although with a slightly higher upper mantle viscosity of (4-5) x 10^{20} Pa.s, and that three-layer models are adequate. Like Tushingham and Peltier (1992), he found no evidence for a low viscosity sub-lithospheric layer. Recent results (Lambeck and others, submitted) confirm that three-layer models are adequate, although the best solution can be obtained using a five-layer model in which viscosity increases with depth. This work also shows that previous published conclusions of higher or lower mantle viscosities (Tushingham and Peltier 1992, Fjeldskaar and Cathles 1992) were influenced by inadequate exploration of the parameter space, particularly with regard to the lithospheric thickness adopted.

7.3 Methods

Although the configuration of the Antarctic Ice Sheet at the LGM is well constrained in a few places (see Chapter 4), there is no general consensus concerning the volume or general style of expansion; specifically, whether the former ice sheet was significantly higher than the present, or wider, or both, or neither. As long as such fundamental problems remain, there is little value in constructing detailed "realistic" models for the purpose of modelling sea-level change. By comparing the sea-level predictions of the endmember simple models with each other and with the observed sea-level curves, we can draw general conclusions which will aid the construction of a realistic model. As described in Chapter 5, the three sets of parameters which influence sea-level change by glacio-hydro-isostasy are the ice, ocean and earth models. The classes of models used in this section are presented here.

7.3.1 Ice sheet configuration

The ice models used in this section are similar to those described in Chapter 5: they are circular, and have a parabolic semi-profile defined by the equation

$$h = H\sqrt{(R-r)} \tag{7.1}$$

where h is the height of the ice sheet at a distance r from its centre, H is the maximum height of the ice sheet, and R is the radius (Paterson 1994). The applicability and limitations of this model have been treated in Chapter 5, and will not be discussed further here. The most important difference between the models used here and those described in Chapter 5 is that ice remains on the Antarctic continent after the postglacial melting is complete. This feature distinguishes the Antarctic Ice Sheet from the LGM ice sheets in the northern hemisphere, which melted almost completely. Figure 7.3 demonstrates the fundamental difference between these situations. In both models, the shape of the ice sheet as melting occurs is constrained by holding the parameter b constant, where

$$b = \frac{H}{\sqrt{R}} \tag{7.2}$$

In this situation, both height and radius decrease with decreasing volume. Two models are considered. In model A, the initial profile is shown in Figure 7.3 as curve *a)* and the entire ice sheet melts, with the greatest thickness of ice removed from the centre of the sheet. In model B, with the initial profile *b)* in Figure 7.3, the same volume of ice is removed, but an ice sheet remains, shown as curve *c)*. In this case, the greatest thickness of ice is removed from near the circumference of the ice sheet. Clearly, the earth's isostatic response to these scenarios will differ markedly in the near-field, although the effects in the far-field are virtually indistinguishable. All models considered in this section are of the same form as model B.

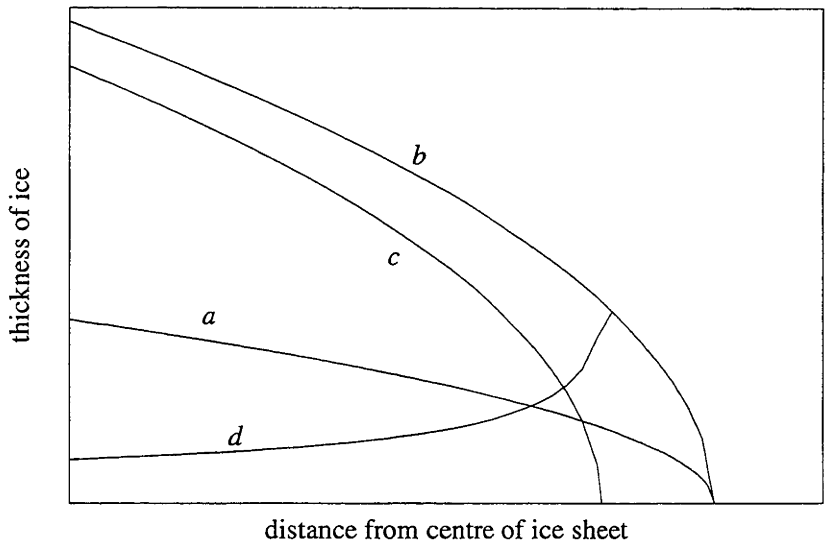

Figure 7.3 : Distribution of ice load for axisymmetric models A and B, discussed in the text. In model A (curve a), the ice sheet melts completely, so the maximum load is in the centre. In model B, a larger ice sheet (curve b) partially melts to leave an ice sheet whose profile is indicated by curve c. The distribution of ice removed is shown as curve d. Although the total volume of ice removed is the same as in the former case, the maximum change in ice load occurs at the ice sheet margin.

Models have been constructed to study the effects of former ice distribution on both regional and continental scales. The regional models simulate the amount and timing of deglaciation over regions on the order of 1000 km across, and do not necessarily apply to the ice sheet as a whole, so are not used to infer the total volume of melting which occurred. The continental-scale models, which model the entire Antarctic Ice Sheet, are less useful for comparison with local observations, but can be used with sea-level observations at sites distant from Antarctica to constrain the total volume change.

7.3.2 Regional models

The regional models were constructed in order to determine how far the LGM ice sheet extended beyond its present position, and the timing of its retreat, at several coastal Antarctic sites using sea-level records from those sites, without attempting to model the entire ice sheet. To do this, we must assume that the ice-load component of sea-level change there is dominated by regional (<1000 km away) changes in ice distribution.

To choose the most appropriate size and shape of a circular model to simulate regions on the Antarctic coast, transects of the ice sheet inland from the main sea-level observation sites were compared with theoretical profiles. The transects were made from each coastal site to the nearest elevation maximum (ice dome summit or ridge crest) on the interior of the

East Antarctic Ice Sheet, using the ice thickness and elevation data of Drewry (1983), interpolated onto a 20 km grid by Jenssen (pers. comm.). The average distance from the coast to the top of each transect is 1100 - 1200 km (Figure 7.4), so model ice sheets were constructed with a radius of 10° (1112 km).

Several theoretical profiles were compared with the transects, to obtain the best approximation. A least-squares fit of the general formula for two-dimensional ice sheets in equilibrium on a flat surface (Paterson 1993, p243) showed that the ice behaves as an almost perfectly plastic medium, which results in the parabolic profile given in equation (7.1). Using this equation, the best fit to the observed transects is obtained using H~3700 m (Figure 7.4). This model ice sheet, designed to represent a segment of the present

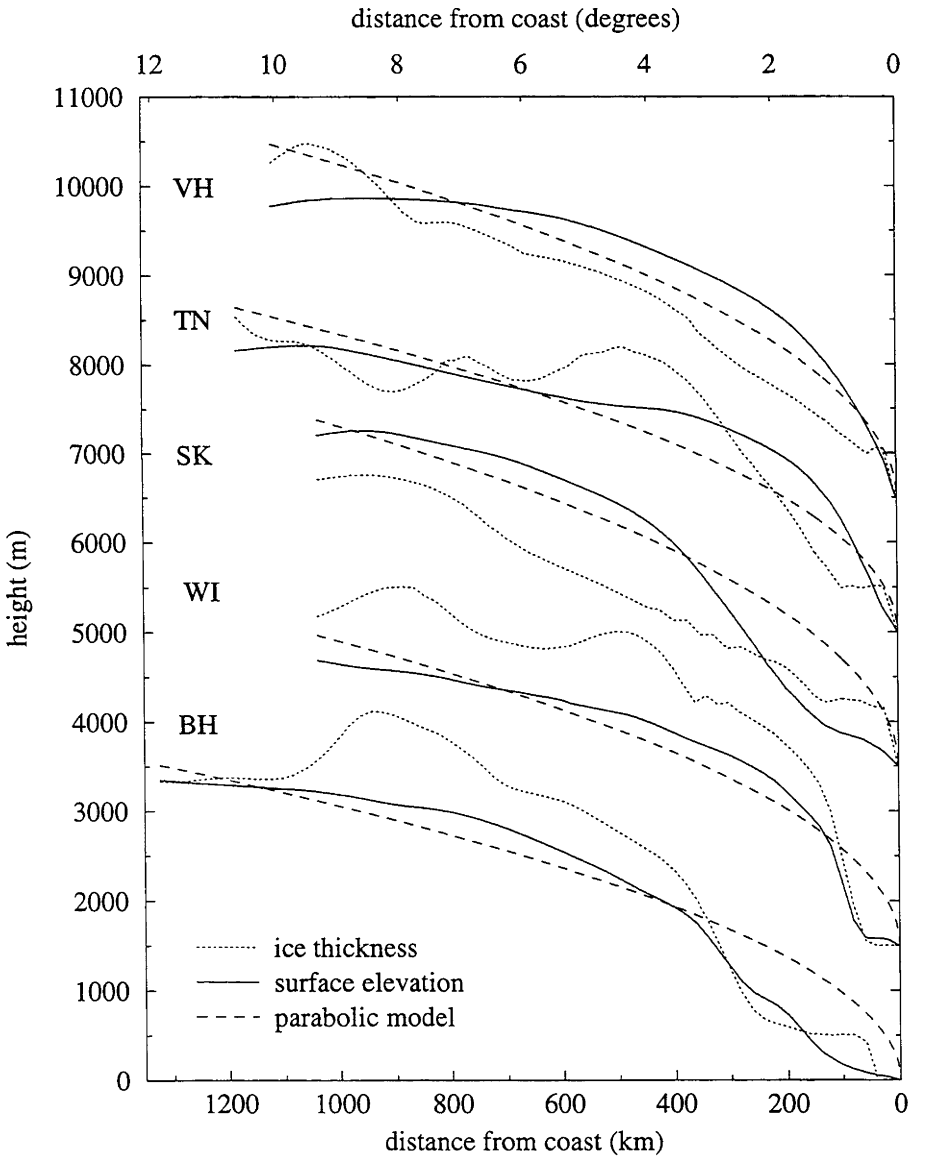

Figure 7.4 : Transects of the Antarctic Ice Sheet at five locations, showing ice thickness and surface elevation. The surface elevation is adequately described by a parabolic model (equation 7.1). Profiles are offset vertically for easier comparison. VH=Vestfold Hills; TN=Terra Nova Bay; SK=Skarvsnes; WI=Windmill Islands; BH=Bunger Hills.

Antarctic Ice Sheet margin, is the configuration to which all the regional models used in this section evolve.

Three aspects of deglaciation are varied in these models: the amount of ice sheet retreat; the distribution of ice in the former ice sheet; and the timing of the melting. The combinations of these parameters, discussed in the following paragraphs, form the set of regional models which have been examined.

Ice sheet retreat

The continental shelf around Antarctica is up to 150 km wide, with an average of about 100 km, apart from in the Ross and Weddell Seas, where it extends about 1000 km beyond the present grounding line of the Antarctic Ice Sheet. Marine coring studies indicate that in some places ice did advance this far during the LGM (see Chapter 4). The regional models therefore consider a range of former ice sheets whose radius at 18 ka is up to ~130 km larger than their final (present) state. Because of the way in which the models are constructed, the various ice models are parameterised by volume, rather than radial expansion, but the relationship between the two is almost linear over the range studied here. The models in this range contribute up to 5 m ESL to sea-level rise. For comparison with observations from Antarctic sites, the sea-level predictions of these models are combined with a modelled contribution from distant ice sheets, accoring to Nakada and Lambeck (1988), which is scaled so that the total ESL rise is the same in all cases.

Distribution of ice removed

The distribution of the additional ice in the former ice sheet has been modelled in two ways. The first is as described above (equation 7.1), with the parameter b (equation 7.2) held constant. As melting takes place, both the height and the radius of the ice sheet decrease, resulting in the removal of an ice load whose shape is shown in Figure 7.5. In Patterson's derivation (1994, p242) for ice sheets in equilibrium,

$$b^2 = \frac{2\tau_b}{\rho g} \tag{7.3}$$

where τ_b is the basal shear stress, ρ is the density of ice and g is gravitational acceleration. This model thus corresponds to an ice sheet with constant basal shear stress. In this model, the radius of the final ice sheet is 1112 km and its maximum thickness is 3700 m, as described above. The corresponding value of τ_b is about 54 kPa which is close to the observed mean of around 50 kPa (Patterson, 1994, p242), and well within the range of 0 to 100 kPa, suggested as reasonable for ice sheets in equilibrium (Patterson, 1994, p242).

The second style of melting modelled involves retreat of the ice sheet margin while the height remains constant. The distribution of ice removed during melting using this model is shown in Figure 7.5. Changing R while H remains constant means that the parameter b, and hence the basal shear stress τ_b, vary as melting proceeds. From equations (7.2) and (7.3) above, we obtain

$$\tau_b = \frac{\rho g H^2}{2R}. \tag{7.4}$$

A model in which L decreases by 100 km while H is held constant requires τ_b to increase steadily during melting from 50 kPa to 54 kPa.

The effective basal shear stress of an ice sheet depends on many variables, including the roughness and slope of the bed, the degree of basal melting and the amount of sediment-laden basal ice (MacAyeal 1992). These properties vary considerably over the extent of the Antarctic ice sheet, so it is not meaningful to interpret these changes in basal shear stress in terms of any physical parameter. It is enough to note that the range of values is close to the suggested value for ice sheets of 50 kPa (Patterson 1994).

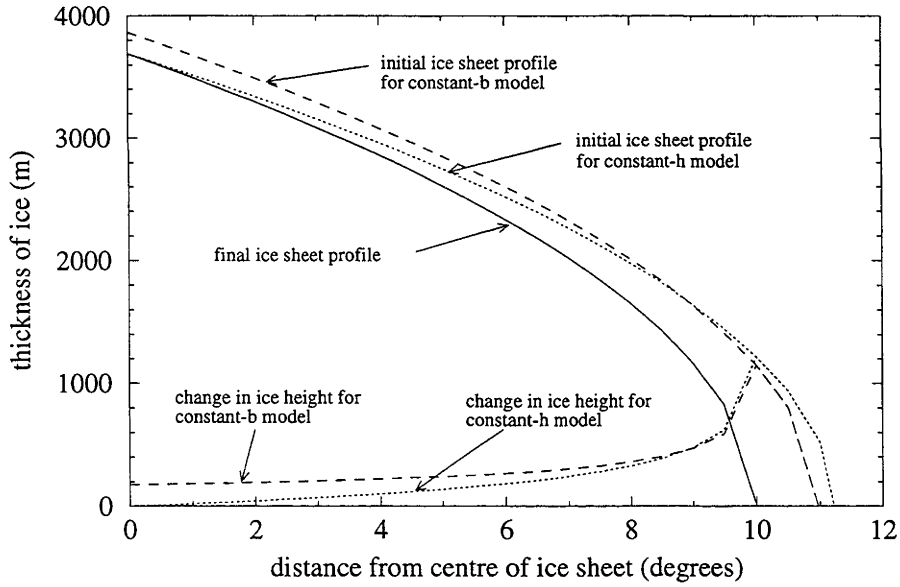

Figure 7.5 : Distribution of ice removed for constant-height and constant-b models.

Timing of melting

The timing of the retreat of the ice sheet has direct effects on the resulting sea-level curve: recently deglaciated regions are presently undergoing faster uplift than those uncovered thousands of years ago. Sea-level observations far from Antarctica indicate that significant melting took place between 10 ka and 6 ka (Nakada and Lambeck 1988), whereas radiocarbon ages from

coastal oases indicate that the ice sheet margin has been stable for at least 10,000 years (Chapter 4). To test whether ice was removed from the coastal region during this time, models have been constructed in which melting ceases at either 6 ka or 10 ka. Melting begins at 18 ka in both cases. In the former case, the melting history, or equivalent sea-level curve, is proportional to that of the entire Antarctic Ice Sheet as described by model ANT3 of Nakada and Lambeck (1988). For models in which melting ceases earlier, the melting curve is the same until 12 ka, when it accelerates to complete melting by 10 ka (Figure 7.6). This melting style is only applied to the regional component of sea-level - the remainder remains proportional to that of ANT3.

Sea-level observations from north Queensland, Australia, indicate that eustatic sea-level rise in the last 6 kyr contributed 3 - 6 m ESL to the oceans (Chapter 6). This style of melting is applied to the regional models to examine its effect on near-field sea-levels. The regional models, however, do not represent the volume of the entire ice sheet, so it would be unrealistic to model this situation using the entire estimate of melting since 6 ka. Using the total Antarctic contribution of 37 m ESL (Nakada and Lambeck 1988), the late Holocene ESL rise is approximately 10% of the total melt volume. Regional model were therefore constructed with 10% of their melting taking place since 6 ka. This represents a scenario in which all the late Holocene eustatic sea-level rise was due to melting at the Antarctic margin, and is shown in Figure 7.6 as model 6a. Models are also considered in which the late Holocene melting was not sourced from the regional models, but is included in the far-field contribution to sea-level change.

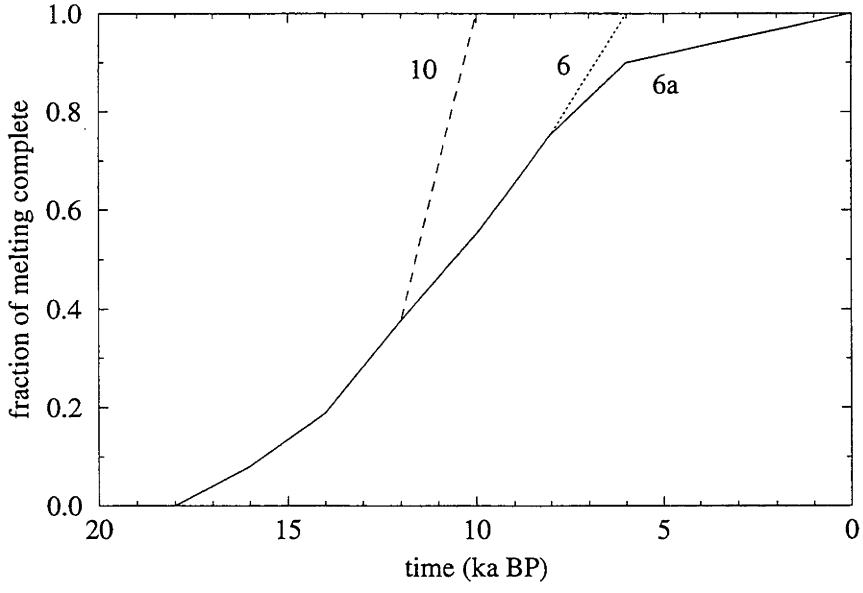

Figure 7.6 : Three melting curves used for the regional-scale ice sheet models. Model 6 corresponds to model ANT3 of Nakada and Lambeck (1988).

Table 7.2: The three ESL models used in association with the regional ice sheet models. The actual melting curves are shown graphically in Figure 7.6.

ESL model	Description
6	Melting is proportional to model ANT3 of Nakada and Lambeck (1988), ceasing at 6 ka
6a	Identical to model 6 before 8 ka, when melting slows so that 10 % of total melting occurs after 6 ka.
10	Identical to model 6 before 12 ka, when melting accelerates so that melting is complete at 10 ka.

7.3.3 Continental-scale models

The "continental-scale" models were constructed in order to investigate the dependence of global sea-level change on the total volume of ice removed from the Antarctic Ice Sheet since the LGM. In these models, the entire Antarctic Ice Sheet is approximated by a single circular ice sheet. The shape of the ice sheet remaining after melting is completed varies between models, according to the distribution of the ice removed by melting, but in all cases contains 60 m ESL, closely approximating the actual value of 59 m (derived from Drewry 1983).

The axisymmetric ice sheet models used in this section are constrained by two variables: ESL history, and the prescribed height, radius or aspect ratio (parameter *b*) history.

As described above, published estimates for the Antarctic contribution to postglacial sea-level rise range from 37 m ESL (Nakada and Lambeck 1988) to less than 2.5 m (Colhoun and others 1992). Two extreme models are presented here - one contributing 37 m ESL, and the other 5 m (Table 7.3).

Distribution of ice removed

Five continental-scale models for the distribution of the melted ice were investigated. As for the regional models, melting schemes with constant height and constant "*b*" were produced. In addition, a model was made in which the radius is constant, and volume reduction is accommodated by height reduction. Modelling was also performed using model ice sheets with a prescribed margin retreat history. These models forced the ice sheet to retreat only ~150 km, roughly the width of the continental shelf around East Antarctica. Two different retreat models were used: one with retreat ceasing 6000 years ago, when melting largely ceased, and the other with retreat ceasing 10,000 years ago. These melting models are summarised in Table 7.4. The initial and final ice sheet dimensions for each model and the range of implied basal shear stress values are shown in Table 7.5.

Timing of melting

Two melting curves were used in association with these models: models ANT3 and ANT3a of Nakada and Lambeck (1988). As noted in the description of regional-scale models, the ANT3 model has no melting occurring after 6 ka, whereas ANT3a contributes 3 m ESL after that time.
In this study, 10% of the ice sheet (3.7 m ESL) melts in the late Holocene, based on new comparisons between model predictions and Australian sea-level records (Chapter 6).

Table 7.3: Equivalent sea-level models used in the continental-scale ice sheet models.

ESL model	Melt volume (ESL)	Description of ESL curve
3	37 m	Model ANT3 of Nakada and Lambeck (1988) (ie, ceasing 6000 years ago)
4	37 m	Proportional to northern hemisphere melting until 8 ka, then slowing to allow 3.7 m melting in the last 6 ka.
7	5 m	Proportional to model ANT3a of Nakada and Lambeck (1988)

Table 7.4: Removed ice distribution models used in the continental-scale ice sheet models.

Melting style	Description
b	parameter "*b*" (equation (7.2)) held constant
h	height of ice sheet constant
r	radius of ice sheet constant
f3	radius of ice sheet retreats from 21.4 to 20 degrees, in phase with northern hemisphere melting.
f4	radius of ice sheet retreats from 21.4 to 20 degrees, with retreat ceasing 10,000 years ago.

Table 7.5: Initial and final dimensions of the continental-scale ice sheet models, and the implied change in effective basal shear stress. † The name of the ice model is a combination of the codes for the ESL model (Table 7.3) and melting style (Table 7.4) used.

Ice model†	$R_{initial}$ (km)	R_{final} (km)	$H_{initial}$ (m)	H_{final} (m)	τ_b (kPa)
4b	2380	1962	4086	3710	31
4h	2380	1867	4086	4086	31 - 39
4r	2380	2380	4086	2527	12 - 31
4f3	2380	2222	4086	2895	17 - 31
4f4	2380	2222	4086	2895	17 - 31
7b	2380	2304	2378	2694	10 - 14
7h	2380	2284	2378	2378	10 - 11
7r	2380	2380	2378	2527	10 - 12
7f3	2380	2222	2378	2895	10 - 17
7f4	2380	2222	2378	2895	10 - 17

7.3.4 Ocean models

The model Antarctic Ice Sheet rests on a circular continent, on a model earth with another circular continent at the far pole, so that the fraction of the surface covered by ocean is 70 %, as on the real earth. This means that the equivalent sea-level rise caused by melting an ice sheet on the model earth is the same as that caused by melting an ice sheet of the same volume on the real earth.

Because the continental-scale models were not intended to model sea-level change in the near-field accurately, a static coastline was used when calculating the water load term. The continent on which the ice sheet sits is as large as the maximum extent of the ice sheet. For the regional ice sheet models, both static- and moving-coastline models were investigated.

Static coastline models

To accurately simulate the real course of events, the position of the model coastline should change with time. This is obvious from the observation that the ocean now covers the region adjacent to the ice sheet, which could not have been water-covered at the LGM if the ice sheet extended beyond its present limit. The effect of moving coastlines on sea-level change was discussed by Johnston (1993), who concluded that at far-field coastlines the error due to using a static coastline model could be significant with respect to the accuracy of observations. For a transgression of 500 km and 125 m ESL rise, the static coastline model underestimates the sea-level highstand at 6 ka by 1.4 m at the coast and by 1.8 m 150 km offshore (Johnston 1993).

In the near-field the situation is more complex, because isostatic rebound and ocean refilling are functions of the time-dependent regional

bathymetry. The water load may be positive or negative, depending on the relative magnitudes of the rebound and ocean refilling. In cases of high rebound rate and deep bathymetry, the water load will be negative, as the ocean shallows due to uplift. This is the case in the centres of former ice sheets, such as Hudson Bay in Canada and the Gulf of Bothnia in Europe. If sea-level rise due to ocean refilling is greater than the rebound, then the coastline may move landwards, causing a positive water load in the transgressed region. The North Sea and Irish Sea, which were exposed at the LGM, are examples of this situation. As rates of ocean refilling and rebound change, the sign of the water load may vary with time.

As Johnston (1993) points out, the predicted motion of coastlines in the near-field is dependent on the ice and earth models and the local bathymetry. He suggests that simple models of coastline movement in this zone are unlikely to yield results that are representative of models with realistic ice and ocean geometries. Nevertheless, by considering the probable evolution of the Antarctic coastline we can estimate the nature and magnitude of the errors which would result from using a model with a fixed coastline.

The Antarctic continental shelf is relatively deep (up to ~500 m), and was probably not above sea-level at the last glacial maximum, since global sea-levels were only ~130 m lower and the continental shelf was probably depressed by the increased ice load at the time. The present ice sheet is largely bounded by the ocean, and it is widely believed that the retreat of the Antarctic Ice Sheet was initiated and controlled by sea-level rise caused by melting of the northern hemisphere ice sheets (Alley and Whillans 1984, Denton and others 1986). Therefore, it is reasonable to assume that the edge of the ice sheet has formed the Antarctic coastline throughout the late Pleistocene and Holocene.

To approximate this, the sea-level predictions of two fixed-coastline models may be calculated - one with the coast at the initial position of the ice sheet margin; the other with the coast at the final position. The former model results in an under-estimation of the 6 ka highstand at the present coast, since it does not include the positive water load which occurs as the shoreline moves landward. The latter model, on the other hand, over-estimates the 6 ka highstand at the present coast, as it assumes a negative water load in the near-shore region due to the sea-level fall caused by isostatic uplift. The difference in the predicted 6 ka highstand at the present coast due to these models is ~2.6 m for a regional ice sheet model contributing 5 m ESL. Since the second iteration of the water load in this region is dominated by the effect of postglacial rebound, not ocean refilling, this difference probably does not need to be increased to include the effects of 125 m ESL rise.

An uncertainty of 2.6 m is significant compared with the accuracy to which the elevation of the 6 ka highstand is known at several locations. The best estimate of sea-level change using fixed-coastline models would probably be

the average of the two models described above, but it is clearly desirable to include the effects of a moving coastline when predicting sea-level change.

Moving coastline models

As described above, the edge of the Antarctic Ice Sheet probably extended beyond its present margin and formed the Antarctic coastline at the LGM and during deglaciation. The ice sheet was grounded below sea-level throughout this period, since the deglaciated region is presently covered by 200 - 500 m of water, even after the uplift due to the ice removal. The effective thickness of the ice load in this situation is called the grounded ice thickness, I_G, equal to

$$I_G = I - \frac{\rho_w}{\rho_i} .W \qquad (7.5)$$

where I is the total thickness of the ice, W is the water depth, and ρ_w and ρ_i are the densities of water and ice, respectively. If the ocean function (the region over which the water load is applied - see Chapter 5) is calculated from a model of the bedrock topography (Case (i) in Figure 7.7), the water load in the ice-covered region below sea-level, and hence the effective ice load, will change as sea-level changes. Alternatively, if the ocean function is defined so that it extends only to the edge of the ice sheet, regardless of water depth (Case (ii) in Figure 7.7), then the total ice thickness can be used to calculate the ice load, since it is equal to the sum of the grounded ice load and the water load:

$$\begin{aligned} \text{grounded ice load + water load} &= \rho_i.(I - \frac{\rho_w}{\rho_i} .W) + \rho_w .W \qquad (7.6) \\ &= \rho_i.I \\ &= \text{total ice load} \end{aligned}$$

The position of the ice sheet margin is defined in the ice model, whereas the water depth W at any time must be calculated at each step. Thus, it is easier to perform the calculation of the ice and water loads using a moving coastline (Case (ii)).

If we assume that the edge of the ice sheet was always grounded below sea-level, it is not necessary to model the bathymetry of the deglaciated region accurately, since the buoyancy and water-load terms in the ice-covered region are incorporated into the ice-load term, and the ocean function is restricted to the region offshore. The bathymetry model need only be deep enough in this region to ensure that it remains below sea-level at all times. The bathymetric models used in this chapter have a constant depth of 1000 m with a vertical boundary at 10°, so this condition is fulfilled.

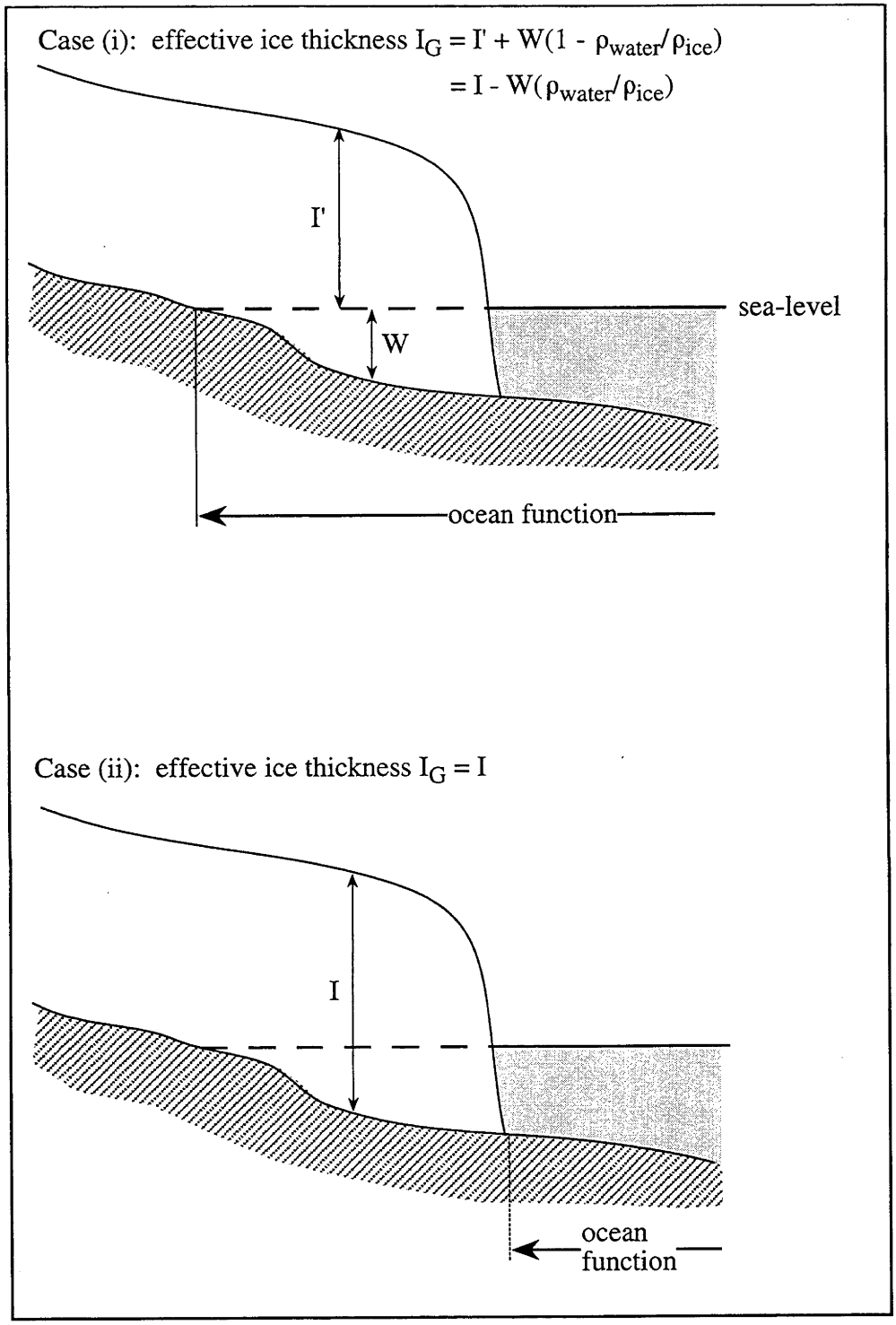

Figure 7.7 : Where an ice sheet is grounded below sea-level, the ice and water loads can be calculated in two ways. In case (i), the extent of the ocean function is determined by the bedrock bathymetry, and the ice load must be adjusted to allow for buoyancy. Alternatively, if the ocean function is determined by the edge of the ice sheet (case (ii)), then the load calculation is simpler, since the sum of the ice and water loads is equivalent to the total ice thickness (equation 7.6).

Iterations of the sea-level equation

As discussed in Chapter 5, the water load is dependent on the sea-level change, so the sea-level equation must be iterated in order to obtain an accurate sea-level prediction. In far-field oceanic regions, one iteration of the equation is sufficient, as the "eustatic" sea-level rise closely approximates the water load. At far-field coastlines, two iterations may be required, as the deformation caused by eustatic sea-level rise changes the water load slightly. In the near-field more iterations are required, as the large rebound due to the ice load changes the water load significantly. For these models, it was found that three iterations are sufficient for convergence within 0.1 m.

7.3.5 Earth model

Sea-level predictions are calculated using a range of earth models similar to that investigated by previous workers (Table 7.6). This range includes the optimum model of Nakada and Lambeck (1989), which was obtained using sea-level observations in the Australian region. This model has Hl = 100 km, $\eta_{um} = 2 \times 10^{20}$ Pa.s, and $\eta_{lm} = 10^{22}$ Pa.s, and is used as the standard model throughout this chapter. Only three-layer viscosity models are considered, but realistic elasticity and density profiles are used, taken from the PREM model (Dziewonski and Anderson 1981).

Table 7.6: The ranges of parameters used to describe the rheological models in this chapter.

Parameter	Range of values
lithospheric thickness (Hl)	50 - 200 km
upper mantle viscosity (η_{um})	10^{20} - 10^{21} Pa.s.
lower mantle viscosity (η_{lm})	10^{21} - 2×10^{22} Pa.s.

7.3.6 Estimation of total relative sea-level change

For comparison with observed sea-level records, we need to predict the total relative sea-level change, not just that due to the Antarctic Ice Sheet. Realistic models of the melting of the northern hemisphere ice sheets have been made (Peltier and Andrews 1976, Nakada and Lambeck 1988, Tushingham and Peltier 1992) and the predictions of these models for Antarctic sites are added to the predictions of the simple Antarctic models to estimate the total relative sea-level change. The ice model used in this work is model ARC3 of Nakada and Lambeck (1988), which includes the Laurentide, Fennoscandian and Barents-Kara ice sheets, and contributes 89 m ESL.

7.4 Results - Regional models

In this section, the general features of sea-level change predicted by the regional ice sheet models will be described, and their sensitivity to the various model parameters will be investigated. Comparison with sea-level observations will be made in the next section, and the optimum earth and ice models will be inferred.

There are seven parameters influencing the sea-level change predicted by these simple models. The rheological model of the Earth is described by three parameters: lithospheric thickness (H_l), and the viscosities of the upper and lower mantle (η_{um} and η_{lm}); and the ice model is described by four: the volume of melt (expressed in metres equivalent sea-level), the distribution of the ice removed (constant height or basal shear stress of the ice sheet), the time of cessation of melting of the regional ice, and the degree of late Holocene melting (both from regional and far-field sources).

7.4.1 Pattern of deformation

Because the distribution of ice removed from these regional models is at a maximum at the present edge of the ice sheet, the isostatic rebound is also greatest there (Figure 7.8). The pattern of deformation is dominated by the ice-load component, with RSL fall occurring over the entire continental shelf region. The ESL rise and the water-load component are indicated only by the small landward migration of the "hinge point".

Approximately 5 degrees to either side of the centre of the removed ice, a rise in relative sea-level is caused by the collapse of the "peripheral bulge" due to mantle flow into the uplifting region (see chapter 3.1). This "bulge" is not necessarily a topographic feature, but is deformation of the sea floor due to the regional component of the ice load. Nevertheless, the removal of ice will result in crustal subsidence in peripheral regions. The predicted subsidence of the interior of the ice sheet is reinforced by the removal of ice from the opposite coast of the regional model. Since the models simulate a continent with a radius of 10 degrees, and the Antarctic continent has an approximate radius of 20 degrees, the opposite coasts are actually twice as far apart as modelled and this reinforcement would not actually occur (Figure 7.9). Thus, the amount of subsidence expected in the interior of the real ice sheet would be less than that predicted by these models (~25 m for the model in Figure 7.8). This subsidence is too small to be observable on its own, and would be dominated by local changes in ice thickness. This is discussed in more detail later in this chapter.

7.4.2 Shape of the RSL curve

The components of the relative sea-level curve produced by the regional models are shown in Figure 7.10. The regional contribution is dominated by the uplift due to ice removal. This uplift lags the removal of ice, and continues after melting ceases with a decaying exponential pattern. The far-

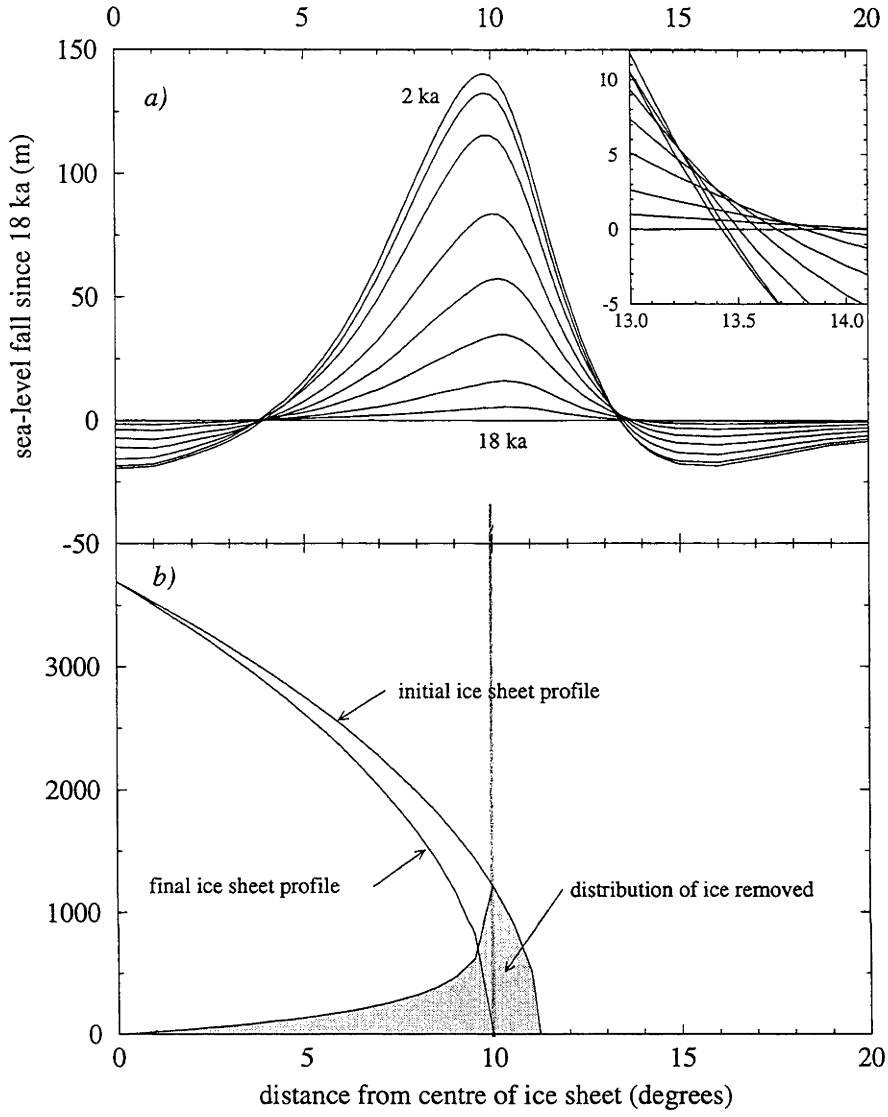

Figure 7.8 : a) the regional contribution to sea-level change as a function of time and distance from the centre of the ice sheet compared with b) the ice load. Due to the asymmetry of the ice load, the maximum rebound is slightly displaced from the location of maximum ice thickness change. A "peripheral" bulge collapses in the centre of the ice sheet as well as beyond its margin.

field contribution is composed of the effects due to the combined northern hemisphere ice sheets, and distant (non-regional) Antarctic ice. The sea-level rise due to ocean refilling makes up most of the far-field contribution, but after melting has ceased the coastal uplift due to the water load on the continental shelf is apparent.

In the example shown in Figure 7.10, the gradients of the regional and far-field components are almost equal, so that sea-level remains almost constant until 6 ka, when the two components reinforce each other and sea-level falls monotonically to the present level. For the period 18 ka - 6 ka the

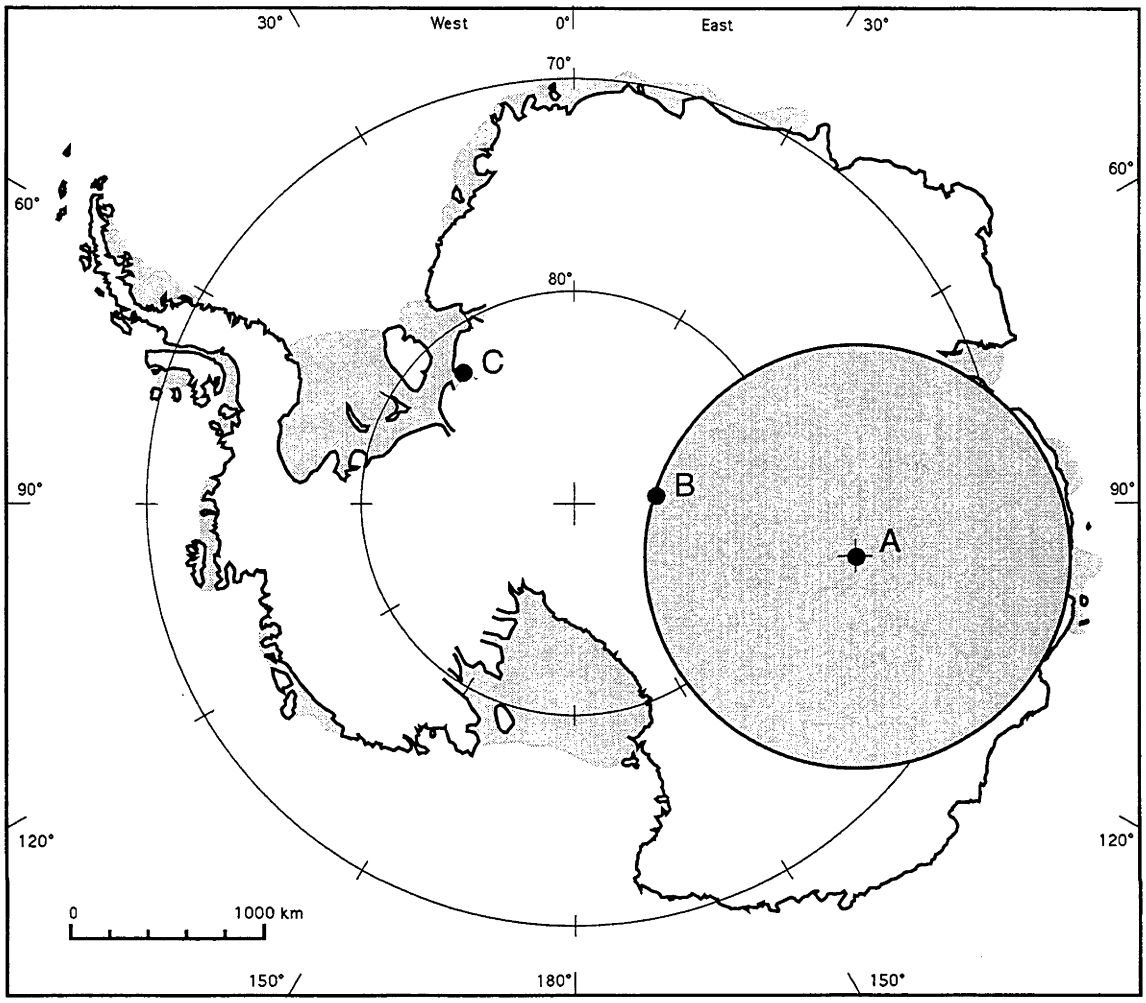

Figure 7.9 : The regional models (small circle) are approximately half the width of the actual Antarctic Ice Sheet. The predicted deformation in the interior of the ice sheet (point A) is therefore not realistic, since the ice load of the opposite "coast" (point B) of the regional model is much closer than is actually the case (point C).

shape of the total curve depends on the relative magnitudes and rates of the two components. This relationship is sensitive to several model parameters, as will be discussed below. In contrast, the form of the predicted sea-level curve since 6 ka is relatively insensitive to model parameters, with all models predict falling sea-level over this period. The sea-level highstand (and in some cases a sea-level maximum) at 6 ka is common to all predictions, and is also within the period for which sea-level observations are most often available. Its magnitude is therefore an important parameter in comparing various model predictions and sea-level observations.

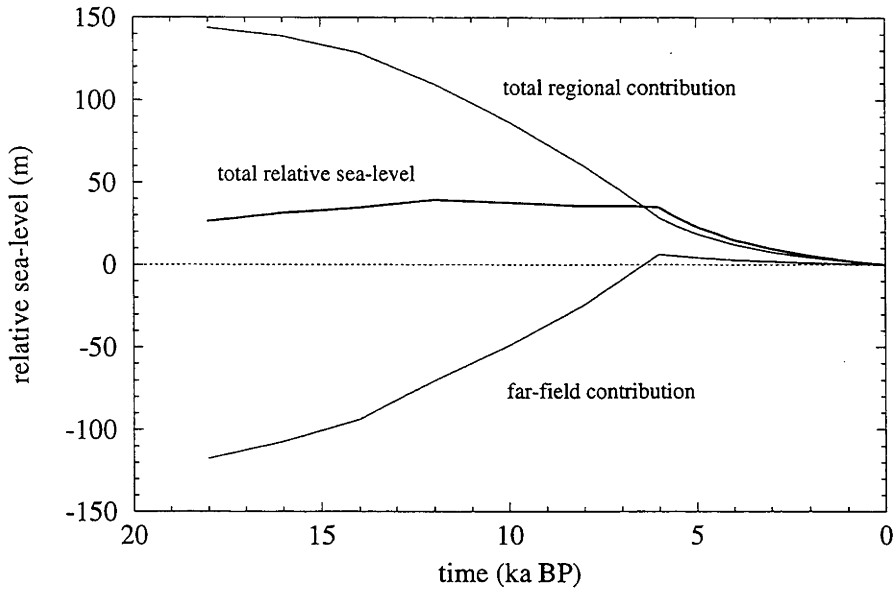

Figure 7.10 : The relative sea-level history of a site on the present ice sheet margin. The regional and far-field components are similar in magnitude.

7.4.3 ESL model

Three models of equivalent sea-level change were considered in conjunction with the regional ice load models: curves 6, 6a, and 10, as shown in Table 7.2 and Figure 7.6. In addition, the far-field component was modelled both with and without late Holocene melting. These combinations thus result in six possible melting models, whose effect on sea-level change at the edge of the ice sheet is shown in Figure 7.11 for the standard earth model.

Models 6 and 6a produce similar sea-level predictions, although in model 6a the reduction in melting rate between 8 ka and 6 ka contributes to the occurrence of a short-duration sea-level maximum at 6 ka. Continued melting throughout the late Holocene in model 6a also makes the ice-load component of sea-level change larger than that of the other models during this time (Figure 7.12), which contributes to the 6 ka highstand. In the near-field, this contribution is larger than the fall in relative sea-level caused by the addition of meltwater since that time, so the 6 ka highstand predicted by the 6a melting model is larger than that predicted by model 6.

Model 10 produces significantly different sea-level predictions: because melting ceases earlier, the rate of rebound becomes lower than the rate of ocean-refilling ("eustatic" sea-level rise) at around 8 ka, resulting in a prominent sea-level maximum at 6 ka, when both the regional and far-field components of sea-level change become negative. Other effects of the earlier cessation of melting which may be observable are a higher predicted RSL at the LGM compared to the predictions of models 6 and 6a (because the

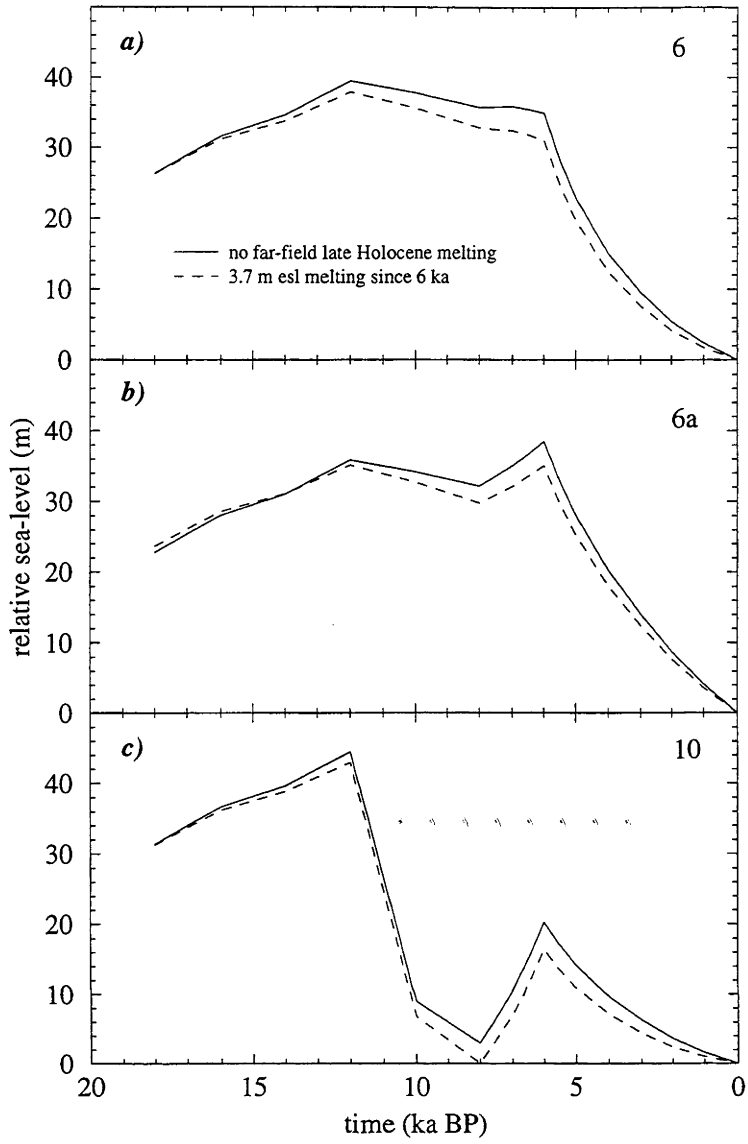

Figure 7.11 : The effect on the predicted relative sea-level history at a coastal site of 3.7 m of eustatic sea-level rise since 6 ka. Graph a: melting model 6. Graph b: melting model 6a. Graph c: melting model 10. Solid line: standard esl model (no melting since 6 ka). Dashed line: 3.7 m esl melting since 6 ka.

model has accomplished more rebound), and a lower 6 ka highstand (because the recent rate of rebound is lower, as the model is closer to isostatic equilibrium).

Including 3.7 m ESL of late Holocene melting in the far-field component has a small but significant effect on the relative sea-level prediction. There is very little difference in the predicted RSL at the start of melting (Figure 7.11), since both models contribute the same total meltwater volume. As melting proceeds, the late-melting model predicts slightly lower sea-levels, because the rate of far-field melting throughout this period is slower. When the standard model has completed melting at 6 ka, the late-melting model predicts sea-levels 3.7 m lower - the volume of far-field ice remaining to melt. Throughout the late Holocene, this ice melts and contributes to sea-

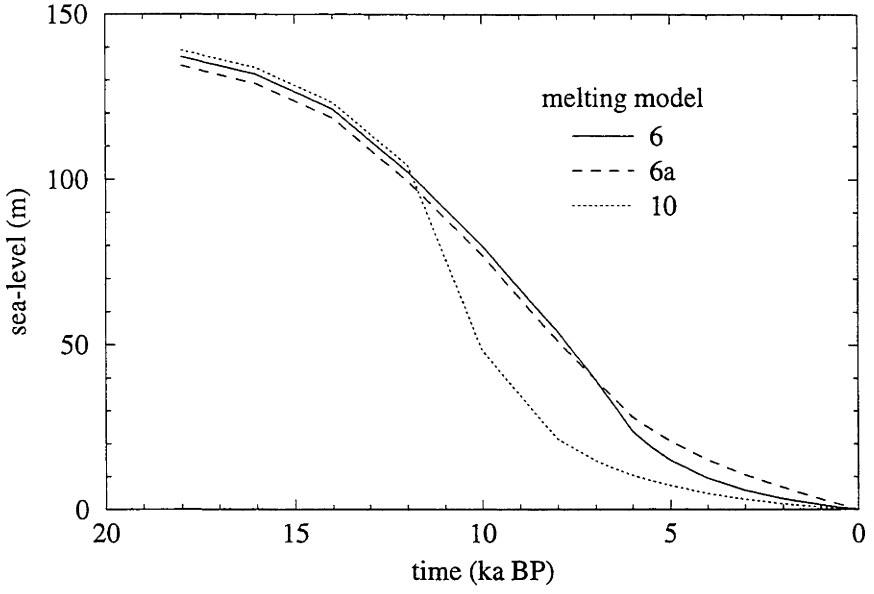

Figure 7.12 : Ice load component of sea-level change at a coastal site predicted by the three regional ice-melting curves. Constant-*h* model, standard earth rheology model.

level rise, reducing the effect of RSL fall due to isostatic uplift. The inclusion of late Holocene far-field melting consistently predicts a 6 ka highstand 3.7 m lower than the standard model. This is a significant effect, since the magnitude of the 6 ka highstand is also dependent on the magnitude and melting curve of the regional ice model. Apart from this feature, the predicted sea-level curves are otherwise very similar. Comparison with near-field sea-level observations alone, therefore, cannot determine whether late melting did occur. If, however, such melting is indicated from far-field observations (see Chapter 5), then the other model parameters will have to be adjusted in order to obtain the same 6 ka highstand.

7.4.4 Ice load distribution

At the present-day margin of the regional model ice sheet (10 degrees from the centre), where the sea-level curve is calculated, the difference between ice models of constant height (constant *h*) and models of constant basal shear stress (constant *b*) is essentially a difference in the height of the former ice sheet at that position. Because the constant-*b* models remove more ice from the interior of the ice sheet, the height of ice removed from the coast is smaller than for constant-*h* models of the same volume change (Figure 7.5). Consequently, the RSL curves predicted by the constant-*b* models are influenced more by the far-field component (Figure 7.10 shows an example of the regional and far-field components). This may result in a local maximum (crest) in the curve at 6 ka when the constant-*h* model has none (Figure 7.13 a), and a sharper crest when both curves exhibit one (Figure 7.13 b and c). The difference between the predictions of the constant-*b* and constant-*h* models decreases towards the present: since sea-level observations are mostly limited to the last 6 ka, it will be difficult to

determine which model is more appropriate. If sea-level measurements from the early post-glacial period can be made, perhaps from sediment cores on the continental shelf, we may be able to conclude from further modelling whether ice thicknesses in the Antarctic interior decreased or not. Currently, ice-core studies indicate that ice thickness in the interior has not changed significantly (Chapter 4), so the constant-*h* models may be considered more appropriate. These have the advantage that, as the thickness of ice removed decreases to zero inland, the results from the small ice sheets in these models can be more easily applied to the margin of a larger ice sheet without requiring elevation change in the interior.

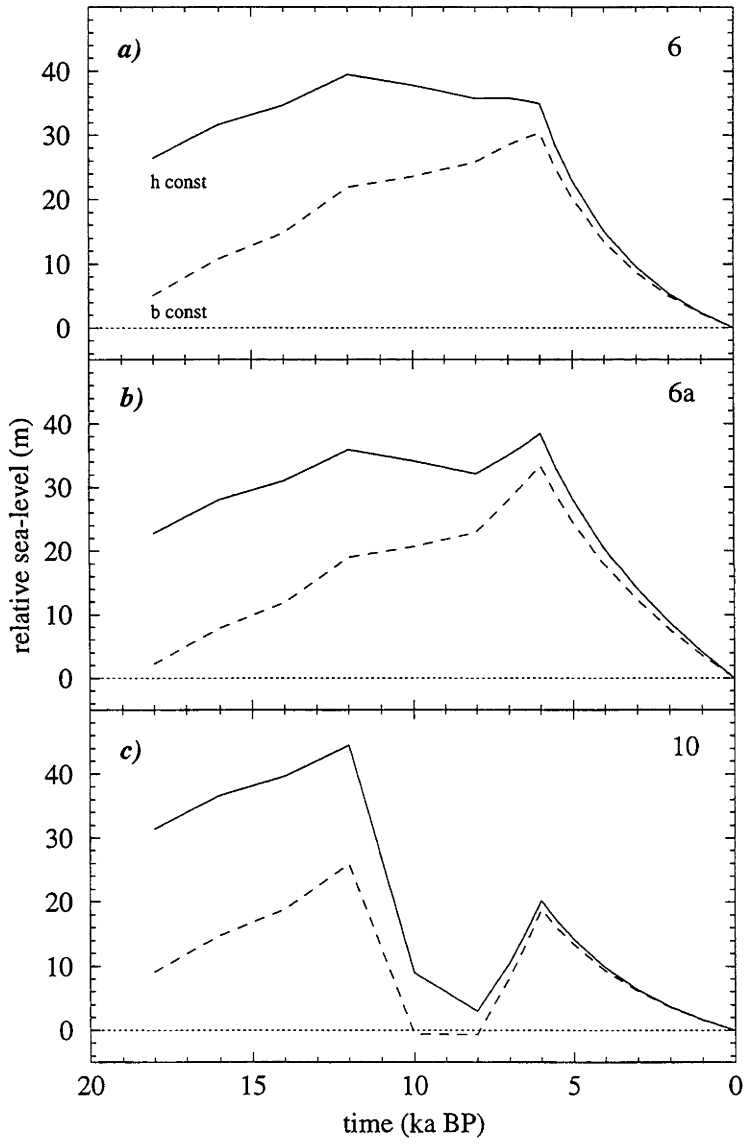

Figure 7.13 : Predicted relative sea-level curves at a coastal site for constant-h and constant-b ice sheets and three melting histories. Graph a: melting model 6. Graph b: melting model 6a. Graph c: melting model 10. Solid line: constant-height model. Dashed line: constant-b model.

7.4.5 Ice volume

The regional contribution to sea-level change is almost directly proportional to the ice volume removed from nearby. This linear relationship is due to the similarity in the ice load distribution over the range of ice models used, and the linear rheology assumed. When combined with the far-field contribution, these models produce RSL curves (Figure 7.14) for which both the sea-level at the LGM and the 6 ka highstand are very sensitive to the regional ice volume. For the models in which the regional melting ceases at 10 ka (Figure 7.14 c), the magnitude of the sea-level "trough" preceding the 6 ka highstand is also very dependent on the regional ice volume. This feature may be useful in the future, if sea-level observations can be extended beyond 10 ka.

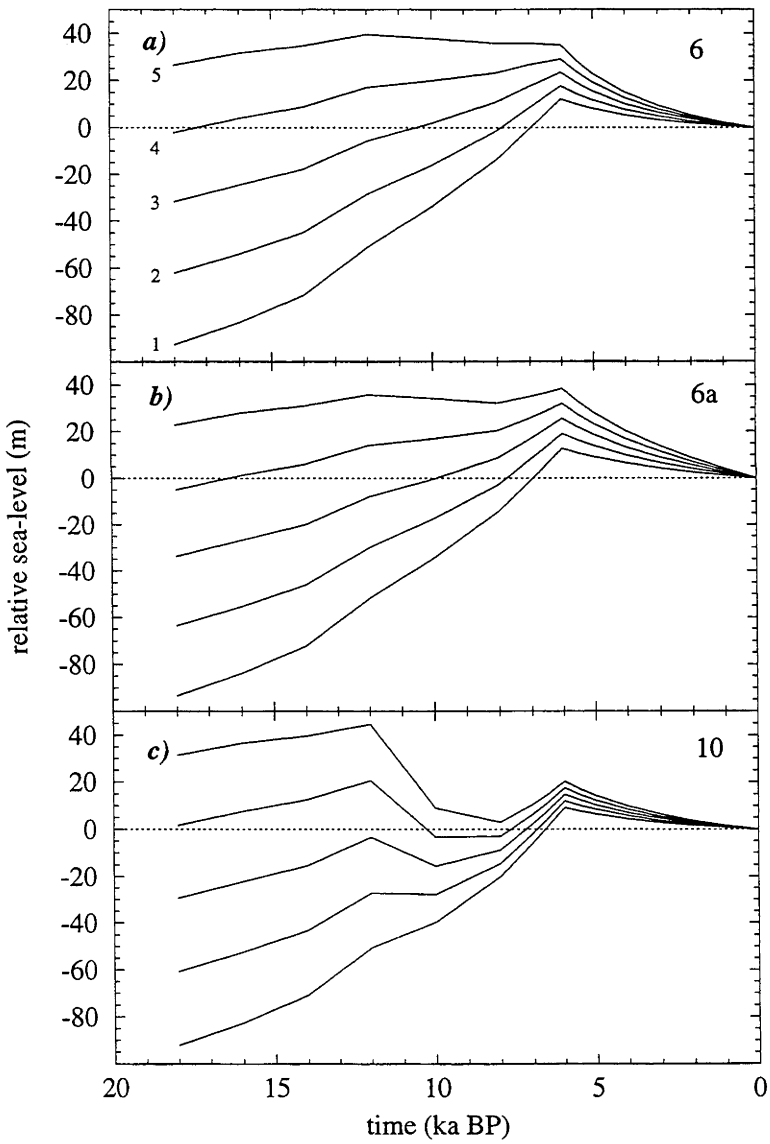

Figure 7.14 : The effect on the predicted relative sea-level history at a coastal site of the volume of the regional ice sheet model. Graph a: melting model 6. Graph b: melting model 6a. Graph c: melting model 10. In graph a) the curves are annotated with the volume contribution (in m esl) of the corresponding ice model.

7.4.6 Lithospheric thickness

In the region of maximum ice load (10 degrees from the centre), the sensitivity of the RSL curve to lithospheric thickness (Figure 7.15 A) is similar in form and magnitude to the dependence on regional ice volume, discussed above. A lithosphere 50 km thick distributes the load less than thicker lithospheres would, so the isostatic response at the centre of the load is greater, although over a narrower region (Figure 7.15 B). Although the sensitivity of the sea-level curve to lithospheric thickness and ice volume are similar in the region of maximum load (Figures 7.14 and 7.15 A), the width of the deformed region is dependent only on the thickness of the

A)

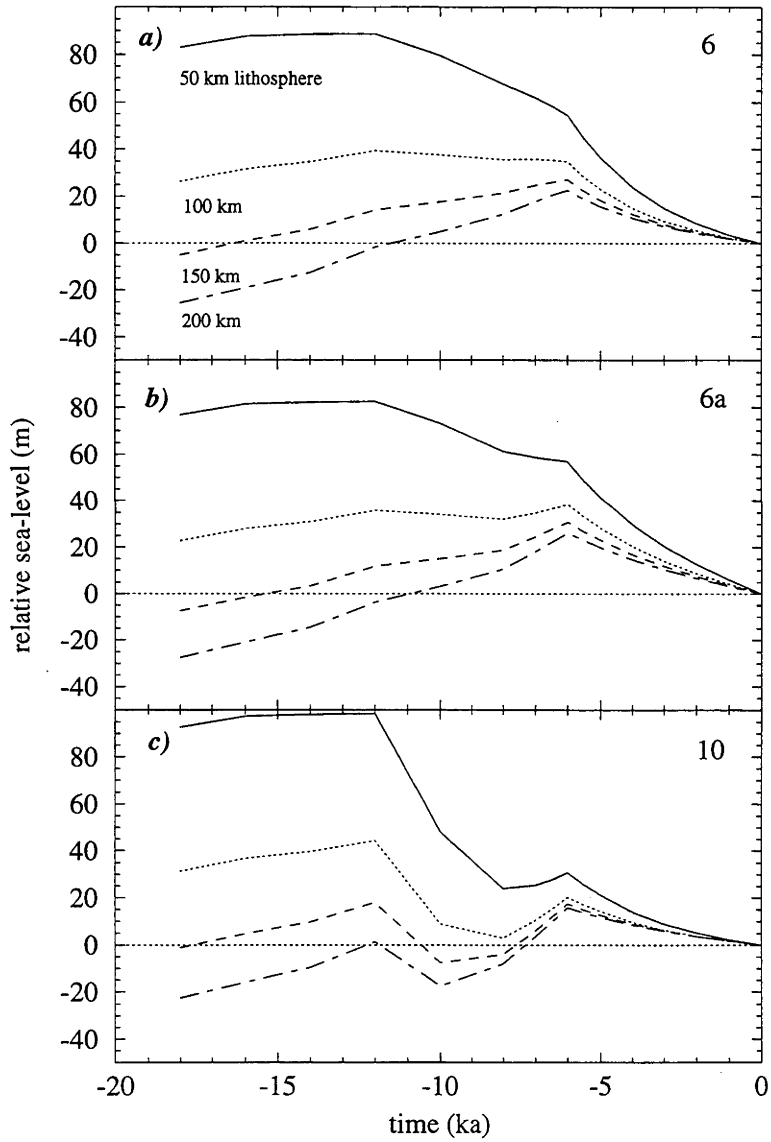

Figure 7.15 : The effect on the predicted relative sea-level history at a coastal site of lithospheric thickness. A: Relative sea-level histories. B: regional component of relative sea-level at 6 ka as a function of distance from the centre of the ice sheet, showing that thickher lithospheres produce a wider zone of rebound of lower amplitude. Graph a: melting model 6. Graph b: melting model 6a. Graph c: melting model 10.

lithosphere. This means that if additional observations are available from sites away from the maximum load, the ice volume and lithospheric thickness may be separately constrained (all other parameters being held constant), as in the work of Lambeck (1993b). For example, an observed 6 ka highstand at the centre of the load could be explained by either a thin lithosphere and small ice volume change, or by a thicker lithosphere and larger volume. A sea-level observation at the same time from another site within the same region but at a different distance from the ice sheet would constrain the spatial gradient uplift, and allow us to determine the optimum thickness and volume values.

B)

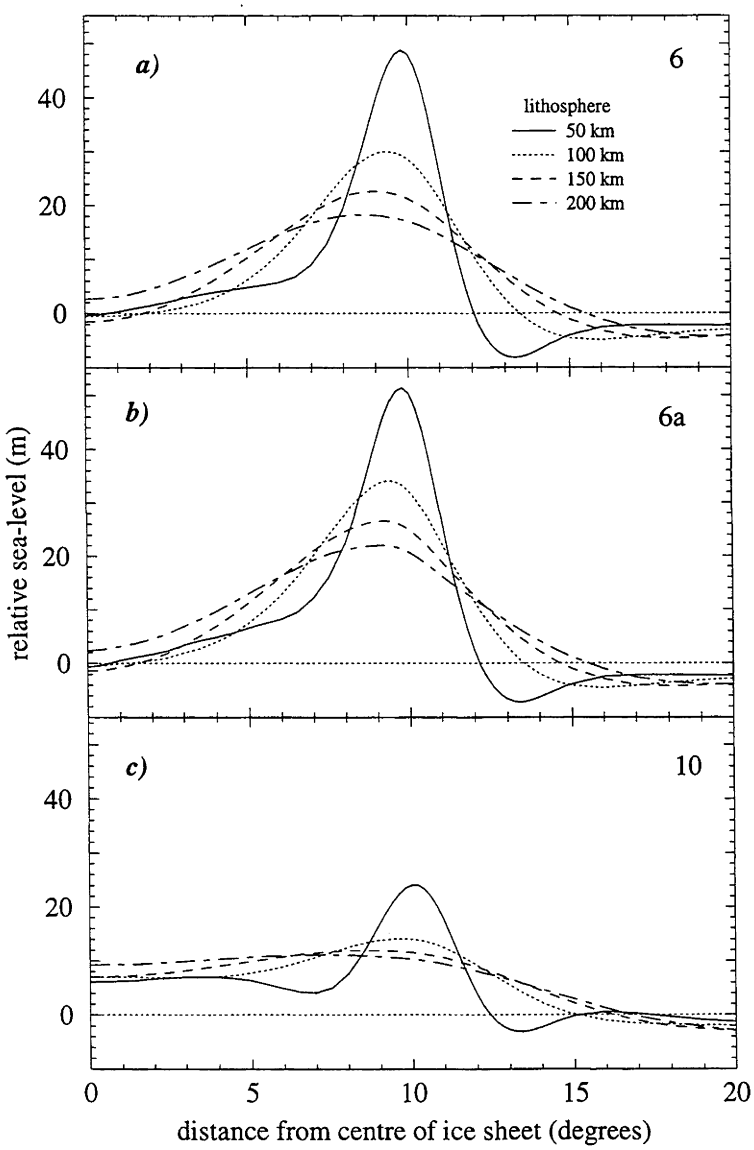

7.4.7 Upper mantle viscosity

The viscosity of the upper mantle determines the time lag between the changing surface loads and the viscous response, for short to intermediate wavelength loads. This time lag is evident in the resulting sea-level curves, because the postglacial period is long enough that the less viscous (ie lower viscosity) models can almost complete their isostatic adjustment, whereas the more viscous models cannot. This has two effects: the more viscous models do not achieve as much compensation as the less viscous models over this time period; and the rates of deformation of the different models differ through time. Because less compensation has been achieved so far,

A)

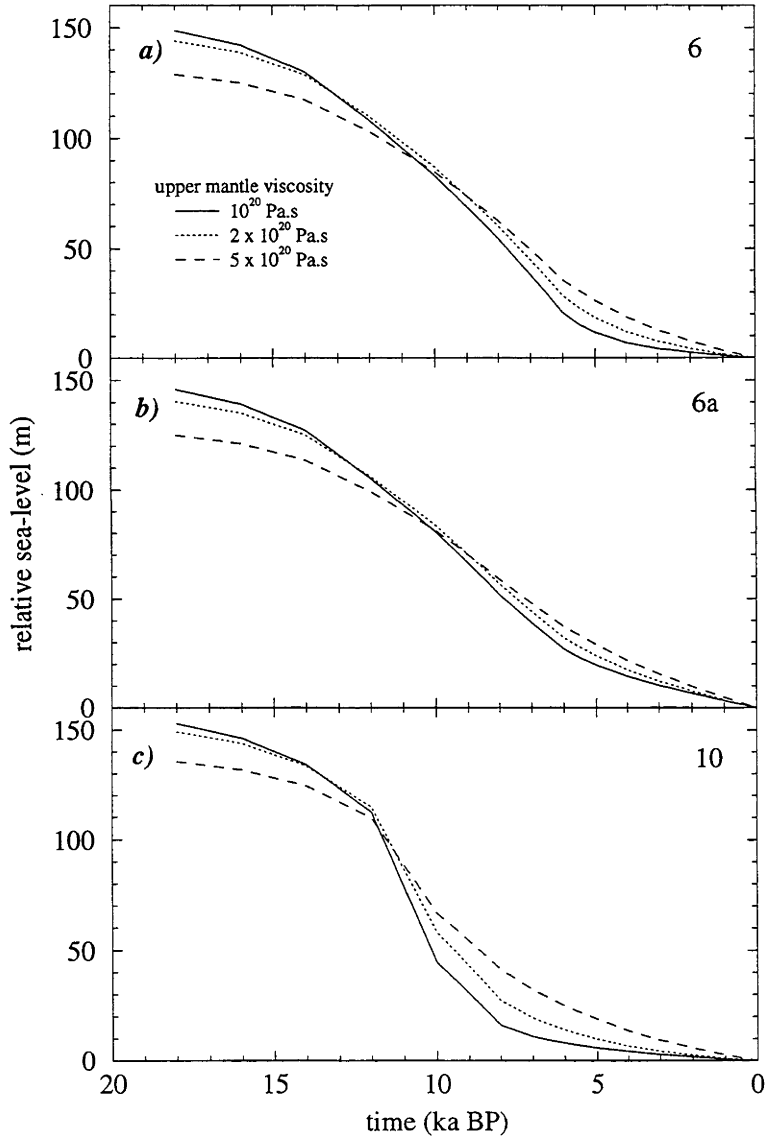

Figure 7.16 : The effect on the predicted relative sea-level history at a coastal site of upper mantle viscosity. The viscosity of the upper mantle in the standard model is 2 x 10^{20} Pa.s. A: regional component only; B: relative sea-level.

the models with a more viscous upper mantle predict lower relative sea-level at the LGM than the other models (Figures 7.16 A and B). And because the more viscous models are still rebounding significantly while other models have almost achieved equilibrium, the rate of rebound in the late Holocene is greater for the more viscous models, and hence the 6 ka highstand is greater (Figures 7.16 B). Clearly sea-level change is sensitively dependent on the viscosity of the upper mantle, and this dependence will be used below to constrain this aspect of the Earth's rheology.

B)

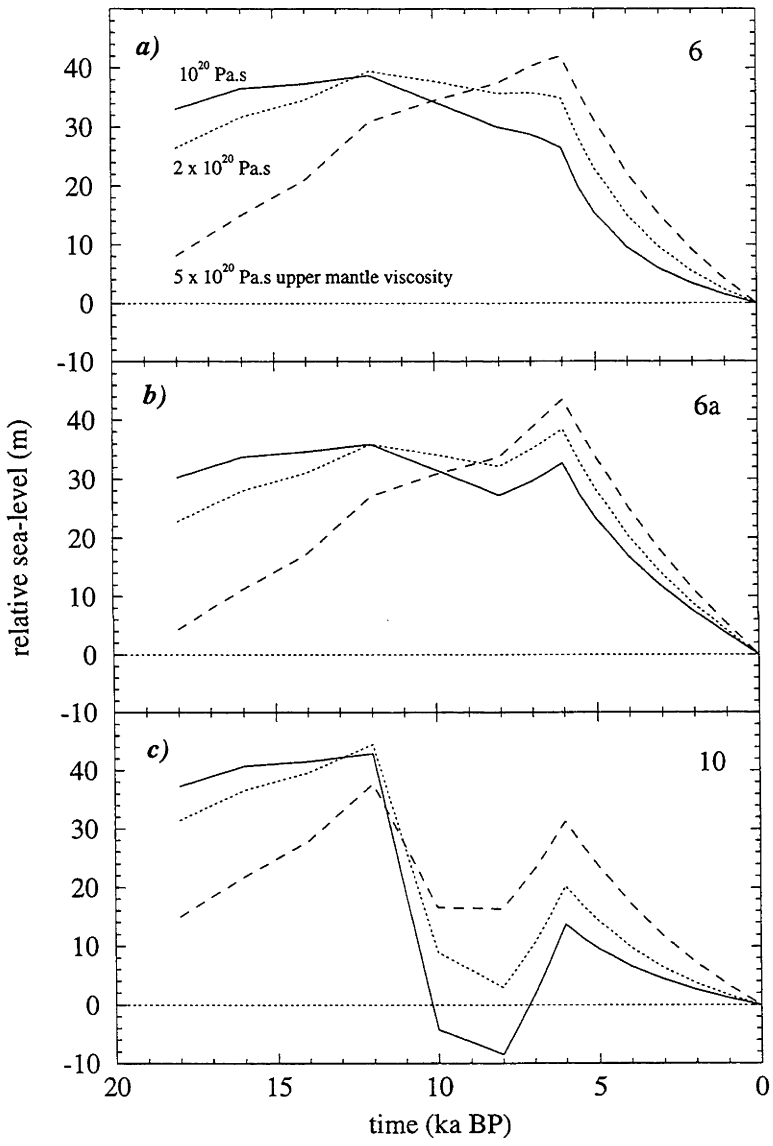

7.4.8 Lower Mantle Viscosity

The lower mantle is not significantly deformed by loads the size of these regional models, so changes in its viscosity have little effect on the resulting sea-level changes (Figure 7.17). Models with a more viscous lower mantle deform somewhat less than less viscous models on deglacial time-scales, but the difference in the last 6 kyr, the time period for which most observational constraints exist, is insignificant. The effect of the water load, which is much broader than the ice load, is more sensitive to the lower mantle viscosity, but is much smaller in magnitude in the near-field, and so does not greatly influence the predicted sea-level change. Only if we have high accuracy observations from localities with markedly different coastal geometries will it be possible to constrain the viscosity of the lower mantle.

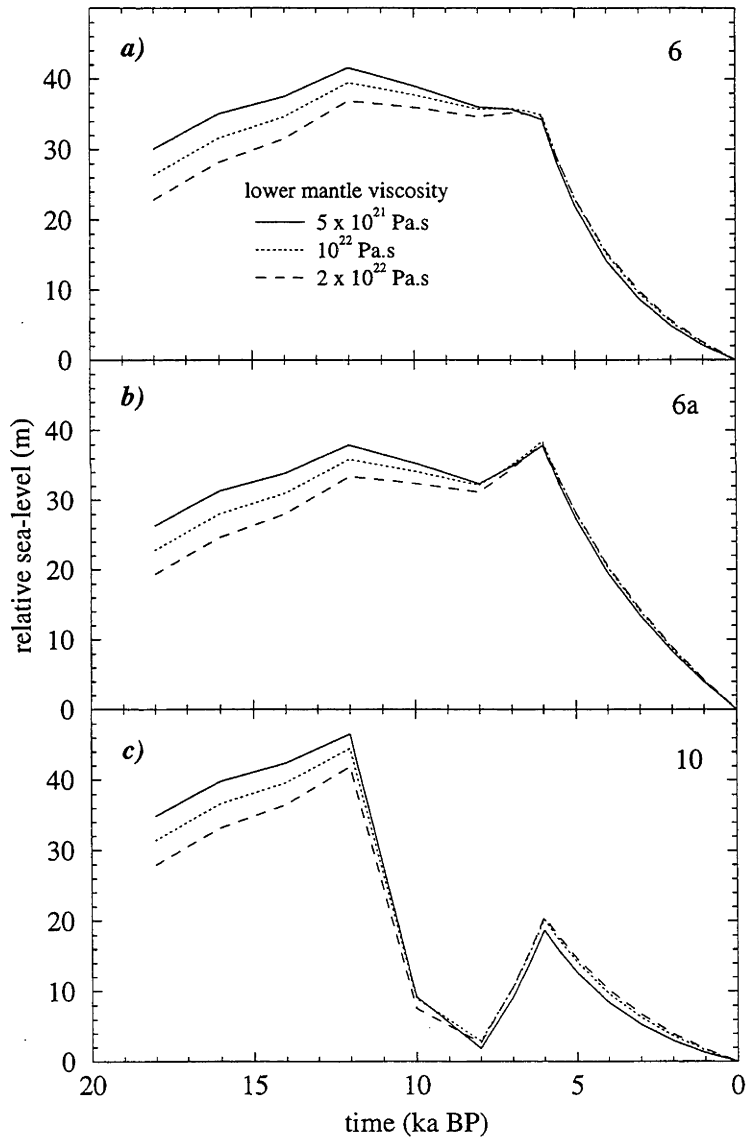

Figure 7.17 : The effect on the predicted relative sea-level history at a coastal site of lower mantle viscosity.

For the range of models depicted in Figure 7.17, the difference in the far-field contribution at 18 ka is ~1.2 m , and at 6 ka is only ~0.7 m. The regional models, in association with available observations, are unable to constrain the viscosity of the lower mantle.

7.4.9 Time extent of models

The models discussed so far present only the changes in sea-level due to deglaciation. These simulate the actual postglacial changes only if the earth was in equilibrium at the LGM. To test the consequences of this assumption, models were constructed with the assumption of isostatic equilibrium at the end of the last interglacial period, at ~120 ka. Even if this assumption is incorrect, after 100 kyr the contribution of the initial disequilibrium to present sea-level change would be negligible, so this model effectively tests the assumption of equilibrium at the LGM. The ice sheet model was constructed in the same manner as the models of deglaciation, using a simplified ice-volume function based on the marine oxygen-isotope curve (Chappell and Shackleton 1986). This ice volume function represents the growth of the ice sheet to its LGM state. It was assumed that the Antarctic Ice Sheet changed volume in proportion to the changes in global ice volume.

It is found that using this long-term model does not significantly change the sea-level predictions for the deglacial period. This is largely because the growth of the ice sheet to its LGM state was slow (~100 kyr) compared with the response time of the Earth. This allowed a state of isostatic near-equilibrium to be maintained. In contrast, deglaciation was relatively rapid (~10 kyr), and the Earth has not yet attained isostatic equilibrium after these changes. These tests indicate that it is sufficient to only model changes in the Antarctic Ice Sheet since the LGM.

7.4.10 Summary

With the exception of lower mantle viscosity, the parameters of the regional models have a significant effect on the relative sea-level curves. The influence of each parameter on two aspects of the sea-level curve is summarised in Table 7.7. Using observations from a limited time period and from only one site per region, trade-offs between the various parameters are able to produce very similar sea-level curves from a range of models. Estimating the optimum combination of ice and earth models will be discussed later in this section.

While all models predict a sea-level highstand (sea-level higher than present) at 6 ka, a local maximum at this time is not always evident. Identification of a crest in the sea-level record, as in the Vestfold Hills (Chapter 3), is thus a very useful feature for constraining the ice and earth model parameters.

Table 7.7: Effect on observable features of the RSL curve of increasing the value of the model parameters.

parameter	RSL feature	
	RSL at 18 ka	6 ka highstand
Ice model		
ice volume	increases	increases
late melting	~ no change	decreases
age of melt cessation	increases	decreases
Earth model		
H_l	decreases	decreases
η_{um}	decreases	increases
η_{lm}	decreases	~ no change

7.5 Continental models

The continental-scale models are not intended to model accurately the changes in ice distribution at the margin of the ice sheet, so the sea-level predictions at marginal sites (corresponding to the sites from which observed sea-level records have been obtained) are probably not useful. Rather, the sea-level predictions of these models at locations far from the main ice sheet changes are investigated.

7.5.1 Elevation change inland

One aspect of the Antarctic Ice Sheet history which the regional-scale ice sheets cannot adequately model is the change in elevation in the interior of the ice sheet. The elevation change at the centre of the ice sheet is simply the combination of the relative sea-level change and the ice thickness change, and can be discussed in the same terms. The equation describing elevation change, analogous to the sea-level equation (Chapter 5) is:

$$\Delta\zeta(\lambda,t) = \Delta\zeta^{e}(t) + \Delta\zeta^{i}(\lambda,t) + \Delta\zeta^{w}(\lambda,t) + \Delta\zeta^{h}(\lambda,t) \qquad (7.7)$$

where $\Delta\zeta(\lambda,t)$ is the change in elevation at a given colatitude λ and time t relative to the present; $\Delta\zeta^{e}(t)$, $\Delta\zeta^{i}(\lambda,t)$, and $\Delta\zeta^{w}(\lambda,t)$ are the sea-level components as described in Chapter 5; and $\Delta\zeta^{h}(\lambda,t)$ is the change in thickness of the ice sheet, measured with respect to bedrock.

The equivalent sea-level term, $\Delta\zeta^{e}(t)$, is the same at all locations and does not depend on the distribution of the ice load. For sites in the interior of the ice sheet, far from the coast, the water-load term $\Delta\zeta^{w}(\lambda,t)$, is positive and is also independent of the ice distribution. These two terms depend only on the volume increase of the oceans. Using the total ESL rise ($\Delta\zeta^{e}(t)$) of ~125 m, $\Delta\zeta^{w}(\lambda=0,t=18$ ka) is found to be ~27 m, by scaling the predictions of the continental-scale models. Thus the surface of the ice sheet would experience a lowering in elevation with respect to sea-level of ~100 m, without considering the effects of any changes in ice sheet thickness. The remaining terms, $\Delta\zeta^{i}(\lambda,t)$ and $\Delta\zeta^{h}(\lambda,t)$, depend on the distribution of the ice load, and analysing their effects on elevation change allows us to use the observed elevation history (see Chapter 4) to constrain the former ice sheet configuration.

In general, if the thickness of the ice sheet is reduced, the isostatic rebound will result in the ice sheet surface being raised by a smaller amount, in proportion to the ratio of the densities of ice and the mantle. This would be the case for a wide load of constant thickness. For the ice sheets modelled here, which are circular and of varying thickness change, the result is more complex, since the ice thickness term at a given point, $\Delta\zeta^{h}$, is equal to the local ice thickness change, whereas the ice load term, $\Delta\zeta^{i}$, depends on the change in ice thickness at distant sites. To estimate the influence on

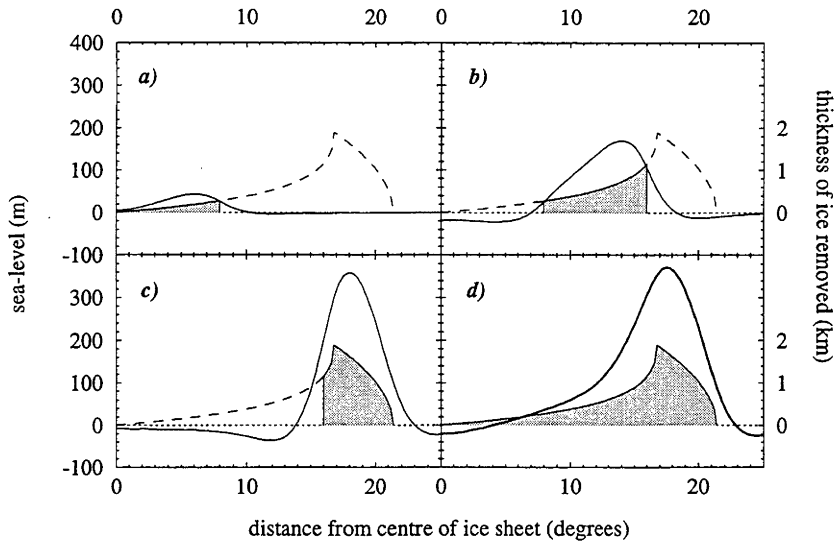

Figure 7.18 : The effect of a changing ice load can be divided into components due to the removal of annular rings of ice. Each annulus produces rebound locally, but peripheral subsidence in the regions of the other annuli. Graph d) shows the sum of the components shown in a), b) and c).

rebound of the radial distribution of ice, the change in ice load can be divided into three components according to their distance from the centre - a central disc surrounded by two annular rings - and the isostatic response to each component calculated separately (Figure 7.18).

For a parabolic ice sheet whose maximum thickness remains constant during melting, the thickness of ice removed, $\Delta\zeta^h$, is zero at the centre of the ice sheet, increases slowly to a maximum at the final radius of the ice sheet, and drops rapidly from there, following the original profile of the ice surface (Figure 7.5). At the centre of the ice sheet, the response to the removal of the small central load is one of minor uplift. Much more ice is removed from the outer rings, which causes significant uplift regionally, but their distance from the centre of the ice sheet means that this point lies on the flank of the "peripheral bulge" of these loads, and so subsidence, rather than uplift, is the result when the load is removed. For constant-height models, the subsidence due to the outer loads dominates the uplift due to the small central load. Since there is no change in the ice thickness at the centre of the ice sheet, this subsidence translates directly to a lowering of the surface. Two constant-height models are examined here: one with a volume change of 37 m ESL and the other of 5 m ESL (models 4h and 7h respectively - see table 7.5). Assuming that the constant-h model is valid, these two models probably bound the actual situation for the Antarctic Ice Sheet. Based on the ice sheet reconstructions reviewed in Chapter 4, model 7h probably produces a reasonable description of the ice sheet retreat around most of the ice sheet margin, whereas 4h represents the larger degree of deglaciation which may have occurred in the Ross and Ronne-Filchner Ice Shelves. The elevation change term $\Delta\zeta^i(\lambda=0,t=18$ ka) predicted by these

models therefore ranges between -4 and -20 m. The total elevation change predicted by these models is presented in Table 7.8.

Treated in the same way, models 4f3 and 7f3 (see Table 7.5) reveal more about the predicted elevation changes in the centre of the ice sheet. These models are constrained by a prescribed margin retreat history (see previous section and Table 7.5 for details), and the distribution of ice removed is determined by the ESL curve of each model and the requirement that the ice sheet remains parabolic in cross section. Because of the difference in melt volume between continental ice models 4 and 7, these melting models result in strikingly different distributions of removed ice (Figure 7.19 d). In the case of model 4f3, the effect of the prescribed margin retreat is insignificant with respect to that of the total melt volume, as most of the ice is removed from the interior. The removal of ~1100 m ($\Delta\zeta^h(\lambda=0,t=18$ ka)) from the central disc causes ~280 m ($\Delta\zeta^i(\lambda=0,t=18$ ka)) of rebound after 18,000 years, which is partly offset by subsidence caused by the removal of a similar thickness of ice from the outer parts of the ice sheet. These figures indicate that isostatic compensation is about 90% complete in this case, since

$$\Delta\zeta^i(\lambda=0,t=18 \text{ ka}) \cdot \rho_{mantle} \approx 90\% \cdot \Delta\zeta^h(\lambda=0,t=18 \text{ ka}) \cdot \rho_{ice}$$

When the contributions of the outer components of the ice sheet are included, the total rebound is about 245 m. The removal of ~1100 m of ice from the central portion of the ice sheet thus results in a surface lowering of ~955 m (see Table 7.8). It should be noted that the peripheral subsidence due to the middle annulus is larger in the interior of the ice sheet than on the outer side, because it is reinforced by the subsidence caused by the other side of the annulus.

In contrast to this, the prescribed margin retreat of 150 km imposed on the initial ice sheet would cause an ice volume reduction larger than the 5 m of ESL model 7. To compensate for this, model 7f3 requires a thickening of ~155 m in the interior of the ice sheet (Figure 7.19 h) in order to maintain the desired total ice volume change. In this situation, the addition of new ice in the centre and the removal of ice from the margin both contribute to isostatic subsidence in the centre of the ice sheet. The total subsidence is ~37 m, so the total elevation change in the centre of the ice sheet due to this model would be an increase of ~20 m (=155-37-126+27).

The third class of models, those with a constant aspect ratio and basal shear stress, produce predictions which lie between those of the other two melting styles. Surface lowering is predicted at the centre of the ice sheet (Table 7.8), as ice is removed from that location for both ESL volumes considered here.

The models investigated here show that the elevation change of the ice sheet surface is dominated by two terms - the equivalent sea-level rise, $\Delta\zeta^e$, and the change in ice sheet thickness, $\Delta\zeta^h$. The water load and ice load

terms, $\Delta\zeta^w$ and $\Delta\zeta^i$, are smaller and generally act to reduce the effects of the larger terms.

Table 7.8: Surface elevation changes (in metres) since 18 ka at the centre of the ice sheet for some continental-scale models. $\Delta\zeta_{total}$ is the total predicted elevation change, and $\Delta\zeta^e$, $\Delta\zeta^h$, $\Delta\zeta^w$ and $\Delta\zeta^i$ are the equivalent sea-level, ice thickness change, water load, and ice load terms respectively. $\Delta\zeta^e$ and $\Delta\zeta^w$ include the contributions from all ice sheets, assuming a total postglacial ESL rise of 126 m.

	4h	4b	4f3	7h	7b	7f3
$\Delta\zeta h$	0	-377	-1191	0	-44	+157
$\Delta\zeta i$	-20	65	243	-4	8	-37
$\Delta\zeta e$	-126	-126	-126	-126	-126	-126
$\Delta\zeta w$	27	27	27	27	27	27
$\Delta\zeta_{total}$	-119	-411	-1047	-103	-135	+21

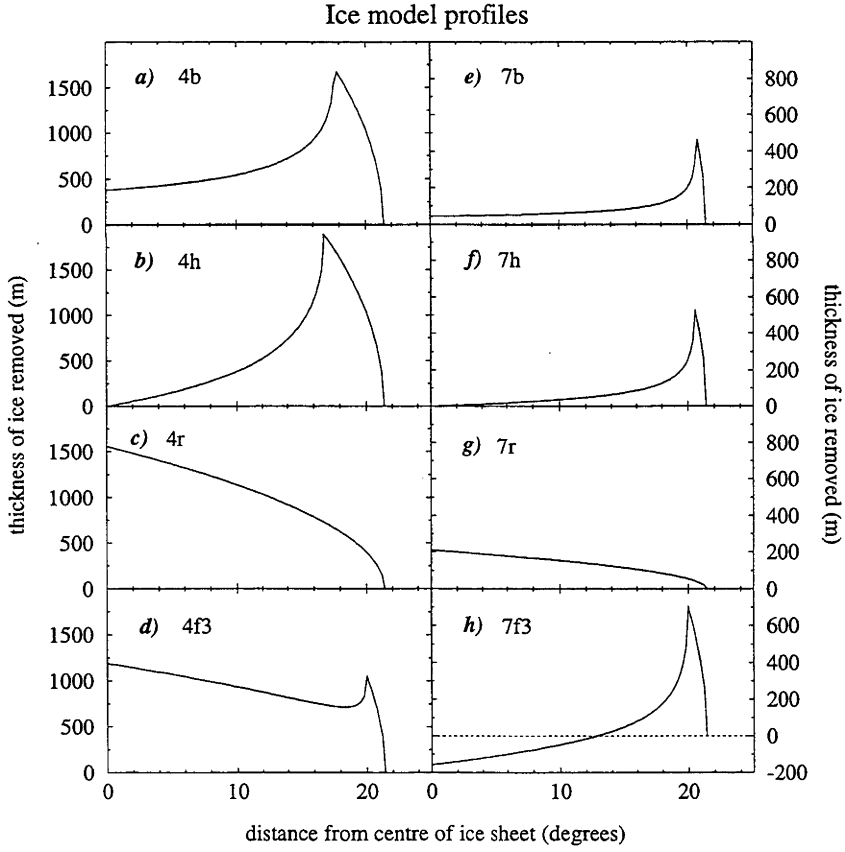

Figure 7.19 : The distribution of removed ice for several melting styles and two values of total ice volume. Models 4x contribute 37 m to globbal sea-level, whereas models 7x contribute 5 m. The melting styles are described in more detail in Table 7.4

7.5.2 Distant effects

The results of this chapter so far highlight the ambiguity of inverting sea-level observations from the Antarctic coastline to obtain the history of the ice sheet. Significantly different models can produce similar sea-level predictions at Antarctic coastal sites, and the differences between sea-level changes at several sites could easily be attributed to regional variation in the style of melting. To find a useful sea-level record that is insensitive to small-scale variations in ice distribution, we need to look further away from the ice sheet, yet close enough to observe effects that can be confidently associated with the Antarctic ice sheet, and not some other far-field source of meltwater. The most appropriate region for these observations is on the far side of the peripheral bulge that formed at the time of maximum loading. The position of the peripheral bulge depends mainly on the width of the load. After the load is removed, the peripheral bulge collapses and migrates towards the centre of rebound. For the axisymmetric continental-scale models of the Antarctic ice sheet studied here, which are approximately 20 degrees in radius, the crest of the peripheral bulge at 6 ka, when significant melting has ceased, lies about 25-30 degrees from the centre of the ice sheet. For these models, the far side of the bulge slopes away gently to a colatitude of around 90 degrees (the ice sheet's 'equator') where there is no observable gradient. In any case, a site beyond 90 degrees must be closer to another ice sheet.

To investigate the predicted sea-level changes in the peripheral bulge zone, we will only consider the ice load component ($\Delta\zeta^i$), which includes both the isostatic and gravitational effects of the changing ice sheet. The other components ($\Delta\zeta^e$ and $\Delta\zeta^w$) depend only on the total ESL rise, which is the same for all models. We will compare the shape of the peripheral bulge at 6 ka for a range of earth and ice models. The amplitude and decay of the peripheral bulge are insensitive to the distribution of ice, but strongly dependent on the total volume of ice removed, as shown in Figure 7.20. This suggests that sea-level observations from the peripheral bulge zone may be able to constrain the total contribution of the Antarctic ice sheets to postglacial sea-level rise. Dependence on the upper mantle viscosity is greater (Figure 7.21), with higher viscosities causing less sensitivity to the total melt volume, although the larger ice sheet (37 m ESL, model 4b) still shows a significantly higher bulge and a greater gradient in the ice load component in the region between the bulge and the equator (30 - 90 degrees colatitude). The amplitude of the bulge at ~30 degrees colatitude is strongly dependent on the lithospheric thickness (Figure 7.22), but this dependence is insignificant in the region between 40 degrees and the equator, where the relevant observations are more likely to be found in the southern hemisphere.

The gradients involved are extremely small - the predicted bulge heights at 6 ka are only 1 - 5 m, and decrease to zero over approximately 7000 km. The greatest gradient occurs within about 2000 km of the crest of the bulge, which is in the Southern Ocean where no reliable Holocene record has yet

been obtained. However, sea-level observations from the late Holocene can be made with a precision of better then 0.5 m, and the far-field effects of the Antarctic Ice Sheet may be observable as far away as Australia if other influences on sea-level change can be well constrained. These observations are discussed in Section 7.8 below.

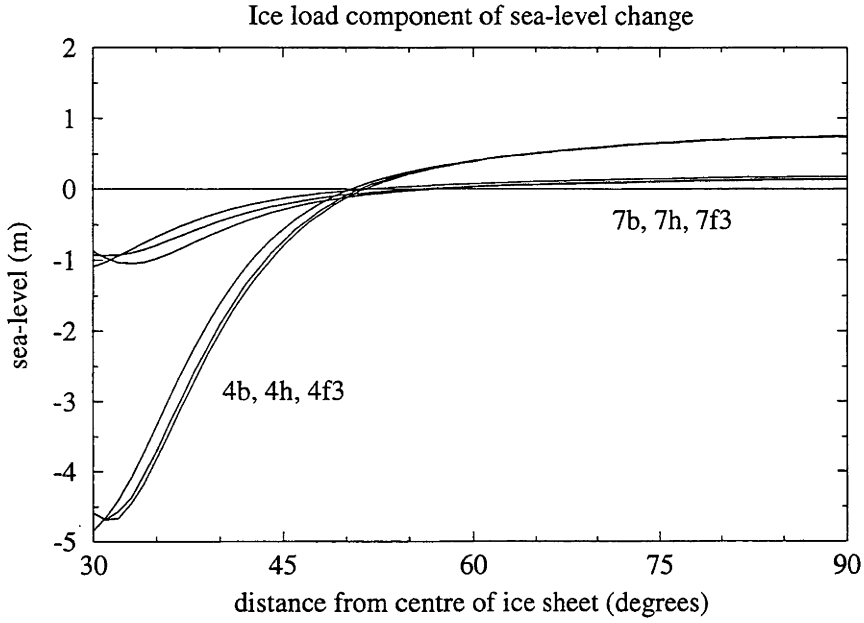

Figure 7.20 : The effect of ice volume and distribution on predicted sea-level change in the region beyond the peripheral bulge. The ice-load component of sea-level at 6 ka is plotted.

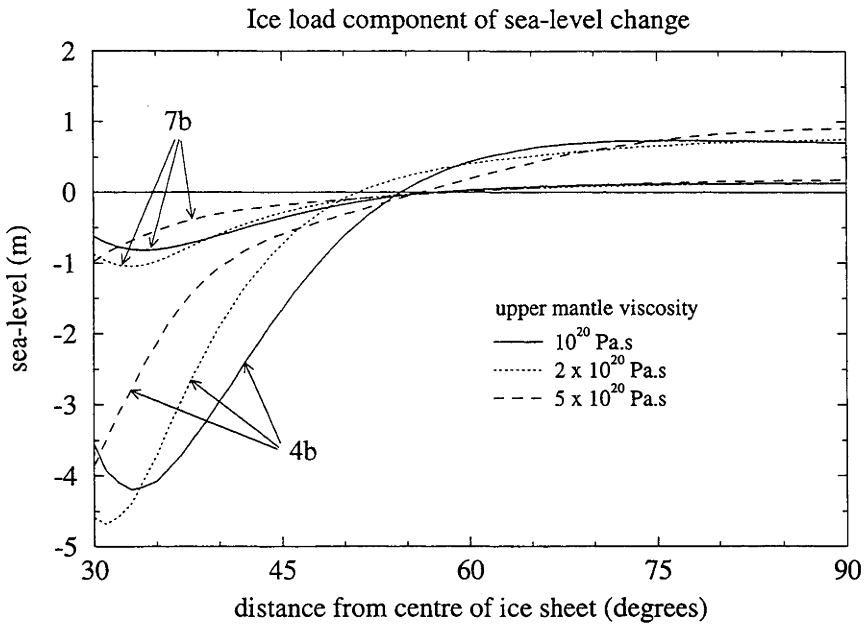

Figure 7.21 : The effect of upper mantle viscosity on predicted sea-level change in the region beyond the peripheral bulge. The ice-load component of sea-level at 6 ka is plotted.

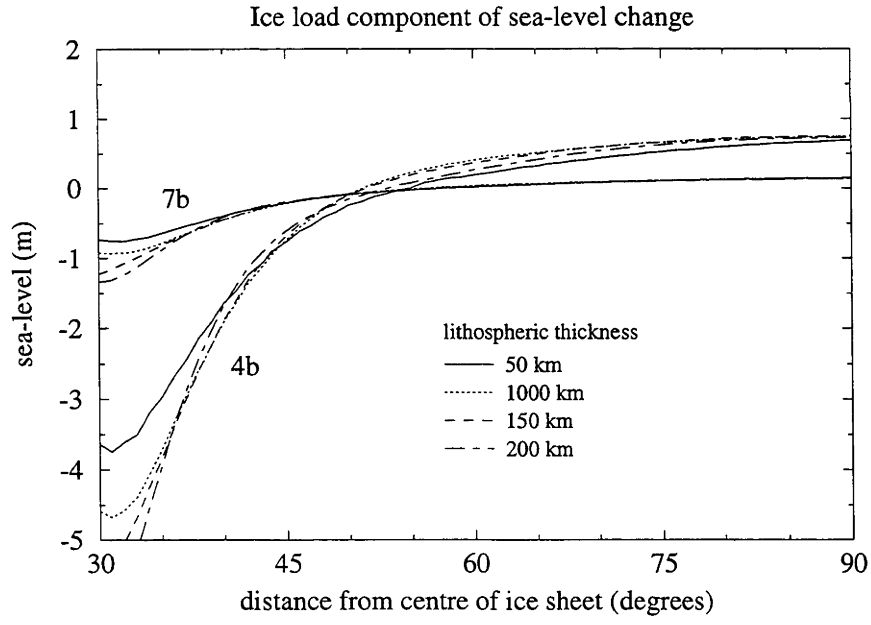

Figure 7.22 : The effect of lithospheric thickness on predicted sea-level change in the region beyond the peripheral bulge. The ice-load component of sea-level at 6 ka is plotted.

7.6 Regional models: Comparison with Antarctic observations

As illustrated in the previous section, trade-offs between pairs of variables result in similarly realistic sea-level predictions from a range of models within the chosen parameter space, making it difficult to determine the optimum combination of ice and earth models. In this section, the sea-level predictions of all models within the chosen parameter space are compared with the best sea-level records from the Antarctic coast. The goodness of fit between the predictions and the models, and the effect of varying the model parameters on the degree of fit, will indicate the optimum combination of models and the suitability of this class of models.

7.6.1 Calculation of variance

The quality of fit between the sea-level predictions and observations is measured using the variance, defined as

$$v = \frac{1}{N} \sum_{i=1}^{N} w_i \left(\frac{p_i - o_i}{\sigma_i} \right)^2 + P \qquad (7.8)$$

where N is the number of points in the observed sea-level curve, p is the relative sea-level predicted by the model, o is the observed sea-level, σ is the error associated with the sea-level observation, w is the weight assigned to each sea-level observation, proportional to the time interval between adjacent observations from the same locality, and P is a penalty function, described below. It should be noted that in many cases σ does not represent any statistical measure of the error, since the observational records are not in the form of an estimate with associated uncertainty. For example, in the case of the records from McMurdo Sound and Terra Nova Bay the observations can only be used to infer upper and lower limits to the relative sea-level curve. In these cases, o_i is estimated to be the mid-point of the sea-level envelope at time i, and σ_i is half the range between the upper and lower bounds. The size of σ thus represents the degree of uncertainty in o, but is not necessarily comparable between sites, so the calculated variance can only be used to compare the quality of fit of different models' predictions to the observed sea-level change at a given site.

If σ were a true measure of the standard deviation, variance values close to unity would indicate that the model adequately explains the observations. Higher values indicate poor fit, and lower values may indicate "over-fit" due to the inclusion of too many parameters in the model, or allowing the parameters to vary unrealistically. As mentioned above, in the data sets used here, σ does not consistently represent a true statistical measure of observational uncertainty. Therefore, the variance values of the best-fitting models differs between sites by more than two orders of magnitude, from ~0.03 at McMurdo Sound, to ~5.0 at Skarvsnes. This difference is not necessarily a measure of the relative degree of fit, but is rather due to poor estimation of the values of σ_i.

To simplify the comparison of the predictions with observations from several sites, the values of o_i were interpolated from the sea-level curves (Figure 3.21) every 1000 years throughout the Holocene, and every 500 years close to 6 ka. Uncertainty in the time of the interpolated observations was not included in the calculation of variance.

The penalty function P is used to incorporate into the variance calculation "limiting observations", that is, observations which are incomplete regarding either the age or elevation of former sea-level. These observations include cases in which we know that sea-level was above or below a point at a certain time (from the presence of dated marine or sub-aerial deposits), and also observations of the marine limit. In the latter case we know that sea-level stood at the level of the marine limit, but do not know when. The penalty function is simply an arbitrary constant value that is added to the variance if the predicted sea-level curve does not satisfy the limiting observations. The constant value of P is chosen to be high, so that unsuitable models are eliminated from further consideration. Consideration of these constraints is crucial to determining the optimum ice and earth models, since the reliable sea-level observations (from which the variance is calculated) lie almost exclusively after 6 ka, when the sea-level predictions from all models are very similar. For the sites studied here, limiting observations are only available for the Vestfold Hills, the Bunger Hills, and Terra Nova Bay (see Chapter 3 for details).

For all combinations of earth model and ice melting style (distribution and timing), the ice volume which results in the lowest variance has been determined for each site where observations exist. Only these models are considered from here on. Removing this variable has the effect of diminishing the variance's sensitivity to changes in the other model parameters, since these changes are optimally compensated for by a change in the ice volume removed. For example, for models with different upper mantle viscosities, the ice volume of the best fitting prediction will be greater for the more viscous model. The volume change of the regional ice model does not actually correspond to the volume of melt from that region of the Antarctic coast, as the model ice sheet is circular, with a radius of 10 degrees, whereas the observation site is on the margin of a much larger ice sheet. However, some ice model parameters which may be directly compared to observations, such as the distance that the ice sheet retreated, and the former ice thickness at any point, can be calculated from the optimum ice volume.

7.6.2 Optimum ice model

Ice thickness and retreat distance

After the optimum value of ice volume change was determined at each site, the rheological model which produced the lowest variance was selected at each site and for each ice model. Although the ice volume change of these best-fitting models generally varies by at least a factor of two at each site, the

distance of ice margin retreat and the former ice thickness at the observation site are fairly consistent at each site but different for each site (Table 7.9), indicating that the optimum regional ice sheet reconstruction is sensitive to the constraints of the sea-level observations and is substantially independent of the earth model.

In Table 7.9, the estimated values of Δh and ΔR are presented with the width of the continental shelf at each site. The shelf width is defined here as the distance from each observation site to the 500 m bathymetric contour. This is the usual depth of the shelf edge around Antarctica, considerably deeper than at most continental margins. The shelf width is a maximum limit for the former extent of ice, and if the ice sheet advance was primarily controlled by the exposure of the continental shelf caused by falling sea-levels then the 100 or 200 m contours may be more realistic upper limits to ice sheet expansion.

Table 7.9: Estimated former ice thicknesses and margin retreat distances at sites in East Antarctica. The "best" values are the range of optimum values from each value of lithospheric thickness, but with the mantle rheology and ice melting history unconstrained. The "overall" values include the optimum reconstructions for all melting styles and lithospheric thicknesses, but still with the mantle rheology unconstrained. Δh is the former ice thickness at the observation site, and ΔR is the distance which the ice sheet margin retreated. In all cases, the present ice margin is at the observation site.

Site	best		overall		shelf
	Δh (m)	ΔR (km)	Δh (m)	ΔR (km)	width (km)
Vestfold Hills	600 - 700	30 - 40	500 - 800	20 - 60	200
Skarvsnes	850 - 950	60 - 80	700 - 1100	40 - 100	100
Bunger Hills	520 - 630	25 - 33	520 - 870	25 - 65	200
Terra Nova Bay	1400 - 1750	160 - 320	900 - 1900	70 - 370	>500
McMurdo Sound	650 - 740	35 - 50	650 - 980	35 - 85	>500
Windmill Islands	960 - 1135	80 - 110	960 - 1320	80 - 150	<100

The optimum values of Δh and ΔR presented in Table 7.9 represent the best estimates from the entire range of model space investigated in this study, and are drawn from a wide range of earth models. While there is little justification either for proposing or rejecting variable earth rheology around the Antarctic margin, it is worthwhile to consider the optimum ice models for each site when only one earth rheological model is considered. This has been done using the best rheological model of Nakada and Lambeck (1989) for the Australasian region. The range of estimates has been further constrained by only considering melting models which include 3.7 m of eustatic sea-level rise during the late Holocene. Under these constraints, two estimates of the ice sheet changes are obtained, from the constant-height and constant-*b* models. The resulting estimates of Δh and ΔR (Table 7.10) are generally slightly larger than if all rheological models are considered.

Table 7.10: Estimated former ice thicknesses and margin retreat distances at sites in East Antarctica, using a standard earth model and only considering models which include significant late-Holocene melting. The model used is based on the optimum model of Nakada and Lambeck (1989), with H_l = 100 km, $\eta_{um} = 2 \times 10^{20}$ Pa.s, and $\eta_{lm} = 10^{22}$ Pa.s.

Site	constant-height		constant-b	
	Δh (m)	ΔR (km)	Δh (m)	ΔR (km)
Vestfold Hills	718	45	720	42
Skarvsnes	1014	91	1021	85
Bunger Hills	809	56	789	51
Terra Nova Bay	1356	174	1342	147
McMurdo Sound	891	69	901	66
Windmill Islands	1162	122	1179	113

These estimates of Δh and ΔR can be compared with previous estimates from the same locations. At all sites, the estimated Δh is greater than those of Colhoun and others (1992), which were based on simplistic local isostatic arguments. The difference is probably not so much due to the application of the principle of isostasy, as to the different interpretation of the various sea-level records.

Excluding rebound observations, constraints on the former ice cover of the Vestfold Hills are few. On land, the highest exposed rock at 158 m asl is striated, but there is no guarantee that this occurred during the LGM, and the "discontinuous line of moraines" on Broad Peninsula cited by Pickard (1986) as a possible former ice margin position could have been deposited at any stage of the last retreat of the ice sheet across the hills. Offshore, sediment cores from ODP site 740 (Domack and others 1991) and the Four Ladies Bank (O'Brien 1994) indicate that the Amery Ice Sheet extended to the continental shelf edge, far beyond the 30-40 km of retreat indicated by the regional-scale ice sheet modelling, but again there are no time constraints.

No direct observation-based estimates have been made of the former ice thickness and extent around Skarvsnes, in Lützow-Holm Bay, although radiocarbon ages from marine sediments from two other coastal oases in the Bay, Langhovde and the Ongul Islands, have led Moriwaki (pers. comm. 1994) to propose that these areas remained ice-free throughout the LGM. He suggests, however, that the ice sheet may have expanded around these oases, which remained ice-free because they were sheltered from the advance of the ice. The advance of 60 - 80 km estimated from the regional models would make this scenario implausible, requiring very steep gradients on the ice sheet surface to maintain these oases. If the expansion of the ice sheet in this region was mainly due to growth of the Shirase Glacier at the southern end of Lützow-Holm Bay, then the possibility of Langhovde and the Ongul Islands, which lie 25 km and 50 km north of Skarvsnes respectively, remaining ice free is more plausible.

No estimates of the LGM ice thickness at the Bunger Hills has been made apart from those based on interpretation of the sea-level record. The best estimate of the regional-scale ice models, of Δh = 520 - 630 m and ΔR = 25-33

km, suggest that the ice sheet did not advance far beyond the extent of the oasis itself, which is about 30 km wide, perpendicular to the ice sheet margin. The width of the continental shelf at the Bunger Hills (to the 500 m bathymetric contour) is around 200 km, but water depths of >250 m have been measured close offshore of the Bunger Hills, and the Shackleton Ice Shelf, which is afloat 50 km to the North of the Bunger Hills and is >100 km wide in places, indicates that regionally the continental shelf is quite deep. It is possible that the continental shelf exposed by ~100 m of sea-level fall would amount to only ~30 km, and that this region was completely occupied by the Antarctic Ice Sheet at the LGM.

The regional-scale circular ice sheet models are probably less applicable to Terra Nova Bay and McMurdo Sound than to the other coastal sites, due to the proximity of the former Ross Ice Sheet, which may have extended east of these sites for around 1000 km with uniform ice thickness (Denton and others 1989b). The former ice heights estimated from the regional models should therefore be greater than the actual values. At Terra Nova Bay, the elevation of the Terra Nova Drift indicates that the region was covered by 500 m of ice at the LGM (Orombelli and others 1990), which is about one-third the regional estimate of 1400 - 1750 m. Although these results are not contradictory, no useful constraints can be determined from the new estimate. At McMurdo Sound, the LGM ice thickness varied from ~700 m to zero, as it flowed in from the Ross Ice Sheet and terminated in the Dry Valleys (Stuiver and others 1981). It is therefore impossible to interpret the estimate from the regional models in any realistic form.

The presence of Law Dome adjacent to the Windmill islands makes the applicability of the regional ice models there questionable, but the radius of the dome is ~100 km, so the perturbation on the regional models, which have a radius of 10° (~1100 km), should not be too great. Budd and Morgan (1977) used ice core measurements from Law Dome to propose that the ice at the LGM extended ~60 km beyond its present position, and was ~1200 m thick at the present coastline. This is in excellent agreement with the estimates derived from the regional-scale ice models, which suggest ice 960 - 1135 m thick at the Windmill Islands, and an ice margin retreat of 35 - 50 km.

An estimate of Δh can also be made for the Sør Rondane Mountains using the regional-scale models. Here, the maximum former ice height on the northern side of the mountains has been measured at ~400 m (Moriwaki and Hirakawa 1990), although there are no age constraints on this reconstruction, and it may not have occurred at the LGM. From the Sør Rondane Mountains to the coast, a distance of ~200 km, the ice sheet surface is adequately described using the parabolic models used for the ice sheet models in this section. Greater changes in ice sheet elevation were reported further south in the mountains (Chapter 4), but the ice surface gradient changes dramatically here, and the simple parabolic models are no longer applicable. No constraints are available from isostatic arguments on the former ice sheet size on the Princess Ragnhild Coast, but if we assume that

the ice advanced to the edge of the continental shelf (20 km), the change in elevation which would occur at the Sør Rondane Mountains, 200 km inland, is only about 50 m. Since the ice margin could not have expanded beyond the continental shelf, the anomalously large Δh raises at least two possibilities: the extra ice thickness could have been compensated for by an increase in the basal shear stress of the ice sheet, perhaps caused by changes in the basal melting regime; or the maximum recorded ice thickness could be much older than the LGM, and the apparent decrease in ice height could be due to slow tectonic uplift over a long period of time. Unless the former ice limits can be dated, or the tectonic regime be constrained, the validity of these scenarios cannot be ascertained.

Distribution of removed ice

As well as attempting to estimate the former extent of the ice sheet margin, we wish to determine the distribution of ice removed from the ice sheet since the LGM. As described above, this distribution was examined by using constant-height and constant-*b* ice sheet models. The applicability of these models may be estimated from the variance between their sea-level predictions and the observed sea-level history at each site where observations exist. As described above, the optimum ice sheet model for both the constant-h and constant-*b* scenario was determined at each site for all melting histories. The average variance of these models' predictions was then calculated. Because the actual variance differs greatly between sites, the results were normalised to the variance of the constant-h model (Figure 7.23).

When the optimum ice models for all melting styles are considered, no distinction can be drawn between the fit of the constant-h and constant-*b* models (Figure 7.23 A). If, however, only the three best models are considered (Figure 7.23 B), the data from the three best-controlled sites indicate a preference for one model or the other, although they do not all prefer the same model. At the Vestfold Hills, the "constant-*b*" models are preferred, whereas the "constant-height" models are preferred at Skarvsnes and Terra Nova Bay.

Skarvsnes is located on a relatively uniform section of the ice sheet margin, which should be adequately simulated by the regional models. The preference for constant-height models here therefore indicates that little if any ice was removed from the interior of the ice sheet in this region during deglaciation. The Vestfold Hills, on the other hand, are adjacent to the Lambert Glacier and the Amery Ice Shelf, both of which may have been

A)

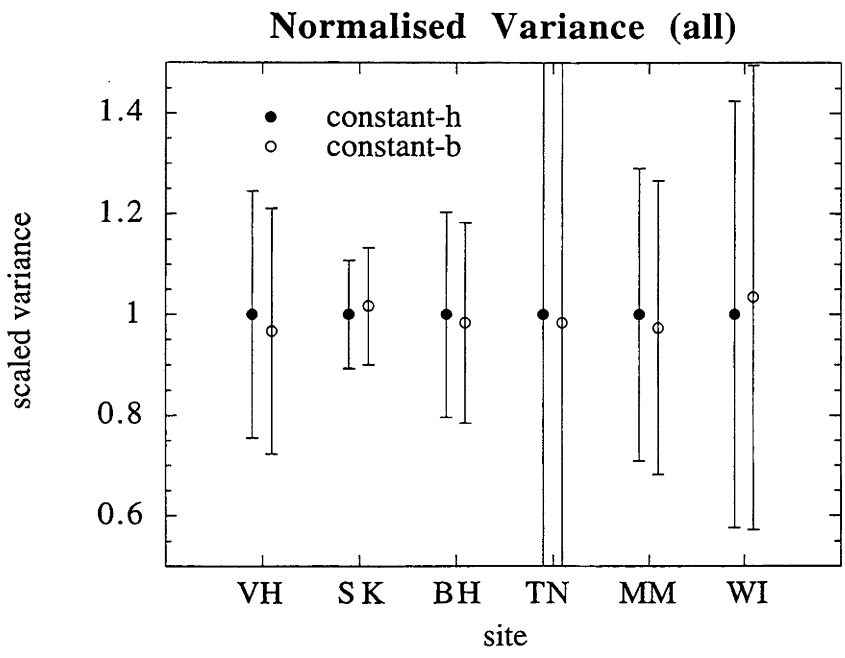

B)

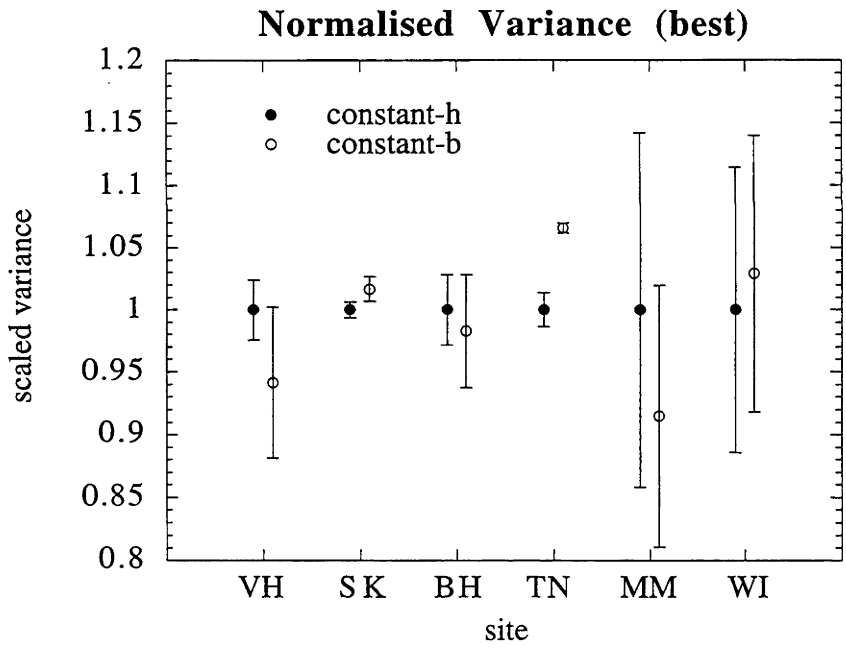

Figure 7.23 : Variance between regional model predictions and sea-level observations, normalised so that values are comparable between sites. A) Comparing the optimal predictions for all melting styles, there is no preference for either constant-h or constant-b ice sheet models. B) Considering the three best models, Skarvsnes and Terra Nova Bay sea-level observations are modelled better by the constant-h models, wheras the Vestfold Hills observations indicate a preference for constant-b models. VH=Vestfold Hills; SK=Skarvsnes; BH=Bunger Hills; TN=Terra Nova Bay; MM=McMurdo Sound; WI=Windmill Islands.

considerably larger at the LGM. Therefore the regional models may not be so appropriate here, and preference for constant-*b* models at this site, which would ideally indicate thinning of the interior of the ice sheet, may instead reflect the removal of ice from the Amery-Lambert system, at a similar distance.

In general, the observations do not allow us to discriminate between the two proposed styles of ice-load distribution. The similar success of the two models in fitting the observations, and the similar former ice thicknesses proposed, indicate that sea-level is controlled more by the nearby changes in ice thickness than by changes on the order of 1000 km away.

Timing of melting

The optimal melting curve differs between the six sites used in this study, indicating that the retreat of ice was not uniform around the Antarctic Ice Sheet. At Skarvsnes and Terra Nova Bay, the lowest variances were obtained using the model in which local melting ceased at 10 ka ("model 10"), wheras all other sites indicate that significant melting continued until 6 ka and that 10% of the total regional melting took place since then ("model 6a").

The preference for melting model 6a at the Vestfold Hills, Bunger Hills and Windmill Islands raises interesting questions regarding the state of these coastal oases at the LGM. If melting of the Antarctic Ice Sheet occurred mainly in response to rising sea-level, as has been suggested elsewhere (Denton and others 1986), then it seems reasonable that significant melting should cease around 6 ka, when the northern hemisphere ice sheets were exhausted. On the other hand, radiocarbon ages from these sites show that the Vestfold and Bunger Hills were ice-free at ~10 ka, and the Windmill Islands at ~8 ka. This situation could occur if the ice margin had retreated uniformly to its present position by 10 ka, and further melting took place without margin retreat, but this is incompatible with the notion of melting in response to rising sea-level. A possible scenario is initially rapid margin retreat in response to global sea-level rise, followed by the establishment of a new equilibrium profile of the remaining ice. Alternatively, the coastal oases were ice-free while regionally the ice sheet was still advanced relative to its present state. In this case, we are required to find a reason for their exposure at that time. Two possibilities exist: either the oases were ice-covered until ~10 ka, when they emerged from the ice prematurely with respect to adjacent sites, perhaps because of divergence in the local iceflow; or they were ice-free throughout the last glaciation, and the 10 ka limit of radiocarbon ages represents the onset of biological production, perhaps controlled by climatic warming.

Which of these explanations is correct is unimportant if we are only interested in the regional-scale ice-sheet history - the local sea-level history records the regional ice sheet history. However, the question is of significant interest to those studying the geomorphic evolution of the coastal oases. Exposure records derived from cosmogenic isotope

determination or sediment thermoluminescence ages may provide the answer, though both of these methods are susceptible to the effect of snow cover, as opposed to glacial over-riding.

The difference in preferred melt timing between the two sites in the Ross Sea probably reflects the retreat of the Ross Ice Sheet across the region. At Terra Nova Bay, the sea-level observations are fitted best by model 10, whereas the data from McMurdo Sound, around 300 km to the south, prefer model 6a. This result is compatible with the oldest radiocarbon ages obtained from the two sites, which indicate that the coast at Terra Nova Bay was ice-free before ~7.5 ka (Orombelli and others 1990), compared to ~5.7 ka in McMurdo Sound (Stuiver and others 1981). The value for Terra Nova Bay may be significantly younger than the actual age of retreat of the Ross Ice Sheet from that region, as coastal ice is strongly influenced there by major outlet glaciers, which is not the case in McMurdo Sound. Only two models of melt timing were included in this work. Future modelling including a range of times may place stronger constraints on the retreat of the Ross Ice Sheet.

Late Holocene melting

As demonstrated in Chapter 6, the sea-level record from Australia indicates that 3 - 6 m equivalent sea-level has been added to the world's oceans since 6 ka, reducing the highstand caused by isostatic uplift. A nominal value of 3.7 m was used here. This extra meltwater was included in the regional-scale ice sheet models presented in this section, with a constant rate of meltwater addition over the 6000 years. At most sites, however, the inclusion of this term increased the variance of the best-fitting model sea-level curve. This may be due to the fact that, in order to compensate for the reduced Holocene sea-levels, a larger local ice load must be modelled to obtain the minimum variance. This results in a more concave sea-level curve over the last 6 kyr, since the isostatic uplift component of sea-level change is correspondingly larger. At most sites, the best-fitting models are more concave than the observations, and the increased concavity of the late-melting models almost always increases the variance.

The actual ESL curve since 6 ka, as estimated by Lambeck (1993b) and in Chapter 6, is not linear, but decreases in gradient towards the present, as shown in Chapter 6, and by Nakada and Lambeck (1988) and Lambeck (1993b). The effect of the late Holocene melting would therefore be to make the relative sea-level curves at each site slightly straighter than the result of the linear model which was used. Using a realistic model of the late Holocene melting would therefore produce a better match of the predictions with the observations. The magnitude of these effects is large enough to influence the calculated variance, and hence the estimated ice sheet and earth model parameters. In future modelling of the Antarctic Ice Sheet, it would be advantageous to include a realistic estimate of the late Holocene melting curve, derived from far-field observations, such as that presented in Chapter 6.

7.6.3 Optimum Earth model

Lithospheric thickness

Sea-level change at the Antarctic margin in the last 6,000 years is fairly insensitive to changes in lithospheric thickness, when the models using the optimum ice volume (as described above) are compared. For models with high upper mantle viscosity, varying the lithospheric thickness produces negligible changes in the fit of the sea-level prediction, even at the Vestfold Hills, which has the best-constrained relative sea-level history . In this case, the effect of varying lithospheric thickness is less than observational error, so no optimum thickness can be determined unequivocally, although the lowest variances are consistently obtained using models with a 50 km lithosphere, all other parameters being held constant. If the upper mantle is less viscous, the effect of changing lithospheric thickness is more pronounced, with a thinner lithosphere allowing more mantle deformation following deglaciation (resulting in higher rsl at 18 ka), and a faster rate of change of rebound (causing a more concave-upward rsl curve).

Overall, the lowest variances at all sites except Terra Nova Bay are obtained using the thinnest model lithosphere, 50 km. This is lower than the values obtained from similar studies in Australia (70 - 80 km, Nakada and Lambeck 1989), Britain (65 km, Lambeck 1993), and from analysis of a global data set (120 km, Tushingham and Peltier 1992). In the latter study, a separate treatment of data from the Antarctic margin, using sea-level observations from 5 sites, showed a preference for the lowest modelled lithospheric thickness, 71 km.

Stern and others (1991) estimated the effective lithospheric thickness in the Ross Sea near McMurdo sound by measuring the crustal flexure caused by the load of the volcanic Ross Archipelago over 5 Myr, obtaining a value of 24 km. This value and the estimates derived here are consistent with the apparent change in flexural rigidity with duration of loading (Walcott 1970, Beaumont 1978), but the degree of uncertainty in this dependence on timescale means that all the lithospheric thicknesses considered here would be equally consistent.

Upper mantle viscosity

The fit of the sea-level prediction to the observations is quite sensitive to the value of the upper mantle viscosity used. However, because of the uncertainties in the other parameters of these models, we cannot constrain the upper mantle viscosity with any real confidence. Rather, we can describe the effect of varying this parameter on the variance at each site, and determine the range of values which produces the lowest variance, in combination with the optimum values of all the other parameters.

In general, the optimum value of η_{um} when late Holocene melting is included in the model is higher than if no eustatic sea-level rise occurs after

6 ka. In the latter models, the optimum value of η_{um} is often well-constrained within the range of viscosities examined. When late melting is included, however, the optimum upper mantle viscosity is in almost all cases the maximum in the range examined. This partially compensates for the increased curvature of the predicted sea-level curve caused by the inclusion of the late melting, as discussed above. In spite of this adjustment, the best-fitting curves which include late melting are usually more concave than the observed rsl history, indicating that the effective upper mantle viscosity may be higher than the range examined here.

At all sites except Terra Nova Bay, the combination of parameters which produces the lowest variance includes the highest value for upper mantle viscosity which was included in these models, 10^{21} Pa.s. As discussed above, this site is not well suited to simulation by the regional-scale models used here. If this is the reason for the different results regarding optimum mantle viscosity, however, we would expect the results from McMurdo Sound to be similar. As they are not, the cause of the Terra Nova Bay data's preference for a less viscous upper mantle may be due to inadequate interpretation of the sea-level observations. The curve to which the predictions were compared is the centre of the envelope described by Baroni and Orombelli (1991). Clearly, the actual sea-level curve may be more or less concave than this adopted line. For example, choosing a less concave sea-level curve within the envelope would result in preferred mantle viscosities similar to those obtained from the other observation sites. More precise observations of former sea-levels will be required to determine whether the apparently less viscous mantle in this region is simply an artefact of inadequate observational data.

Lower mantle viscosity

As indicated by the general model results presented in the previous section, sea-level change is not very sensitive to changes in the viscosity of the lower mantle. In the contour plots of variance against mantle rheology , this is indicated by variance contours which are almost parallel to the lower mantle viscosity axis, especially in the case of models with a thin lithosphere. Despite this lack of resolution, some general observations are possible: the Bunger Hills, McMurdo Sound and Windmill Islands sites consistently prefer the most viscous lower mantle among the models considered (2×10^{22} Pa.s.), whereas the results from the Vestfold Hills, Skarvsnes and Terra Nova Bay were much more variable, with the lowest variance occurring throughout the range of viscosities considered.

7.6.4 Local spatial gradients in sea-level change

In this chapter, when comparing model sea-level predictions with observations, it has been assumed that the observation site is a point on the present ice sheet margin. In actual fact, for most of the observed data, the region from which observations were collected is not small compared to the retreat distance of the ice sheet, so spatial variation in sea-level change over

these regions may be significant. In this study, I have not attempted to correct for this variation when comparing predictions and observations, as this extra degree of freedom is not warranted in such simple models, but by looking at the predicted spatial gradients in sea-level change, we can estimate the confidence in the solutions we have already obtained (for example, low gradients would mean that the spatial effect is less important, and so the solutions are more likely to be correct) and determine whether the gradients are large enough that we may have to apply corrections to field observations in future studies. The sea-level highstand at 6 ka is probably the most commonly preserved feature in Antarctic sea-level records, and can be estimated from incomplete records. Here, therefore, only the spatial variation in sea-level change since 6 ka will be investigated.

The eustatic component of sea-level change, by definition, is the same at all locations, but the ice-load and water-load terms both vary spatially. Therefore, these terms both contribute to spatial variation in sea-level change.

In the constant-height and constant-*b* ice sheet models used here, the present coast is the location where the maximum change in ice load has occurred, but the maximum ice-load component of sea-level change actually occurs slightly inland, due to the asymmetry of the ice load (Figure 7.8). The coastal region is thus between the location of maximum uplift and the peripheral bulge, where subsidence occurs, so the ice load component will decrease offshore in this region.

In calculations including two or more iterations, the water load is mainly due to relative sea-level fall caused by isostatic uplift, so its maximum occurs in the region immediately offshore. Because of landward migration of the shoreline through time, as the ice sheet retreats, the "average" position of the coast is offshore from the present position, so the maximum water-load component of sea-level change is also offshore, and decreases landwards. Because their spatial gradients have opposite sense, the relative sizes of the ice-load and water-load terms will determine the magnitude and direction of any spatial gradient in sea-level change.

The gradient in the water load component has been estimated from a combination of first and higher iteration calculations. The third iteration of the water load due to the regional model includes the effect of uplift-induced sea-level fall, as described above. Added to this is a first-iteration estimate of the water load due to "far-field" (ie not included in the regional model) melting. This component is the same as the water-load term of sea-level change at a coastline far from any ice sheets, and is almost invariant between the various regional models since it is caused by a sea-level rise which is large (~120 m) compared to the contribution from the regional model. The contribution of this component to the spatial gradient in the 6 ka highstand is a decrease of ~16 mm per km offshore from the ice sheet margin, ie a seaward tilting of the coastal region.

The predicted gradients in sea-level change since 6 ka are presented in table 7.11. Because these calculations involve second and higher iterations of the water-load, the difference between these simple models and the real earth may be considerable, as the effects of regional coastline geometry may be significant. These estimates are based on the optimum simple ice models determined above, and should indicate whether this effect requires consideration in further interpretation of sea-level observations and numerical modelling.

Table 7.11: Spatial gradient in the height of the 6 ka sea-level highstand predicted by the optimum ice and earth model combinations at each location. All values are positive (ie seaward tilting), indicating that the ice load component of sea-level change is dominant.

site	uplift gradient (mm/km)
Vestfold Hills	58
Skarvsnes	76
Bunger Hills	50
Terra Nova Bay	20
McMurdo Sound	64
Windmill Islands	110

The Vestfold Hills occupy a region of approximately 20 km x 20 km. Thus, we can expect a difference in elevation of the 6 ka highstand of ~1.1 m across the region. This difference is larger than the observational uncertainty for the complete set of lake-isolation records presented in Chapter 3, but might not be detectable using the raised marine deposits. The six lakes which constrain the 6 ka highstand can be divided into the southern group of Lakes Druzhby, Anderson and Watts, and a group ~15 km north, Highway, Ace, and Organic Lakes. As presented in Figure 3.10, these sites can be treated together to obtain the sea-level record for the Vestfold Hills. Considered separately, there is no evidence for a difference in highstand elevation of ~87 cm, which is predicted by the estimated uplift gradient. This indicates that either the spatial gradient in sea-level change at the Vestfold Hills is considerably smaller than estimated, or that the two groups of sites considered here do not lie along the direction of maximum gradient. In fact, the two groups of sites are roughly equidistant from the present ice sheet margin, which runs roughly north-south. The present observational coverage of the region cannot support or dismiss the estimated gradient. However, the Vestfold Hills have been investigated for records of sea-level change in considerable detail, and it seems unlikely that new records of sufficient accuracy to resolve the spatial gradient of sea-level change remain to be discovered.

Skarvsnes is a small oasis, only ~ 5 km across, so the gradient in the 6 ka highstand is not observable there using the present record of raised marine sediments. Also in Lützow-Holm Bay, there are two other oases from which raised marine sediments have been sampled: Langhovde and the Ongul Islands, approximately 25 and 50 km to the north respectively. So far, insufficient observation have been made to determine the 6 ka sea-levels at these sites.

The Bunger Hills oasis extends ~20 km perpendicular to the ice sheet margin, providing good potential for observing any gradient in sea-level change. So far, the sea-level record consists only of dated raised marine sediments, which do not constrain the sea-level history with sufficient accuracy to detect the predicted difference of ~1 m over this distance. Some lake cores have been collected from the Bunger Hills (Melles and others 1994) and it is anticipated that more will be collected in the future with the aim of establishing an accurate sea-level history for the region. If enough such observations are made throughout the oases, the spatial gradient in sea-level change should be detectable.

Because the region-scale circular ice sheet models do not simulate the conditions in the Ross Sea well, it is not expected that the gradients estimated here accurately model the actual gradients in sea-level change. In any case, the sea-level records currently available, consisting of envelopes defined by upper and lower limits on past sea-levels, are not precise enough to detect spatial variation in sea-level change over the regions studied.

In the Windmill Islands, the dated sea-level record is too poor to determine the existence or magnitude of spatial gradients in sea-level change. However, marine limit observations made by Goodwin (1993) show an increase towards the south of ~5m over 30 km. These marine limits are not necessarily contemporaneous at all sites, but it is not unreasonable to suppose that they all represent sea-level at 6 ka, since this was probably the highest stand of sea-level since the site became ice-free following the LGM. If this is the case, then the implied spatial gradient in the 6 ka highstand is 167 mm/km, about 50% larger than the estimate obtained from the regional-scale models. This is reasonable agreement, given the uncertainty in both the LGM ice configuration and the earth's rheological parameters in that region. However, although this observation is consistent with the modelling results, the same gradient could be obtained from many different combinations of ice sheet change and earth rheology.

7.6.5 Discussion

The optimum earth model frequently lies on the boundary of the chosen parameter range. Does this indicate that these earth models are unrealistic? A further constraint on these parameters is available from other studies of sea-level and earth rheology, which find that earth models in this range give optimum fits to sea-level curves in other ice-proximal and formerly ice-covered regions such as NW Europe and Great Britain (Lambeck 1993b). Lateral variation in the rheological properties of the mantle on these time-scales is poorly controlled, but there seems no reason to expect the earth rheology to be greatly different in the Antarctic. If the estimated mantle viscosities are in fact in error, this could be due to deficiencies in either the ice models or the observational data.

The estimation of the northern hemisphere component, dominated by the water-load term, is very simplistic. As the northern hemisphere water-load

term is similar in magnitude to the ice-load term of the regional model, improving the realism of the models may have an important effect on the optimum ice models. For example, at sites within coastal embayments, such as Skarvsnes, the simple models will underestimate the water-load term.

Similarly, the simplistic assumption that "distant" ice load changes elsewhere in Antarctica do not significantly affect sea-level change may be erroneous. The effect of these loads may be a small relative sea-level rise, if the observation sites lie in their "peripheral bulge" zone. If this is the case, slightly larger regional ice sheet changes would be predicted, which would cause greater uplift to counteract the "peripheral bulge" subsidence. These simple models cannot justify this correction.

If the rheological model is limited to the optimum model of Nakada and Lambeck (1989), then all sites indicate a preference for the constant-*b* models, and all sites except Terra Nova Bay prefer melting model 6a.

7.7 Continental-scale models: Comparison with observations

7.7.1 Elevation change inland

The gas content of ancient ice can be used as a paleobarometer (see Chapter 4) allowing the deduction of the elevation history in the interior of an ice sheet. This is an unusual and potentially useful record, as it provides an indirect relative sea-level record at a location remote from the sea. As discussed in Chapter 4, ice core data from sites in the Antarctic interior indicate that there has been no significant lowering since the LGM, and possibly a height increase of 100 - 200 m of both the East and West Antarctic Ice Sheets (Lorius and others 1984, Raynaud and Whillans 1982, Ritz and others 1982, Jenssen 1983). The uncertainty associated with these measurements is large, however, with scatter in the Vostok data set of ±400 m, so the elevation change of -300 m to 600 m is possible. The profiles of LGM moraines deposited by outlet glaciers in the Transantarctic Mountains also indicate that any elevation change in the Antarctic interior was small. One interpretation of the paleotemperature record from the Vostok ice core (Robin 1985) suggests that the elevation of that region has increased by 200 - 300 m since the LGM.

The results of continental-scale ice sheet models, presented in the previous section, show that any change in ice sheet thickness in the Antarctic interior does not simply result in an equal elevation change, since it is partly buffered by the isostatic response, and is combined with elevation decrease of ~100 m due to global postglacial sea-level rise. Furthermore, regardless of ice thickness changes in the interior, the removal of ice from the margin of the ice sheet (which is a universally accepted reconstruction) results in a small lowering of the interior, due to its position in the "peripheral bulge" zone of the marginal load.

Thus, even with no ice thickness change at the centre of the ice sheet, we can expect a surface lowering of ~100 - 120 m. The observed elevation change above therefore suggests that the ice sheet in the vicinity of the Vostok site and its catchment has become changed by -300 - +700 m in the last 18,000 years. The ANT3 model of Nakada and Lambeck (1988) includes a maximum thickening of the ice sheet in this region of around 500 m, although thinning of up to 1000 m is suggested over most of East Antarctica. The observational record of surface elevation from ice cores only provides local constraints on the ice thickness history, and data from more sites will be needed to constrain the history of the entire ice sheet.

7.8 Comparison with Australian Holocene sea-levels

Australia lies between approximately 15° and 45° South, in the region beyond the crest of the peripheral bulge due to the Antarctic Ice Sheet. Several observations of the highstand at 6 ka are available from Australia ranging from Cape York in the north to Tasmania in the south (see Table 7.12). Sea-level at some sites (eg Karumba and Port Augusta) is strongly influenced by the water load term, as they are effectively a long way inland. Nevertheless, even at first glance, there is an apparent north-south gradient from ~1 m at sites on Cape York Peninsula in Far North Queensland, through 0.5 m at Moruya on the NSW South Coast to Tasmania, where no mid-Holocene highstand has been found. Two observations from New Zealand show a similar trend. This is the expected effect of mantle flow towards Antarctica due to ice unloading: sites closer to the crest of the bulge sink further as the bulge collapses, so receive a smaller sea-level contribution from the ice load, and hence form a lower mid-Holocene highstand.

The observations are all based on raised coastal geomorphic features, except in Tasmania, where no Holocene highstand is found. Although the absence of observable raised sea-level indicators does not unequivocally indicate the absence of a highstand, Tasmania has environments (such as large estuaries) which are suitable for the preservation of such features, and geomorphologists have searched for such a record without success. It is therefore suggested that there has been no relative sea-level fall in Tasmania during the Holocene, and that there could in fact have been a relative sea-level rise. This is supported by the presence of the Last Interglacial shoreline 20 m above present sea-level at Mary Ann Bay, near Hobart (Murray-Wallace and Goede 1991) which has been dated at ~80,000 - 150,000 years BP from U-series measurements on shells (K. Lambeck, pers. comm.). If this shoreline corresponds to sea-level 120,000 years ago, when global sea-level was similar to the present, then the implied tectonic uplift rate of 0.6 mm/yr would have resulted in 1 m of uplift in the last 6,000 years. If no highstand from this time is observed, sea-level must have been at least 1 m below its present level. This value is used throughout this discussion, although it represents a maximum sea-level estimate for that time.

To investigate the variation of the 6 ka highstand with distance from the Antarctic Ice Sheet, we need to remove the effects of other spatially variable contributions to sea-level. As shown in Chapter 6, and in previous work by Nakada and Lambeck (1988, 1990), sea-level variation around Australia can be modelled with sufficient accuracy for us to be confident that residual variations represent real contributions to sea-level change. Since we are interested in the variation in sea-level due to the Antarctic ice load, we must make corrections for a) the ice-load term due to the northern hemisphere ice sheets; and b) the water load term including the effects of the migration of Australia's coastline as sea-level rose and the second iteration of the sea-level equation.

Term a) is calculated using the ice model ARC3 of Nakada and Lambeck (1988), and is almost invariant in the Australian region (see Table 7.12). Term b) is calculated using the entire 126 m of postglacial eustatic sea-level rise which results from ARC3 and the Antarctic Ice Sheet model ANT3. The assumption in these models that the Antarctic Ice Sheet contributed 37 m to sea-level rise does not prejudice this investigation of Antarctica's contribution, since even if the contribution is in fact much smaller than ANT3 suggests, the total sea-level rise would still be the same, and it is safe to assume that no ice sheet existed at the LGM closer to Australia than Antarctica.

Estimation of the effect of the second iteration is not simple in this case, since a significant part of the difference between the first and second iterations of the sea-level equation is due to the collapse of the peripheral bulges of the former ice sheets. The subsidence of the bulge causes an increase in the water load over that region, which in turn causes further subsidence. This effect is greatest where bulge subsidence is greatest, and so reinforces the ice-load component of sea-level change in this region. To avoid circular argument, the second iteration correction due to the 89 m of eustatic sea-level rise from ARC3 has been scaled to represent the entire 126 m of postglacial sea-level change. The rheological model used to calculate these corrections is that which Nakada and Lambeck (1989) found to be most suitable for the Australian region. The northern hemisphere ice load component (term a)) and the first iteration of the water load component were calculated to degree 240, while the moving coastline and second iteration contributions were only calculated to degree 80.

In models ARC3 and ANT3, eustatic sea-level has been constant for the last 6,000 years, but previous comparison of these models with Australian sea-level data (Chapter 6) indicates that in fact a correction of 3 - 6 m needs to be included over this time. This contribution is not included in any of the ice- or water-load terms, but is small (~3 % of the total eustatic sea-level rise) and recent, so the effect of this omission is negligible. The exact magnitude of this term is also unimportant, since it is the same for all sites, and does not affect any spatial gradient which is present.

The subtraction of the predicted components of the 6 ka highstand from the observed value yields a residual which should show variation which is dependent on the Antarctic ice load term, $\Delta\zeta_{ice}^{ant}$. This residual highstand, $\Delta\zeta_{res}$, is defined by:

$$\Delta\zeta_{res} = \Delta\zeta_{obs} - \left(\Delta\zeta_{ice}^{ARC3} + \Delta\zeta_{water}^{total} + \Delta\zeta_{3\text{-}step} + \Delta\zeta_{2it}^{ARC3} \times \frac{126}{89} + \Delta\zeta_{f\text{-}f}\right) \quad (7.9)$$

where $\Delta\zeta_{obs}$ is the observed sea-level highstand; $\Delta\zeta_{ice}^{ARC3}$ is the ice-load contribution from the ARC3 ice sheets; $\Delta\zeta_{water}^{total}$ is the predicted contribution from the entire water load; $\Delta\zeta_{3\text{-}step}$ is the correction for a 3-step moving

coastline model; $\Delta\zeta_{2it}^{ARC3}$ is the second iteration correction for the ARC3 model; and $\Delta\zeta_{f\text{-}f}$ is the "far-field correction" of 3.7 m due to late Holocene melting.

The observed sea-level highstands and the predicted components of sea-level change since 6 ka are shown in Figure 7.24 a. It is clear from this graph that most of the variation between Australian sites is due to the water load terms. The only other term which shows significant variation is the

Table 7.12: Relative sea-level at 6 ka at several East Australian sites, and predicted contributions to it. The terms are defined in the text. In the absence of observational errors and subject to model limitations, the residual highstand $\Delta\zeta_{res}$ should correspond to the ice-load contribution from the Antarctic Ice Sheet, $\Delta\zeta_{ice}^{ant}$. The ice-load contribution of model ANT3 is given in the last column, for comparison, and also in Figure 7.24. All sea-level contributions were calculated using earth model 614 (H_l=100 km, η_{um}=2 x 10^{20} Pa.s, η_{lm}=10^{22} Pa.s) which was found to be the most appropriate for the Australian region by Nakada and Lambeck (1989). References: 1=Lambeck and Nakada 1990; 2=Chappell and others 1983; 3=McLean and others 1978; 4=this work, Chapter 2; 5=Belperio and others 1984; 6=Burne 1982; 7=Belperio and others 1983; 8=Short and others 1986; 9=Thom and Roy 1983; 10=Gibb 1986; 11=Hopley 1987.

Site	ref	$\Delta\zeta_{obs}$	$\Delta\zeta_{ice}^{ARC3}$	$\Delta\zeta_{water}^{total}$	$\Delta\zeta_{3\text{-}step}$	$\Delta\zeta_{2it}^{ARC3}$	$\Delta\zeta_{res}$	$\Delta\zeta_{ice}^{ANT3}$
Cape York -10°35',142°40'	1	0.8±0.5	0.899	1.584	0.793	0.609	0.362	0.733
Cape Melville -14°30',145°00'	2,3	1.0±0.3	0.888	2.103	0.438	0.419	0.678	0.645
Karumba -17°25',140°50'	2	2.5±0.3	0.873	4.546	0.554	0.542	-0.540	0.567
Orpheus Island -18°36',146°30'	2,4	1.2±0.2	0.877	3.377	0.380	0.504	-0.448	0.533
Rockingham Bay -32°10',115°13'	2	1.0±0.3	0.876	2.749	0.083	0.556	0.205	-0.103
Port Augusta -32°30',137°27'	5,6	3.0±0.5	0.865	5.494	0.215	0.450	-0.511	-0.108
Cape Spencer -35°15',136°50'	7,8	0.5±0.5	0.876	2.301	0.292	0.554	-0.053	-0.324
Moruya -35°56',150°06'	9	0.5±0.5	0.858	3.202	0.118	0.533	-0.733	-0.359
Weiti River -36°25',175°00'	10	0.9±0.5	0.873	1.812	0.125	0.700	0.799	-0.346
Tasmania -42°50',147°49'	11	-1.0±0.5	0.871	1.046	0.121	0.437	0.043	-1.209
Christchurch -43°25',172°50'	10	0.0±1.0	0.875	2.529	0.150	0.736	-0.896	-1.101

predicted Antarctic ice load term $\Delta\zeta_{ice}^{ANT3}$, which we are attempting to constrain. The residual sea-level highstand, defined above in equation 7.9, is plotted in Figure 7.24 b along with the predicted ice load contribution from ice model ANT3 (Nakada and Lambeck 1988) and two continental-scale axisymmetric ice sheets discussed earlier in this section. It is immediately clear that the residual highstands do not form the smooth trend which all three models predict. This is at least partly due to uncertainty in the observations, which is large compared with the predicted variation in the highstand.

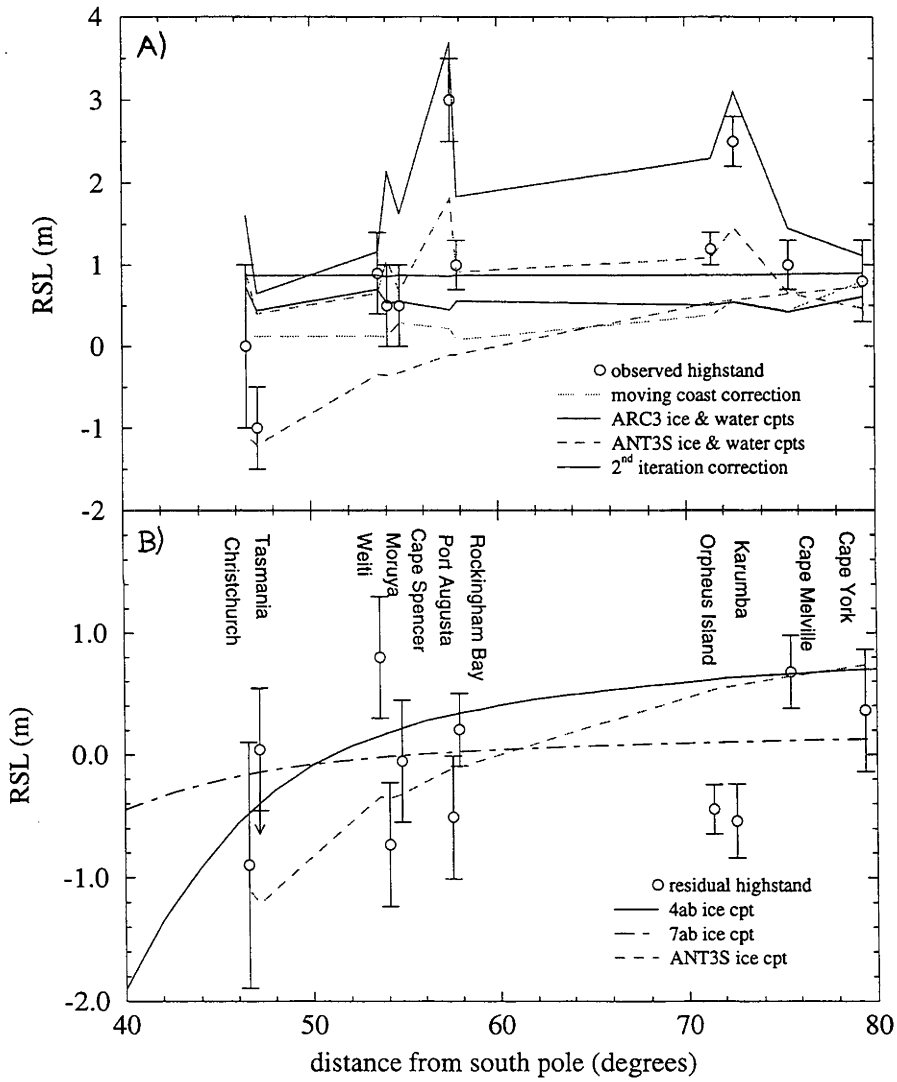

Figure 7.24 : Comparison between observed and predicted sea-level in the Australasian region. A: observed highstand at 6 ka and the predicted contributions to variation between locations. B: Residual highstand observations compared with the predicted ice-load component of sea-level change for three ice sheet models.

Some of the deviation from the region of predicted values can be explained: the Tasmanian data point is a maximum limit only, so its position above the group is consistent with the observation. Using the value of -1±0.5 as the upper limit, we see that the residual lies at most 1 m above the other data points. This suggests that if a record of sea-level at 6 ka is preserved in Tasmania, it will be found 1 - 2 m below present sea-level, after the effect of tectonism has been removed. The residual from Weiti River also lies above the expected range. A possible explanation for this is that the 2nd iteration correction has been underestimated. This could occur because this term was only calculated to degree 80, compared to degree 240 for the ice- and water-load terms. The Weiti River mouth lies on the North Island of New Zealand, at a point where the island is around 50 km wide. At the lower resolution to which the correction terms were calculated, this site would appear more similar to a mid-ocean island, so a smaller sea-level highstand is predicted, resulting in smaller correction terms. Calculation of the correction terms at higher resolution should be done to resolve this possibility.

The residuals at Karumba and Orpheus Island both lie below the predicted range, as do those from Moruya and Port Augusta, although the latter are within their error limits. These four sites are the locations with the largest water-load term, and the fact that these residuals lie below the expected range suggests that this term may have been overestimated. The most likely reason for this would be that the rheological model used to calculate the term has too low a lithospheric thickness or mantle viscosity. An alternative explanation, that these residuals are small because of overestimation of the 2nd iteration or moving coastline correction terms, is less likely, as the sites in question are on the margin of the Australian continent, which is more adequately described by a degree 80 spherical harmonic expansion than New Zealand is.

A southward-decreasing trend in the residual highstand is quite pronounced, whether or not the Karumba and Orpheus Island values are included. If they are excluded, the difference in highstand from Cape York to Christchurch is around 1.2 m compared to 1.8 m predicted by model ANT3 and 1.1 m for model 4b, which both contribute 37 m to sea-level rise. At the other extreme, if the Karumba and Orpheus Island values are used in preference to those from Capes Melville and Cape York, the difference in the observed ice load component becomes ~0.6 m. This is still around twice the variation predicted by model 7b (which contributes 5 m ESL), although the observational uncertainties are so large that the observations do not explicitly exclude this model, if the two northernmost data points are discarded. There is no justification for doing this, so these observations indicate that such a low-volume ice model is unlikely, and are compatible with much larger models, although no ice volume can be directly inferred.

Unfortunately, these observations fall in a range of latitudes in which the predicted variation in the ice-load term is small, limiting our ability to use observations of the mid-Holocene highstand to constrain the volume reduction of the Antarctic Ice Sheet on deglaciation. More, and better-

constrained sea-level observations from this time, especially at sites south of 45°S where the predicted ice-load term is more significant, should allow this method to produce useful constraints on the postglacial volume change of the Antarctic Ice Sheet.

7.9 Realistic models

The reconstructions of the Antarctic Ice Sheet used in previous glacio-hydro-isostatic calculations of sea-level change have been simplistic, since few sea-level records were available from Antarctica to constrain the reconstruction, and the detailed distribution of ice is irrelevant when calculating sea-level changes in the far-field. The total volume change and melting history have been estimated from far-field observations (Nakada and Lambeck 1988, Peltier 1994), and the ice distribution has followed the reconstruction of Hughes and others (1981). Alternative reconstructions for some regions have been published since these models were adopted (see Chapter 4), but they have not been incorporated into these ice models. Currently-used models (Figures 7.25 and 7.26) show major ice-thickness changes in the West Antarctic Ice Sheet and its extensions into the Ross and Weddell Seas. These regions remain more poorly-constrained than the East Antarctic Ice Sheet, although Denton and others (1989) suggest that the observed ice thickness changes of ~1500 m in the Ross Sea were due to grounding of the Ross Ice Shelf, and may not have extended into the interior of the ice sheet.

7.9.1 Estimating the total volume change of the Antarctic Ice Sheet

The regional estimates of changes in the Antarctic Ice Sheet obtained in this chapter can be combined with reconstructions from other parts of Antarctica to estimate the total contribution to sea-level rise since the LGM. The

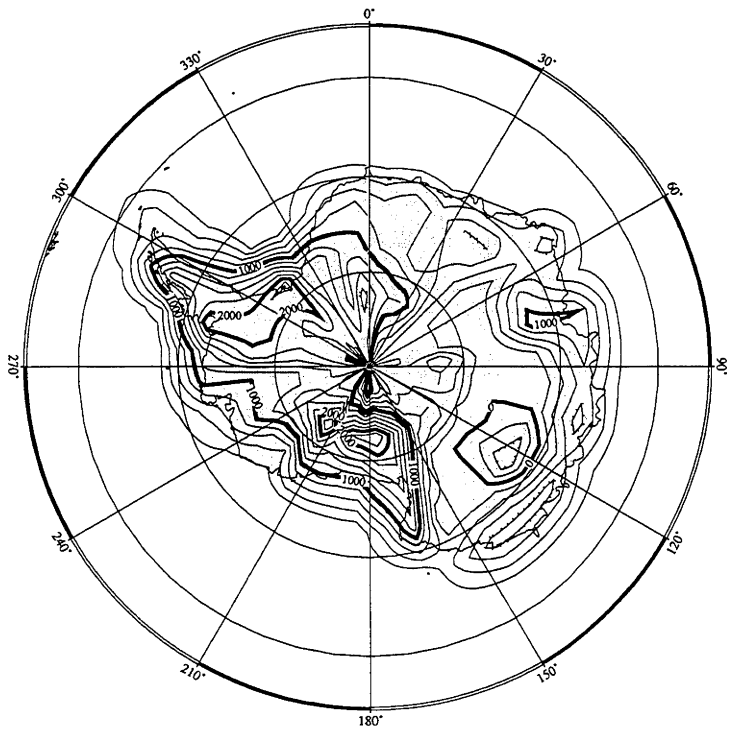

Figure 7.25 : The ANT3 reconstruction of the LGM Antarctic Ice Sheet currently used in modelling of global sea-level change (Nakada and Lambeck 1988).

regional icesheet models can be used to constrain the former ice sheet over ~1000 km of coast, but the coastline of East Antarctica is ~9100 km long, and there are no constraints on the ice sheet history in regions far from any of the observation sites. Therefore, to estimate the sea-level contribution from coastal East Antarctica the cross-sectional area of the ice sheet change at each site has been calculated from the values in Table 7.9, and its average applied over the 9100 km coastline. The resulting volume change of East Antarctica is (1.1 - 2.1) x 10^6 km^3, which corresponds to a global sea-level rise of 2.9 - 5.4 m. This is several times larger than the estimate of 0.73 m over the same region by Colhoun and others (1992).

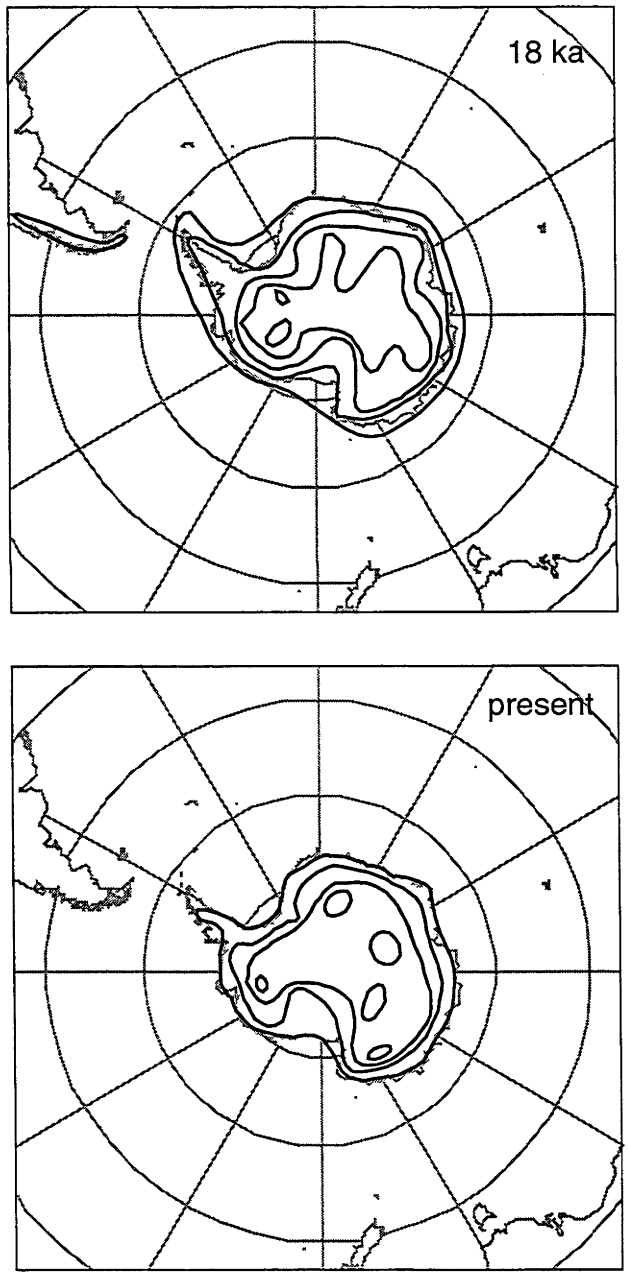

Figure 7.26 : The ICE-3G reconstruction of the LGM Antarctic Ice Sheet currently used in modelling of global sea-level change (Tushingham and Peltier 1992). Contour interval is 1 km.

To estimate the total Antarctic contribution, we must add the effects from other parts of Antarctica. Assuming an ice thickness change of 200 m in the lower Lambert Glacier ice drainage, Colhoun and others (1992) estimated a sea-level contribution of 0.13 m from this region. If, in fact, the thickness change was as much as 500 m (see Chapter 4 for discussion) then this contribution would be 0.33 m.

Reconstructions of the West Antarctic Ice Sheet vary greatly, but if the history of coastal ice resembles that of East Antarctica, then the resulting sea-level contribution would be 0.8 - 1.5 m. In fact, if ice sheet expansion was controlled by the advance of the grounding line, then the West Antarctic Ice Sheet, which flows into the shallow Ross and Weddell Seas, may have expanded proportionally more.

Theoretical reconstructions of the ice sheet over the Antarctic Peninsula suggest that this region contributed 0.8 - 1.9 m to sea-level rise (Huybrechts 1990, Payne and others 1989).

The sea-level contribution from the Ross Ice Sheet can be estimated from the maximum reconstruction of Denton and others (1989) to be ~1.9 m. There are few constraints on the ice history of the Weddell Sea, but if it is assumed that the Ronne-Filchner Ice Sheet extended to the edge of the continental shelf and was similar to the Ross Ice Shelf in form, then its volume contribution may have been ~2.1 m.

Table 7.13: Estimated contribution to global sea-level change from regions of the Antarctic Ice Sheet since the LGM.

Region	sea-level contribution (m)
Coastal East Antarctica	2.9 - 5.4
Lambert ice drainage	0.13 - 0.33
Coastal West Antarctica	0.8 - 1.5
Antarctic Peninsula	0.8 - 1.9
Ross Sea	~1.9
Weddell Sea	~2.1
Total	8.6 - 12.1

These estimates are summarised in Table 7.13, and the total sea-level contribution of Antarctic Ice since the LGM is estimated to be 8.6 - 12.1 m. This contrasts strongly with previous estimates of 37 m (Nakada and Lambeck 1988, based on Hughes and others 1981) and 21.8 m (Peltier 1994). The main difference between these models and the new one presented here is in the West Antarctic Ice Sheet, which remains poorly constrained. More glaciological, geological and sea-level observations are required to obtain an accurate reconstruction for this region. Theoretical reconstructions (Huybrechts 1990, 1992) suggest a total Antarctic sea-level contribution of 12 - 16 m ESL, compared with the low estimate made here based on similarity of the East and West Antarctic ice sheets.

If this estimate of ice volume change is correct, then another reservoir must have existed at the LGM for up to 10 - 25 m ESL, depending on the model used for the other ice sheets, and the total eustatic sea-level rise adopted. Small ice caps and expanded mountain glaciers, which would not cause significant observable isostatic effects may account for some of this.

7.10 Summary

In this chapter, I have presented a set of simple axisymmetric ice models representing the Antarctic Ice Sheet. Models were constructed on two scales, to constrain different aspects of Antarctica's glacial history:

"Regional-scale" ice sheets ~1000 km in radius were used to predict sea-levels at sites on the coast of East Antarctica, and these predictions were quantitatively compared with observations from six locations to obtain estimates for the ice sheet history and earth rheology parameters in those regions. Ice sheet retreats of 25 - 100 km since the LGM are indicated, with the former ice thickness at most sites around 500 - 1000 m. Despite evidence that most sites have been exposed since ~10 ka, a preference is shown for models in which significant melting does not cease until 6 ka, and some melting continues through the Holocene. Earth rheology models with high upper and lower mantle viscosities (10^{21} and 2×10^{22} Pa s respectively) produce predictions which fit the observations best, although this may be an artefact caused by generally poorly constrained observations.

"Continental-scale" ice sheet models were constructed to investigate phenomena which depend on the past behaviour of the Antarctic Ice Sheet as a whole. One such phenomenon is the spatial variation in the height of sea-levels 6000 years ago in Australasia, caused by the continuing slow subsidence of the ice sheet's peripheral bulge. This is a subtle effect, predicted to be on the order of 2.5 m over 4000 km, yet observations corrected for all other spatially varying components of sea-level change are consistent with a large (~37 m) sea-level contribution from Antarctica since the LGM.

This conclusion is somewhat at odds with another estimate of the total volume change of the ice sheet since that time, based on the regional-scale models for East Antarctica as well as previously published reconstructions for the rest of the continent. These reconstructions produce an estimate of 8.6 - 12.1 m ESL, although this is poorly constrained. West Antarctica remains the most likely site for a large accumulation of ice during the LGM, which must have existed somewhere if current estimates of the total postglacial sea-level rise are correct. It is interesting to note that this large volume could until recently be attributed to the whole of Antarctica, since constraints on the ice sheet did not exist. Now that there is reason to believe that the contribution from East Antarctica was small compared with early estimates, further constraints on the history of the West Antarctic ice sheet are critical for evaluating current models of the earth's recent glacial history.

Chapter 8

Conclusion

In the absence of vertical tectonic movements, sea-level change over thousands of years can be attributed to the movements of ice and water masses on the surface of the earth, and the gravitational and isostatic responses to these movements. As described in Chapter 5, these sea-level changes can be described and calculated using the sea-level equation, as formulated in Farrell & Clark (1976) and Nakada & Lambeck (1987):

$$\Delta\zeta(\lambda,\phi,t) = \Delta\zeta^{e}(t) + \Delta\zeta^{i}(\lambda,\phi,t) + \Delta\zeta^{w}(\lambda,\phi,t) \qquad (8.1)$$

where $\Delta\zeta(\lambda,\phi,t)$ is the sea-level relative to its present value, at time t, latitude λ, and longitude ϕ. The first term on the right hand side of the equation is the eustatic sea-level, which is uniform over the whole earth and is only a function of time. Over Quaternary time, the eustatic sea-level is essentially a measure of the amount of water stored on land in ice sheets. The remaining two terms are the vertical isostatic responses to the loads of ice and water on the surface of the earth. These terms depend on the geographic distribution of the loads, and on the rheology of the earth.

The aim of studies in glacio-hydro-isostasy is to use observations of sea-level change (the left side of equation 8.1) to constrain the parameters which control the terms on the right hand side. Previous workers have produced adequate models for the ice sheets of the northern hemisphere for the last 18000 years and for the rheology of the earth, but few constraints have been placed on the history of the Antarctic ice sheet, because sea-level change in most parts of the world is not sensitive to the geographic distribution of mass changes so far away. The goal of this thesis has been to obtain new estimates for the size and shape of the Antarctic ice sheet since the last glacial maximum (LGM), using sea-level observations from the Antarctic and Australian coasts.

8.1 New Antarctic sea-level observations

In Chapter 3, a new sea-level record was determined for the Vestfold Hills, East Antarctica, by dating the lacustrine-marine and marine-lacustrine transitions in sediment cores from lakes which were formerly connected to the sea. Using cores from lakes with sill heights up to 40 m above present sea-level (a.s.l.), a well-constrained record was obtained for the period back to ~8 ka. At 8 ka, sea-level was about 7.5 m higher than present. Sea-level rose until ~6.2 ka, when it reached a highstand 9 - 9.5 m a.s.l, after which it fell

steadily until the present. The maximum at 6.2 ka is clearly seen in two sediment cores, where a lacustrine-marine-lacustrine succession records the transgression of the lakes by rising sea-level and their subsequent isolation as sea-level fell.

Evidence for sea-level change was also compiled from other sources for several other sites in East Antarctica: McMurdo Sound, Terra Nova Bay, the Windmill Islands, the Bunger Hills, and Skarvsnes in Lützow-Holm Bay. Evidence at a site in the Antarctic Peninsula region, King George Island, was also investigated, but the results were not used in subsequent sea-level modelling due to the complexity of the ice sheet history in that region. At all sites, sea-level appears to have fallen throughout the last 6000 years, without any evidence of oscillations during this time. Apart from the Vestfold Hills record, no evidence is seen for a local sea-level maximum, a period of sea-level rise preceding the mid-late Holocene fall. This does not necessarily mean that such a maximum did not occur, but reflects the greater accuracy and completeness of the new lake-isolation record compared to the dating of raised shoreline features, which is the most common source of information on former sea-levels.

8.2 Regional ice sheet reconstructions

To study the influence of ice sheet changes on sea-level at East Antarctic sites, a range of plausible simplified models of the ice sheet margin were constructed (Chapter 7). These models were based on glaciological principles, constraints from the ice sheet at the study sites, and published evidence indicating that the elevation change in the interior of the ice sheet has been small since the LGM (Chapter 4). They do not attempt to simulate the behaviour of the entire Antarctic ice sheet, but only a region on the margin, on the order of 1000 km.

Using published models of the earth's response to surface loads (Farrell and Clarke 1976, Nakada and Lambeck 1987, Johnston 1993), the regional ice models described above were used to predict sea-level histories at coastal sites. A large range of scenarios was investigated, allowing for variation in the maximum extent of the ice and its melting history, the rheological parameters of the earth, and the global eustatic sea-level curve, particularly with respect to the existence of late Holocene eustatic rise. The component of sea-level change not due to the regional ice sheet model was calculated from the northern hemisphere ice sheet models of Nakada and Lambeck (1988).

The observed sea-level records at each site were compared with the prediction of each combination of ice and earth model parameters, and the degree of fit of the predictions to the observations was measured using the variance, based on the uncertainty in the observations. The combination of ice model and earth rheology which produced the lowest variance was determined at each site. The results indicate noticeably different ice sheet

histories for each site, indicating that the optimum reconstruction is sensitive to the constraints of the sea-level observations, and are fairly insensitive to the choice of earth model.

The optimum ice sheet histories indicate that at the LGM the East Antarctic ice sheet margin advanced 25 - 100 km beyond its present position, resulting in ice thicknesses of 500 - 1000 m at sites now on the coast. At the Windmill Islands, these results are in excellent agreement with the reconstruction based on ice core data from the adjacent Law Dome (Budd and Morgan 1977). The estimates for McMurdo Sound and Terra Nova Bay are larger than those of reconstructions based on the glacial geology, perhaps reflecting the influence of the expanded Ross Ice Sheet. No good constraints have previously been obtained from the other observation sites.

8.3 Total Antarctic ice sheet volume change

Current estimates of the total extra ice stored in the Antarctic ice sheet at the LGM used in glacio-hydro-isostatic modelling range from 37 m ESL (Nakada and Lambeck 1988) to 25 m equivalent sea-level (ESL) (Tushingham and Peltier 1992). These estimates are poorly-constrained, but are consistent with estimates of the total global ice sheet volume at the LGM based on sea-level at that time. Reconstructions of the ice sheet based on a numerical thermomechanical model (Huybrechts 1990, 1992) indicate that the sea-level contribution from Antarctica since the LGM was 12 - 16 m ESL, and a simplistic treatment of the available rebound data from the Antarctic coast (Colhoun and others 1992) yielded a volume difference of only 0.5 - 2.5 m ESL.

The reconstructions of the former ice thickness at the six East Antarctic sites discussed above were used to estimate the total volume of the Antarctic ice sheet at the LGM. Applying the results from East Antarctica above to the margin of the West Antarctic ice sheet, and using published reconstructions to calculate the contributions from the Ross and Ronne-Filchner Ice Shelves (Chapter 4), a total Antarctic contribution of 8.6 - 12.1 m ESL is obtained (Chapter 7). The extrapolation of results from the sites in East Antarctica to the West Antarctic may not be valid, because the two ice sheets are fundamentally different: the former is land-based, whereas the latter is a marine ice-sheet, grounded below sea-level and supported in part by the buttressing effect of the ice shelves. The ice shelves probably advanced significantly more during the LGM than the rest of the ice sheet margin (eg Denton and others 1991), which may have caused correspondingly larger changes to the West Antarctic Ice Sheet, compared to the East. The total volume change obtained here should therefore be regarded as a minimum estimate.

The total volume change of the Antarctic ice sheet since the LGM was also investigated using sea-level observations in eastern Australia. After the melting of Antarctic ice, isostatic rebound at the location of the former ice

causes inward flow in the mantle, which may be observed as the subsidence of the "peripheral bulge" around Antarctica. The amount of subsidence which occurs is dependant on the total volume of ice removed, and is insensitive to its geographic distribution. The subsidence reaches a maximum in the Southern Ocean between Antarctica and Australia, and decreases northwards. This subsidence contributes a component of sea-level rise to the total sea-level change occurring at Australian sites, although until ~6 ka this rise is indistinguishable from the much larger eustatic rise. After 6 ka, sea-level change at most Australian coastal sites is dominated by the uplift caused by the increased water load in the oceans, but the subsidence due to bulge collapse continues, and contributes to the differences in sea-level between sites. Thus, if we can remove the effects of other spatially variable sea-level changes, such as the water-load term, we expect to see higher sea-level in the north of Australia than at sites further south. The north-south variation in sea-level may provide an indication of the amount of peripheral bulge subsidence, and hence the amount of ice removed from the Antarctic ice sheet since the LGM.

Numerical model predictions show that the difference in sea-level at 6 ka over Australia would be around 1.7 m if 37 m ESL was removed from the Antarctic ice sheet, but only 0.5 m if the total melting was 5 m ESL (Chapter 7). Sea-level observations from that time in Australia and New Zealand were compiled, and corrections for the other spatially variable components of sea-level change were applied, using the ARC3 ice model of Nakada and Lambeck (1988) and the standard earth rheological model derived using observations from Australasia (Nakada and Lambeck 1989). The north-south gradient in the residual sea-levels is consistent with the larger ice volume model, although uncertainties in the sea-level observations at this time are generally on the order of 0.5 m, and there are some outliers to the general trend.

The discrepancy between the coastal observations from East Antarctica, which indicate a small ice-volume change in Antarctica since the LGM, and the Australian observations, which are consistent with a large one, indicate that a well-constrained reconstruction of the West Antarctic Ice Sheet is required in order to obtain a consistent model of ice sheet and sea-level changes since the LGM. Sea-level records from the West Antarctic coast would be extremely useful for constraining a glacio-hydro-isostatic reconstruction similar to those performed here for East Antarctic sites.

8.4 Late Holocene melting

The ESL history for the Antarctic ice sheet used in the models described above has been that of the model ANT3 (Nakada and Lambeck 1988), which is similar to the ESL history of the northern hemisphere ice sheets. In these models, no eustatic sea-level rise occurs after 6 ka. However, sea-level predictions after 6 ka based on these models are consistently higher than observations, indicating that some eustatic rise has in fact occurred. Because

the Laurentide and Fennoscandian ice sheets did not exist during this time, the Antarctic ice sheet is the main candidate for the source of this water.

The amount of eustatic sea-level rise which has taken place since 6 ka can be estimated from the difference between sea-level predictions and observations. Nakada and Lambeck (1989) estimated that ~3 m ESL of melting had occurred, using Australian sea-level observations. In a more detailed study using sea-level observations from the British Isles, Lambeck (1993b) estimated 1.7±1 m ESL rise since 6 ka, with the rate of rise decreasing with time.

In Chapter 6, a compilation of new and published sea-level observations from north Queensland was used to obtain a new estimate for the mid-late Holocene ESL curve. The result is dependant on the rheological model used to calculate the predictions, although all estimates show a curve similar in shape to that obtained by Lambeck (1993b). Using the range of earth models considered suitable for the Australian region (Nakada and Lambeck 1989), the total ESL rise since 6 ka is estimated to be 3 - 6 m. This is larger than Lambeck's (1993b) estimate from the British Isles, and could indicate slow tectonic subsidence in north Queensland. Though unproven, this would be consistent with the absence of last interglacial (~120 ka) shoreline features in north Queensland.

Appendix

Site Reports

FAR NORTH QUEENSLAND FIELD WORK, NOVEMBER 1992

Eleven islands on the northern Great Barrier Reef were visited between November 16 and 27, 1992. The sites studied and samples taken are described here, with the elevation of each sample. Levels were determined using a staff and level in the field, measuring the height of each sample relative to water level at low tide. These were reduced to Tidal Datum using the secondary port corrections to the Cairns tide observations (supplied by the National Tidal Facility, Flinders University) and then converted to heights above the level of mean low water spring tides (MLWS). To approximate the heights of the daily low tides and MLWS above tidal datum at each island, the Lizard Island values were used for Nymph, West Pethebridge, the Turtle Islands and Fly Reef; the Howick Island values were used for Houghton, Leggatt and Noble Islands; and the Flinders Island values were used for the Cliff Islands and Clack Island. The total uncertainty due to levelling at the site and extrapolation of the tidal observations to sites for which the secondary correction is unknown is estimated to be ±0.2 m.

Nymph Island **14° 39' S** **145° 15' E** **16 November**

The site visited is in the southwest of the island, at the mouth of the channel linking the central lagoon with the sea, and in the moated inlet just to the south. Dead microatolls are found among mangroves to the south of the channel, and beneath the cemented platform on the north side of the inlet.

Sample	Height (MLWS)	Description
NY 9201	1.30±0.2	microatoll
NY 9202	1.36±0.2	microatoll
NY 9203	1.40±0.2	microatoll
NY 9204	1.36±0.2	microatoll, sample kept by David Hopley
NY 9205	1.22±0.2	microatoll, sample kept by David Hopley
NY 9206	1.39±0.2	microatoll
NY 9207	1.38±0.2	microatoll, large *Porites*
NY 9208	0.73±0.2	microatoll, approx 10 cm thick, overlying black organic mud and coral rubble, sample kept by David Hopley.
NY 9209	1.03±0.2	microatoll, horizontal core, sample kept by David Hopley
NY 9211	1.04±0.2	microatoll

Turtle I **14° 44' S** **145° 11' E** **17 November**

A field of dead raised microatolls on Turtle I is located on the south side of the island, approximately 100 m from the western end. The microatolls are found in a embayment about 20 m across, where the cemented platform has eroded more than elsewhere, exposing the corals below. The site is presently moated by a shingle rampart about 1 m high, which is covered at high tide. Microatolls were found in the centre of the bay, and in the mangroves to either side.

Sample	Height (MLWS)	Description
T1 9201	1.14±0.2	Highest of a cluster of microatolls, well-bedded in reef flat material.
T1 9202	0.96±0.2	microatoll
T1 9203	1.08±0.2	*Favites*, no obvious flat upper surface, but upright and in place.
T1 9204	1.21±0.2	*Porites* microatoll, adjacent to cemented platform. Rim raised ~ 0.15 m above centre of coral, indicating possible moating or windward rim on open reef flat.
T1 9207	1.11±0.2	*Porites* microatoll ~ 2 m across, with raised rim.

Turtle II **14° 44' S** **145° 12' E** **17 November**

At the west end of Turtle II, a small stream draining the central lagoon flows across intertidal reef flat containing dead microatolls. Immediately to the south, and extending along the southern edge of the island, a platform of cemented rubble about 1 m thick overlies abundant preserved microatolls. The stream which drained the lagoon to the north side of the island in 1973 is apparently now blocked by a rubble beach ridge (David Hopley, pers. comm.).

Sample	Height (MLWS)	Description
T2 9201	1.15±0.2	*Porites* microatoll in stream bed
T2 9202	0.86±0.2	microatoll in stream bed
T2 9203	0.65±0.2	microatoll in stream bed
T2 9204	0.84±0.2	microatoll under cemented platform
T2 9205	0.80±0.2	microatoll under cemented platform
T2 9206	0.85±0.2	microatoll
T2 9207	0.85±0.2	microatoll

West Pethebridge Island **14° 44' S** **145° 05' E** **18 November**

Abundant dead microatolls were found at the west end of West Pethebridge Island, immediately south of the narrow shingle spit extending to the west. Those sampled were on the edge of or just within the mangroves, and were occasionally overlain by eroded slabs of cemented rubble, which exists as a continuous platform a little inland and extends around the southern edge of the island.

Sample	Height (MLWS)	Description
WP 9201	0.91±0.2	large *Porites* microatoll
WP 9202	0.90±0.2	*Porites* microatoll
WP 9203	0.90±0.2	microatoll, 2 bags of sample
WP 9204	1.07±0.2	microatoll, 2 bags of sample
WP 9205	0.94±0.2	microatoll
WP 9206	1.12±0.2	microatoll, dirty sample
WP 9207	0.61±0.2	microatoll
WP 9208	0.92±0.2	*Porites* microatoll
WP 9209	0.55±0.2	*Favites*? microatoll
WP 9210	0.87±0.2	microatoll
WP 9211	0.90±0.2	microatoll

Fly Reef **14° 30' S** **145° 09.5 E** **19 November**

At the north end of Fly Reef is a small sand cay, about 20 m long at low tide. The reef is ringed by blocks of coral up to several metres across thrown up during storms, which are emergent at low tide. Dead microatolls were found on the reef flat close to the height of living corals, to the northwest of the cay, and near a bank of rubble extending southeast from the south end of the cay. All dead microatolls seen were in good condition and may be quite young.

Sample	Height (MLWS)	Description
FR 9201	0.11±0.2	*Porites* microatoll
FR 9202	0.02±0.2	*Favites*? microatoll

Lizard Island **14° 40' S** **145° 28' E** **21 November**

Lizard Island has extensive reef flat on the southern side, but with no obvious high fossil microatolls (Kurt Lambeck, pers. comm.). On the western side, the bouldery coast north of Watson's Bay preserves abundant carbonate-cemented rubble in the intertidal zone and above the high-water line. The rubble consists mainly of granite pebbles and quartz granules, and small coral heads, probably thrown up during storms from the adjacent fringing reef. Small bivalve shells are also incorporated.

At the first cliff-like outcrop of granite basement heading northwest from the beach, a massive accumulation of barnacle shells, and a single oyster, were found on a large boulder well above their modern growth limits. In a crack in the cliff behind this boulder, a large fragment of coral was sampled from an accumulation of cemented rubble.

Further to the northwest, approximately 50 m north of Turtle Beach, a large deposit of oyster shells was found on the underside of a large granite boulder at the head of a small bouldery embayment. The oyster shells form a layer a few cm thick, cemented to the boulder in growth position. The deposit has no obvious upper limit, as the top has been eroded away, and extends for approximately 2 m horizontally and 0.5 m vertically.

The sand and rubble between the boulders along this part of coast appear to be developing an interstitial carbonate cement, where the sediment contains enough fine-grained material to retain sea-water after wetting at high tide, and accumulate carbonate as the water evaporates.

Sample	Height (MLWS)	Description
LI 9201	2.25±0.2	coral fragment from cemented rubble
LI 9202	2.16±0.2	oyster shells, from top of deposit

Houghton Island **14° 31.5' S** **144° 58' E** **22 November**

Two sites were sampled on Houghton Island. The mangrove-enclosed area of reef flat on the northern side of the island contains a large field of high dead microatolls. They are generally large and well-formed, and cover an area several hundred metres long. At the inland edge, the microatolls are covered by a beach ridge, and they were not seen under the denser mangrove swamp beyond. A transect was sampled at a break in the front line of mangroves.

The origin of the line of mangroves enclosing the area of reef flat is unknown. It is possible that they are growing along the line of a rubble bank or storm deposit of some sort, which would suggest that the high microatolls may be moated. However, there is no evidence of any such sediment at the base of the mangroves, and the line of their growth may be controlled by wave action during storms, which should simply be a function of distance from the reef edge.

A single sample was taken from beneath the cemented platform at the western end of the island, as some protection against the possibility that the better site was moated.

Sample	Height (MLWS)	Description
HO 9201	1.18±0.2	microatoll, highest in transect
HO 9202	1.09±0.2	microatoll
HO 9203	1.04±0.2	microatoll
HO 9204	0.84±0.2	microatoll
HO 9205	0.56±0.2	microatoll, lowest in transect, outside mangroves
HO 9206	0.45±0.2	modern microatoll, not sampled
HO 9207	0.93±0.2	*Porites* microatoll under platform

Leggatt Island **14° 33' S** **144° 40' E** **23 November**

On the south side of Leggatt Island, there is a cluster of high dead microatolls extending underneath a steep beach ridge composed of coral rubble. No microatolls were seen in the mangrove swamp behind the beach ridge. Dead microatolls were also sampled from the modern reef flat, though this is presently moated above low-water.

The microatolls closest to the ridge (within the line marked on the map) exhibit raised rims; those nearer the coast within the same cluster do not. The line between the two groups is quite sharp - it even appears to truncate one individual microatoll, which has a raised rim on the landward side only. A possible explanation for this is the development of a rampart across the reef flat while the microatolls were alive, raising the water level inside and causing the corals to grow to the surface, forming rims. At the east end of the island, the modern rubble rampart is forming over living microatolls, and more than one was seen half buried and still alive, providing a modern analogue for the dead microatoll with a half-rim.

Sample	Height (MLWS)	Description
LE 9201	0.95±0.2	rimmed microatoll, sample from rim
LE 9202	0.81±0.2	microatoll outside rim line
LE 9203	0.75±0.2	microatoll outside rim line
LE 9204	0.61±0.2	microatoll from reef flat
LE 9205	0.59±0.2	microatoll from reef flat

West Cliff Island **14° 13' S** **143° 47' E** **25 November**

Although there is a modern reef flat around this and East Cliff Island, no high dead microatolls were seen. The northern edge consists of a line of cliffs around 15 m high, with many large blocks and overhangs at the base. The line of overhang probably represents the modern wave-cut notch, as modern debris was found throughout. No ancient oyster shell accumulations were found on the rocks or boulders, probably because the sandstone substrate in eroding too fast to preserve them. In some places the rock crumbled easily, and everywhere the erosion appeared active. A high retreat rate of the coast explains why no high microatolls were found.

At the beach on the west end of the island there is beach rock, composed mainly of carbonate-cemented quartz sand (derived from the sandstone) but also containing coral and shell fragments.

At the east end of the island, there is a sandstone platform about 30 m across and sloping along-shore from near sea-level to about 5 m elevation, bounded by a 3 m cliff. While it is likely that this terrace was wave-cut at a time of higher sea-level, its height is clearly lithology-controlled - it follows a single bed - so is not a useful sea-level indicator.

Mangroves grow in the intertidal zone on the south side of the island, with a sandy terrace about 10 m wide just above the high-water line. This is bounded on the inland edge by a degraded sandstone scarp about 5 m high.

Sample	Height (MLWS)	Description
CL 9201	~ 0.5 m	Beach rock, sample from top of deposit ~ 1 m thick.

Clack Island **14° 04' S** **144° 15' E** **26 November**

At the south end of Clack Reef, there are two rocky islands. A spit of cemented platform extends southwest from the larger (south) island, protecting a dense mangrove swamp to the north. Along the southern edge of the platform there are a few dead microatolls, underwater at low tide when visited and not far above the living coral. At the end of the spit is a field of large dead microatolls, well-formed and emergent at low tide.

Sample	Height (MLWS)	Description
CK 9201	0.21±0.2	microatoll
CK 9202	0.23±0.2	microatoll
CK 9205	0.69±0.2	*Porites* microatoll
CK 9206	0.87±0.2	microatoll
CK 9207	0.88±0.2	microatoll
CK 9208	0.78±0.2	living microatoll, not sampled.

Sample CK 9208 is somewhat puzzling, as microatolls are generally understood to live only below MLWS in open water, and this site did not appear to be moated. When observed, however, low tide covered this microatoll, and possibly the site is in fact moated at lower tides. Clack Island is quite close to the nearest Secondary Place for tide predictions (Flinders Island), and it is unlikely that tide levels differ by as much as 0.78 m.

Noble Island **14° 30' S** **144° 46' E** **27 November**

The site studied on Noble Island is an embayment at the south end of the mangrove swamp on the western side of the island. The bay opens to the southwest, and has a rocky shore on the south side. Many microatolls are present in the north and east of the bay, forming an almost continuous platform. Isolated dead microatolls were found further out on the reef flat. A large giant clam (*Tridacna*) was also found in growth position embedded in the platform, truncated at the level of the surrounding corals.

Sample	Height (MLWS)	Description
NO 9201	0.99±0.2	microatoll
NO 9202	0.99±0.2	microatoll
NO 9203	1.00±0.2	microatoll
NO 9204	1.00±0.2	microatoll
NO 9205	0.76±0.2	microatoll
NO 9206	0.80±0.2	microatoll
NO 9207	0.85±0.2	microatoll
NO 9208	0.91±0.2	*Tridacna* shell material

CAPE TRIBULATION FIELD WORK, OCTOBER 1993

Two coastal fringing reefs near Cape Tribularion were visited in October 1993. The sites studied and samples taken are described here, with the elevation of each sample. Levels were determined using a staff and level in the field, measuring the height of each sample relative to water level at low tide. These were reduced to Tidal Datum using the Cairns tide observations (supplied by the National Tidal Facility, Flinders University) and then converted to heights above the level of mean low water spring tides (MLWS).

Rykers Reef **16° 2 S** **145° 29 E** **12 October**

Rykers Reef is a roughly semicircular fringing reef developed at the mouth of Rykers Creek, on the point immediately north of Cape Tribulation. The edge of the reef is living, while the inner part consists of a sandy flat which is emergent at low tide and has numerous exposed dead microatolls. The samples were mostly taken from the southern end of the reef.

Sample	Height (MLWS)	Description
RY 9301	0.32±0.2	*Porites* microatoll
RY 9303	0.32±0.2	*Porites* microatoll
RY 9304	0.27±0.2	*Porites* microatoll
RY 9306	0.47±0.2	*Porites* microatoll

Myall Reef **16° 5 S** **145° 30 E** **13 October**

Myall Reef is a long shore-parallel fringing reef on the coast to the south of Cape Tribulation. The reef was studied immediately north of the mouth of Myall Creek. An outer ridge with living coral on the seaward side and dead microatolls on top is separated from the beach by a low sand flat, which is exposed at low tide. Some dead microatolls are exposed at the base of the beach, on the landward side of the sand flat.

Sample	Height (MLWS)	Description
MY 9301	0.42±0.2	*Porites* microatoll
MY 9302	0.52±0.2	*Porites* microatoll
MY 9303	0.28±0.2	*Porites* microatoll
MY 9305	0.11±0.2	*Porites* microatoll

Bibliography

Adamson, D.A. and Pickard, J., 1983. Late Quaternary ice movement across the Vestfold Hills, East Antarctica. In *Antarctic Earth Science*, (R.L. Oliver, P.R. James and J.B. Jago, Eds), Australian Academy of Science, 465-469.

Adamson, D.A. and Pickard, J., 1986. Cainozoic history of the Vestfold Hills. In *Antarctic Oasis*, (J. Pickard, Eds), Academic Press, 63-97.

Adie, R.J., 1964. Sea-level changes in the Scotia Arc and Graham Land. In *Antarctic Geology*, (R.J. Adie, Eds), Wiley, 27-32.

Agassiz, A., 1898. *Harvard Mus. comp. Zoology Bull.*, **28**, 93-148.

Aldaz, L. and Deutsch, S., 1967. On a relationship between air temperature an oxygen isotope ratio of snow and firn in the south pole region. *Earth and Planetary Science Letters*, **3**, 276-274.

Alley, R.B. and Whillans, I.M., 1984. Response of the East Antarctica Ice Sheet to Sea-Level Rise. *J. Geophys. Res.*, **89**, 6487-6493.

Anderson, J.B., Shipp, S.S., Bartek, L.R. and Reid, D.E., 1992. Evidence for a grounded ice sheet on the Ross Sea continental shelf during the Late Pleistocene and preliminary paleodrainage reconstruction. In *Contributions to Antarctic Research III*, (D.H. Elliot, Eds), American Geophysical Union, **57**, 39-62.

Anderson, J.B. and Thomas, M.A., 1991. Marine ice-sheet decoupling as a mechanism for rapid, episodic sea-level change: the record of such events and their influence on sedimentation. *Sed. Geol.*, **70**, 87-104.

Andrews, J.T., 1968. Postglacial rebound in Arctic Canada: similarity and prediction of uplift curves. *Canadian Journal of Earth Sciences*, **5**, 39-47.

Andrews, J.T., 1975. *An approach to glaciers and their environments.* Duxbury Press, Massachusetts.

Anundsen, K., 1985. Changes in shore-level and ice-front position in Late Weichsel and Holocene, southern Norway. *Norsk. Geogr. Tidsskr.*, **39**, 205-225.

Augustinus, P.G.E.F., 1989. Cheniers and chenier plains: a general introduction. *Marine Geol.*, **90**, 219-229.

Bard, E., Fairbanks, R., Arnold, M., Maurice, P., Duprat, J., Moyes, J. and Duplessy, J.-C., 1989. Sea-Level Estimates during the Last Deglaciation Based on $\delta^{18}O$ and Accelerator Mass Spectrometry ^{14}C Ages Measured in *Globigerina bulloides*. *Quaternary Res.*, **31**, 381-391.

Bard, E., Hamelin, B., Fairbanks, R.G. and Zindler, A., 1990. Calibration of the ^{14}C timescale over the past 30,000 years using mass spectrometric U-Th ages from Barbados corals. *Nature*, **345**, 405-410.

Barker, P.F. and party, L.1.s.s., 1987. Glacial History of Antarctica. *Nature*, **328**, 115-116.

Barnes, R.D., 1984. *Morphogenesis of a nearshore windward fringing reef, Orpheus Island*. James Cook University.

Barnola, J.M., Raynaud, D., Korotkevich, Y.S. and Lorius, C., 1987. Vostok ice core provides 160,000-years record of atmospheric CO_2. *Nature*, **329**, 403-414.

Baroni, C., 1990. The Hells Gate and Backstairs Passage Ice Shelves. *Memorie Società Geologica Italiana*, **34**, 123-144.

Baroni, C. and Orombelli, G., 1991. Holocene Raised Beaches at Terra Nova Bay, Victoria Land, Antarctica. *Quaternary Research*, **36**, 157-177.

Baroni, C. and Orombelli, G., 1994. Holocene glacier variations in the Terra Nova Bay area (Victoria Land, Antarctica). *Antarctic Science*, **6**, 497-505.

Beaman, R., Larcombe, P. and Carter, R.M., 1994. New evidence for the Holocene sea-level high from the inner shelf, central Great Barrier Reef, Australia. *J. Sed. Res.*, **A64**, 881-885.

Beaumont, C., 1978. The evolution of sedimentary basins on a viscoelastic lithosphere: theory and examples. *Geophys. J. Roy. Astr. Soc.*, **55**, 471-497.

Belperio, A.P., Hails, J.R. and Gostin, V.A., 1983. A review of Holocene sea-levels in South Australia. In *Australian Sea Levels in the Last 15000 Years: A Review (Monograph series 3)*, (D. Hopley, Ed), James Cook University Geography Department, 37-47.

Bentley, C.R. and Giovinetto, M.B., 1992. Mass balance of Antarctica and sea-level change. *EOS, Transactions, AGU*, **73**, 203.

Bird, M.I., Chivas, A.R., Radnell, C.J. and Burton, H.R., 1991. Sedimentological and stable-isotope evolution of lakes in the Vestfold Hills, Antarctica. *Palaeogeogr. Palaeoclimatol. Palaeoecol.*, **84**, 109-130.

Blanchon, P. and Shaw, J., 1995. Reef drowning during the last deglaciation: Evidence for catastrophic sea-level rise and ice-sheet collapse. *Geology*, **23**, 4-8.

Bockheim, J.G., Wilson, S.C., Denton, G.H., Andersen, B.G. and Stuiver, M., 1989. Late Quaternary Ice-surface Fluctuations of Hatherton Glacier, Transantarctic Mountains. *Quaternary Res.*, **31**, 229-254.

Bolshiyanov, D., Verkulich, S., Pushina, Z. and Kirienko, E., 1991. Some features of the Late Pleistocene and Holocene history of the Bunger Hills (East Antarctica). *Abstracts, Sixth International Symposium on Antarctic Earth Sciences*, 66-71.

Bond, G. and others, a.t., 1992. Evidence for massive discharges of icebergs into the North Atlantic ocean during the last glacial period. *Nature*, **360**, 245-249.

Bronge, C., 1989. Holocene Climatic Fluctuations Recorded from Lake Sediments in Nicholson Lake, Vestfold Hills, Antarctica. Stockholms Universitet Naturgeografiska Institutionen, Report.

Budd, W.F. and Morgan, V.I., 1977. Isotopes, climate and ice sheet dynamics from core studies on Law Dome, Antarctica. *IAHS publication*, **118**, 312-321.

Burgess, J.S., Spate, A.P. and Shevlin, J., 1994. The onset of deglaciation in the Larsemann Hills, Eastern Antarctica. *Antarctic Science*, **6**, 491-495.

Cameron, R.L., 1964. Glaciological studies at Wilkes Station, Budd Coast, Antarctica. In *Antarctic Research Series 2*, (M. Mellor, Eds), American Geophysical Union, 1-36.

Carter, R.M., Johnson, D.P. and Hooper, K.G., 1993. Episodic post-glacial sea-level rise and the sedimentary evolution of a tropical continental embayment (Cleveland Bay, Great Barrire Reef shelf, Australia). *Aust. J. Earth Sci.*, **40**, 229-255.

Cathles, L.M., 1975. *The Viscosity of the Earth's Mantle.* Princeton University Press, 386.

Chappell, J., 1974. Late Quaternary glacio- and hydro-isotasy, on a layered Earth. *Quaternary Res.* **4**: 429-440.

Isotopes and Deep-sea Temperatures. *Journal of Geography*, 103, 820-840.

Chappell, J., Chivas, A., Wallensky, E., Polach, H.A. and Aharon, P., 1983. Holocene palaeo-environmental changes, Central to North Great Barrier Reef Inner Zone. *BMR J. Aust. Geol. Geophys.*, **8**, 223-235.

Chappell, J. and Grindrod, J., 1984. Chenier plain formation in northern Australia. In *Coastal Geomorphology in Australia*, (B.G. Thom, Eds), Academic Press, 197-231.

Chappell, J. and Shackleton, N.J., 1986. Oxygen isotopes and sea-level. *Nature*, **324**, 137-140.

Chappell, J.M.A., Rhodes, E.G., Thom, B.G. and Wallensky, E., 1982. Hydro-isostasy and the sea-level isobase of 5500 B.P. in north Queensland, Australia. *Marine Geology*, **49**, 81-90.

Clark, J.A. and Lingle, C.S., 1979. Predicted Relative Sea-Level Changes (18,000 Years B. B. to Present) Caused by Late-Glacial Retreat of the Antarctic Ice Sheet. *Quaternary Res.*, **11**, 279-2948.

Colhoun, E.A. and Adamson, D.A., 1992. Raised Beaches of the Bunger Hills, Antarctica. Report 136, Australian Antarctic Division.

Colhoun, E.A., Mabin, M.C.G., Adamson, D.A. and Kirk, R.M., 1992. Antarctic ice volume and contribution to sea-level fall at 20,000 yr BP from raised beaches. *Nature*, **358**, 316-319.

Cook, P.J. and Mayo, W., 1977. Sedimentology and Holocene history of a tropical estuary (Broad Sound, Queensland). *BMR, Australia, Bulletin*, 170.

Dansgaard, W. and others, a.t., 1993. Evidence of general instability of past climate from a 250-kyr ice-core record. *Nature*, **364**, 218-220.

Denton, G.H., Bockheim, J.G., Wilson, S.C., Leide, J.E. and Andersen, B.G., 1989a. Late Quaternary Ice-surface Fluctuations of Beardmore Glacier, Transantarctic Mountains. *Quaternary Res.*, **31**, 183-209.

Denton, G.H., Bockheim, J.G., Wilson, S.C. and Stuiver, M., 1989b. Late Wisconsin and Early Holocene Glacial History, Inner Ross Embayment, Antarctica. *Quaternary Res.*, **31**, 151-182.

Denton, G.H., Hughes, T.J. and Karlén, W., 1986. Global Ice-Sheet System Interlocked by Sea Level. *Quaternary Res.*, **26**, 3-26.

Denton, G.H., Prentice, M.L. and Burkle, L.H., 1991. Cainozoic history of the Antarctic ice sheet. In *The Geology of Antarctica*, (R.J. Tingey, Ed), Bureau of Mineral Resources, Geology, and Geophysics, 365-433.

Domack, E.W., Jull, A.J.T., Anderson, J.B. and Linick, T.W., 1991. Mid-Holocene ice sheet recession rom the Wilkes Land continental shelf, East Antarctica. In *Geological Evolution of Antarctica*, (M.R.A. Thomson, J.A. Crame and J.W. Thomson, Eds), Cambridge University Press, 693-698.

Domack, E.W., Jull, A.J.T. and Donahue, D.J., 1991. Holocene chronology for the unconsolidated sediments at hole 740A: Prydz Bay, East Antarctica. *Proceedings of the Ocean Drilling Program, Scientific Results*, **119**, 747-750.

Drewry, D.J., 1979. Late Wisconsin Reconstruction for the Ross Sea Region, Antarctica. *J. Glaciology*, **24**, 231-243.

Drewry, D.J., 1980. Pleistocene bimodal response of Antarctic ice. *Nature*, **287**, 214-216.

Drewry, D.J., 1983. Antarctica: Glaciological and Geophysical Folio. Cambridge, Scott Polar Research Institute,

Drewry, D.J., Jordan, S.R. and Jankowski, E., 1982. Measured properties of the Antarctic ice sheet:surface configuration, ice thickness, volume and bedrock characteristics. *Annals Glaciology*, **3**, 83-91.

Dziewonski, A.M. and Anderson, D.L., 1981. Preliminary Reference Earth Model. *Phys. Earth Planet. Inter.*, **25**, 279-356.

Elverhoi, A., 1981. Evidence for a late Wisconsin glaciation of the Weddell Sea. *Nature*, **293**, 641-642.

Elverhøi, A., Fjeldskaar, N., Solheim, A., Nyland-Berg, M. and Russwurm, L., 1993. The Barents Sea ice sheet: a model of its growth and decay during the last ice maximum. *Quat. Sci. Rev.*, in press.

Endean, P., Stephenson, W. and Kenny, R., 1956. The ecology and distribution of intertidal organisms on certain islands off the Queensland coast. *Aust. J. Marine and Freshwater Res.*, **7**, 317-342.

Fairbanks, R.G., 1989. A 17,000-year glacio-eustatic sea level record: influence of glacial melting rates on the Younger Dryas event and deep-ocean circulation. *Nature*, **342**, 637-642.

Farrell, W.E. and Clark, J.A., 1976. On Postglacial Sea Level. *Geophys. J. Roy. astr. Soc.*, **46**, 647-667.

Fjeldskaar, W. and Cathles, L., 1992. The present rate of uplift if Fennoscandia implies a low-viscosity asthenosphere. *Terra nova*, **3**, 393-400.

Flood, P.G. and Frankel, E., 1989. Late Holocene Higher Sea Level Indicators From Eastern Australia. *Marine Geol.*, **90**, 193-195.

Gagan, M.K., Johnson, D.P. and Crowley, G.M., 1994. Sea level control of stacked late Quaternary coastal sequences, central Great Bariier Reef. *Sedimentology*, **41**, 329-351.

Gat, J.R. and Gonfiantini, R., 1981. Stable Isotope Hydrology. Vienna, International Atomic Energy Agency,

Genthon, C., Barnola, J.M., Raynaud, D., Lorius, C., Jouzel, J., Barkov, N.I., Korotkevich, Y.S. and Kotlyakov, V.M., 1987. Vostok ice core: climatic response to CO_2 and orbital forcing changes over the last climatic cycle. *Nature*, **329**, 414-418.

Gibb, J.G., 1986. A New Zealand regional Holocene eustatic sea-level curve and its application to determination of vertical tectonic movements. *Roy. Soc. N.Z. Bull.*, **24**, 377-395.

Gillespie, R. and Polach, H.A., 1979. The suitability of marine shells for radiocarbon dating of Australian prehistory. In *Radiocarbon Dating: Proceedings of the 9th International Radiocarbon Dating Conference, Los Angeles*, University of California Press, 404-421.

Gillieson, D., Burgess, J., Spate, A. and Cochrane, A., 1990. *An atlas of the lakes of the Larsemann Hills*. Australian Antarctic Division, 173.

Gillieson, D.S., 1991. An environmental history of two freshwater lakes in the Larsemann Hills, Antarctica. *Hydrobiologia*, **214**, 327-331.

Goodwin, I.D., 1993. Holocene Deglaciation, Sea-Level Change, and the Emergence of the Windmill Islands, Budd Coast, Antarctica. *Quaternary Res.*, **40**, 70-80.

Gordon, J.E. and Harkness, D.D., 1992. Magnitude and geographic variation of the radiocarbon content in Antarctic marine life: implications for reservoir corrections in radiocarbon dating. *Quaternary Sci. Rev.*, **11**, 697-78.

Grindrod, J.F. and Rhodes, E.G., 1984. *Holocene sea-level history of a tropical estuary: Missionary Bay, north Queensland*. Academic Press, Sydney, 151-178. in Thom, B G (ed) 'Coastal Geomorphology in Australia'

Grobe, H., Huybrechts, P. and Fütterer, D.K., 1993. Late Quaternary record of sea-level changes in the Antarctic. *Geologische Rundschau*, **82**, 263-275.

Grootes, P.M. and Stuiver, M., 1986. Ross Ice Shelf Oxygen Isotopes and West Antarctic Climate History. *Quaternary Res.*, **26**, 49-67.

Grootes, P.M. and Stuiver, M., 1987. Ice sheet elevation changes from isotopic profiles. *IAHS Publication*, **170**, 269-281.

Hafsten, U., 1983. Biostratigraphical evidence for Late Weichselian and Holocene sea-level changes in southern Norway. In *Shorelines and Isostasy*, (D.E. Smith and A.G. Dawson, Eds), Academic Press, London, 161-181.

Harris, P.T. and Davies, P.J., 1989. Submerged reefs and terraces on the shelf edge of the Great Barrier Reef, Australia. *Coral Reefs*, **8**, 87-98.

Harris, P.T., Davies, P.J. and Marshall, J.F., 1990. Late Quaternary sedimentation on the Great Barrier Reef continental shelf and slope east of Townsville, Australia. *Marine Geol.*, **94**, 55-77.

Hayashi, M., 1994. Coastal geomorphology in the Lützow-Holm Bay region, East Antarctica. *Proceedings of the NIPR Symposium on Antarctic Geosciences*, **7**, 189.

Hays, J.D., 1978. A review of the Late Quaternary climatic history of Antarctic Seas. In *Antarctic Glacial History and World Paleoenvironments*, (E.M. van Zinderen Bakker, Eds), A.A. Balkema, 57-70.

Herron, S.L. and Langway, C.C.J., 1987. Derivations of paleoelevations from total air content of two deep Greenland cores. *IAHS Publication*, **170**, 283-295.

Hirakawa, K. and Moriwaki, K., 1990. Former ice sheet based on the newly observed glacial landforms and erratics in the central Sør Rondane Mountains, East Antarctica. *Proceedings of the NIPR Symposium in Antarctic Geoscience*, **4**, 41-54.

Hirvas, H., Nenonen, K. and Quilty, P., 1993. Till stratigraphy and glacial history of the Vestfold Hills area, East Antarctica. *Quaternary Int.*, **18**, 81-95.

Hjort, C., Björck, S. and Ingolfsson, O., 1991. The last major deglaciation in the Antarctic Peninsula region. *Abstracts, Sixth International Symposium on Antarctic Earth Sciences*, 229.

Hjort, C., Ingólfsson, Ó. and Björk, S., 1992. The last major deglaciation in the Antarctic Peninsula region - a review of recent Swedish Quaternary research. In *Recent Progress in Antarctic Earth Science*, (Y. Yoshida, Eds), TERRAPUB, 741-743.

Hollin, J.T., 1962. On the glacial history of Antarctica. *J. Glaciology*, **4**, 173-195.

Hopley, D., 1971. The origin and significance of north Queensland island spits. *Zeitschrift für Geomorphologie, N. F.*, **15**, 371-389.

Hopley, D., 1978. Sea level change on the Great Barrier Reef: an introduction. *Phil. Trans. R. Soc. Lond.*, **A 291**, 159-166.

Hopley, D., 1982. *The geomorphology of the Great Barrier Reef: Quaternary Evolution of Coral Reefs.* John Wiley - Inerscience, New York, 453.

Hopley, D., 1986a. Beachrock as a sea-level indicator. In *Sea-level Research*, (O. van de Plassche, Ed), Geo Books, 157-173.

Hopley, D., 1986b. Corals and reefs as indicators of paleo-sea levels. In *Sea-level Research*, (O. van de Plassche, Eds), Geo Books, 195-228.

Hopley, D., 1987. Holocene sea-level changes in Australasia and southern Pacific. In *Sea Surface Studies: A Global Review*, (R.J.N. Devoy, Ed), Croom Helm, 375-408.

Hopley, D., McLean, R.F., Marshall, J. and Smith, A.S., 1978. Holocene - Pleistocene boundary in a fringing reef: Hayman Island, North Queensland. *Search*, **9**, 323-325.

Hughes, T.J., Denton, G.H., Andersen, B.G., Schilling, D.H., Fastook, J.L. and Lingle, C.S., 1981. The Last Great Ice Sheets: A Global View. In *The Last Great Ice Sheets*, (G.H. Denton and T.J. Hughes, Eds), John Wiley and Sons, 263-317.

Huybrechts, P., 1990. A 3-D model for the Antarctic ice sheet: a sensitivity study on the glacial-interglacial contrast. *Climate Dynamics*, **5**, 79-92.

Huybrechts, P., 1992. The Antarctic ice sheet and environmental change: a three-dimensional modelling study. *Rep. Polar Res.*, **99**, 241.

Jacobs, S.S., 1992. Is the Antarctic ice sheet growing? *Nature*, **360**, 29-33.

Jenssen, D. and Radok, U., 1982. On the joint interpretation of total gas contents and stable isotope ratios in ice cores. *Annals Glaciology*, **3**, 152-155.

Jenssen, D., 1983. Elevation and climatic changes from total gas content and stable isotopic measurements. In *The Climatic Record in Polar Ice Sheets*, (G.d.Q. Robin, Ed), Cambridge University Press, 138-144.

Johnsen, S.J., Dansgaard, W., Clausen, H.B. and Langway Jr, C.C., 1972. Oxygen isotope profiles through the Antarctic and Greenland ice sheets. *Nature*, **235**, 429-434.

Johnston, P.J., 1993. *Deformation of the Earth by surface loads.* The Australian National University.

Johnston, P.J., 1993. The effect of spatially non-uniform water loads on prediction of sea-level change. *Geophys. J. Int.*, **114**, 615-634.

Jongsma, D., 1970. Eustatic Sea Level Changes in the Arafura Sea. *Nature*, **228**, 150-151.

Jouzel, J., Lorius, C., Petit, J.-R., Genthon, C., Barkov, N.I., Kotlyakov, V.M. and Petrov, V.M., 1987. Vostok ice core: a continuous isotope temperature record over the last climatic cycle (160,000 years). *Nature*, **329**, 403-408.

Jouzel, J. and Merlivat, L., 1984. Deuterium and Oxygen 18 in Precipitation: Modeling of the Isotopic Effects During Snow Formation. *J. Geophys. Res.*, **89**, 11749-11757.

Jouzel, J., Raisbeck, G., Benoist, J.P., Yiou, F., Lorius, C., Raynaud, D., Petit, J.-R., Barkov, N.I., Korotkevich, Y.S. and Kotlyakov, V.M., 1989. A Comparison of Deep Antarctic Ice Cores and Their Implications for Climate between 65,000 and 15,000 Years Ago. *Quaternary Research*, **31**, 135-150.

Kaminuma, K. and Nagao, T., 1983b. Ground tilt observations at Syowa Station, Antarctica. Part 2. Water-tube Tiltmeter. *Memoirs of the National Institute of Polar Research, Special Issue*, **28**, 33-41.

Kaminuma, K., Nagao, T. and Ito, K., 1983a. Ground tilt observations at Syowa Station, Antarctica. Part 1. Borehole Tiltmeter. *Memoirs of the National Institute of Polar Research, Special Issue*, **28**, 27-32.

Kaup, E., Klokov, V., Vaikmäe, E.R., Haendel, D. and Vierath, R., 1989. Hydrochemical and isotope hydrological investigations in the Bunger Oasis. *Geodätische und Geophysikalische Veröffentlichengen*, **1**, 245-359.

Kirk, R.M., 1991. Raised beaches, late Quaternary sea-levels and deglacial sequences on the Victoria Land coast, Ross Sea, Antarctica. In *Quaternary research in Australian Antarctica: Future directions*, (D.S. Gillieson and S. Fitzsimons, Eds), Department of Geography and Oceanography, University College, Australian Defense Force Academy, **Special Publication No. 3**, 85-105.

Lambeck, K., 1980. *The Earth's Variable Rotation: Geophysical Causes and Consequences*. Cambridge University Press, 450.

Lambeck, K., 1981. Flexure of the ocean lithosphere from island uplift, bathymetry and geoid height observations: the Society Islands. *Geophys. J. Roy. astr. Soc.*, **647**, 91-114.

Lambeck, K., 1990. Glacial rebound, sea-level change and mantle viscosity. *Quaterly Journal of the Royal Astronomical Society.*, **31**, 1-30.

Lambeck, K., 1990. Late Pleistocene, Holocene, and present sea-levels: constraints on future change. *Palaeogeogr. Palaeoclimatol. Palaeoecol. (Global and Planetary Change section)*, **89**, 205-217.

Lambeck, K., 1993a. Glacial rebound of the British Isles - I. Preliminary model results. *Geophys. J. Int.*, **115**, 941-959.

Lambeck, K., 1993b. Glacial rebound of the British Isles - II. A high-resolution, high-precision model. *Geophys. J. Int.*, **115**, 960-990.

Lambeck, K., 1995. Constraints on the late Weichselian ice sheet over the Barents Sea from observations of raised shorelines. *Quaternary Sci. Rev.*, **14**, 1-16.

Lambeck, K., Johnston, P., Smither, C. and Nakada, M., submitted. Glacial rebound of the British Isles - III. Constraints on mantle viscosity.

Lambeck, K. and Nakada, M., 1990. Late Pleistocene and Holocene sea-level change along the Australian coast. *Palaeogeogr. Palaeoclimatol. Palaeoecol.*, **89**, 143-176.

Lambeck, K. and Nakada, M., 1992. Constraints on the age and duration of the last interglacial period and on sea-level variations. *Nature*, **357**, 125-128.

Lambeck, K. and Nakiboglu, S.M., 1981. Seamount loading and stress in the ocean lithosphere 2. Viscoelastic and elastic-viscoelastic models. *J. Geophys. Res.*, **86**, 6961-6984.

Larcombe, P., Carter, R.M., Dye, J., Gagan, M.K. and Johnson, D.P., 1995. New evidence for episodic post-glacial sea-level rise, central Great Barrier Reef, Australia. *Marine Geol.*, **125**,

Larter, R.D. and Vanneste, L.E., 1995. Relict subglacial deltas on the Antarctic Peninsula outer shelf. *Geology*, **23**, 33-64.

Lehman, S.J. and Keigwin, L.D., 1992. Sudden changes in North Atlantic circulation during the last deglaciation. *Nature*, **356**, 757-762.

Levin, I., Kromer, B. and Francey, R., 1994. Continuous measurements of ^{14}C in atmospheric CO_2 at Cape Grim. In *Baseline Atmospheric Program, Australia*, (A.L. Dick and J.L. Gras, Eds), CSIRO Division of Atmospheric Research,

Lewis, A., 1994. *An Environmental History of Anderson Lake (Vestfold Hills, Antarctica) Derived from Lake Sediments*. University of Tasmania.

Lighty, R.G., Macintyre, I.G. and Stuckenrath, R., 1982. Acropora palmata reef framework: a reliable indicator of sea-level in the western Atlantic for the past 10 000 years. *Coral Reefs*, **1**, 125-30.

Lingle, C.S. and Clark, J.A., 1979. Antarctic ice-sheet volume at 18,000 years B. P. and Holocene sea-level changes at the West Antarctic margin. *Journal of Glaciology*, **24**, 213-230.

Løken, O.H., 1959. Evidence of higher sea-levels in the Windmill Islands. In *Ohio State University Research Foundation Report 825-1, Part 3*, (R.L. Cameron, O.H. Løken and J.R.L. Molholm, Eds), 28-32.

López-Martínez, J., Martínez de Pisón, E. and Arche, A., 1992. Geomorphology of Hurd Peninsula, Livingston Island, South Shetland. In *Recent Progress in Antarctic Earth Science*, (Y. Yoshida, Eds), TERRAPUB, 751-756.

Lorius, C., Jouzel, J., Ritz, C., Merlivat, L., Barkov, N.I., Korotkevich, Y.S. and Kotlyakov, V.M., 1985. A 150,000-year climatic record from Antarctic ice. *Nature*, **316**, 591-596.

Lorius, C., Raynaud, D., Petit, J.-R., Jouzel, J. and Merlivat, L., 1984. Late-Glacial Maximum-Holocene atmospheric and ice-thickness changes from Antarctic ice-core studies. *Annals of Glaciology*, **5**, 88-94.

Mabin, M.C.G., 1986. The Ross Sea section of the Antarctic ice sheet at 18,000 yr B.P.: evidence from Holocene sea-level changes along the Victoria Land Coast. *South African Journal of Science*, **82**, 506-508.

Mabin, M.C.G., 1992. Late Quaternary ice-surface fluctuations of the Lambert Glacier. In *Recent Progress in Antarctic Earth Science*, (Y. Yoshida, Eds), TERRAPUB, 683-687.

MacAyeal, D.R., 1992. Irregular oscillations of the West Antarctic ice sheet. *Nature*, **359**, 29-32.

Marchant, D.R., Denton, G.H., Bockheim, J.G., Wilson, S.C. and Kerr, A.R., 1994. Quaternary changes in level of the upper Taylor Glacier, Antarctica: implications for paleoclimate and East Antarctic Ice Sheet dynamics. *Boreas*, **23**, 29-43.

Marshall, J.F., 1995. Late Quaternary sedimentation on a rimmed continental shelf: northern Great Barrier Reef, Australia. *MS*,

Mäusbacher, R., 1992. Distribution and stratigraphy of raised interglacial marine sediments on King George Island, South Shetlands, Antarctica. *Zeitschrift für Geomorph. N. T. Suppl.-Bd*, **86**, 113-123.

Mäusbacher, R., Müller, J. and Schmidt, R., 1989. Evolution of postglacial sedimentation in Antarctic lakes (King George Island). *Zeitschrift für Geomorphologie N. T.*, **33**, 219-234.

Maxwell, W.G.H., 1968. *Atlas of the Great Barrier Reef.* Elsevier, 258.

McCulloch, M.T., Gagan, M.K., Mortimer, G.E., Chivas, A.R. and Isdale, P.J., 1994. A high-resolution Sr/Ca and $\delta^{18}O$ coral record from the Great Barrier Reef, Australia, and the1982-1983 El Niño. *Geochim. Cosmochim. Acta*, **58**, 2747-2754.

McLean, R.F., Stoddart, D.R., Hopley, D. and Polach, H., 1978. Sea level change in the Holocene on the northern Great Barrier Reef. *Phil. Trans. R. Soc. Lond.*, **A 291**, 167-186.

Meguro, H., Yoshida, Y., Uchio, T., Kigoshi, K. and Sugawara, K., 1963. Quaternary marine sediments and their geological dates with reference to the geomorphology of Kronprins Olav Kyst. In *Antarctic Geology*, (R.J. Adie, Eds), Scientific Committee on Antarctic Research, 73-80.

Meier, M.F., 1984. Contribution of small glaciers to global sea level. *Science*, **226**, 418-421.

Melles, M., Verkulich, S.R. and Hermichen, W.-D., 1994. Radiocarbon dating of lacustrine and marine sediments from the Bunger Hills, East Antarctica. *Antarctic Science*, **6**, 375-378.

Mitrovica, J.X. and Peltier, W.R., 1991. Radial resolution in the inference of mantle viscosity from observations of glacial isostatic adjustment. In *Glacial Isotasy, Sea Level and Mantle Rheology*, (R. Sabadini, K. Lambeck and E. Boschi, Eds), Kluwer Academic Publ., 63-78.

Moriwaki, K., Iwata, S., Matsuoka, N., Hasegawa, H. and Hirakawa, K., 1994. Weathering stage as a relative age of till in the central Sør-Rondane. *Proc. NIPR Symp. Antarct. Geosci.*, **7**, 156-161.

Murray-Wallace, C.V. and Belperio, A.P., 1991. The last interglacial shoreline in Australia - a review. *Quaternary Sci. Rev.*, **10**, 441-461.

Murray-Wallace, C.V. and Goede, A., 1991. Aminostratigraphy and electron spin resonance studies of late Quaternary sea level change and coastal neotectonics in Tasmania, Astralia. *Z. Geomorph. N.F.*, **35**, 129-149.

Nakada, M. and Lambeck, K., 1987. Glacial rebound and relative sea-level variations: a new appraisal. *Geophys. J. Roy. astr. Soc.*, **90**, 171-224.

Nakada, M. and Lambeck, K., 1988. The melting history of the late Pleistocene Antarctic ice sheet. *Nature*, **333**, 36-40.

Nakada, M. and Lambeck, K., 1989. Late Pleistocene and Holocene sea-level change in the Australian region and mantle rheology. *Geophys. J.*, **96**, 497-517.

Nakada, M. and Lambeck, K., 1991. Late Pleistocene and Holocene Sea-Level Change: Evidence for Lateral Mantle Viscosity Structure? In *Glacial Isotasy, Sea Level and Mantle Rheology*, (R. Sabadini, K. Lambeck and E. Boschi, Eds), Kluwer Academic Pub.l, 79-94.

Nakiboglu, S.M. and Lambeck, K., 1982. A study of the Earth's response to surface loading with application to Lake Bonneville. *Geophys. J. Roy. astr. Soc.*, **70**, 577-620.

Nakiboglu, S.M. and Lambeck, K., 1991. Secular Sea-Level Change. In *Glacial Isotasy, Sea Level and Mantle Rheology*, (R. Sabadini, K. Lambeck and E. Boschi, Eds), Kluwer Academic Publ., 237-258.

Nakiboglu, S.M., Lambeck, K. and Aharon, P., 1983. Postglacial sealevels in the Pacific: Implications with respect to deglaciation regime and local tectonics. *Tectonophysics*, **91**, 335-358.

Nichols, R.L., 1966. Geomorphology of Antarctica. In *Antarctic Soils and Soil Forming Processes*, (J.C.F. Tedrow, Eds), American Geophysical Union, **8**, 1-46.

Nichols, R.L., 1968. Coastal geomorphology, McMurdo Sound, Antarctica. *J. Glaciology*, **7**, 449-478.

O'Brien, P.E., 1994. Morphology and Late Glacial History of Prydz Bay, Antarctica, Based on Echo Sounder Data. *Terra Antarctica*, **1**, 403-405.

O'Brien, P.E., 1994. Morphology, Seismic Stratigraphy and Sedimentation History of the Mac. Robertson Shelf, East Antarctica. *Terra Antarctica*, **1**, 407-408.

Odamaki, M., Michida, Y., Noguchi, I., Iwanaga, Y., Ikeda, S. and Iwamoto, K., 1991. Mean sea-level observed at Syowa Station, East Antarctica. *Proceedings of the NIPR Symposium on Antarctic Geosciences*, **5**, 20-28.

Omoto, K., 1991. Late Holocene sea-level fluctuations in Lützow-Holm Bay, East Antarctica. *Abstracts, Sixth International Symposium on Antarctic Earth Sciences*, 460.

Orheim, O., 1993. Iceberg calving rates and the mass balance of Antarctica. *paper presented at the Fifth International Symposium on Antarctic Geology*,

Orombelli, G., Baroni, C. and Denton, G.H., 1990. Late Cenozoic glacial history of the Terra Nova Bay region, Northern Victoria Land, Antarctica. *Geogr. Fis. Dinam. Quat.*, **13**, 139-163.

Otvos, E.G. and Price, W.A., 1979. Problems of chenier genesis and terminology - an overview. *Marine Geol.*, **31**, 251-263.

Paine, A.G.L., Gregory, C.M. and Clarke, D.E., 1966. Geology of the Ayr 1:250 000 sheet area. Bureau of Mineral Resources, Geology and Geophysics, Report # 68

Paterson, W.S.B., 1994. *The Physics of Glaciers*. Pergamon, 480pp.

Paterson, W.S.B. and Hammer, C.U., 1987. Ice core and other glaciological data. In *North America and adjacent oceans during the last deglaciation*, (W.F. Ruddiman and H.E.J. Wright, Eds), Geological Society of America, 91-109.

Payne, A.J., Sugden, D.E. and Clapperton, C.M., 1989. Modelling the Growth and Decay of the Antarctic Peninsula Ice Sheet. *Quaternary Res.*, **31**, 119-134.

Peltier, R.W., 1994. Ice Age Paleotopography. *Science*, **265**, 195-201.

Peltier, W.R. and Andrews, J.T., 1976. Glacial-isostatic adjustment — 1. The forward problem. *Geophys J. Roy. astr. Soc.*, **46**, 605-646.

Peltier, W.R., Farrell, W.E. and Clark, J.A., 1978. Glacial isostasy and relative sea level: A global finite element model. *Tectonophysics*, **50**, 81-110.

Peterson, J.A., Finlayson, B.L. and Zhang, Q., 1988. Changing distribution of late Quaternary terrestrial lacustrine and littoral environments in the Vestfold Hills, Antarctica. *Hydrobiologia*, **165**, 221-226.

Pickard, J., 1986. Antarctic oases, Davis station and the Vestfold Hills. In *Antarctic Oasis*, (J. Pickard, Eds), Academic Press, 1-19.

Pickard, J., Adamson, D.A. and Heath, C.W., 1986. The evolution of Watts Lake, Vestfold Hills, East Antarctica, from marine inlet to freswater lake. *Palaeogeography, Palaeoclimatology, Palaeoecology*, **53**, 271-288.

Pickard, J. and Seppelt, R.D., 1984. Holocene occurrence of the moss Bryum algens Card. in the Vestfold Hills, Antarctica. *J. Bryology*, **13**, 209-217.

Pope, P.G. and Anderson, J.B., 1992. Late Quaternary glacial history of the Northern Antarctic Peninsula's western continental shelf: evidence from the marine record. In *Contributions to Antarctic Research III*, (D.H. Elliot, Eds), American Geophysical Union, **57**, 63-91.

Queensland, Ministry of Transport, 1992. *Queensland Tide Tables.* Queensland Govt.,

Quinlan, G. and Beaumont, C., 1982. The deglaciation of Atlantic Canada as reconstructed from the postglacial relative sea-level record. *Canadian Journal of Earth Sciences,* **19**, 2232-2246.

Raynaud, D. and Lebel, B., 1979. Total gas content and surface elevation of polar ice sheets. *Nature,* **281**, 289-291.

Raynaud, D. and Lorius, C., 1973. Climatic Implications of Total Gas Content in Ice at Camp Century. *Nature,* **243**, 283-284.

Raynaud, D. and Lorius, C., 1977. Total gas content in polar ice: rheological and climatic implications. *IAHS publication,* **118**, 326-335.

Raynaud, D., Lorius, C., Budd, W.F. and Young, N.W., 1979. Ice flow along an IAGP flow line and interpretation of data from an ice core in Terre Adélie, Antarctica. *J. Glaciology,* **24**, 103-115.

Raynaud, D., Mazaudier, D., Lorius, C., Barkov, N.I. and Lipenkov, V., 1987. Elevation changes over the past 160,000 years near Vostok, East Antarctica, from air content in ice. *IAHS publication,* **170**, 297.

Raynaud, D. and Whillans, I.M., 1982. Air content of the Byrd core and past changes in the West Antarctic ice sheet. *Annals Glaciology,* **3**, 269-273.

Rhodes, E.G., 1980. *Modes of Holocene coastal progradation, Gulf of Carpentaria.* Australian National University. PhD Thesis

Rhodes, E.G., 1982. Depositional model for a chenier plain, Gulf of Carpentaria, Australia. *Sedimentology,* **29**, 201-221.

Ritz, C., Llibourty, L. and Rado, C., 1982. Analysis of a 870 m deep temperature profile at Dome C. *Annals Glaciology,* **3**, 284-289.

Robin, G.d.Q., 1977. Ice cores and climate change. *Phil. Trans. R. Soc. Lond. B,* **280**, 143-168.

Robin, G.d.Q., 1985. Contrasts in Vostok core - changes in climate or ice volume? *Nature,* **316**, 578-579.

Salama, M.S., 1990. *Late Quaternary sedimentary characteristics, processes and evolution of the Princess Charlotte Bay area: A Great Barrier Reef province.* University of Queensland.

Scoffin, T.P. and Stoddart, D.R., 1978. The Great Barrier Reef and the Great Barrier Reef Expedition 1973. *Phil. Trans. R. Soc. Lond.,* **B 284**, 99-122.

Shackleton, N.J., 1987. Oxygen Isotopes, Ice Volume and Sea Level. *Quaternary Sci. Rev.*, **6**, 183-190.

Siegenthaler, U., 1979. Stable Hydrogen and Oxygen Isotopes in the Water Cycle. In *Lectures in Isotope Geology*, (E. Jäger and J.C. Hunziker, Eds), Springer-Verlag, 264-273.

Skjold, L.J., 1988. *A Seismic and Sedimentary study of the late Quaternary development of the Lloyd Bay area, Northern Great Barrier Reef, Australia.* University of Queensland.

Slocombe, A.M., 1981. *The Structure and Development of the Fringing Reefs in Pioneer Bay, Orpheus Island.* James Cook University.

Smart, J., 1976. The nature and origin of beach ridges, western Cape York Peninsula, Queensland. *BMR J. Aust. Geol. Geophys.*, **1**, 211-218.

Smart, J., 1977. Late Quaternary sea-level changes, Gulf of Carpentaria, Australia. *Geology*, **5**, 755-759.

Steers, J.A., 1929. The Queensland coast and the Great Barrier Reefs. *Geographical Journal*, **74**, 232-257, 341-370.

Steers, J.A., 1937. *Geogr. J.*, **89**, 1-28 and 119-139.

Steers, J.A., 1938. *Rep. Great Barrier Reef Comm.*, **4**, 51-96.

Stein, M., Wasserburg, G.J., Aharon, P., Chen, J.H., Zhu, Z.R., Bloom, A. and Chappell, J., 1993. TIMS U-series dating and stable isotopes of the last interglacial event in Papua New Guinea. *Geochim.Cosmochim.Acta*, **57**, 2541-2554.

Stern, T.A., Davey, F.J. and Delisle, G., 1991. Lithospheric flexure induced by the load of Ross Archipelage, southern Victoria Land, Antarctica. In *Geological Evolution of Antarctica*, (M.R.A. Thomson, J.A. Crame and J.W. Thomson, Eds), Cambridge University Press, 323-328.

Stoddart, D.R., 1978. The Great Barrier Reef and the Great Barrier Reef Expedition 1973. *Phil. Trans. R. Soc. Lond.*, **A 291**, 5-22.

Stoddart, D.R., McLean, R.F. and Hopley, D., 1978. Geomorphology of reef islands, northern Great Barrier Reef. *Phil. Trans. R. Soc. Lond.*, **A 291**, 39-61.

Stuiver, M., Hughes, T.J., Denton, G.H. and Fastook, J.L., 1981. History of the marine ice sheet in West Antarctica during the last glaciation: a working hypothesis. In *The Last Great Ice Sheets*, (G.H. Denton and T.J. Hughes, Eds), John Wiley and Sons, 319-436.

Svendsen, J.I. and Mangerud, J., 1987. Late Weichselian and Holocene sea-level history for a cross-section of western Norway. *J. Quaternary Sci.*, **2**, 113-132.

Symonds, P.A., Davies, P.J. and Parisi, A., 1983. Structure and stratigraphy of the central Great Barrier Reef. *BMR Journal of Australian Geology and Geophysics*, **8**, 277-291.

Thom, B.G. and Chappell, J., 1978. Holocene sea-level change: an interpretation. *Phil. Trans. R. Soc. Lond.*, **A 291**, 187-194.

Thom, B.G. and Roy, P.S., 1983. Sea level change in New South Wales over the past 15000 years. In *Australian Sea Levels in the Last 15000 Years: A Review (Monograph series 3)*, (D. Hopley, Ed.), James Cook University Geography Department, 3-26.

Tushingham, A.M. and Peltier, R.W., 1991. Ice-3G: A New Global Model Of Late Pleistocene Deglaciation Based Upon Geophysical Predictions of Post-Glacial Relative Sea-level Change. *Journal of Geophysical Research*, **96**, 4497-4523.

Tushingham, A.M. and Peltier, R.W., 1992. Validation of the ICE-3G Model of Würm-Wisconsin Deglaciation Using a Global Data Base of Relative Sea-level Histories. *Journal of Geophysical Research*, **97**, 3285-3304.

van Andel, T.H. and Veevers, J.J., 1967. *Morphology and Sediments of the Timor Sea.* BMR Bulletin 83

Veeh, H.H. and Veevers, J.J., 1970. Sea Level at -175 m off the Great Barrier Reef 13,600 to 17,000 Year Ago. *Nature*, **226**, 536-537.

Verkulich, S.R. and Hiller, A., 1994. Holocene deglaciation of the Bunger Hills revealed by ^{14}C measurements on stomach oil deposits in snow petrel colonies. *Antarctic Science*, **6**, 395-399.

Walbran, P.D., 1994. The nature of the pre-Holocene surface, John Brewer Reef, with implications for the interpretation of Holocene reef development. *Marine Geol.*, **122**, 63-79.

Walcott, R.I., 1972. Past sea levels, eustasy and deformation of the earth. *Quaternary Research*, **2**, 1-14.

Walcott, R.I., 1973. Structure of the Earth from glacio-isostatic rebound. *Ann. Rev. Earth Planet Sci.*, **1**, 15-37.

Walcott, R.I., 1975. Recent and Late Quaternary Changes in Water Level. *EOS*, **56**, 62-72.

Warrick, R. and Oerlemans, J., 1990. Sea Level Rise. In *Climate Change : The IPCC Scientific Assesment*, (J.T. Houghton, G.J. Jenkins and J.J. Ephraums, Eds), Press Syndicate of the University of Cambridge, 257-281.

Woodroffe, C. and McLean, R., 1990. Microatolls and recent sea level change on coral atolls. *Nature*, **344**, 531-534.

Yiou, F., Raisbeck, G.M., Bourles, D., Lorius, C. and Barkov, N.I., 1985. ^{10}Be in ice at Vostok, Antarctica during the last climatic cycle. *Nature*, **316**, 616-617.

Yoshida, Y. and Moriwaki, K., 1979. Some considerations on elevated coastal features and their dates around Syowa Station, Antarctica. *Memoirs of the National Institute of Polar Research, Special Issue*, **13**, 220-226.

Zhang, Q. and Peterson, J.A., 1984. A geomorphology and Late Quaternary geology of the Vestfold Hills, Antarctica. ANARE,